Local ice load data relevant to Grand Banks structures

K.R. Croasdale & Associates Ltd.

Publisher's version / Version de l'éditeur:
https://doi.org/10.4224/12328497
PERD/CHC report; no. 20-61, 2001-03

Local Ice Load Data Relevant to Grand Banks Structures

Report for:
National Research Council of Canada

Contract Number: 40731

PERD/CHC Report 20-61

01680
March 2001

K.R. Croasdale & Associates Ltd.

In Association with:

Avron Ritch Consulting Ltd.
C-CORE
Ian Jordaan & Associates Inc.
Sandwell Inc.
Westmar Consultants Inc.
B. Wright & Associates Ltd.

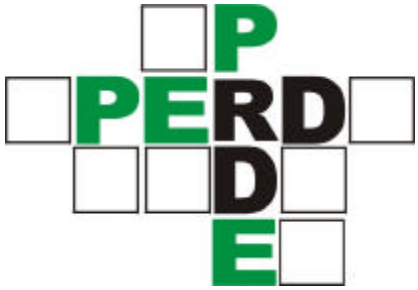

Executive Summary

Development of oil and gas on the Grand Banks requires facilities that are capable of being operated in an environment in which icebergs, pack ice and severe storms can be present. Designing for icebergs can add to the cost of a fixed platform. In particular, the local design loads on the walls of a platform are much higher when ice is present, and this can add considerably to the costs (several $100 million - in the case of Hibernia). So, there is a clear incentive to develop authentic local ice load design criteria for the Grand Banks (as there is in any ice covered region).

Given this incentive, the objectives of this study are:

- To identify, assess and compile all the data sources available on local ice loads that could be applied to the design of fixed and floating platforms on the Grand Banks, due to iceberg impact.

- To review the methodology for inferring local ice pressures as a function of area, and other relevant parameters for each set of key data.

- To rank data sets as to their value and relevance to local ice pressure design for the Grand Banks.

- To comment on the state of knowledge, deficiencies and make recommendations for future work, especially in relation to Code revisions.

During the course of this study, over 20 data sets relevant to local ice loads, and spanning almost a 30 year period, were examined and catalogued. The main categories of data are:

- Indentation experiments on full-thickness ice sheets.
- Indentation tests into the sides of icebergs and multi-year ice.
- Flaking tests on first year and lake ice.
- Iceberg impact experiments.
- Measurements of local loads on instrumented structures.
- Measurements of local loads on ice breaking vessels.

A description of each data set is provided according to a standard format.

Most data sets will yield pressure/area curves which show decreasing ice crushing pressure with increasing area, which can be used for local load design. However, it is clear that where aspect ratio (width divided by height of contact area) is reported, most data also show a significant decrease in ice pressure with increasing aspect ratio. Most iceberg interactions maintain a relatively low aspect ratio and so there may be a concern in using pressure/area curves which contain high aspect ratio data.

Another way of stating this problem is that local ice pressures over a given area may be higher, if the distance to a free edge is greater (giving a greater degree of confinement).

It is recommended that all data sets being used for local pressure design be examined and reprocessed to recognize this issue. This is nothing new, and Masterson and Spencer (2000) have recently re-introduced the inclusion of aspect ratio in recommendations for global ice pressures.

When deriving local pressure design criteria for the Grand Banks, it may also be appropriate to have criteria which are scenario specific. Three scenarios should be considered, these are:

1) Fixed Platforms
2) Floating Platforms
3) Tankers and Supply Vessels

The scale of the interactions in each of these scenarios is quite different, therefore, a local area of a given size may be subject to a range of confinements which may require different criteria.

The use of a probabilistic approach as discussed in this report, also requires the separation of criteria by scenario because the exposures are different. This is an important issue for the Grand Banks where certain extreme interactions will occur only rarely.

The use of the traditional pressure/area curve to derive ice pressures during impact calculations is questioned, because high ice pressures during the initial stages of the interaction are not as likely as the pressure/area curves predict. A new model is discussed, and further work to refine it is recommended.

Finally, during the course of this study, an important new field experiment was conducted. The icebreaker “The Terry Fox” was instrumented and impacts made against glacial ice. This data will be an important addition to the data base.

TABLE OF CONTENTS

TABLE OF CONTENTS *(continued)*

TABLE OF CONTENTS *(continued)*

TABLE OF CONTENTS *(continued)*

1 Background

Development of oil and gas on the Grand Banks requires facilities that are capable of being operated in an environment in which icebergs, pack ice and severe storms can be present. Designing for icebergs can add to the cost of a fixed platform. For example, in order to resist the global loads from an iceberg impact, the structural shape developed will also attract high wave loads. This is exemplified in the design of the Hibernia platform. Without icebergs, structural shapes much more transparent to waves can be developed at lower cost than a structure required to resist both.

In addition, the local design loads on the walls of a platform are much higher when ice is present, and this can add considerably to the costs (several $100 million - in the case of Hibernia). So, there is a clear incentive to develop authentic local ice pressure design criteria for the Grand Banks (as there is in any ice covered region). Although the primary focus of this study is local ice loads, the issue of a rational transition between local and global loads is also an issue and is touched on in the work.

The Hibernia oilfield is in production using a fixed concrete gravity platform. Global and local design ice loads were based on indentation experiments conducted in tunnels dug into a grounded iceberg (Masterson et al, 1992). These experiments were conducted on ice in a confined state, and at the time were considered relevant to small areas of crushing within larger areas. The Terra Nova field is being developed with a floating production system which will avoid large icebergs. The interactions with smaller bergs will be less confined than the larger icebergs acting on Hibernia. In recognition of this, experiments were performed by towing small icebergs into an instrumented panel mounted on a cliff face at Grappling Island (Crocker et al, 1996). These results were used as input to global and local ice design criteria for the Terra Nova FPSO.

The recognition that local ice pressures are higher than global ice pressures goes back many decades. Early codes for ice breaking vessels recognized the problem and early indentation tests showed this effect, e.g., the Imperial Oil Tests on Eagle Lake (Taylor et al, 1981). For most of these tests, the results were plotted as a function of aspect ratio, but the data can also be plotted as a function of nominal contact area - showing the well known drop in pressure with area (see results plotted in *Section 5*). However, it should be noted that pressure/area curves obtained from one kind of test cannot necessarily be used directly for local ice pressure design. For example, in the Eagle Lake tests, the ice was not confined at the top and bottom surfaces (as it would be on small areas within larger areas). As well, the Eagle Lake tests were performed starting with undisturbed ice at relatively slow strain rates. Despite this recognition and concerns about different test conditions, Sanderson (1988) was one of the first to promote the concept of combining data from all sources into one pressure/area curve. The attraction was that it seemed as though all data could be bounded on a log plot using a simple relationship (e.g., $p = 10A^{-0.5}$).

Another data plot was developed by Masterson & Frederking (1992), in which many tests and data representing local pressures within a larger area were plotted. However, the data still represented a wide range of different conditions such as impact speeds, structure shape, contact geometry and ice type.

Since the work of Masterson and Frederking in 1992 (which was incorporated into both the CSA and API codes), there has been no attempt to consolidate new data into a similar analysis. For example, the most recent data from Grappling Island has not yet been integrated into the existing body of empirical data. On the other hand, there has been some very focussed work on ice crushing processes, as well as the collection of new data and re-analysis of existing data. The intent of this study is to ensure that all new relevant and re-analyzed data is brought together, but within a framework which recognizes new insights into the ice crushing process. For example, work by Jordaan and his research team at Memorial has recognized the high pressure zones which exist over small areas, and which have been observed in indentation tests and ship measurements (Johnston et al, 1998; Riska et al, 1990). These high pressure zones (typically 20 MPa or more), exist over a very small area (0.1 m^2) and they exist for only fractions of seconds in one location. It is also believed that around the edges of a contact zone, ice pressures are significantly affected by spalling (see *Figure 1.1* and the later discussions in *Sections 15 and 16*). Clearly, if this is the appropriate model, then the issue of the nominal contact area versus the area of high contact pressure near the centre needs to be carefully considered in how data is processed and then used in design. It should also be noted that there are data in the literature for which only the average pressure over the whole nominal contact area is known.

Another data analysis concept which will need to be kept in mind is the presentation of ice crushing pressures in a probabilistic format (see Jordaan, 1999, and the discussion in *Section 16*).

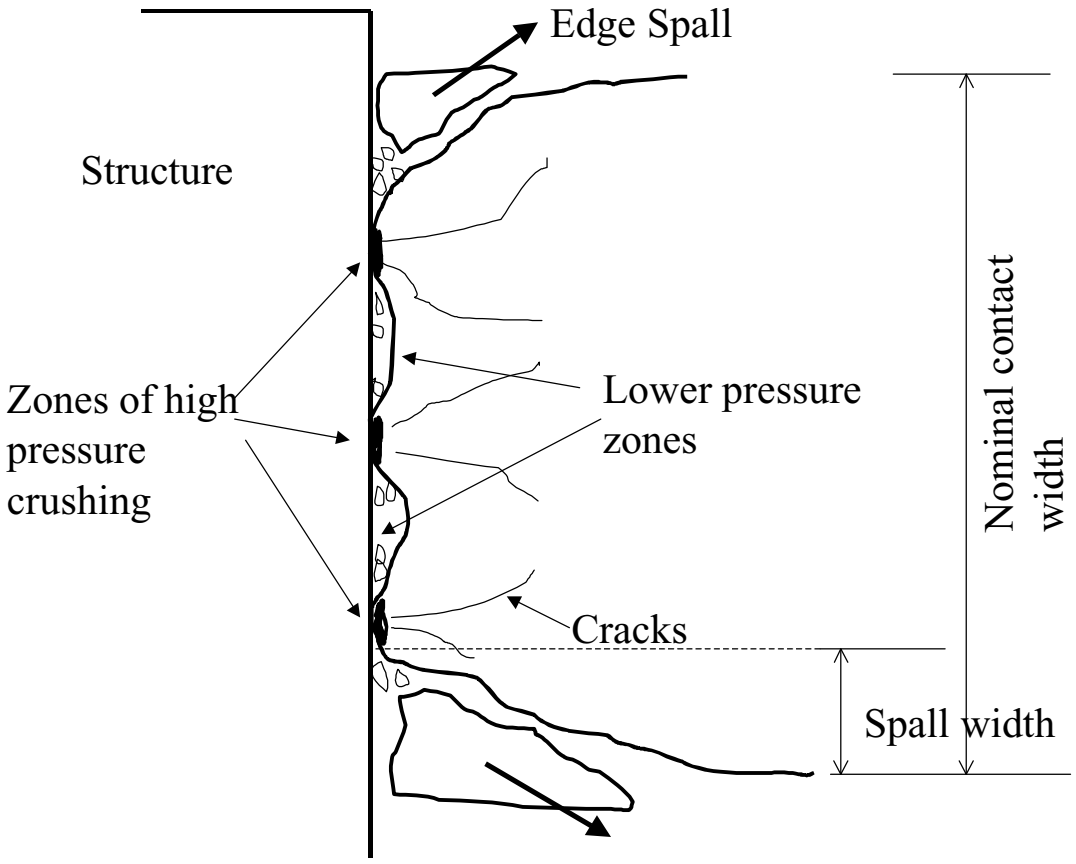

FIGURE 1.1: Conceptual Model for Ice Crushing

2 Study Objectives

The objectives of this study are as follows:

- To identify, assess and compile all the data sources available on local ice loads that could be applied to the design of fixed and floating platforms on the Grand Banks due to iceberg impact.

- To review the methodology for inferring local ice pressures as a function of area and other relevant parameters for each set of key data.

- To rank data sets as to their value and relevance to local ice pressure design for the Grand Banks.

- To comment on the state of knowledge, deficiencies and make recommendations for future work, especially in relation to Code revisions.

3 Work Scope

The study was conducted in three tasks:

Task 1 - Review of Data Sources for Local Ice Loads

Based on their own knowledge and experience, the team compiled a list of relevant data sets, old and new. A short description of the data sets, known strengths, and weaknesses was provided, recognizing that ideally the data sets should be amenable to time series analysis of pressure versus area, but also have information on ice type, contact shape including aspect ratio, structure characteristics, ice type, etc. Based on the preliminary review, key data sets were selected for further review and analysis. A standard approach was developed to catalogue and describe the data including the attributes described in the RFP (see *Appendix A*). The work was divided among the team according to familiarity with the data sets.

Task 2 - Ranking of Data in Terms of Quality and Usefulness for the Grand Banks

Inherent in the activities in Task 1 was a qualification of each data set and event analysis in terms of quality and relevance of the data to iceberg impacts. Quality assessment included a review of the instrument and Data Acquisition (DA) resolutions etc., as well as how the ancillary data was documented and its likely accuracy. Also, the issues of aspect ratio, confinement and ice type were discussed in terms of how these may affect direct application of the data to the Grand Banks. Recognizing the potential to ultimately treat local pressures within a probabilistic framework, the number of potential data points within a data source was commented on. An example of the treatment of one data set in a probabilistic manner has been developed.

Task 3 - Reporting

The report includes a full listing, with attributes, of sources of data for local ice pressures, as well as sample time series with accompanying analyses of the pressure/area data contained in some of the key data sets. Comments are provided on the suitability of the data for use in determining local load criteria for Grand Banks facilities.

4 Data Sources

Data on local ice loads and pressures can be categorized and summarized as follows:

- Indentation experiments on full-thickness ice sheets.
- Indentation tests into the sides of icebergs and multi-year ice.
- Flaking Tests on first year and lake ice.
- Iceberg impact experiments.
- Measurements of local loads on instrumented structures.
- Measurements of local loads on ice breaking vessels.

4.1 Indentation Experiments on Ice Sheets

In a typical indentation test, an indentor is pushed into the edge of an ice sheet, simulating the movement of ice into a structure of similar shape and size as the indentor. These kinds of tests were initiated on full thickness ice sheets in the late 1960's (Croasdale, 1970). They continued for several years and included indentation tests with indentors up to 3.65 m wide (Taylor, 1973 and Taylor et al, 1981). The main rationale for the tests was to investigate the effects of aspect ratio, contact area and strain rate on ice pressures.

The advantage of indentation data is that it is usually well-controlled in terms of strain rate, nominal contact area and the load being measured accurately. The degree of confinement is also well known. The disadvantages of much of the early data are that tests were usually performed on undamaged ice and strain rates were often too low to establish brittle failure. The work of Kry (1978, 1980) focussed on continuous crushing and is more typical of most ice structure interaction.

Typical results and attributes of indentation tests on full-thickness ice sheets are reviewed in more detail in *Section 5*.

4.2 Indentation Tests into the Sides of Icebergs and in Multi-Year Ice: Flaking Tests

In 1984, Masterson et al (1992), conducted an ambitious series of indentation tests into the sides of tunnels dug into a grounded iceberg in Pond Inlet. The work was conducted to develop ice pressure design criteria for the Hibernia platform design. The indentors in this case were spherical and ranged up to 3 m^2 in contact area. The indentors penetrated initially undamaged ice and the state of the ice was confined. A range of data was obtained and plotted as ice pressure versus contact area. These tests were the first to provide indentation crushing pressures for iceberg ice.

The same apparatus was later used in the Arctic. (Frederking et al, 1989) for tests on multi-year ice.

Results from the Pond Inlet tests are reviewed in more detail in *Section 6*. The multi-year ice tests are reviewed in *Section 7*.

A series of specialized flaking tests were conducted to assess free edge and indentor stiffness effects. These are reported in *Section 8*.

4.3 Iceberg Impact Experiments

The concept of towing icebergs into an instrumented structure attached to a cliff face was first proposed in about 1983 as a way of developing the ice design criteria for Hibernia. Some initial scoping of this approach indicated that it was feasible, but expensive and relatively high risk. Therefore, it was decided in 1984, to implement the somewhat easier method of conducting indentation tests into iceberg ice, as described in *Section 4.2*.

However, the idea of conducting such tests lived on. Especially as it became obvious that the Pond Inlet test results were likely too conservative to apply to the less confined situation of the impact of smaller bergs with floating production units. The merits of conducting such tests were promoted by C-CORE and K. R. Croasdale. In 1993, a small effort was funded to investigate sites and develop design concepts for the load panel and towing arrangements. The Grappling Island iceberg impact experiments were conducted in 1995 and are now public. A detailed description of the tests and samples of the results, are given in *Section 9*.

4.4 Measurements of Local Loads on Instrumented Structures

Most work on the measurements of ice loads (hence ice pressures) on actual structures subject to ice action has been in the context of verifying and/or studying global loads. These kinds of measurements date back to the 1960's when there was a focussed effort to measure bridge pier ice loads (Neill, 1970; Lipsett and Gerard; 1980, Schwarz, 1970). As well, at about the same time, the oil industry was installing oil production platforms in Cook Inlet, Alaska. Ice load measurements on one platform have been reported by Blenkarn (1970). The measurement of ice loads on Beaufort Sea islands and caissons received much attention through the 1970's and 1980's. Again, much of this work was aimed at global loads and its use for local loads is limited. A review of structures instrumented for ice loads was performed by Croasdale and Frederking (1987). *Table 1* is based on this review, and has been updated to the present.

It should be pointed out that the measurement of both global and local ice loads on structures is not straightforward. The simplest approach is to use strain gauges to measure structure response. However, most structures have redundant load paths, therefore, back-calculating a load from strain data is subject to uncertainty, especially if the exact point of application of the load is not well known. As well, structures can vibrate under load and may have a dynamic deformation greater than the equivalent quasi-static load applied. As a result, strain gauge data may over-estimate the applied load due to the dynamic magnification which may be occurring. The same concerns apply to other techniques which measure structure response such as inclinometers and tiltmeters. Foundation instruments can also be in error due to inertia effects of the structure. In this case, these instruments may under-estimate the ice load because the structure response time may be longer than the ice load "spike" time.

An alternative to monitoring the structure response is to install ice load cells and panels at the interface between the structure and the ice. The technology for ice load panels was actually developed in the context of measuring in-situ stresses in an ice sheet. For this application, they had to be thin and penetrate the full ice thickness. But because they were likely to be installed in land-fast ice which exhibits rather slow stress changes, their response time was not too important. Consequently, some panels later used on structures had response times that were too slow to pick up short term load peaks. Even so, properly installed load panels at the ice interface have provided good quality data on ice loads. The Molikpaq caisson structure, for example, was equipped with ice load panels across certain lengths of the ice line.

The volume and quality of ice load data that was collected on the Molikpaq during its Beaufort Sea operations is well known. During the 1990's attention was given to compiling a number of high quality events which can be used for detailed analysis. For the purposes of this study, specific multi-year ice interaction events of relevance have been identified and examples of the local ice load information obtained during these events provided. A detailed review of the Molikpaq data is provided in *Section 10*.

TABLE 1: Catalogue of Structures Instrumented for Ice Loads

Site	Initiation Date	Company or Agency	Method, Size and Instruments	Reference
Hondo Bridge, Alberta	1967	Alberta Research Council & Alberta Highways	Nose section hinged at bottom, load cell at top. 2.3 m diameter 23 degrees from vertical. Ice thickness to 1 m.	Sanden and Neill (1968). Lipsett and Gerard (1980).
Pembridge	1969	Ditto	Hinged pile with load cell. 0.86 m diameter. Ice thickness 0.5 m.	Montgomery and Others (1980). Lipsett and Gerard (1980).
Eider River Estuary	1967	University of Hannover	Array of 50 load cells covering 0.6 m width and 1.5 m high. Ice to 0.4 m.	Schwarz (1970).
Yukon River Alaska	1977	CRREL and U of Alaska	1.8 m x 1.8 m plates on load cells. Accelerometers.	McFadden et al (1981).
Ottauquechee River, Vermont	1982	CRREL	Four 0.56 m x 1.22 m panels covering 2.5 m vertical height of V shaped pier.	Sodhi et al (1983).
St. Regis River, New York	1990	CRREL	Simply supported beam with load cell. Ice to 0.2 m.	Haynes et al (1991).
Yamichiche Lightpier, Quebec	1975 and 1985	Transport Canada and NRC	Load panels supported on load cells. Also strain gauged load panel. Ice to 0.5 m.	Danys (1975). Frederking and Sayed (1989) and (1990).
Kemi 1 Lightpier, Finland	1975	University of Oulu	Deformation of structure. 20 cm pressure plates and accelerometers.	Maattanen (1978).
Norstromsgrund Lightpier, Sweden	1972, 1988 and 1999	VBB Consulting	Four accelerometers initially but inclinometers and panels installed later. Subject of LOLEIF research.	Engelbrekston (1978) LOLEIF.
JZ 20 Platform Leg - Bohai Bay, China	1989/90	HSVA	Load panels on 2.3 m diameter leg . Ice to 0.55 m.	Wessels and Jochman (1990).
Cook Inlet – Pile	1963	University of Alaska and Amoco	Beam 0.91 m diameter. Ice to 0.3 m.	Peyton (1966). Blenkarn (1970).
Cook Inlet Platform	1964	Amoco	Strain gauges on structural members of four leg platform.	Blenkarn (1970).
Saroma Lagoon	1976	Mitsui	2.5 m cantilevered cylinder. Strain gauged.	Oshima et al (1980).
Adgo P-25 Artificial Island – 2 m Water – Mackenzie Delta	1974	Imperial Oil	University of Alaska small cylindrical in-situ sensor and Esso thin wide sensors in surrounding ice.	APOA 104. Metge (1976). Nelson and Sackinger (1976).
Netserk South B-44 Island – 4.5 m Water -Beaufort Sea	1975	Imperial Oil	Twenty in-situ ice panels.	APOA 104. Metge (1976).
Netserk North F-40 - 7 m of Water - Beaufort Sea	1976	Imperial Oil	Thirteen in-situ ice panels.	Apoa 105. Strilchuk (1977).

Site	Initiation Date	Company or Agency	Method, Size and Instruments	Reference
Kannerk G-42 and Arnak L-30 Islands in 8 and 8.5 m Water - Beaufort Sea	1977	Imperial Oil	In-situ ice panels.	APOA 122. Semeniuk (1977).
Tarsiut –44 (Caisson Retained Island) in 22 m Water - Beaufort Sea	1981-83	Gulf, Dome, BP	Flat jack panels on caisson. Shear bar plates. Strain gauges. In-situ panels in surrounding ice. Soils instruments.	APOA 197. Weaver and Berzins (1983). Pilkington et al (1983).
SSDC at Uviluk - 31 m Water - Beaufort Sea	1982-83	Dome/Canmar	Medof panels on structure and in surrounding ice. Soils instruments.	Blanchet (1990).
SSDC at Kogyuk - 28 m Water - Beaufort Sea	1983-84	Dome/Canmar	Medof panels on structure. Soils instruments.	Blanchet (1990).
Esso Caisson Retained Island at Kadluk - 14.5 m Water – Beaufort Sea	1983-84	Imperial	Strain gauges and panels on caisson. In-situ ice panels in surrounding ice. Soils instruments.	Johnson et al (1985). Hawkins et al (1983).
Esso CRI at Amerk 0-99 – 26 m Water - Beaufort Sea	1984-85	Imperial	Strain gauges and panels on caisson. In-situ ice panels in surrounding ice. Soils instruments.	Croasdale (1985). Sayed et al (1986).
CIDS Off Alaska	1984	Exxon: Global Marine	In-situ ice pressure panels. Strain gauges. Soils instruments.	Wetmore (1984).
Molikpaq - Water Depth Range 11 m to 32 m	1984 Onwards	Gulf Canada	Medof panels. Strain gauges. Extensometers on structure. Soils instruments.	Wright et al (1998).
SSDC at Phoenix, Aurora, Fireweed and Cabot – 16 to 21 m Water – US Beaufort Sea	1986-92	Canmar	Medof panels on structure and in ice. Soils instruments.	Blanchet et al (1987) (1988).
Molikpaq on Piltun Astokhskoye Field Off Sakhalin Island Russia in 31 m Water	1998 On	Sakhalin Energy Investment Co.	Flat jack panels on structure (18). Over 80 strain gauges. Soils instruments.	Weiss et al (2001).
Piers of the Confederation Bridge – Canada - Water Depth to 30 m	1997 On	Public Works Canada Strait Crossing Industry JIP	Inclinometers. Load panels.	Brown (2001).

4.5 Measurements of Local Loads on Ice Breaking Vessels

Over the last 20 years, local ice pressures have been measured on the bow of a variety of icebreakers during ice breaking operations in various ice conditions. Examples of such data sets include, but are not limited to, data from the various Polar Sea/Star Voyages, Robert Lemeur, Kigoriak, PolarStern, Oden 1991 and 1996 North Pole Voyage, and the 1994 Louis S. St-Laurent North Pole voyage. During these voyages, the various vessels encountered large amounts of thick multi-year ice in the form of floes and ridges.

The impact of a vessel against a thick multi-year ice feature is very similar to a vessel impacting a bergy bit or growler and is therefore a very important source of information for the prediction of pressure/area curves for east coast applications. The key differences and issues are: difference in the failure behaviour of the glacial ice versus multi-year ice, possible differences between the dynamics or motions of a floe/ridge versus a free floating piece of glacial ice and associated limited momentum, and possible differences in shape of the contact zone. Incorporation of ship data into this study needs to recognize these potential difficulties. Ship data is derived almost entirely from the interpreted measurements of strain gauges on the ships hull. As such, these measurements are subject to the potential inaccuracies, already discussed in the context of strain gauged structures.

Statistically, the ship data provides thousands of ship-ice interaction events. For each of these events, time history data was collected. Depending on when the data was collected the time history data is stored in various forms. The data can be broken up into three basic groups:

1990 - Present

- During the 1990's, data onboard such trials such as the 1991 and 1996 Oden Voyage and the 1994 Louis S. St-Laurent voyage were collected on HP based systems. This data was later transferred from the HP format to an ASCII format readable by modern PC computers.

1982 - 1990

- In the early 1980's, Hewlett Packard Series 9000 systems were used to collect the data for tests using the Robert Lemeur and Kigoriak in 1981; and also for the Polar Sea/Star trials. Much of this data is still stored in the original HP formats. Some of this data exists in various databases which members of the project have used.

Pre 1981

- The time history data for the earliest impact tests (e.g., Dome Petroleum, 1981) are in the form of paper traces and/or stored on old data storage media. This digital data is very difficult to access.

During this study, the Louis S. St-Laurent data has been reviewed in detail in *Section 11*. Reviews of the 1991 and 1996 Oden data are given in *Sections 12 and 13* respectively. The 1981 Kigoriak data is reviewed in *Section 14*.

Note that during the course of this study, a new series of ship impact tests has been conducted using the Terry Fox in collision with small icebergs. This data is not yet available, but will be an important addition to the relevant data on local ice loads for the Grand Banks.

4.6 Recognition of Randomness in the Data

The events of interest here involve interactions between ice and structures at speeds in which considerable brittleness of the ice is found. Repetitions of such ice-structure interaction events that are similar in observable aspects generally can result in very different pressures from one interaction to another or during different time periods. This results from the extreme randomness of the interaction process. For effective probabilistic analysis, it is most important that a clearly defined maximum pressure over a known area, for an interaction with a known duration be obtainable. Repetitions of such events are amenable to statistical analysis. Longer events will result in higher maxima (on average), so that the duration is important to obtain an estimate of the exposure of the structural element. It is the extreme values that are of interest in engineering. For this reason a plot of the ranked data is useful, and it has been found that an exponential distribution fits the tail of the data very well; this procedure has been applied to the Kigoriak data and to some of the Polar Sea data. Once the distribution of the tail has been found, a methodology can be applied to find a probabilistic estimate of the peak pressure for any given exposure. This general methodology is based on a Poisson process, and is valid for a wide range of practical cases. In particular, it can be adapted to the present situation of interest. The results using the methodology have been found to be consistent with the ASPPR revisions, and have been verified using an analysis of high-pressure zones based on data from the Louis S. St-Laurent. This resulted in confirmation of the key pressure/area relationship. Aspects of describing local ice pressures in a probabilistic format are reviewed in more detail in *Section 16*.

5 Indentation Tests (Full Thickness Sheet Ice)

5.1 Imperial Oil Indentation Tests: 1970-1975

5.1.1 Summary

Data Source:	Imperial Oil Indentation Experiments
Geographic Location:	Arctic (Tuktoyatuk) and Eagle Lake (Alberta)
Time Period:	1970 - 1975
Ice Types:	Low-salinity Arctic ice; natural and seeded lake ice
Range of Contact Areas:	0.3 to 3 m^2
Relevance to Icebergs:	Of medium relevance. The data can be used to set bounds and help provide an understanding of aspect ratio and non-simultaneous processes.

5.1.2 Background

This series of tests was conceived late 1960's when Imperial Oil and others were preparing to design offshore structures for drilling and development in the Southern Beaufort. At that time, the main source of design criteria and experience for structures in ice came from bridge pier experience and practice. In moving into Arctic regions there was concern that the colder ice would lead to higher crushing strengths and ice pressures. Therefore, the first series of tests was performed in the Arctic (in Tuktoyaktuk Harbour) (Croasdale, 1970). The tests were repeated the following winter. Indentors ranged in size from 0.76 m diameter to 1.52 m. Ice thickness was up to about 1.5 m. This was the first time that indentation experiments had been conducted in the field to study ice crushing pressures.

It was known, that in addition to ice temperature, the geometry of the contact zones, contact areas and strain rates were also likely to have an influence on the measured ice pressures. However, tests in the Arctic were logistically difficult and wide ranges of these parameters were not easily studied. Therefore, a new series of tests was commenced on Eagle Lake near Calgary (Croasdale, 1971). In this new series of tests, the indentors were placed in openings cut into the ice sheet. In the tests conducted in the years 1973 and 1974, a large apparatus was used with two loading rams that could exert up to 1,000 tonnes force each. Loading faces up to 12 ft. (3.66 m wide) were tested. The apparatus was supported through an opening in the ice from a gantry with legs that sat on the lake floor (see Taylor et al, 1981). In many tests, "test ponds" were created within the ambient ice sheet into which the indentors could be pushed. The advantage of the test ponds was that a range of ice thicknesses could be tested. Also, the ice could be "seeded" to ensure a horizontal c-axis ice (as is typical in Arctic regions).

The main aim of the 1973 and 1974 tests was to examine "aspect ratio" effects (width/thickness) in order to help in the design of wide structures such as caissons and islands. (Taylor, 1973; Taylor et al, 1981). Most structures being considered by Imperial Oil at that time were in landfast ice. Therefore, the primary interest was in the condition where the ice had grown in place around the structure prior to a sudden motion. So most of the indentation tests were aimed at getting the initial peak ice pressure with good contact between the structure and the ice. The ice pressures reported, however, represent an average pressure over the whole contact area.

By 1975, it was apparent from observations at drilling islands in the Beaufort Sea that across a wide structure, the ice failed in a non-simultaneous manner. Imperial Oil developed a stochastic failure model to model this process (Kry et al,1978). The model needed a time trace of crushing pressure with distance (or time) that could be used to represent one zone of a multizonal model. So the final series of tests on Eagle Lake, were conducted with a single ram and a 1.2 m indentor. The ram was extended full stroke to get several crushing peaks. Then the test was continued with a spacer behind the ram to extend further the number of pressure peaks. This mode of ice failure was termed "continuous crushing".

It is of interest to note that using Kry's model and the data from the continuous crushing tests at Eagle Lake, the ice pressure criteria across a typical 100 m wide structure subject to 1.8 m ice was developed in 1975 to be 250 psi (1.7 MPa). This value compared well to the subsequent measurements on wide caissons such as the Molikpaq subject to non-simultaneous crushing.

5.1.3 Data Attributes

The main parameters of the tests and the data attributes for each of the test programs are contained in the referenced reports. Most of these are available from either the Arctic Institute in Calgary or the National Research Council in Ottawa. In general, the range of indentor widths was from 0.75 to 3.66 m; and ice thickness from about 0.3 to 1.5 m. Strain rates ranged from the ductile to the brittle regime. Contact conditions ranged from "frozen-in" to "continuous crushing".

5.1.4 Data Quality

All time series data was recorded in analogue format on paper rolls. The applied load was usually derived from pressure transducers at the inlets and outlets of the hydraulic rams. Indentation distance was recorded using linear potentiometers. Ice thickness was measured by drilling prior to or after the test. The load levels, the contact areas and hence the maximum ice crushing pressures are considered to be accurate within plus or minus 10%.

5.1.5 Examples of Time Series Data

An example of ice stress and indentor deflection versus time from an early "nutcracker test" in Tuk Harbour is given as *Figure 5.1*. As can be seen, all high frequency variations (if any) have been dampened out by the data acquisition system. The same data plotted as failure stress versus deflection is given as *Figure 5.2*. Note that this test is relevant to a "frozen in" condition, which likely led to the relatively high ice failure pressure of about 5 MPa.

In contrast the data plots shown in *Figure 5.3* are from the last series of tests on Eagle Lake by Kry. In this case, the dynamic fluctuations associated with continuous crushing have been captured.

5.1.6 Examples of Processed Data

Some of the data obtained at Eagle Lake in 1973 is shown in *Table 2*. This includes all tests except those with the indentors frozen to the ice.

The plot of ice pressure versus aspect ratio (*Figure 5.4*) gives an upper envelope curve which follows the classic trend of lower ice pressure with aspect ratio. On the other hand, the same data plotted as ice pressure versus area also gives a strong pressure/area trend (see *Figure 5.5*). The pressure/area data is plotted on log scales in *Figure 5.6*. An upper bound line can be expressed as:

$$p = 5A^{-0.5}$$

where: p is in MPa and A is in square metres.

Note that in many of the tests, the ice failure process was ductile. This was due to the relatively slow velocities and the relatively warm ice. The ice pressure versus indentor speed is plotted in *Figure 5.7*.

TABLE 2: Eagle Lake Data 1973

Indentor Width (D) (m)	Ice Thickness (t) (m)	Contact Area (m^2)	Indentor Speed (cm/s)	D/t	Peak Crushing Pressure (MPa)
1.22	0.60	0.74	0.54	2.02	2.96
1.22	0.61	0.74	0.50	2.00	2.61
1.22	0.56	0.68	0.53	2.18	6.07
1.52	0.56	0.85	0.53	2.73	4.86
1.22	0.64	0.77	0.52	1.92	2.32
1.52	0.64	0.97	0.52	2.40	1.85
1.22	0.65	0.79	0.36	1.88	2.41
1.22	0.67	0.82	0.69	1.81	5.10
1.22	0.67	0.82	0.07	1.81	5.65
1.22	0.66	0.81	0.01	1.85	1.83
0.61	0.67	0.41	0.15	0.91	8.24
0.61	0.69	0.42	0.14	0.89	5.24
0.61	0.67	0.41	0.12	0.91	3.41
0.30	0.66	0.20	0.14	0.46	5.24
0.30	0.75	0.23	0.17	0.41	2.90
2.44	0.75	1.83	0.23	3.25	1.69
2.44	0.76	1.86	0.18	3.20	1.48
2.44	0.75	1.83	0.18	3.25	1.55
2.44	0.76	1.86	0.18	3.20	1.42
2.44	0.51	1.24	0.18	4.80	1.81
2.44	0.41	0.99	0.22	6.00	3.64
3.66	0.76	2.79	0.20	4.80	1.80
3.66	0.77	2.83	0.16	4.72	1.35
3.66	0.43	1.58	0.09	8.47	4.09

Indentor Width (D) (m)	Ice Thickness (t) (m)	Contact Area (m^2)	Indentor Speed (cm/s)	D/t	Peak Crushing Pressure (MPa)
3.66	0.42	1.53	0.13	8.73	3.83
4.27	0.74	3.14	0.13	5.79	1.94
3.66	0.45	1.65	0.14	8.11	1.88
3.66	0.53	1.95	0.13	6.86	2.17
0.30	0.46	0.14	0.17	0.67	7.93
0.30	0.46	0.14	0.21	0.67	8.27
0.30	0.47	0.14	0.00	0.65	0.76
0.30	0.46	0.14	0.21	0.67	7.58
0.30	0.81	0.25	0.20	0.38	3.55
0.61	0.79	0.48	0.27	0.77	3.52
0.61	0.53	0.33	0.19	1.14	5.69
1.22	0.47	0.57	0.19	2.59	6.21
1.22	0.48	0.59	0.21	2.53	5.86
1.52	0.74	1.12	0.21	2.07	3.07
1.22	0.48	0.59	0.16	2.53	5.93
1.52	0.72	1.10	0.16	2.11	3.17
0.61	0.75	0.46	0.25	0.81	5.24
0.61	0.50	0.30	0.23	1.23	8.96

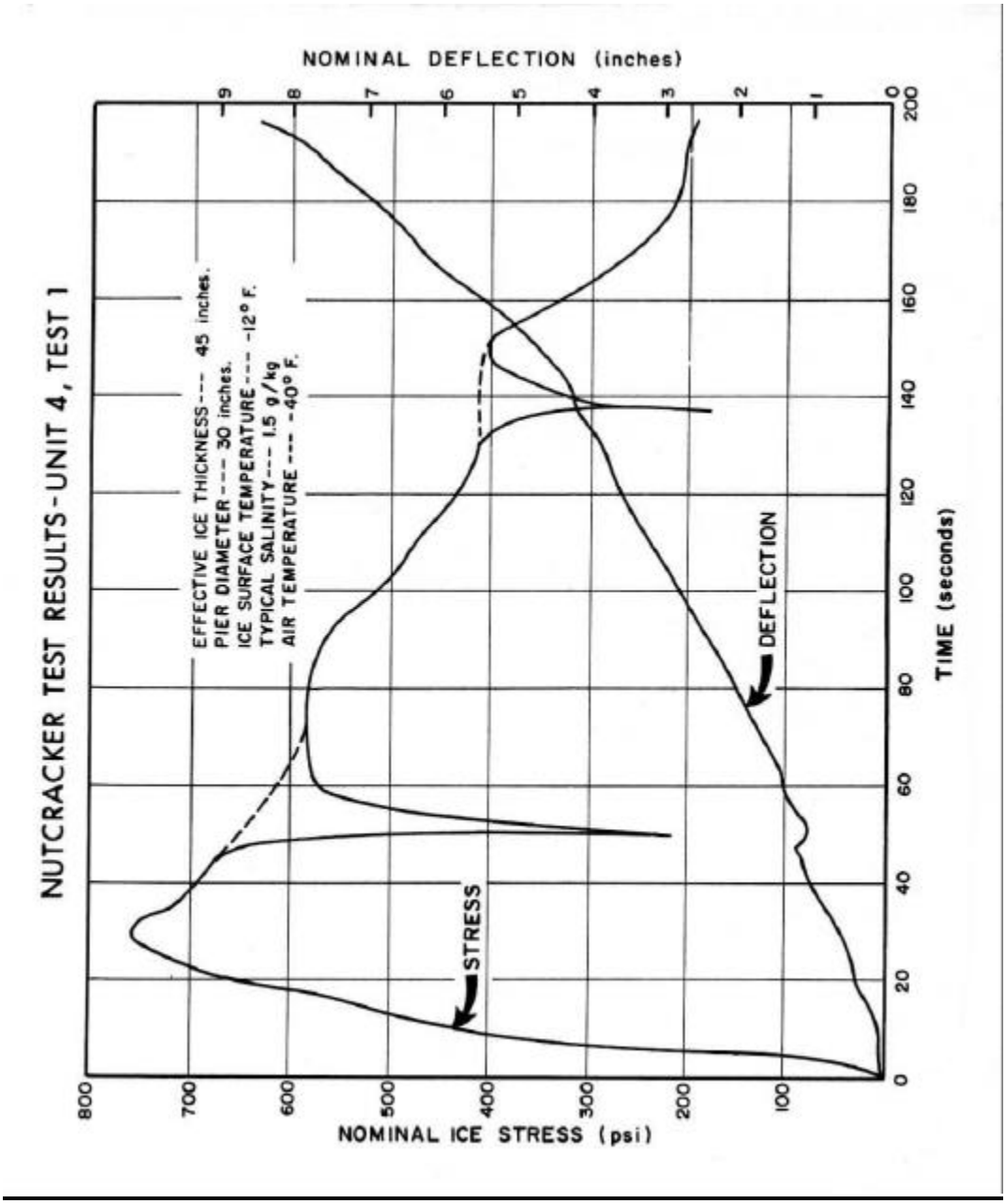

FIGURE 5.1: Time Series Plots from an Early Indentation Test (Croasdale, 1970)

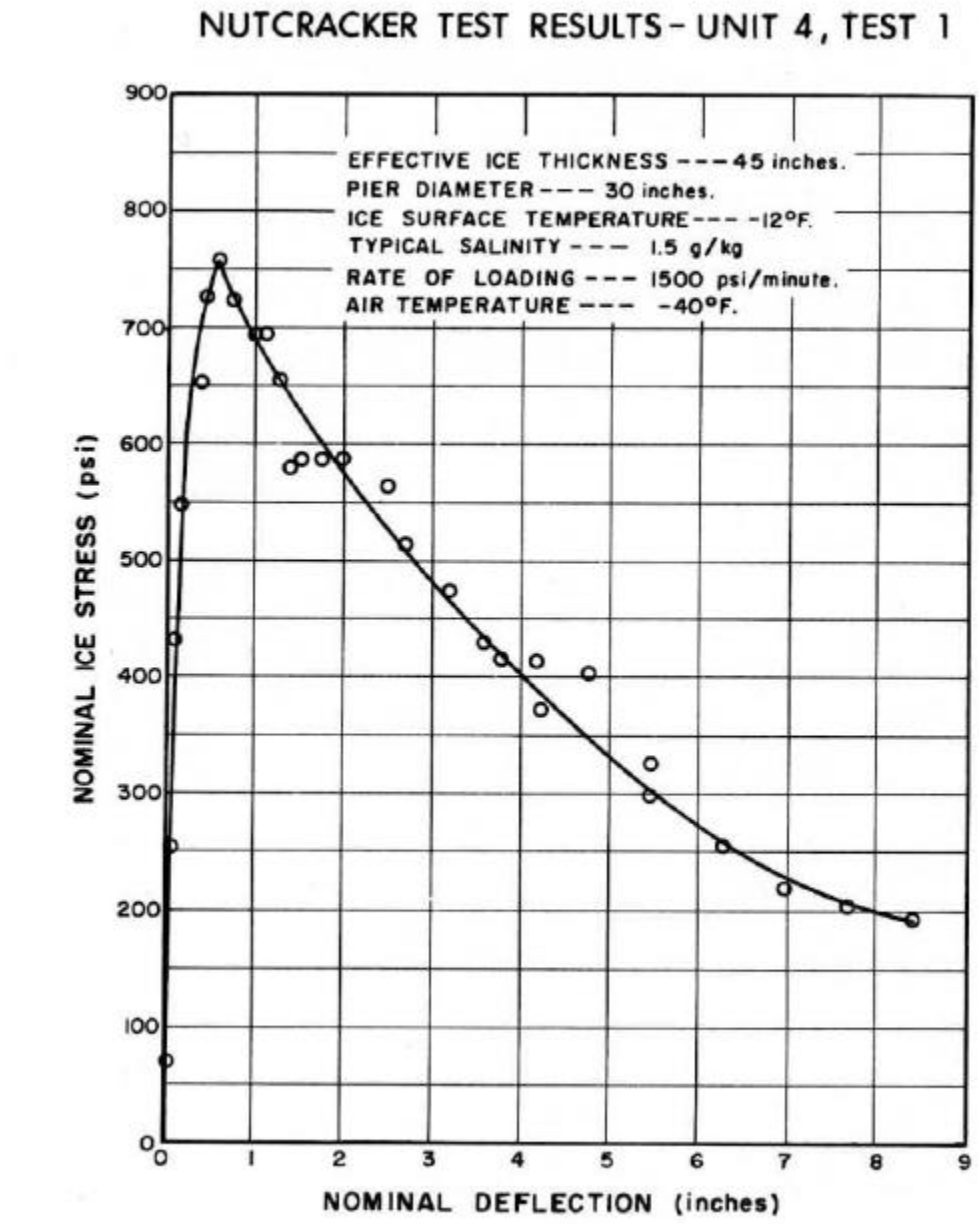

FIGURE 5.2: Early Indentation Data Plotted as Failure Stress Versus Deflection (Croasdale, 1970)

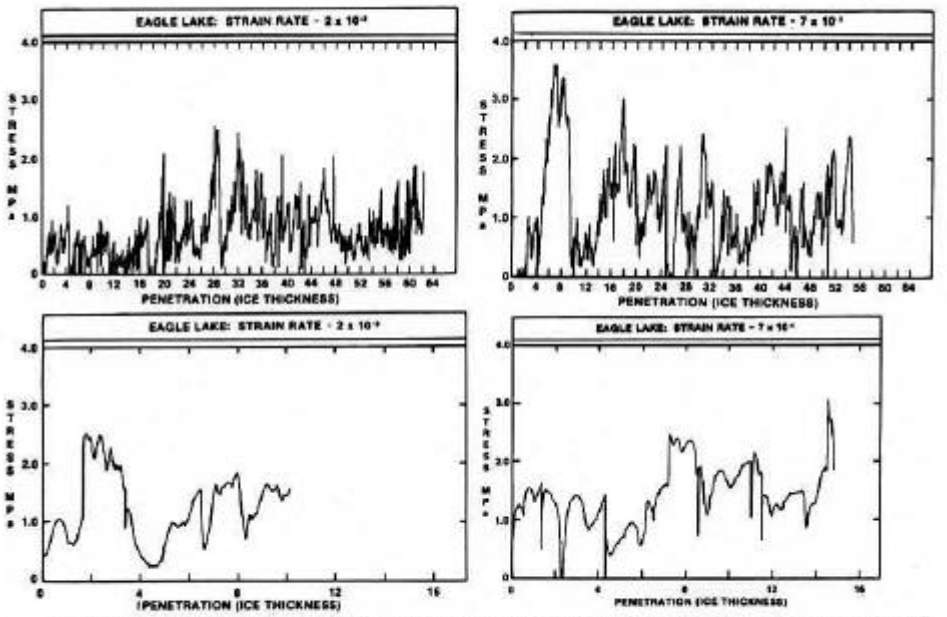

FIGURE 4 Continuous crushing stresses measured at large scale. Results grouped according to penetration rate divided by ice sheet thickness ($7x10^{-4}s^{-1}$, $2x10^{-3}s^{-1}$, $7x10^{-3}s^{-1}$ and $2x10^{-2}s^{-1}$). Total penetration distance normalized by ice sheet thickness penetrated.

FIGURE 5.3: Series Data from "Continuous Crushing" Tests – Eagle Lake, 1975 (Kry, 1981)

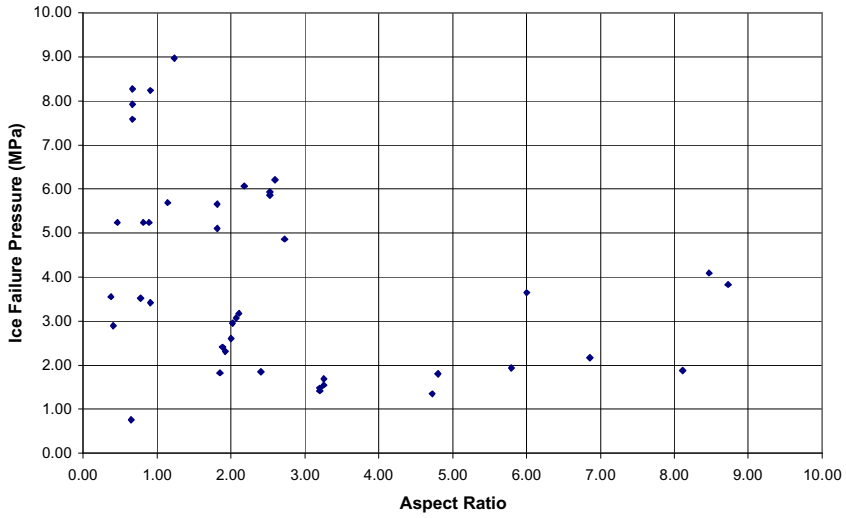

FIGURE 5.4: Eagle Lake Indentation Data Plotted Against Aspect Ratio

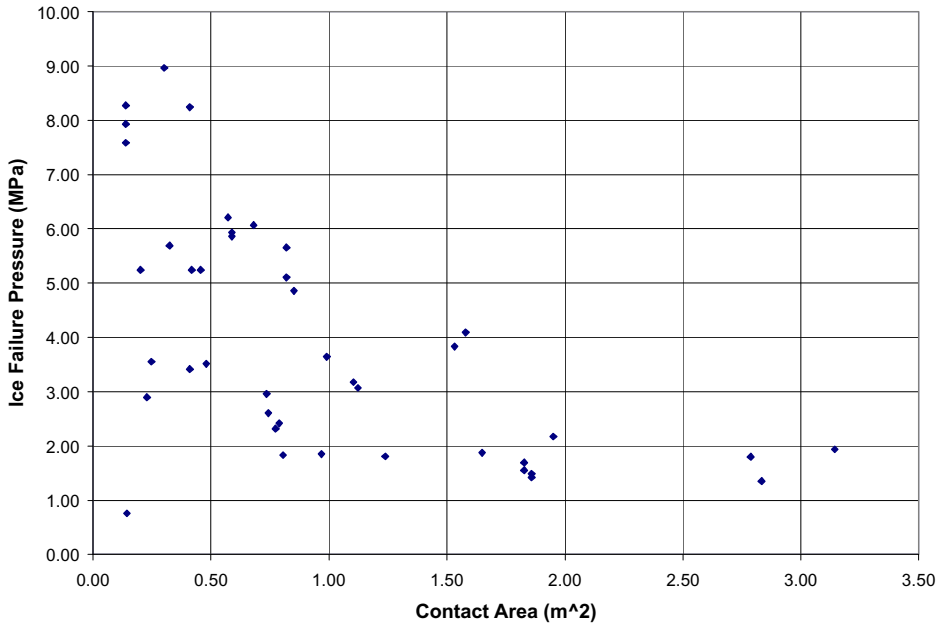

FIGURE 5.5: Eagle Lake Indentation Data Plotted Against Contact Area

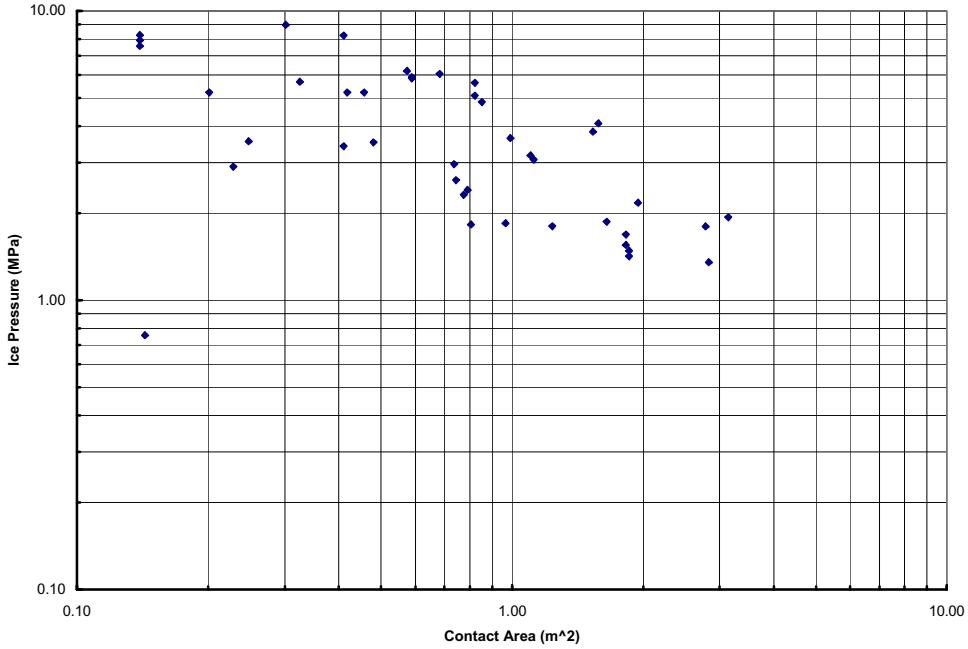

FIGURE 5.6: Eagle Lake Indentation Data Plotted Against Contact Area (Log Scales)

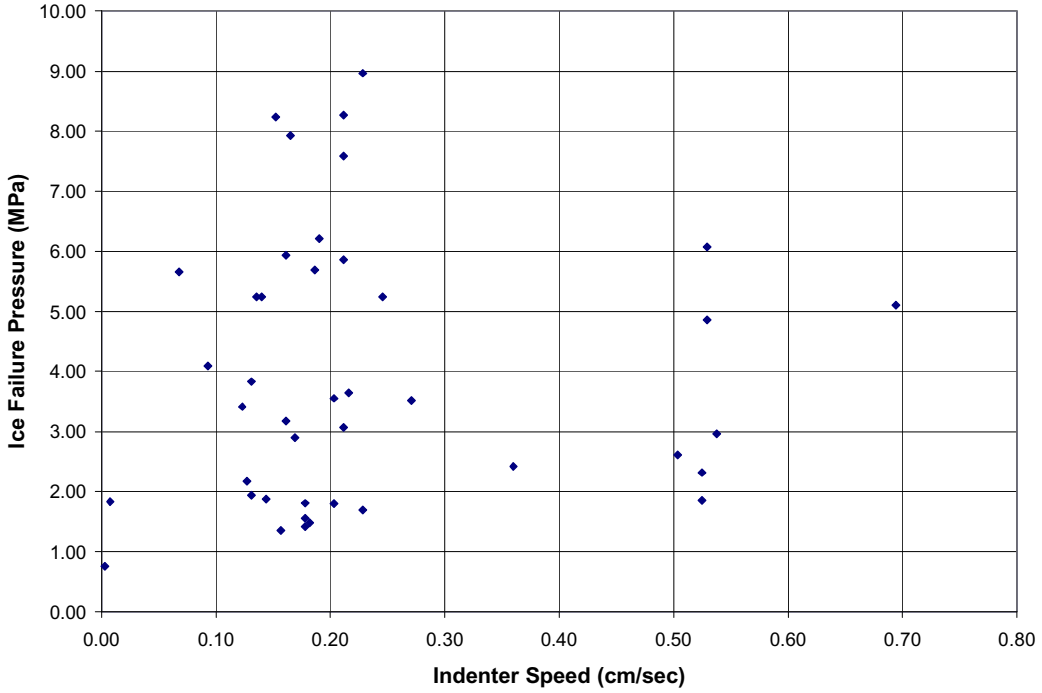

FIGURE 5.7: Eagle Lake Indentation Data Plotted Against Indentor Speed

5.2 JOIA Medium Scale Indentation Tests

5.2.1 Summary

Data Source:	JOIA Medium Scale Field Indentation Test
Geographic Location:	Notoro Lagoon in Hokkaido, Japan (44o05'N, 144o10'E)
Time Period:	Winter 1996, 1997, 1998, 2000 and ongoing
Ice Types:	First Year Sea Ice
Range of Contact Areas:	0.02 to 2.17 m^2
Relevance to Icebergs:	Medium

5.2.2 Background

A series of medium scale field indentation tests (MSFIT) was performed at Lake Notoro in Hokkaido, Japan, as part of the Japan Ocean Industries Association (JOIA) project to determine the scaling effect of ice load. These tests were conducted over four consecutive winter seasons since 1996. The tests consisted of ice indentation tests and measurements of ice sheet deformation and physical properties.

The MSFIT includes experiments using vertically faced model structure up to 6 m wide. The main factors affecting ice loads were investigated through systematically varying structure width, ice thickness, indentation speed. A schematic drawing of the test set-up is shown in *Figure 5.8*. The indentor width ranged from 1.5 to 6.0 m. The maximum jacking capacity against the ice sheet was 200 tons for 4.5 to 6.0 m wide indentors and 1.5 tons for 1.5 and 3.0 m wide indentors. The indentation speed ranged from 0.03 to 3cm/s (e.g., strain rate between 10^{-4}/sec and 10^{-2}/sec). The maximum stroke of the model structure was 120 cm.

A schematic diagram of the model structure and instrumentation is shown in *Figure 5.9*. A 100 ton-capacity load cell was installed behind the hydraulic servo-jack to measure the total ice force. A 10 ton-capacity load cell was installed behind each 10 cm wide segmented indentor panel in the model structure to measure the local ice force. In winter 1998, four pressure sensing panels (0.3 mm thick, 238 mm wide, and 238 mm high) were installed on the face of the indentor to measure pressures at 44 x 44 grid points over an area of 100 mm^2 to determine the ice failure pattern in additional to local ice pressures. Each grid point encompassed a 5.4 by 5.4 mm area. In winter 1999, the smaller pressure sensing panels were replaced by a single panel 480 mm wide by 44 mm high, which measured pressures at 2112 grid points over an area of 100 mm^2. The pressure capacity at each sensing point is 7 MPa.

More than 30 indentation tests were conducted during the four year test period. The displacement rates of a servo-controlled jack, acceleration, inclination of model structure, and ice strength were measured in all tests. The test conditions and results of the 1996, 1997, 1998, and 1999 winters are summarized in *Table 3*. These results were reported in Takeuchi et al (1997 and 2000), Saeki et al (1998), Sodhi et al (1998) and Nakazawa et al (1999).

The physical and mechanical characteristics of first-year sea ice at Notoro Lagoon measured in the four winter seasons from 1996 through 2000 were summarized by Kamio et al (2000). Compressive, bending, shear and splitting tensile strengths were measured and correlated. All tests were conducted at a nominal temperature of -3 deg. C, and a nominal strain rate of 10^{-3}/sec. The compressive strength ranged from 0.5 to 3.0 MPa and the ratio of shear strength, bending strength and tensile strengths to the compressive strength were 0.31, 0.27, and 0.17, respectively. The distribution of compressive strength followed a lognormal distribution or a Weibull distribution. Ice density ranged from 0.79 to 0.91 g/cm^3. The salinity ranged from 2.0 to 7.7 ppt.

The MSFIT research group is conducting detailed analysis and interpretation of data. The availability of the original data for the present study is not anticipated.

5.2.3 Comments on Relevance to Local Ice Loads Due to Icebergs

The introduction of pressure sensing panels permits the visualization of the pressure distribution of the ice at the interface and its change with time at intervals as short as 10 m sec. Detailed analysis of these data has been carried out and the results were published in a number of papers at a recent ISOPE conference (Akagawa et al, 2000; Takeuchi et al, 2000; Matsushita et al, 2000). The data revealed line-like loading and non-simultaneous ice failure predominant at indentation speeds greater than 3 mm/sec as shown in *Figure 5.10*. This speed range is expected during iceberg impact. Minor ice failure events were identified to correspond to ice failure of independent zones. Flaking failure of these independent failure zones may correspond to local peak ice load. Detailed interpretation of the cited publications may contribute to the understanding of the relationship between iceberg impact velocities, contact area, ice failure modes, and ice pressure.

TABLE 3: Summary of the Test Conditions for JIOA Winter 1996, 1997, 1998 and 1999 Test Series

Test Year	Indentor Width (m)	Ice Thickness (cm)	Indentation Velocity (cm/sec)	Sampling Freq. (Hz)		First Peak Force (kN)	Subsequent Force Maximum (kN)	Compressive Strength (MPa)	Salinity (ppt)	Density (g/cm^3)	Ice Temp (deg.)	Intact Ice Condition	Ice Type
				Load Cell	Panel Sensor								
1996	1.5	12	0.3	-	-	44.58	40.43	1.43	5.29	0.86	-	undamaged	refrozen
	3	12	0.61	-	-	126.35	105.55	1.83					
		24	0.61	-	-	573.75	303.17	2.1					
1997	4.5	14	0.96	-	-	128.23	--	0.35	5.5	0.86	-	undamaged	refrozen
		16	0.96	-	-	325.1	258.76	1.21					natural
	6	13.3	1.28	-	-	446.91	450.79	0.72					refrozen
		27.3	1.24	-	-	1303.8	615.75	0.97					natural
1998	1.5	24.1	0.3	-	-	284.16	152.8	1.00	5.78	0.843	-	undamaged	natural
			0.03	-	-	--	270.64					damaged	
			3	-	-	--	112.72					damaged	
		23.8	0.3	-	-	1013.9	236.07	1.56	6	0.907	-	undamaged	refrozen
		18.6	0.03	-	-	--	429.92	1.40				undamaged	
		23.8	3	-	-	--	208.79	1.56				damaged	
1999	0.6	35	0.09	5	3.75	572.7	367.3	1.12	2.5	0.813	-1.96	undamaged	natural
			0.03		1.25	--	383.5					damaged	
		36.5	0.15	10	6.25	749.2	233.6	2.02	2.5	0.847	-2.3	undamaged	

NATIONAL RESEARCH COUNCIL OF CANADA
Local Ice Load Data Relevant to Grand Banks Structures
Contract Number: 40731

Test Year	Indentor Width (m)	Ice Thickness (cm)	Indentation Velocity (cm/sec)	Sampling Freq. (Hz)		First Peak Force (kN)	Subsequent Force Maximum (kN)	Compressive Strength (MPa)	Salinity (ppt)	Density (g/cm^3)	Ice Temp (deg.)	Intact Ice Condition	Ice Type
				Load Cell	Panel Sensor								
1999	0.6	36.5	0.06	5	3.75	--	370.8	2.02	2.5	0.847	-2.3	damaged	natural
		30	0.2	10	8.354	908.5	212.2	2.62	2.9	0.864	-2.82	undamaged	
			0.09	5	3.75	--	239.5					damaged	
		33.9	0.3	50	12.5	751.3	143.4	2.09	3.2	0.881	-2.24	undamaged	
			0.03	5	1.25	--	278.2					damaged	
		37.3	3	200	125	537	135.7	3.26	2.1	0.854	-2.04	undamaged	
			0.03	5	1.25	--	379.6					damaged	

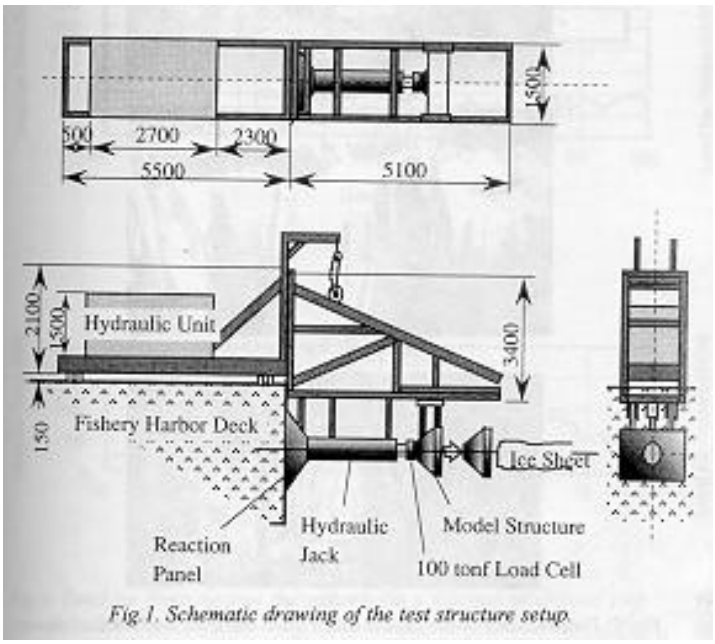

FIGURE 5.8: Schematic Drawing of the Test Structure Set-Up (Taken from Nakazawa et al, 1999)

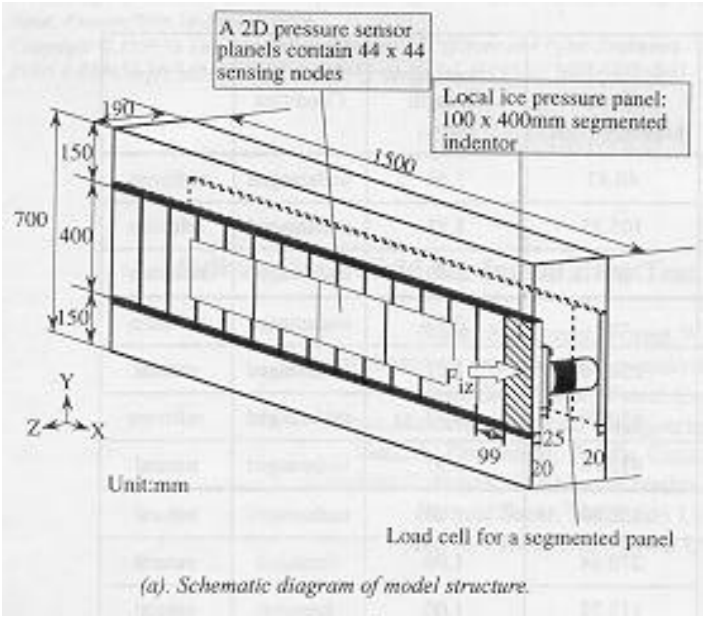

FIGURE 5.9: Schematic Diagram of Model Structure and Instrumentation (Taken from Nakazawa et al, 1999)

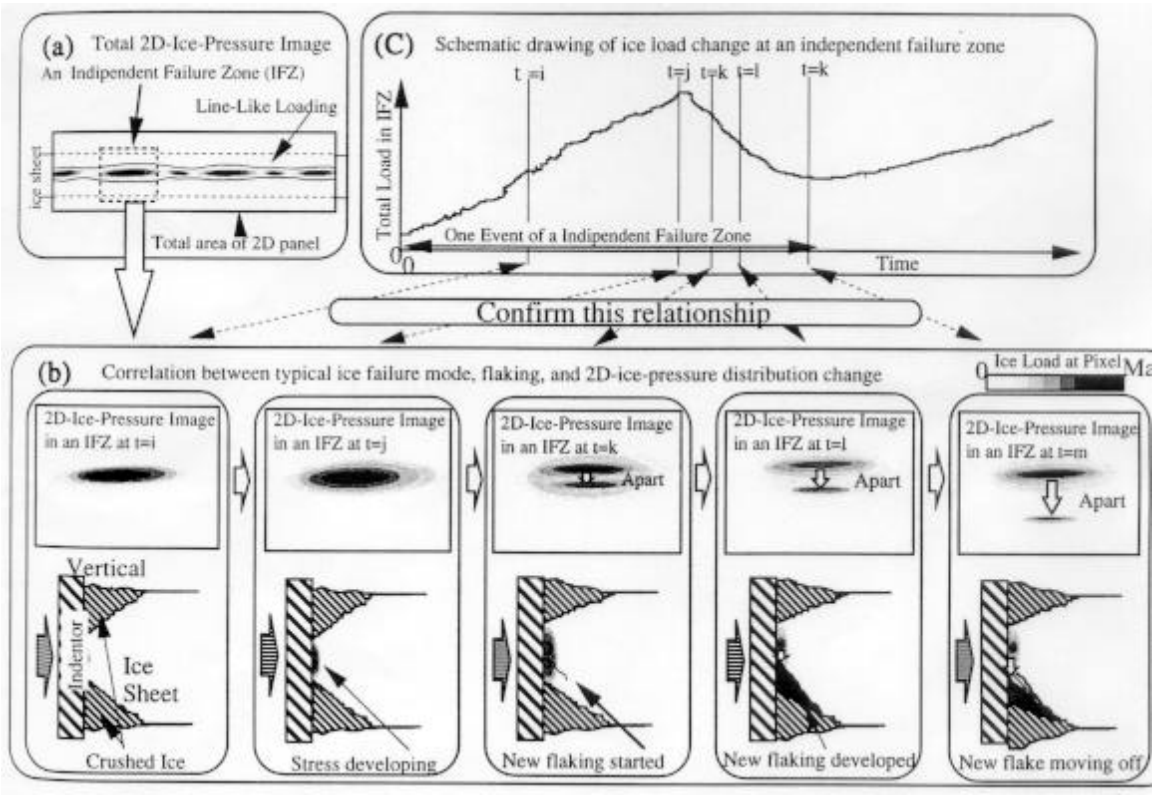

FIGURE 5.10: Relationship Between Flaking Failure and Local Ice Load of Line-Like Independent Failure Zone (IFZ): (a) Total 2D-Ice-Pressure Image Showing an Independent Failure Zone, (b) Correlation Between Typical Ice Failure Mode, Flaking, and 2D-Ice-Pressure Distribution Change, and (c) Schematic Drawing of Ice Lad Change at an Independent Failure Zone

6 Indentation Tests Into Iceberg Walls

6.1 Summary

Data Source:	Iceberg Impact Simulations at Medium Scale (Geotech Project No. 9290)
Geographic Location:	Pond Inlet, Nunavut
Time Period:	1983 - 1984
Ice Types:	Iceberg
Range of Contact Areas:	0 to 3.3 m^2
Relevance to Icebergs:	High

6.2 Background

During the fall and winter of 1983/84 a major research project was undertaken by the Hibernia Partners (Mobil, Chevron, Gulf and Petro-Canada) to simulate the interaction of an iceberg impacting an offshore structure. The theory of lumped ice mass impacts with structures is described in Nevel (1986), along with the basic rational for the testing program.

The tests investigated local pressure versus area effects during iceberg impacts under highly controlled conditions. Complete details of the test program are contained in Masterson et al (1993).

The project was divided into two major components which were the design and fabrication of an impact simulation test machine and the completion of a field testing program. GEOTECH Engineering (now Sandwell Inc.) was contracted to design and build the test apparatus, to manage the project and to conduct the tests. Terra-Tek of Salt Lake City designed and built the servo-control system for the test apparatus.

A total of 21 iceberg impact simulation tests were performed in four (4) tunnels dug into an iceberg grounded off the Hamlet of Pond Inlet, Nunavut. Five spherical indentor plates, each with a specified radius of curvature and maximum area of contact were required for the tests. For descriptive purposes, the indentor plates are distinguished in terms of their nominal maximum areas of contact and ranged from 0.02 to 3 m^2. Two separate ice testing systems were required to accommodate the range of indentor areas. A single hydraulic actuator provided adequate forces to conduct the 0.02 m^2, 0.1 m^2, and 0.5 m^2 indentation tests. For the two largest tests, 1 m^2 and 3 m^2, four actuators acting in parallel were required to generate a force of 18 MN or 4,000,000 lbs. In both systems the rear of each ram was attached to a single back plate and rested against the smooth ice backwall.

The displacement for each test was servo controlled according to the following equation for a quarter of a cycle.

$$x = x_0 \, Sin \, (\omega t)$$

The maximum penetration x_0 was set to 0.1 times the indentor radius R and the initial velocity set to 100 mm/s. The time to maximum displacement x_0 and the frequency ω are listed in *Table 4*. The spherical indentor penetrating into a flat ice surface resulted in a progressive increase of the contact area during a test.

TABLE 4: Defining Parameters of Impact

Test Category	R (mm)	X_0 (mm)	ω Cycles/Sec	t d (secs)	a max (m^2)
3.00 m^2	2,300	230	0.4348	3.613	3.3238
1.00 m^2	1,280	128	0.7813	2.011	1.0294
0.50 m^2	900	90	1.11	1.414	0.5089
0.10 m^2	400	40	2.5	0.628	0.1005
0.02 m^2	200	20	5	0.314	0.0251

The impact simulation tests confirmed that interaction pressure decreases with increasing contact area.

Most of the test results, conform to the following functional relationship:

$$q = k\,(a_c)^{-m}$$

where: q = Average Ice Pressure
k = Constant
a_c = Area of Contact
$m < 1$

However, in certain tests the pressure did not decrease monotonically with increased area of contact. This could be explained by the fact that the actual area of contact with the ice is different than the theoretical area of contact. Because of the brittle and uneven nature of the ice failure in front of the indentor, this discrepancy is understandable. Large chunks of ice were observed to be dislodged from the immediate test area during some of the tests. An examination of the test videos confirms this.

A comparison of the test results from indentors of different sizes and curvatures shows that, as the indentor curvature increases, the pressure for the same contact area decreases. Thus pressure decreases as the curvature (1/R) increases.

6.3 Data Attributes

The test program required measuring indentor loads, pressures along the indentor face, and position. The load was monitored by a load cell in series with each actuator and the displacement by potentiometers referenced to the floor of the tunnel. An estimate of the highest frequency component expected in the data was required in order to select transducers, signal conditioners, and sampling rates. Previous tests with flatjacks and small indentors showed pressure pulses with rise times approaching one millisecond. A bandwidth of DC to 10 kHz was selected as being sufficient to faithfully record the expected signals. A Honeywell Model 101 FM recorder was used with 14 intermediate band record and playback amplifier cards. A separate voice record and playback channel was used to notate the tape. Record speed was 60 in./sec which provided a DC to 40 kHz bandwidth with the intermediate amplifiers.

6.4 Data Quality and Number of Events

TABLE 5: Schedule of Tests

Tunnel No.	Test Date	Test No.	Test Category
1	84-05-02	1	0.02 m^2
	84-05-04	2	0.10 m^2
	84-05-06	3	0.10 m^2
	84-05-13	4	1.00 m^2
	84-05-14	5	3.00 m^2
2	84-05-10	1	0.5 m^2
	84-05-10	2	0.5 m^2
	84-05-17	3	0.1 m^2
	85-05-17	4	0.02 m^2
	84-05-19	5	1.00 m^2
3	84-05-15	1	1.0 m^2
	84-05-16	2	3.0 m^2
	84-05-18	3	0.5 m^2
	84-05-18	4	0.5 m^2
	84-05-19	5	0.02 m^2
4	84-05-21	1	1.00 m^2
	84-05-21	2	3.00 m^2
	84-05-22	3	3.00 m^2
	84-05-22	4	0.10 m^2
	84-05-22	5	0.10 m^2

Force versus time curves were plotted for all of the tests. The output from each load cell was plotted against time and then a total load versus time curve was plotted. In general, the load on any indentor increases as the indentor is pushed into the ice.

Examination of the force versus time curves reveals the following:

A) 0.02 m^2 Tests

The curves are generally smooth with no apparent sawtooth (load increases and decreases in a regular manner) effect.

B) 0.1 m^2 Tests

Four of the five tests of this size showed some sawtooth effect. This sawtooth effect was irregular, having a high frequency and low amplitude. One of these four tests had a very small amplitude sawtooth. Test 1-3 had a regular sawtooth with a decreasing frequency near the end of the test.

C) 0.5 m^2 Tests

Three of these tests had a regular sawtooth imposed on the force versus time curve. They had a higher frequency, small amplitude signal superimposed on the sawtooth. Test 2-1, the test conducted with no servo control, had a frequency for the sawtooth of 27 Hz. One of the four tests, 2-2, had no regular sawtooth imposed on it.

D) 1 m^2 Tests

All four of these tests had a regular sawtooth shape. Tests 1-4 and 4-1 had a very small amplitude, high frequency waveform superimposed on the sawtooth. Tests 2-5 and 2-6 showed a decrease in the frequency of the sawtooth near the end of the test. In Test 2-5, the main load was concentrated on diagonally opposite load cells.

E) 3 m^2 Tests

All tests showed a regular sawtooth pattern in the force versus time curve. Frequencies were a function of time and varied as shown in *Table 6* on the following page.

TABLE 6: Sawtooth Frequency (Hz) During 3.0 m^2 Tests

Test No.	Time Intervals		
	0 to 1 sec	1 to 2 sec	2 to 3 sec
1-5	20	18	10
3-2	29	26	6
4-2	19	17	8
4-3	23	21	10

6.5 Examples of Time Series Data

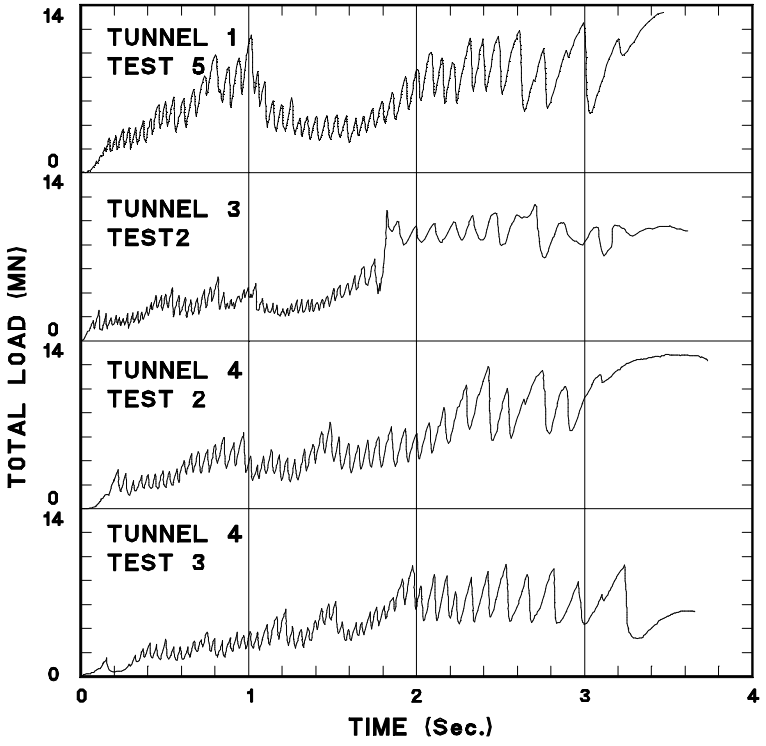

TOTAL LOAD vs. TIME
for
$3m^2$ TEST

FIGURE 6.1: Example of time Series Data for Pond Inlet

6.6 Comments on Relevance to Local Ice Loads Due to Icebergs

Directly relevant, as data were collected on cold intact ice. In an iceberg-structure interaction the contact conditions will not likely be as perfect as was the case for these tests.

7 Indentation Tests into Multi-Year Ice Walls

7.1 Byam Martin Channel Indentation Tests 1985

7.1.1 Summary

Data Source:	Velocity Effects from Multi-Year Ice Tests
Geographic Location:	Byam Martin Channel, Nunavut (Geotech Project No. 9363)
Time Period:	April - May 1985
Ice Types:	Multi-Year
Range of Contact Areas:	0 to 1.4 m^2
Relevance to Icebergs:	High

7.1.2 Background

Multi-year ice poses a major design load on offshore drilling and production platforms in Arctic waters. In order to obtain information on ice pressures that might occur during the contact of a multi-year ice floe with an offshore structure, a joint-industry research project was initiated under the sponsorship of Mobil Research and Development Corporation, Shell Development Company, Chevron USA Incorporated and SOHIO Petroleum Company (British Petroleum). This project was preceded by a similar suite of tests conducted in tunnels excavated into an iceberg grounded in the eastern Arctic (Masterson et al, 1992). Subsequently, field indentation tests on multi-year ice have been conducted to address issues raised by these two programs and to present the data in a summarized form suitable for use in design (Masterson et al, 1993, Masterson and Frederking, 1993, Masterson et al, 1994, Jones et al, 1995, Gagnon et al, 1998, Sodhi et al, 1998). More information on the current project can be found in Masterson et al (1999) OMAE99.

The major objectives of the project were:

- To obtain a relationship between indentation pressure and contact area.
- To determine the effect of indentor velocity on pressure/area relationships and determine the velocity at which maximum indentor pressure occurs.
- To compare the results of cosine velocity function tests to constant velocity function tests.
- To compare the results from penetrating a flat ice surface with a curved indentor to the penetration of a curved ice surface with a flat indentor.
- To determine the relationship between indentor geometry and pressure/area relationships.

In April/May, 1985, GEOTECH (now Sandwell) conducted tests to simulate the interaction of a multi-year floe with an offshore structure. The project involved the design and fabrication of an indentation test apparatus and the completion of 20 medium scale field tests in three trenches excavated into a multi-year floe adjacent to Byam Martin Island, NWT. Also, see Masterson et al, 1992, for more detail on the original apparatus design and function.

During each test, an aluminium indentor was forced against the milled ice surface of a trench wall with three hydraulic rams capable of exerting a combined maximum force of 13.5 MN. A servo system controlled the indentation velocities. Displacement, load and pressure load sensors signals were recorded with a 32 channel, 50 kHz digital data acquisition system.

Three trenches, averaging 50 m long by 2.5 m wide by 3.5 m deep, were excavated into the multi-year ice floe. After the excavation was completed, trench walls were milled to ensure a smooth surface for the indentation tests.

The medium scale ice indentation test apparatus may be divided into four distinct systems: structural, hydraulic, servo control and data acquisition. See also Masterson et al, 1992, Masterson et al, 1993, and Spencer and Masterson, 1993, for more detail. The major components of the structural system consisted of three 200 mm thick aluminium indentors, one mounting plate and three 1.0 m back plates. A distinct radius of curvature and maximum area of contact characterized each indentor. The hydraulic components operated at a pressure of 35 MPa and also had the ability to operate in -40 deg. C temperatures.

The hydraulically powered tri-actuator system was developed to provide the required forces to move the 1.0 m^2 flat, 1.0 m^2 spherical and 2.5 m^2 spherical indentors into the ice wall. The energy for the system was generated by eight air/oil accumulators acting in parallel and mounted on a separate skid.

The on-site computer was used to digitally record the various transducer data. The indentor displacement data was provided by three potentiometers attached to the indentor. The total force exerted by the actuator system was recorded from three load cells mounted in front of the actuators. The local contact pressure was measured with pressure cells 100 mm in diameter in various points on the face of the indentors.

1. The average nominal pressure (32 MPa) peaked at an area of contact of 0.1 m^2. For areas of contact larger than 0.1 m^2, the average nominal pressure, *P*, decreases with increasing area, *A*, and can be expressed as:

$$p = P_0 A^{-a} \quad 0.13 \# . \# 0.5$$

2. The pressure on the face of the indentor was greatest at the point of contact of the indentor and decreased with increasing radial distance from the centre.

3. Contact velocity had a first order effect on the ice pressures recorded during indentation. Significantly different ice pressures and loads are seen in the ductile, brittle and transition modes of ice failure. The highest pressure occurred in the transition zone at a velocity of 3.16 mm/s for the 1.0 m^2 spherical indentor. However, because of lack of larger indentor tests in the transition zone, no information on maximum pressures at areas of contact larger than 1.0 m^2 are available.

4. For the 1.0 m^2 tests (spherical indentor) the maximum nominal pressure (34.3 MPa) occurred at a velocity of 3.16 mm/s. The maximum nominal pressure also occurred at a contact area of 0.1 m^2.

5. The maximum nominal pressure, *P*, for a given area of contact in the ductile region (V < 3.16 mm/s) can be expressed as a power law function of indentation velocity, *V*:

$$P = CV^{\circ} \qquad 0.15 \# \circ \# 0.33$$

6. At velocities less than 3.16 mm/s, the load and pressure curves were smooth and the ice behaviour was consistent with plastic flow and ductile behaviour. At velocities greater than 3.16 mm/s, the load and pressure curves showed a pronounced sawtooth waveform and the ice behaviour was consistent with a brittle failure behaviour. Tests completed at 3.16 mm/s exhibited load and pressure signals, which ranged from a smooth to a more sawtooth shape characteristic of the transition zone between the ductile and brittle mode of failures.

7. There are different patterns of ice failure corresponding to the brittle and ductile modes. Failed ice in the ductile mode tests was typified by:

   - Extensive radial cracking in a conical pattern.
   - A strong tendency for large wedge failure cracks to occur.
   - Pressure melting in the indentation zone.
   - Plastic deformation of ice at the edges of the indentor.

   Failed ice in brittle mode tests was typified by:

   - Extensive radial and circumferential cracking, but more localized than in ductile tests.
   - Extensive crushing and flaking.
   - Two distinctive layers of crushed ice in front of the indentor - the closest being hard and compacted, the second being softer.
   - Ejected ice extruded in pulsating action during failures.

8. The data indicated no direct relationship between pressure distribution across the face of the indentor and the indentation velocity.

9. There are no significant differences in test results between the tests completed at 100 mm/s constant velocity and those completed at 100 mm/s cosine velocity (initial maximum velocity (100 mm/s) is reduced to zero at full penetration).

10. There is a small but consistent difference between nominal pressure for the 2.5 m^2 and 1.0 m^2 indentors. However, there are differences in the pressure cell readings indicating differences in the pressure distribution across the face of the two indentors.

11. There are significant differences between the results of the 1.0 m^2 spherical and 1.0 m^2 flat indentor tests on spherical ice. The peak nominal pressure and the maximum value of the centre pressure transducer P_1 are higher in the case of the spherical indentor loading a flat ice surface than for the flat indentor loading a spherical ice surface. Both P_1 maxima occur at small contact areas. At larger contact areas the two sets of P_1 data tend to be in better agreement. These data suggest that confinement from the surrounding ice may be a key factor governing maximum interaction pressures.

12. Judgement is required in the use of these test results quantitatively for design, especially where geographical location may significantly affect the strength and ductility of the ice.

7.1.3 Data Attributes

During each test, an aluminium indentor was forced against the milled ice surface of a trench wall with three hydraulic rams capable of exerting a combined maximum force of 13.5 MN. A servo system controlled the indentation velocities. Displacement, load and pressure load sensors signals were recorded with a 32 channel, 50 kHz digital data acquisition system. The on-site computer was used to digitally record the various transducer data. The indentor displacement data was provided by three potentiometers attached to the indentor. The total force exerted by the actuator system was recorded from three load cells mounted in front of the actuators. The local contact pressure was measured with pressure cells 100 mm in diameter in various points on the face of the indentors.

TABLE 7: Indentation Test Summary of Maximum Values

Test No.	Indentation Velocity mm/s	Failure Mode	Maximum Penetration (mm)	Maximum Total Load (mm)	Maximum PI Pressure (MPa)	Maximum Nom. Pressure (MPa)	Maximum Specific Energy (MPa)	Maximum Area (m^2)	Nom. Pressure At Max. Area (MPa)
2.5 m^2 Spherical Indentor									
1	0.10	Ductile	100.90	10.50	27.10	16.70	15.70	1.425	5.50
2	1.00	Ductile	44.60	7.00	28.60	32.40	29.00	0.600	11.50
1.0 m^2 Spherical Indentor									
3a	1.00	Ductile	8.10	2.00	49.40	32.10	27.00	0.064	31.00
3b	1.00	Ductile	17.90	3.60	40.60	31.10	24.00	0.142	24.60
4a	10.00	Brittle	18.80	2.20	42.50	25.20	21.00	0.150	5.00
4b	10.00	Brittle	37.20	2.40	56.90	16.40	4.00	0.295	3.00
4c	10.00	Brittle	56.60	3.40	49.70	7.90	2.80	0.440	4.00
4d	10.00	Brittle	83.40	4.10	52.00	9.20	1.60	0.650	1.00
5	10.00	Brittle	125.00	6.40	46.40	23.20	15.50	0.956	5.00
6	100.00	Brittle	116.90	6.90	50.80	25.50	22.00	0.897	6.00
7	100 Cosine	Brittle	126.60	8.00	51.20	21.40	17.00	0.968	9.00
8	100 Cosine	Brittle	127.20	6.30	53.50	23.80	19.00	0.972	1.00
9	100.00	Brittle	119.70	9.20	44.00	26.10	19.50	0.918	3.00
10	10.00	Brittle	121.80	5.70	64.30	27.60	23.50	0.933	2.00
11	1.00	Ductile	29.30	3.90	35.30	27.40	25.50	0.233	16.00
12	3.16	Brittle	110.90	5.30	66.80	34.30	31.00	0.853	5.00
13	1.78	Ductile	29.50	4.50	45.90	32.40	29.50	0.235	19.00
1.0 m^2 Flat Indentor									

Test No.	Indentation Velocity mm/s	Failure Mode	Maximum Penetration (mm)	Maximum Total Load (mm)	Maximum PI Pressure (MPa)	Maximum Nom. Pressure (MPa)	Maximum Specific Energy (MPa)	Maximum Area (m^2)	Nom. Pressure At Max. Area (MPa)
14	10.00	Brittle	122.20	7.90	32.50	23.80	18.50	0.935	6.00
1.0 m^2 Spherical Indentor									
15	0.10	Ductile	71.80	4.40	25.20	10.70	9.80	0.562	8.50
16	0.10	Ductile	51.10	3.70	21.20	13.80	13.00	0.403	10.00
17	0.30	Ductile	56.50	5.20	31.40	19.10	17.00	0.399	7.00
18	3.16	Ductile	55.50	3.50	56.40	28.00	24.00	0.437	9.00
19	1.78	Ductile	20.70	3.90	63.20	32.50	30.00	0.165	23.50
20	3.16	Ductile	59.10	6.40	52.20	31.60	29.00	0.464	14.00

7.1.4 Time Series Data

Time series data from the three types of transducers (displacement, load, and pressure) were recorded during each test. *Figure 7.1* shows examples of time series plots for Test 15 that was performed at 0.1 mm/s with the 1.0 m spherical indentor. These time series plots are typical of tests performed at indentation velocities of less than 3.16 mm/s. At these velocities, transducer signals were generally smooth and characteristic of the ductile ice failure mode.

The transducer signals, for the ductile (V <3.16 mm/s) tests generally conform to the following trends: the displacement signal increased monotonically with time; the load signal also increased monotonically with time and the maximum load occurred at the end of the test; the pressure, recorded from the central pressure cell P_1, always peaked very early in the test. This is also true for the other rings of pressure cells when considering ice contact time delays.

Figure 7.2 shows examples of time series plots for Test 9, which was carried out at 100 mm/s (constant) with the 1.0 m^2 spherical indentor. These time series plots are typical of tests carried out at indentation velocities greater than 3.16 mm/s. At these velocities, transducer signals generally had a pronounced sawtooth appearance characteristic of a brittle ice failure mode.

The transducer's signals, for the brittle (V >3.16 mm/s) tests, generally conform to the following trends. The displacement signal increased in small step increments with time and the load signal exhibited a sawtooth pattern and a general increase in magnitude with time, all due to the brittle nature of the ice failure. In all the constant velocity tests the maximum load occurred at approximately 75 percent of total penetration. The only exception to this trend was the 100 mm/s cosine test (Test 7) and the repeated penetration tests (Tests 4A to 4D). The pressure, recorded from the central pressure cell P_1, also exhibited a sawtooth behaviour. It always peaked early in the constant velocity tests and was immediately followed by a drastic decrease in pressure. After this, the pressure signal reached various smaller peaks with no general trend as to general increase or decrease. Tests 7 and 8 (100 mm/s Cosine) generally experienced a decrease in pressure after the initial peak.

Tests conducted at 3.16 mm/s exhibited both brittle and ductile modes of failure. Test 12 on May 6 had a brittle mode of failure, and Tests 18 and 20 on May 9 and 10 had ductile modes of failure. The load versus time for Test 12 is shown in *Figure 7.3* and displays the typical sawtooth brittle mode of failure. The load versus time for Test 20 is shown in *Figure 7.3* and displays the typical smooth ductile mode of failure. Thus a speed of approximately 3 mm/s may be considered the transitions speed from ductile to brittle failure. The time order of these tests was 12, 18, 20 and during this time, there was a slowly warming trend of the weather. A plausible explanation for observing both ductile and brittle failures at 3.16 mm/s is the ice temperature. The ice temperature was measured for most tests and showed very little difference during the time of these tests. However, it was noted that the sun was not shining on the ice surface of Test 12, but was shining on the ice surface for Test 18.

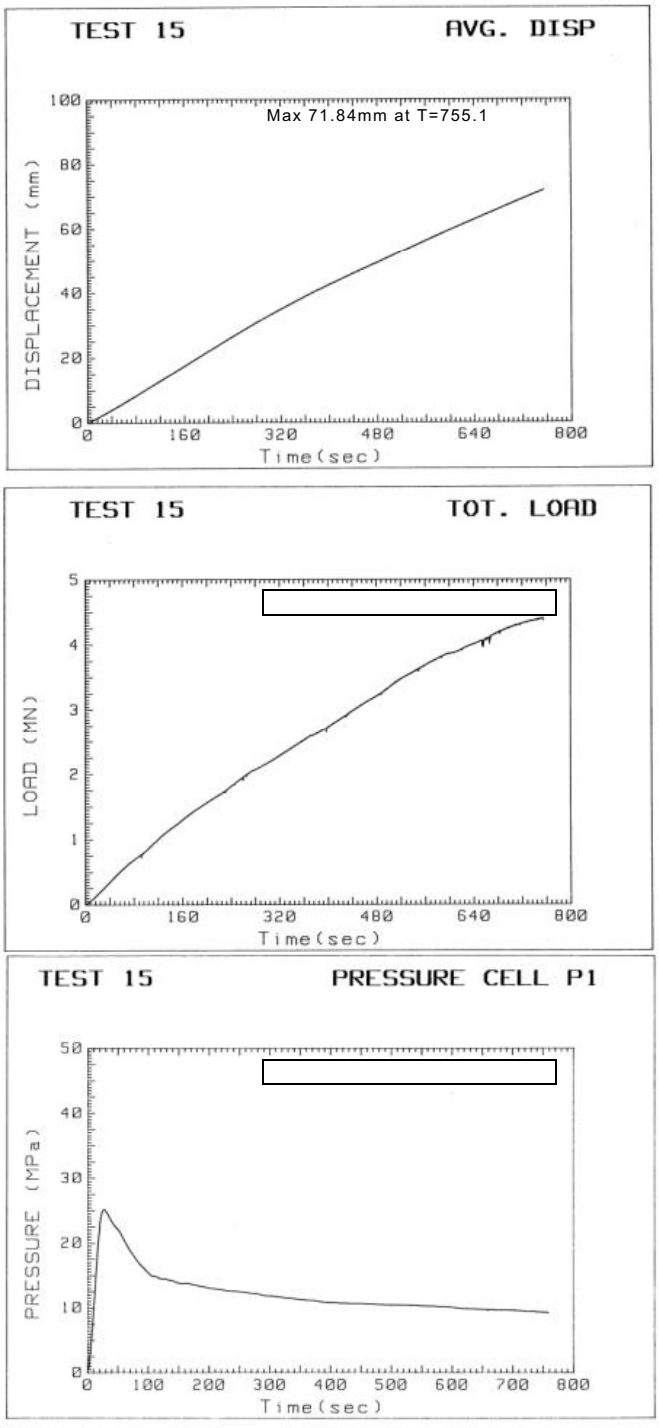

TEST 15 V = 0.1mm/sec.

FIGURE 7.1: Typical Time Series Plots for Ductile Ice Failure

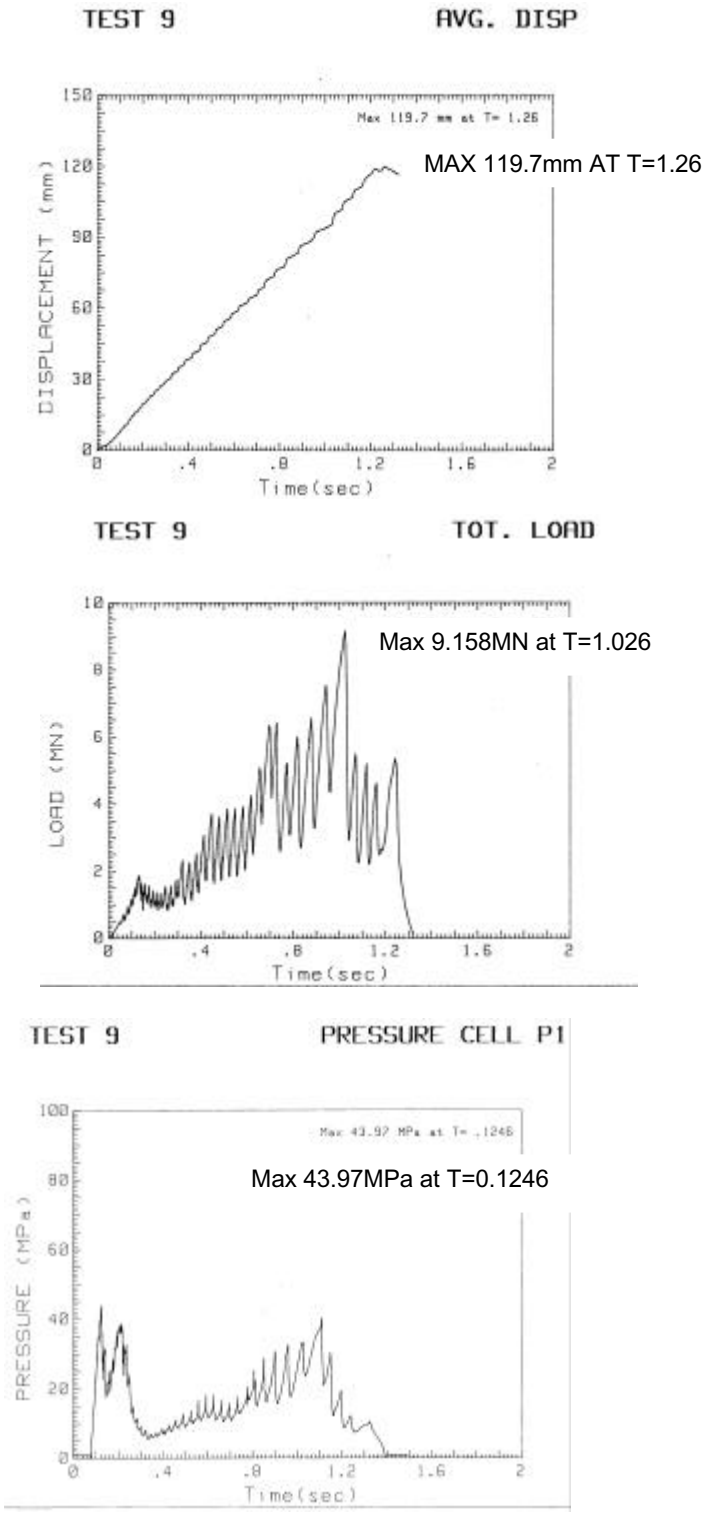

FIGURE 7.2: Typical Time Series Plots for Brittle Ice Failure Mode

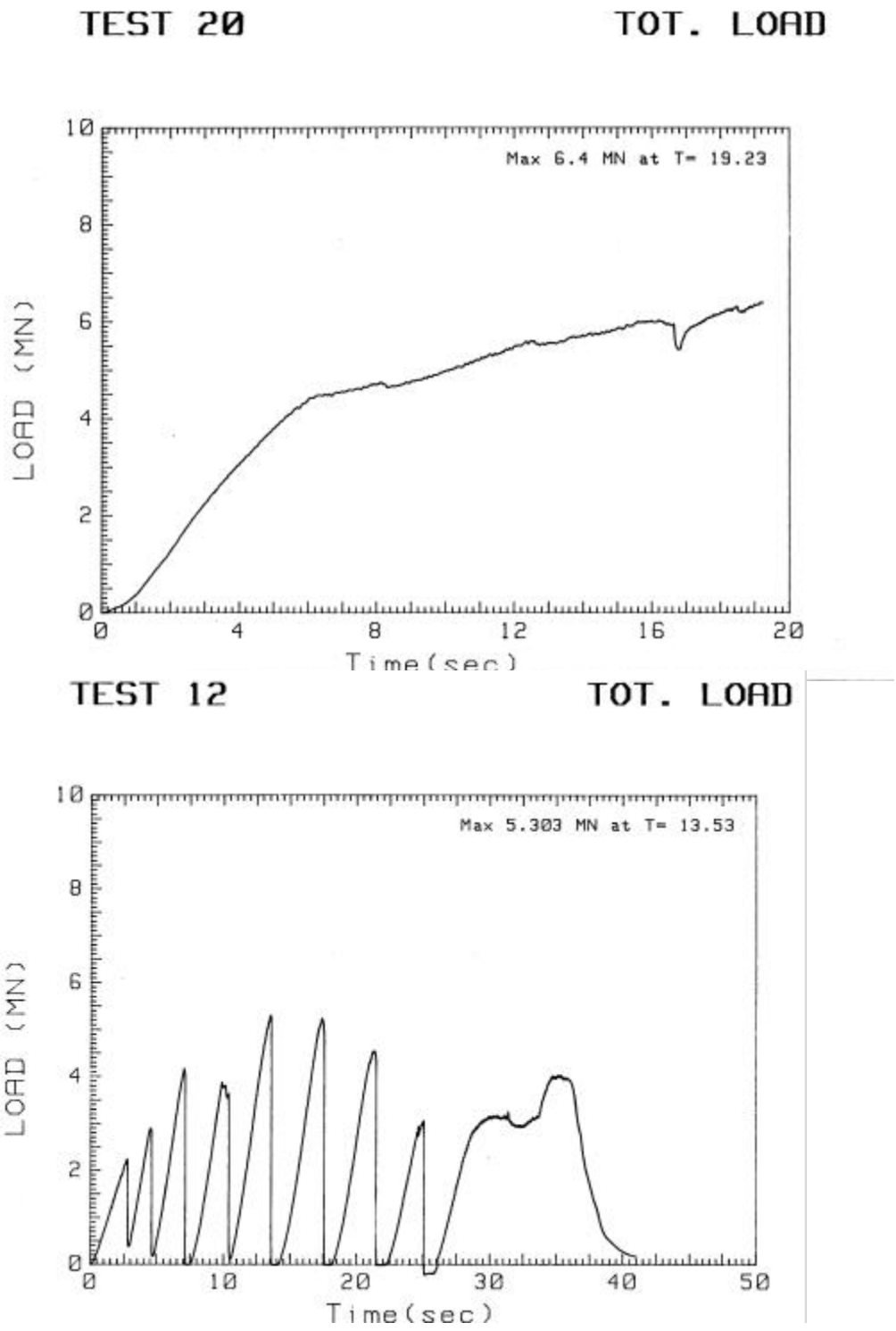

FIGURE 7.3: Time Series Plots for Tests at 3.16 mm/sec

7.1.5 Comments on Relevance to Local Ice Loads Due to Icebergs

Low salinity multi-year ice tests have a high relevance to iceberg loading. Tests show a pronounced effect of impact velocity on contact pressures.

7.2 Hobsons Choice Ice Island Indentation Tests 1989

7.2.1 Summary

Data Source:	Field Tests of Ice Indentation of Medium Scale Hobson's Choice Ice Island, 1989 (Sandwell Job 112034)
Geographic Location:	Hobson's Choice Ice Island, 79^{o} 23.5' N - 102o 20.2' W
Time Period:	April 1989
Ice Types:	Shelf ice and multi-year ice
Range of Contact Areas:	0.2 to 0.5 m^2
Relevance to Icebergs:	Local ice pressures measured on ice of similar strength and stiffness

7.2.2 Background

A series of 11 indentation tests at constant velocities ranging from 0.3 mm s^{-1} to 100 mm s^{-1} were carried out on multi-year sea ice. Memorial University of Newfoundland (MUN), Canadian Coast Guard (CCG), National Research Council of Canada and Sandwell Swan Wooster (now Sandwell Engineering Inc.) collaborated on this project to carry out ice indentation tests in the Arctic during April 1989. This program followed joint industry project indentation tests at Pond Inlet in 1984 and in Byam Martin Channel in 1985. These programs had used indentors up to 3 m^2 in area and at speeds up to 100 mm s^{-1}. These indentors had been rigid spherical or flat, while in this program an indentor more representative of the geometry and stiffness of an actual structures was used. The tests were conducted in a trench excavated in the island's multi-year ice which was 65 m long, 3 m deep and 3 m wide.

The apparatus used was formed from the same equipment used to perform the Pond Inlet and Byam Martin tests. The hydraulic actuator used to propel the indentors had a capacity of 4.5 MN, a stroke of 300 mm and a maximum velocity of 100 mm s^{-1}. Energy to operate the actuator was supplied from a bank of hydraulic accumulators. A high-speed data acquisition system was used to record force, displacements with respect to the ice face, and local ice pressures. The actuator, indentors and base plate were placed across the trench and the trench itself served as the load frame and loaded medium.

Three indentors were used:

- A rigid spherical indentor of 0.8 m^2 area.
- A circular, flat, compliant indentor of 0.8 m^2 area.
- A rigid flat rectangular indentor of 0.375 m^2 area.

Pressure sensors were mounted in each of the indentors.

7.2.3 Data Attributes

Tests were conducted at impact velocities ranging from 0.3 mm s^{-1} to 110 mm s^{-1}. Ice penetration varied from 1 mm to 60 mm, final contact areas varied from 0.18 to 0.54 m^2 and average pressures varied from 6.3 to 21.9 MPa. Data was scanned at rates as high as 1,000 readings per second for each channel.

7.2.4 Data Quality and Number of Events

Good quality data was obtained, which included not only the load, pressure and sensor recordings but as well detailed observations of the ice before and after failure. Eleven tests were performed and are summarized in *Table 8* below. A time series of force and local ice pressures are shown in *Figure 7.4*.

TABLE 8: April 1989 Ice Indentation Test Results

Test No.	Indentor	Ice Face	Rate (mm/s)	Max. Load (MN)	Load Time(s)	Pen (mm)	Final Area (m^2)	Average Press (MPa)
1	Spherical	Flat	~0.3	3.4	99	35	0.31	10.9
2	Spherical	Flat	~2.5	3.8	9.8	60	0.54	7
3	Spherical	Flat	~110	2	0.22	17	0.32	6.3
4.1	Spherical	Flat	~4	3.3	4.6			
4.2	Spherical	Flat	~15	3.5	0.48	19	0.22	16
5	Spherical	Flat	~90	3.6	0.69	22	0.2	18
6	Flexible	1201:3	19	1.8	1.9	30	0.27	6.7
7	Flexible	2701:3	68	4.5	0.4	25	0.37	12.2
8	Rigid	2001:5	~80	3.8	0.56	31	0.27	14
9	Rigid	4001:5	~10	4.4	0.4	1	0.2	21.9
10	Rigid	2001:5	~10	2.8	0.65	12	0.18	15.6

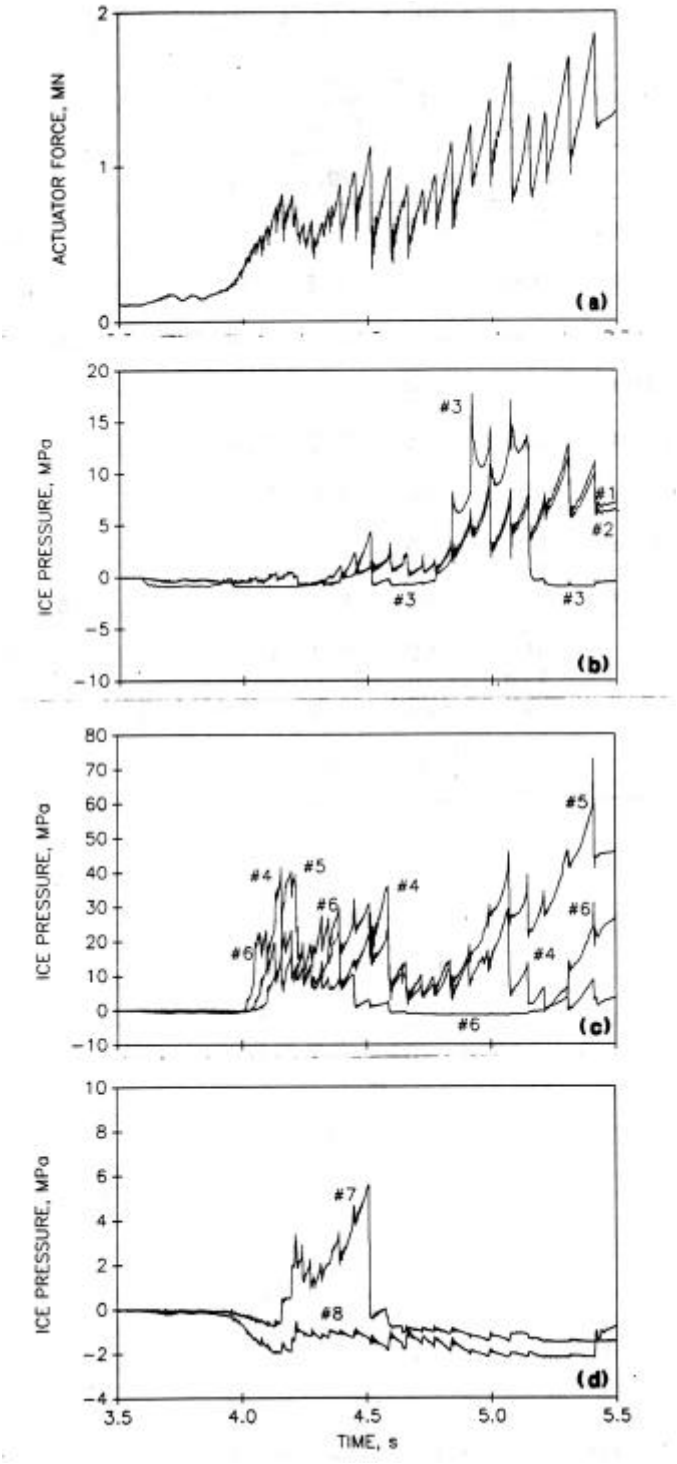

FIGURE 7.4: Time Series of Force and Local Ice Pressures for Test 6

7.2.5 Comments on Relevance to Local Ice Loads Due to Icebergs

The principal failure modes observed in the medium scale tests were crushing and flaking, both on a large scale as well as locally around the perimeter of the contact area. The combination of these modes was related to indentation rate. At low rates (< 3 mm s^{-1}) creep and microfracture occurred at depth in the ice and large flakes, some running right up to the surface occurred. At higher indentation rates, a relatively thin layer of crushed and damaged ice forms and small particles of crushed ice were seen to extrude from this region. The crushed layer was not uniform, but varied in thickness and was characterized by a narrow band of relatively undamaged ice in the central part of the contact zone.

Measurements of local ice pressures in the centre of the contact area indicated they were about three times higher than the average pressure acting over the entire area. It is clear that ice pressures are not uniform over the contact area. Pressure distributions show a systematic pattern of being significantly higher in the centre of the contact area. This confirms the pressure distribution assumed for design purposes and is useful design information for iceberg impact in particular.

7.3 Hobson's Choice Ice Island Indentation Tests 1990

7.3.1 Summary

Data Source:	Multi-Year Ice Indentation Tests at Hobson's Choice - 1990 (Sandwell Job No. 112390)
Geographic Location:	Hobson's Choice Ice Island
Time Period:	April and May 1990
Ice Types:	Multi-Year Ice
Range of Contact Areas:	0.7 m^2 to 1.8 m^2
Relevance to Icebergs:	Local ice pressures on ice with strength and stiffness similar to iceberg ice

7.3.2 Background

The motivation for the field test program was to measure ice contact pressures for various interaction geometries and indentor (structural) stiffness. In previous field indentation programs conducted in 1984, 1985 and 1989, the principal variables have been the contact speed and the contact area.

This field test program was conducted during April and May 1990 adjacent to Canada's former arctic Ice Island research station. The tested ice was in a multi-year floe approximately 10 m in thickness adjacent to the shelf ice. The test program measured ice contact loads at areas up to 1.5 square metres and at speeds of 100 mm/s to 400 mm/s.

The indentors used to crush the ice were a large flat, flexible indentor, area 1.8 m^2; a small flat, flexible indentor, area 0.7 m^2; wedge indentors, one with an included angle of 90 degrees and the other with an included angle of 143 degrees; and a flat, rigid indentor with an area of 1.8 m^2. Fifteen (15) indentation tests were performed.

The two hydraulic actuator assemblies used were a triple actuator system, and a single actuator system. The triple actuator assembly provided up to 12 MN of thrust, with each actuator furnishing up to 4 MN at a servo-controlled speed of 100 mm/s. The second actuator assembly used a single actuator and three servo valves in parallel which allowed for a thrust of 4 MN at servo-controlled speeds of 300 mm/s.

7.3.3 Data Attributes

Time series recordings were made of hydraulic actuator oil pressure (load), actuator displacements, indentor strains, local pressures and ice pressures within the contact area, indentor plate deflections, accelerations, ice temperature during the test and acoustic emissions in the ice.

A flexible indentor simulating plating and framing of a structure was instrumented with strain gauge and a number of local pressure series about 10 mm in diameter.

A 36-element pressure panel supplied by TKK of Finland was installed on the flat-rigid indentor at the locations shown in *Figure 5.3*. It used a 9 x 4 rectangular array of piezoelectric film sensors each approximately 50 mm by 50 mm.

Uniaxial Piezo electric accelerometers were mounted with the sensor axis in the direction of travel and in the mounting bracket for the displacement potentiometers for Actuators 1 and 2 of the test apparatus.

A video camera was installed for recording visual information through the view port on the flat rigid indentor. During the first test, the video camera failed to record the data due to the large vibration levels. A cable was then made which allowed for the storage of the video information on a hand held camera at the surface.

One of the mounts of the local pressure cell was field modified to incorporate a thermocouple for recording ice contact temperatures during the interaction.

A stand-alone sonar system, supplied by the Memorial University of Newfoundland, recorded the acoustic signal of the interaction. The sensor was mounted in a fluid filled borehole in the ice behind the interaction zone.

During the triple actuator series of tests, the data were collected at 2.0 kHz per channel, with an analogue first order low pass filter set at 1.0 kHz. For the single actuator tests, the data were collected at a sample rate of 5.0 kHz per channel, with the first order low pass filter set at 3.0 kHz.

7.3.4 Data Quality and Number of Events

The test matrix is given in *Table 9* which indicates all the tests conducted with the triple and single actuator arrangements and the five indentors.

TABLE 9: Test Matrix

7.3.4.1.1	Date	No. of Actuators	Indentor	Ice Shape	Ice Slope	Initial Contact mm	Initial Speed mm/s
TFF 01	12/05/90	3	Flat Flexible	V * Wedge	3:1	300 x 1500	100
TFF 02	13/05/90	3	Flat Flexible	V * Wedge	3:1	300 x 1500	100
TFF 03	14/05/90	3	Flat Flexible	H * Wedge	3:1	300 x 1200	100
TW1 01	15/05/90	3	1:1 Wedge	Flat	N/A	100 x 1800	100
TW1 02	15/05/90	3	1:1 Wedge	Flat	N/A	100 x 1800	100

7.3.4.1.1	Date	No. of Actuators	Indentor	Ice Shape	Ice Slope	Initial Contact mm	Initial Speed mm/s
TW3 01	Eccentric Load Detector Stopped Test						
TW3 02	Eccentric Load Detector Stopped Test						
TW3 03	Eccentric Load Detector Stopped Test						
TW3 04	16/05/90	3	3:1 Wedge	Flat	N/A	100 x 1800	100
TW3 05	16/05/90	3	3:1 Wedge	Flat	N/A	100 x 1800	100
TFR 01	18/05/90	3	Flat Rigid	V * Wedge	3:1	300	100
TFR 02	18/05/90	3	Flat Rigid	Pyramid	3:1	100 x 100	100
TFR 03	19/05/90	3	Flat Rigid	Pyramid	3:1	500 x 500	100
TFR 04	19/05/90	3	Flat Rigid	Pyramid	3:1	100 x 100	100
TFR 05	19/05/90	3	Flat Rigid	Pyramid	3:1	500 x 500	100
SFF 01	21/05/90	1	Flat Flexible	V * Wedge	3:1	100	400
SFF 02	22/05/90	1	Flat Flexible	V * Wedge	3:1	100	400
SFF 03	22/05/90	1	Flat Flexible	V * Wedge	3:1	100	100

Note: V = Vertical
H = Horizontal

TABLE 10: Ice Face Final Contact Areas

Test	Calculated Area (m^2)	Measured Area (m^2)	Measured/Calculated
TFF 01	1.58	1.50	0.95
TFF 02	1.41	1.30	0.92
TFF 03	1.06	1.08	1.02
TW1 01	-	-	-
TW1 02	-	-	-
TW3 04	-	-	-

Test	Calculated Area (m^2)	Measured Area (m^2)	Measured/Calculated
TW3 05	-	-	-
TFR 01	-	1.35	-
TFR 02	0.80	0.90	1.25
WTFR 03	1.17	1.15	0.99
TFR 04	1.14	1.20	1.05
TFR 05	1.48	0.70	0.47
SFF 01	0.46	0.29	0.63
SFF 02	0.41	0.29	0.70
SFF 03	0.46	0.34	0.74

The test program was successfully completed and a wealth of data collected on multi-year ice contact pressures. The apparatus and testing arrangement worked well, providing data from 15 tests on the effect of different shaped indentors, impact speed and indention stiffness.

The conclusions are as follows:

1. The total load increased with penetration into the ice.

2. The total load versus penetration and nominal pressure versus penetration curves exhibited the typical higher frequency sawtooth behaviour, indicating load build up followed by enhanced ice extrusion rate after pulverization.

3. The total load versus penetration curves demonstrated large load drops during the tests which are indicative of large pieces of ice flaking or spalling. Load build-up resumes after this occurrence.

4. The nominal pressures observed during the 300 mm/s single actuator tests are generally of the same magnitude as those observed during the 100 mm/s tests.

5. The loads and pressures measured with the flat flexible and flat rigid indentors are similar in value, indicating that indentor stiffness does not significantly affect the ice pressures and loads.

6. The tests conducted with flat indentors and wedge shaped ice showed slightly higher pressures than for those conducted with a flat ice surface and wedge shaped indentors. However, this may reflect an aspect ratio effect. The range of indentor wedge angles investigated did not noticeably affect the loads and pressures.

7. Comparing the penetration and acceleration of the indentor results shows a one to one correspondence.

8. Stepping evident in the penetration versus time graphs indicates that, as the ice fails during the sawtooth development, the actuator surges forward and as the load builds the penetration rate decreases. This has important implications on the complete servo-control of the system which is discussed in Spencer and Masterson, (1993).

Peak nominal pressure versus area data from this test series and the data from the Pond Inlet Tests are compared in the paper by Masterson et al, 1992. The agreement is seen to be surprisingly good, the mean of all the 1990 Hobson's Choice data being 6.2 MPa with a standard deviation of the population of 3.4 MPa and the mean of the Pond Inlet data being 4.1 MPa with a standard deviation of the population of 2.7 MPa.

7.3.5 Examples of Time Series Data

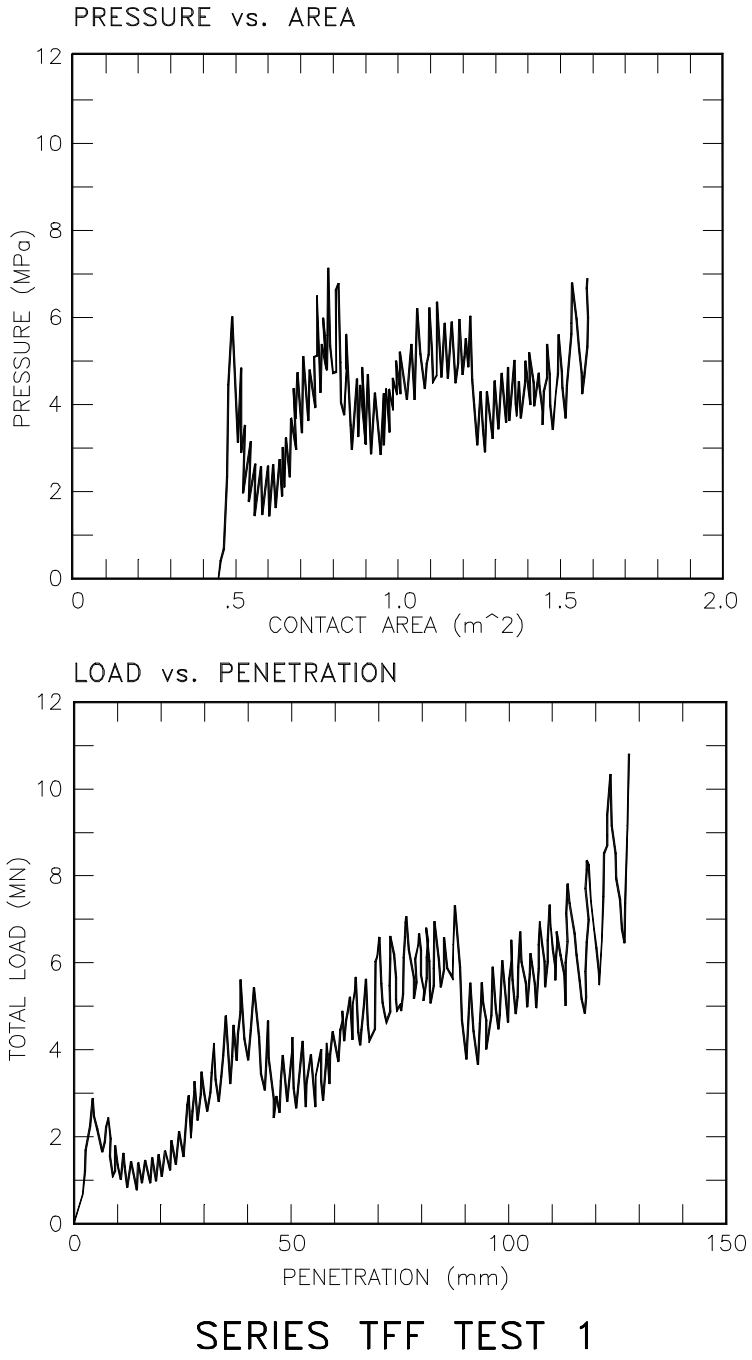

FIGURE 7.5: Time Series of Test TFF 01

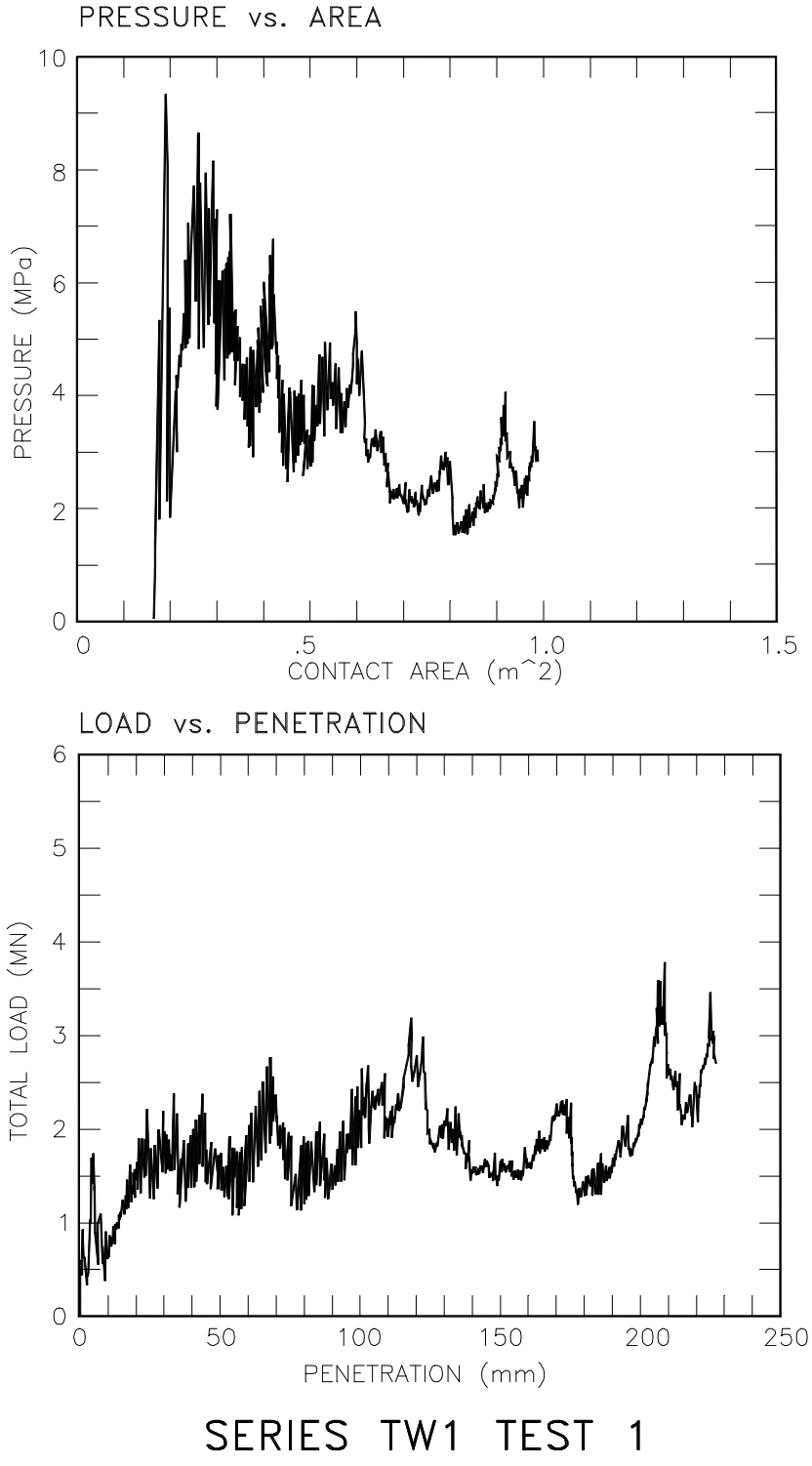

FIGURE 7.6: Test Series of Test TWI 01

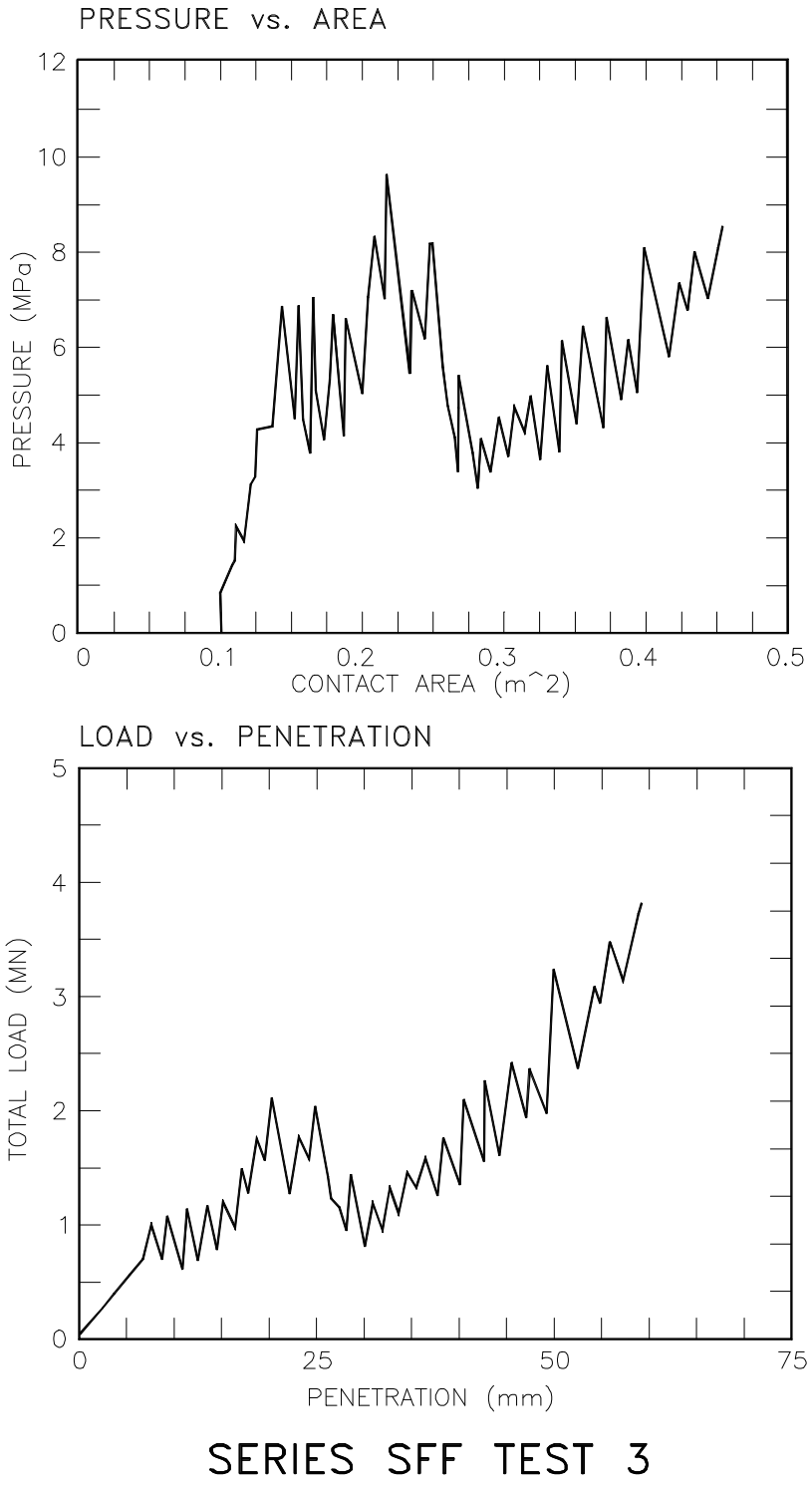

FIGURE 7.7: Time Series of Test SFF 03

7.3.6 Comments on Relevance to Local Ice Loads Due to Icebergs

The ice tested was a cold multi-year ice with strength and stiffness properties similar to those of iceberg ice. The loading scenarios used in the tests are identical to those which would be encountered during an interaction between an iceberg and a structure. Thus the local pressure and loading information is directly applicable to iceberg loading.

8 Flaking Tests in First Year Sea Ice and Lake Ice

8.1 Medium Scale Uniform Pressure Tests: F-Y Sea Ice: 1993

8.1.1 Summary

Data Source:	Medium-Scale Uniform Pressure Tests on First-Year Sea Ice (Sandwell Project No. 113077)
Geographic Location:	Resolute Bay, Nunavut
Time Period:	May 1993
Ice Types:	First-Year 1.8 m thick
Range of Contact Areas:	0.20 to 4.5 m^2
Relevance to Icebergs:	Medium

8.1.2 Background

Loads on Arctic offshore structures generated by ice interactions usually govern their hull design. This is particularly true for icebreakers and bottom founded structures in the Beaufort, Kara and Pechora Seas. While other loading, for example wind, wave or tectonic forces also exist, they are usually of lower magnitude. There is, therefore, considerable economic incentive to quantify the ice generated loads to allow for a safe and efficient design.

A number of medium-scale field test programs to determine the pressures and loads generated by ice crushing against a structure have been conducted over the last fifteen years. The principal advantage of the approach is that it can be conducted at a scale much larger than is possible in a laboratory setting. The disadvantage compared with laboratory tests is that the level of experimental control is less and, in general, because of the higher cost of conducting experiments in the field, only a relatively few tests can be conducted.

Four medium-scale testing programs using hydraulic actuators and indentors have been conducted in the Canadian Arctic, in 1984, 1985, 1989 and 1990. In these programs a rigid indentor was pushed into an ice wall and local pressures and total loads were recorded. The geometry of the test arrangement was chosen so that the propagation of cracks to the free surface would be unlikely. This resulted in the collected pressure data being most applicable to a "local" loading of a structure rather than a "global loading". The principal difference between these two loading situations is the degree of confinement. For local loading, the surrounding ice can provide confinement whereas, for global loading, the full thickness of the ice is loaded and free surfaces can influence the failure mode, average pressure and total loads. Thus there is the possibility for flaking and migration of macroscopic cracks to free surfaces, usually resulting in lower average contact pressures than in the confined configuration. Such full thickness tests have been conducted at medium scale by Esso, the so-called "nutcracker" series of tests in which a cylindrical indentor was forced into the ice sheet. Because the height of the indentor was greater than the thickness of the ice sheet, flaking could occur to the upper and lower surfaces of the ice sheet. In addition, field strength testing using thin walled, highly compliant flatjacks has been conducted in the Beaufort Sea in multi-year ice. The current project expanded upon and complimented the results obtained in these tests, using the flat jacks described in Iyer and Masterson.

The principal aims of the current test program were:

- To conduct tests where the loaded area was close to the top surface of the ice and to investigate the effect of the dimensions of the loaded area on the resulting interaction pressures.

- To reduce the field costs as much as possible without compromising the scientific aims by using a load control system configured for another test program.

In general, the aim was to load as large an area as possible, as quickly as possible in a geometric configuration favourable to the creation of edge flakes. The chosen methodology consisted of placing thin-walled, metal flatjacks into vertical slots cut in the upper portion of the first year ice sheet. The fluid flow into the flatjack(s) was controlled via a high capacity hydraulic servo valve and servo controller. In the majority of the tests, a displacement gauge across the slot near the mid-line of the flatjack was used as the feedback element. With this controlled displacement arrangement the test continued until either the pressure capability of the system was reached or a flake (compression failure) occurred. Because there was a probability that the high fluid pressure would result in failure of the flatjack, a biodegradable hydraulic oil was used (Shell Naturelle HF). The principal independent variables in the test

program were the dimensions of the flatjacks, the configuration of the test slots and the depth below the ice surface at which the flatjacks were mounted. The smallest flatjack was 1.5 x 0.13 m and the largest test comprised two 3.0 x 0.75 m flatjacks. Loading times were in the 0.5 to 50 s range. A total of 26 tests were conducted between May 8 and May 20, 1993 in first year sea ice (Masterson et al, 1994).

8.1.3 Data Attributes

The data acquisition system used a Sheldon 8 channel unit, with 12-bit analogue to digital conversion resolution. This system has built-in low pass filters set to one third of the sampling frequency to avoid aliasing. Generally, data were recorded at 1000 readings per second per channel. The data were automatically transferred to the hard drive of a 486 computer during the test via a RS422 communication bus. After completion of the test, the data were converted into ASCII format and downloaded onto floppy disks. A program written in BASIC was then used to convert the data into a format suitable for entering into a spreadsheet. The spreadsheet program was then used to produce graphs of the data for the test team during the project.

8.1.4 Data Quality and Number of Events

TABLE 11: Test Parameters

Test Number	Max. Recorded Pressure (MPa)	F.J.[1] Width (m)	F.J.* Height (m)	Depth to Top of F.J.* (m)	Aspect Ratio	F.J.* Area (m^2)	Slot Config.[1]	Max. Recorded Load (MN)
1	2.35	0.73	0.73	0	1.0	0.53	S	1.2
2	3.15	0.73	0.73	0	1.0	0.53	S	1.7
3	4.5	0.73	0.73	0	1.0	0.53	S	2.4
4	3.3	1.48	0.21	0	7.2	0.30	S	1.0
5	9.3	1.48	0.21	0	7.2	0.30	S	2.8
6	9.2	1.48	0.21	0	7.2	0.30	S	2.8
7	8.8	1.48	0.21	0	7.2	0.30	S	2.7
8	7.5	1.48	0.11	0	13.3	0.16	S	1.2
9	12.3	1.48	0.11	0.25	13.3	0.16	S	2.0
10	11.5	1.48	0.11	0.5	13.3	0.16	S	1.9
11	11.2	1.48	0.11	0.75	13.3	0.16	S	1.8

Test Number	Max. Recorded Pressure (MPa)	F.J.[1] Width (m)	F.J.* Height (m)	Depth to Top of F.J.* (m)	Aspect Ratio	F.J.* Area (m^2)	Slot Config.[1]	Max. Recorded Load (MN)
12	6.8	1.48	0.11	0	13.3	0.16	H	1.1
13	7.2	1.48	0.11	0.25	13.3	0.16	H	1.2
14	9.8	1.48	0.11	0.5	13.3	0.16	H	1.6
15	10.8	1.48	0.11	0.75	13.3	0.16	H	1.8
16	5.0	0.73	0.73	0	1.0	0.53	H	2.6
17	4.2	0.73	0.73	0	1.0	0.53	H	2.2
18	4.8	1.48	0.73	0	2.0	1.07	H	5.1
19	5.1	2.98	0.73	0	4.1	2.16	H	11.0
20	3.1	5.95	0.73	0	8.2	4.32	H	13.4
21	6.0	2.98	0.73	0	4.1	2.16	S	13.0
22	7.7	1.48	0.73	0	2.0	1.07	S	8.3
23	7.8	1.48	0.73	0	2.0	1.07	S	8.4
24	11.0	0.43	1.48	0	0.3	0.63	S	6.9
25	8.5	0.75	0.73	0	1.0	0.54	S	4.6
26	6.3	5.95	0.11	0	53.6	0.66	S	4.2
Mean	7.2							4.1
Max.	12.3	5.95	1.48	0.75	53.6	4.32		13.4
Min.	2.4	0.43	0.11	0.00	0.3	0.16		1

Notes: *F.J. = Flatjack
1S = Straight Slot
H = H-Shaped Slot

TABLE 12: Flatjack Performance

Test	Number of Flatjackets	Maximum Pressure (MPa)	Flatjack Leaked	Leak Stopped Test
1		2.3		
2		3.2		
3	1	4.4	X	X
4	1	3.5		

Test	Number of Flatjackets	Maximum Pressure (MPa)	Flatjack Leaked	Leak Stopped Test
5	1	9.3	X	
6	1	9.2		
7	1	8.8		
8	1	7.5		
9	1	12.5	X	
10	1	12	X	X
11	1	11.5		
12	1	6.8		
13	1	7		
14	1	9.7		
15	1	10.9		
16	1	5.2		
17	1	4.2		
18	1	4.8		
19	2	5.1		
20	2	2.9		
21	1	4.9	X	
22	1	7.1	X	X
23	1	7.8	X	
24	1	10.5	X	X
25	1	8.1	X	
26	2	6.4		
Total	**27**		**9**	**4**

TABLE 13: Maximum Displacements

Test	Maximum* Displacement (mm)	Time to Maximum Displacement (s)	Time to Maximum Pressure
1	1.9	29.5	29.5
2	3.5	54	54
3	8.4	46	46
4	4	0.53	0.53
5	12.5	2.9	2.9
6	18.7	2.9	2.9
7	12.3	1.9	1.9
8	5	0.48	0.48
9	2.7	3.3	0.9
10	1.3	1	1
11	0.75	3.1	0.9
12	24.6	2.3	1.1
13	--	--	0.62
14	1.3	1.6	1.6
15	1	2.7	2.7
16	13.2	3.2	2.7
17	8.8	1.5	1.5
18	16	4	3.6
19	20.4	3.5	3.2
20	16.1	7.9	7.9
21	19.5	4.4	4.4
22	17.1	2.4	2.4
23	22.7	4.3	4
24	6.2	1	1
25	9.6	1.2	1.2
26	9.4	1.1	1.1

Notes: *LVDT #1 Transducer Movement

8.1.5 Examples of Time Series Data

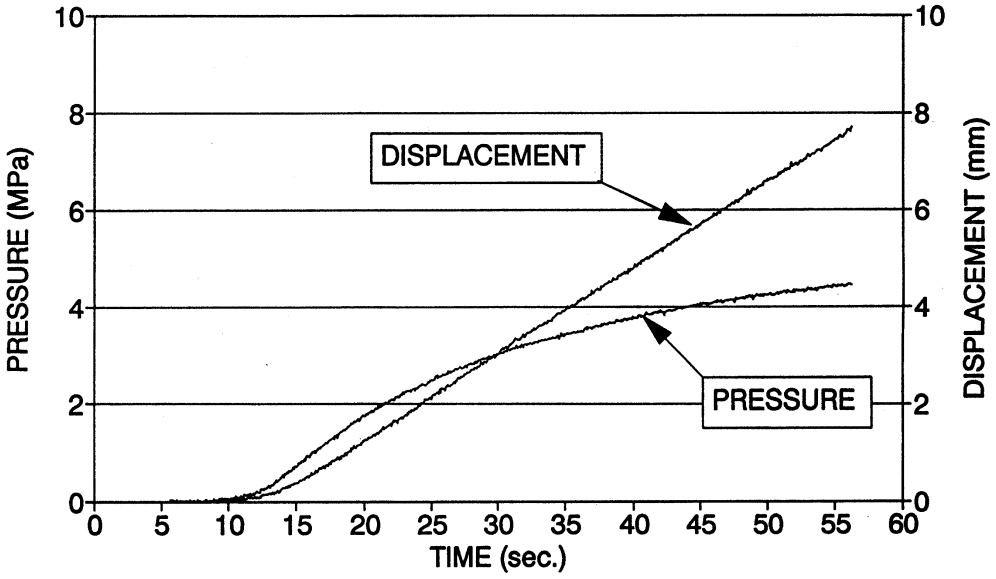

FIGURE 8.1: Example of Time Series

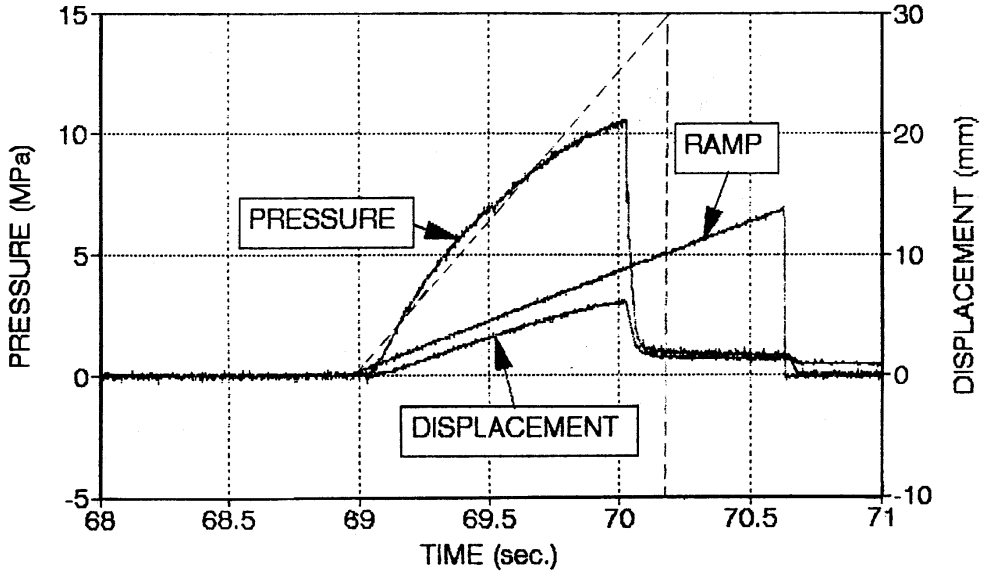

FIGURE 8.2: Example of Time Series

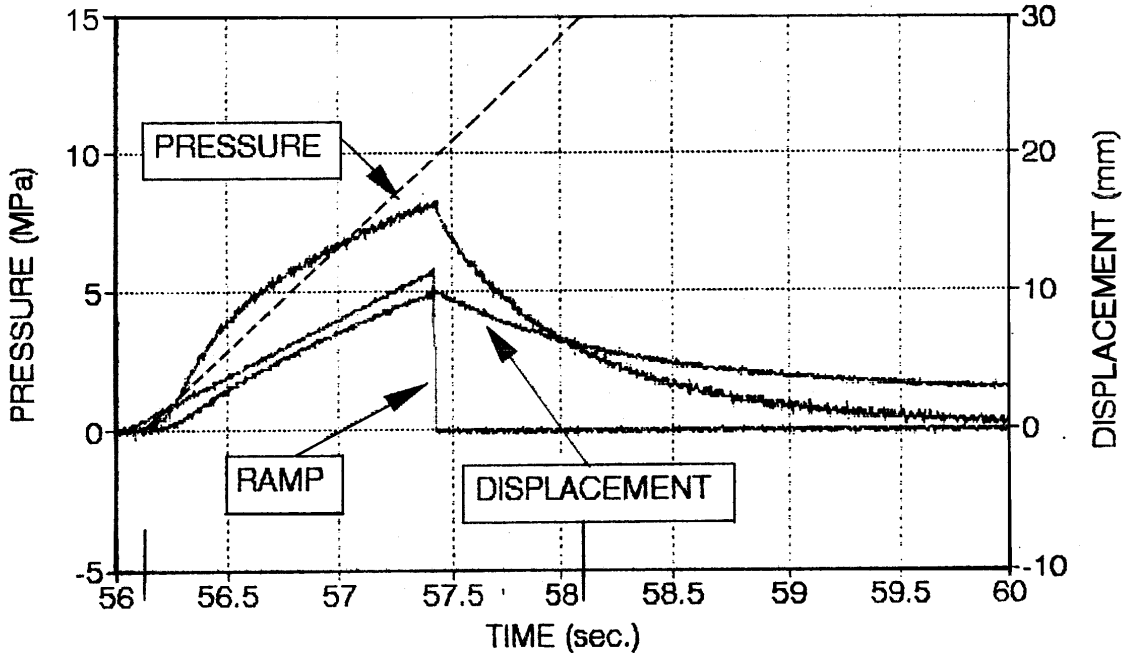

FIGURE 8.3: Example of Time Series

8.1.6 Comments on Relevance to Local Ice Loads Due to Icebergs

Tests were conducted on first year sea ice at relatively slow loading rates, and so have limited application to icebergs. Adjustments for slicing effects resulted in there being essentially no pressure/area dependence up to an area of 4.5 m^2.

8.2 Ice Flaking Tests: Fresh Ice: 1994

8.2.1 Summary

Data Source:	Ice Flaking Tests Conducted with a Gas Actuator System
Geographic Location:	Calgary, Alberta
Time Period:	February 1994
Ice Types:	Fresh

Range of Contact Areas: 0.3 m^2

Relevance to Icebergs: High

8.2.2 Background

Since 1969 when Esso first conducted tests on the first-year ice in Tuktoytaktuk Harbour, NWT by pushing pairs of steel piles against the full ice sheet thickness (the "Nutcracker Tests") to determine the pressure ice could exert on offshore structures, there have been efforts to devise methods of deriving global ice loads on structures by means of small or medium scale tests. Since the time of the early tests, gravity base structures have been placed in the Beaufort Sea and full-scale load measurements have been made. Large-scale data has also been obtained from ship trials wherein load measurements have been made while ramming thick multi-year ice. Forces were also measured at Hans Island when southward drifting multi-year ice impacted the island.

While these measurements have contributed considerably to our knowledge of the global forces on structures and ship hulls, the constraints of the measurement programs result in sufficient uncertainty to cast doubt on the accuracy of the measurements, limiting their reliability for use in design. There is still much controversy over the magnitude of loads experienced by the Molikpaq and the loads measured at Hans Island are considered to be lower bound. Thus there is still a need to develop and utilize methods which will lead to an understanding of the processes at work in ice/structure or ice/hull interaction which will also yield large scale values of ice pressure and load.

A technique for testing ice strength was developed in the 1970's which consisted of using the walls of pits excavated in the ice along with a hydraulic ram and load plates. The ice itself formed the "load frame" with the ram reacting against one wall with a larger plate and the other wall with a smaller plate, under which failure of the ice would occur. These tests were small scale but the plates could be shaped to model structural sections or the entire structure itself. Since the tests could only be reasonably conducted at small or medium scale, it was not possible to model large scale interactions.

The use of the flat jack, a thin walled, flat envelope of steel which is fitted into an ice slot and into which fluid is pumped to achieve the failure load of the ice, made it possible to load much larger areas of the ice at relatively low cost. Tests conducted with these flat jacks to areas of 4.5 m^2 showed that the strength of competent, intact ice did not change significantly with the size of loaded area. The compliant flat jacks themselves provided a perfect loading with no stress concentrations over the loaded area, allowing the ice to fail uniformly and to deform visco-elastically. This was conclusively demonstrated in 1993 during the Resolute Bay tests. In most cases the ice did not fail but deformed sufficiently to allow the flat jack to burst or else the ice was able to simply resist the available pressure from the accumulator.

It was reasoned that if a stiff plate were placed in the ice slot alongside the flatjack, then the resulting stress concentrations from the stiff plate would result in a lower failure pressure more reasonably approximating that measured on large structures and ships. This past program outside Calgary in February 1994 used a 76 mm thick aluminium plate. However, so perfect are the saw cuts made using a specially built guide, that the pressures, while reduced somewhat, still resembled those measured in the laboratory. An aluminium plate 1.5 m by 0.2 m by 76 mm thick was able to produce pressures of around 5.5 MPa. Meanwhile, average pressures on large structures due to global loading of 1 to 2 MPa have been measured.

Some of the tests during this program had been conducted, as at Resolute, with no rigid plate and in some tests the ice had been deformed and damaged but had not flaked. Two additional tests with the rigid indentor were run in this pre-damaged ice and the pressures obtained averaged 1.5 MPa, a value in line with global pressure measured on large structures. This constitutes a very important observation and provides concrete direction for tests aimed at determining global loads on large structures in the future.

8.2.3 Data Attributes

A brief description of the tests is provided below:

Test 1

- First test using an indentor. Maximum flatjack pressure of 5.53 MPa achieved in 2.22 sec. Flaking of ice occurred adjacent to indentor. Cracking of ice adjacent to flatjack but not flaking. Manual flow choke set to limit the loading rate. The motion of indentor after the ice flaking indicated that the indentor tie-downs are important.

Test 2

- First test using a bare flatjack. The pressure reached 4.38 MPa causing extensive cracking but no flaking. The flatjack came out of the slot resulting in flatjack failure. Loading time was 0.53 sec. Because of the low stiffness of the gas within the flatjack the surface flaking events prior to general flaking failure of the ice face are indicated by pressure transients rather than by large pressure drops.

Test 3

- Another test using the rigid indentor plate. Extensive flaking and cracking adjacent to indentor, cracking only adjacent to flatjack. To reduce the possibility of the flatjack coming out of the ice, friction tape was applied to both sides of the flatjack. Friction tape was used in all subsequent tests. Air temperature +4.3 deg. C at test time.

Test 4

- A bare flatjack test, air temperature had reached +8.0 deg. C by test time. The flatjack reached maximum pressure in approximately 3 sec causing extensive cracking and uplifting of ice adjacent to flatjack. No flaking occurred and air supply switch maintained at open. At about 20 sec into the event flaking occurred resulting in the failure of the flatjack.

Test 5

- An test conducted using an air temperature -14.0 deg. C. IMD personnel now on-site to record the ice failure using monochrome 1000 frame/second video camera system. Approximately 2.8 sec loading time with flaking adjacent to indentor.

Test 6

- Test conducting with bare flatjack. However, used the two indentor plates across the flatjack to act as inertial ballast. Loading time 1.9 sec prior to final failure. Two or three flaking events were observed in video.

Test 7

- An indentor test with flaking adjacent to indentor. No failure occurred in the flatjack.

Test 8

- A test conducted using an indentor, flaking occurred at 5.5 MPa. Test conducted late in the day at 5:45 p.m. and the ambient light levels were only sufficient to allow high speed video system to record at 500 or 250 frames/second even with illumination.

- ***Test 9***

  - For all subsequent tests the manual choke at the outlet of the accumulator was set fully open to increase the loading rate. Test conducted using an indentor with pressure reaching 8.43 MPa in 2.33 sec with flaking adjacent to indentor.

Test 10

- Bare flatjack test. Reached the maximum supply pressure with cracking but no flaking. The supply pressure was removed after 3 - 4 sec rather than allowing the ice to creep to failure.

Test 11

- Second loading with bare flatjack using same set-up as Test 10. No flaking occurred but some additional cracking. Again removed pressure after about 4 sec. The flatjack was removed for later use.

Test 12

- Increased the accumulator pressure to approximately 10.8 MPa. Bare flatjack test reached 9.5 MPa in about 1 sec. The ice at one end of the flatjack flaked allowing the flatjack to expand and fail.

Test 13

- Because of the good consistency between bare flatjack tests and because the reduction in flatjack pressure at failure due to the presence of the indentor was only about 20 - 30%, it was decided to investigate damaging the ice prior to a test with an indentor. In this test a series of vertical saw cuts (5 mm wide, 10 mm deep, 100 mm spacing) were made in the ice adjacent to the indentor. Flaking flatjack pressure reached 6.8 MPa in 0.84 sec so no large reduction in pressures due to the presence of the saw cuts.

Test 14

- A continuation of the damaged ice investigation. Used the ice previously loaded during Test 2, to conduct this test using an indentor. The results from Tests 10 and 11 showed that re-loading with the flatjack in exactly the same location resulted in no significant change in maximum pressures, indicating that, while damaged, the ice was not "failed". As illustrated cracks emanate from near the end of the flatjack or indentor. For this test the centre of the indentor was arranged to be at these end cracks. The indentor and flatjack for this test were parallel to the slot for Test 2. Maximum flatjack pressure of 2.08 MPa only was reached in this test!

Test 15

- An indentor test using the predamaged ice from Test 12 location. Similar geometrical arrangement as for Test 14. Only reached 1.54 MPa flatjack pressure before flaking occurred.

Test 16

- A larger 1.5 x 0.5 m flatjack used for full thickness test with bare flatjack. Reached 6.24 MPa pressure and flaking allowed flatjack to expand and fail at both ends. Flatjack landed about 2 m away from test.

8.2.4 Data Quality and Number of Events

TABLE 14: Test Matrix

Test	Date	Time	Configuration	Comments
1	14 Feb.	0.458	1.5 x 0.2m + Indentor	Indentor Test
2	14 Feb.	0.613	1.3 x 0.2m Flatjack	Bare Flatjack
3	15 Feb.	0.583	1.5 x 0.2m + Indentor	Indentor
4	15 Feb.	0.542	1.5 x 0.2m Flatjack	Bare Flatjack
5	16 Feb.	0.469	1.5 x 0.2m + indentor	Indentor Test
6	16 Feb.	0.604	1.5 x 0.2m Flatjack	Bare Flatjack
7	16 Feb.	0.674	1.5 x 0.2m + Indentor	Indentor Test
8	16 Feb.	0.74	1.5 x 0.2m + Indentor	Indentor Test
9	17 Feb.	0.469	1.5 x 0.2m + Indentor	Indentor Test
10	17 Feb.	0.583	1.5 x 0.2m Flatjack	Bare Flatjack
11	17 Feb.	0.604	1.5 x 0.2m Flatjack	Same location as 10
12	17 Feb.	0.653	1.5 x 0.2m Flatjack	Bare Flatjack
13	17 Feb.	0.729	1.5 x 0.2m + Indentor	Indentor Test - Notched Face
14	18 Feb.	0.438	1.5 x 0.2m + Indentor	Damaged Ice Test - Same location as 2
15	18 Feb.	0.51	1.5 x 0.2 m + Indentor	Damaged Ice Test - Same location as 12
16	18 Feb.	0.618	1.5 x 0.5m Flatjack	Full Thickness Test

TABLE 15: Test Data

Test	Ice Temperature (deg. C)	Maximum Flatjack Pressure (MPa)	Cracks Detected at Pressure (MPa)			Indentor Pressure (MPa)	Loading Time (sec)	Loading Rate (MPa/s)
1	-5.6	5.53				4.61	2.22	2.49
2	-4.1	4.38					0.53	8.26
3	-0.8	6.82				5.68	4.21	1.62
4	-0.5	8.01	7.16	7.5	8.0		2.19	3.66
5	-8.0	6.81				5.67	2.78	2.45
6	-7.0	8.32	6.57	7.08	7.42		1.89	4.4
7	-8.0	7.56	7.07			6.30	1.81	4.18
8	-8.0	4.95	4.0			4.12	1.26	3.93
9	-9.2	8.43	7.95	8.35		7.02	2.33	3.62
10	-10.0	8.47	7.07	8.37			1.33	6.37
11	-10.0	8.98					2.33	3.79
12	-9.3	8.71					0.83	10.49
13	-9.8	6.18	4.93			5.15	0.84	7.36
14	-14.0	2.08				1.73	0.26	8
15	-13.0	1.54				1.38	0.27	5.7
16	-13.6	6.24					1.56	4

8.2.5 Example of Time Series Data

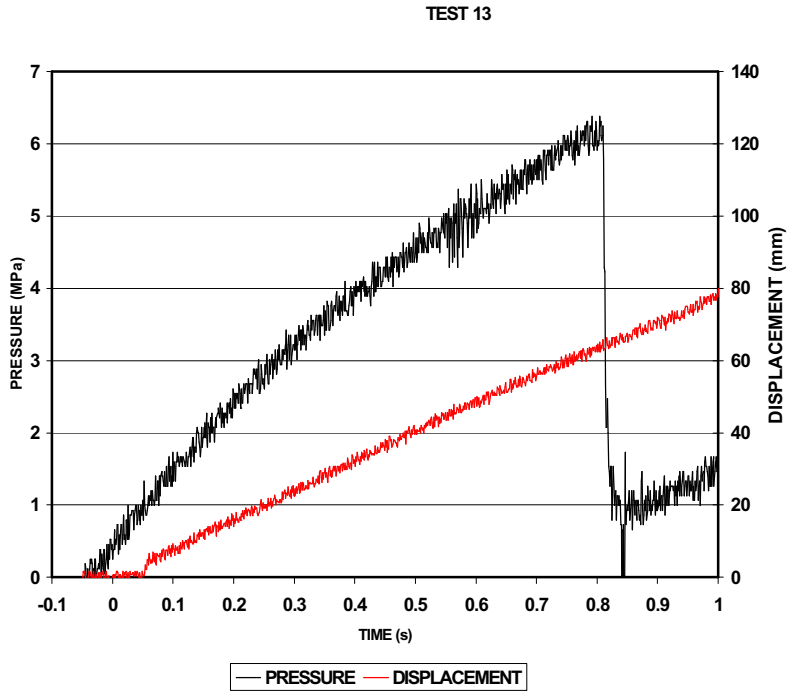

FIGURE 8.4: Time Series for Test 8

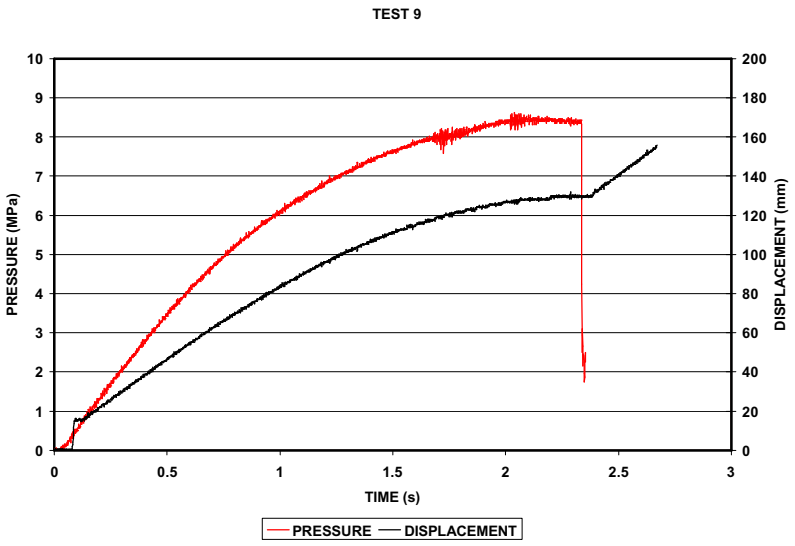

FIGURE 8.5: Time Series for Test 9

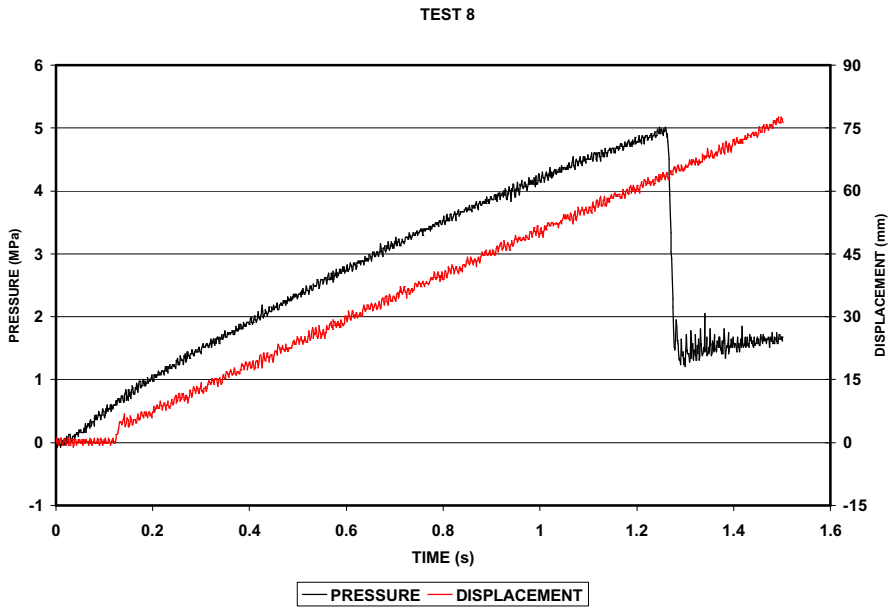

FIGURE 8.6: Time Series for Test 13

8.2.6 Comments on Relevance to Local Ice Loads Due to Icebergs

Tests were conducted on fresh water ice over a range of temperatures directly applicable to iceberg impacts. The tests also indicate that the boundary conditions are important in determining contact pressures and loads and that pre-damaging the ice can result in significant reductions in pressure.

8.3 Flaking/Crushing Tests: Tuktoyaktuk Harbour: 1997

8.3.1 Summary

Data Source:	Large Scale Hull Loading of Ice in Tuktoyaktuk Harbour (Sandwell Project No. 142051)
Geographic Location:	Tuktoyaktuk Harbour, NWT
Time Period:	March - April 1997
Ice Types:	Fresh

Range of Contact Areas: 0.3 m^2

Relevance to Icebergs: High

8.3.2 Background

INSROP (International Northern Sea Route Programme) Project I. 1.7 addressed the issue of large-scale, ship hull - ice loading, which would be encountered sailing along the Northern Sea Route. Previous work done on ship hull - ice loads has either been measurements with actual ships, small-scale model basin tests, or controlled field tests. This project falls into the last category. Phase 1 of this project, (Masterson et al, 1997) identified the need for further tests on sea ice, focussing on the effects of prior damage on strength, as well as control of the rate of loading. To fulfil this requirement, a series of tests was carried out at Tuktoyaktuk in the Canadian Arctic. The concept behind these Phase 2 tests was to simulate the impact of a ship hull with an ice cusp. A hydraulic actuator was used to press an indentor plate against the edge of an ice sheet. The objective was to generate loading over a large contact area, 0.3 m^2 with a high aspect ratio, i.e., the ratio of the length to height of the contact patch was up to 8:1. The results provide information on the strength of damaged ice at large scales. The present paper first summarizes the results of Phase 1, describes the apparatus used, and presents the results of finite element calculations of stress distributions and deformation for intact ice. It then examines trends in the results of the field tests such as degree of damage, loading time and rates. The results are then compared with other field tests and discussed in relation to the recommendations of the Canadian Arctic Shipping Pollution Prevention Regulations for local hull ice pressure.

Phase 1 (Masterson et al, 1997) provided results of flaking tests using flat jacks to measure the large-scale strength of ice. The results showed:

- Gas filled flat jacks worked well provided certain safety precautions were taken.
- The measured flat jack ice strength pressures were high, about 8.5 MPa.
- The use of a stiff aluminium plate in conjunction with the compliant flat jack reduced the measured pressures somewhat, but they were still around 5.5 MPa.
- Two tests on pre-damaged ice gave significantly lower pressures of about 1.5 MPa.

These tests were conducted on lake ice. It was decided, therefore, that Phase 2 should concentrate on studying the effect of prior damage on the strength of sea ice.

Indentor Equipment

The test system is described here is shown schematically in *Figure 8.7*. A rectangular trench 0.7 m across, 0.33 m deep and 2.5 m long was excavated in the ice. Ice thickness was approximately 1.7 m. The loading system could generate a load of up to 2 MN on a 0.3 m^2 (1.5 m wide by 0.2 m high) indentor, through two actuators. The indentor was 184 mm thick aluminium, so it could be considered rigid. A control system allowed actuator rates to be controlled at speeds up to 50 mm/s and for strokes up to 200 mm. The force generated on the ice face was reacted through each actuator to 0.33 m high plates that bore on the back of the trench. The test procedure involved loading the ice at a particular rate to a pre-determined level to produce damage in the ice. This pre- loading could be done with flatjacks, as had been used in Phase 1, or with an expanded metal grill. In the field it was found that the grill was much easier to use than the flatjacks. After being damaged the ice was subsequently loaded to measure the strength of the damaged ice. Damage applied to the ice by the grill was of two types. The first was cracking that extended some distance, about a metre, from the indentor. The second type was quite local damage from the pattern of the grill that extended only a few cm into the ice.

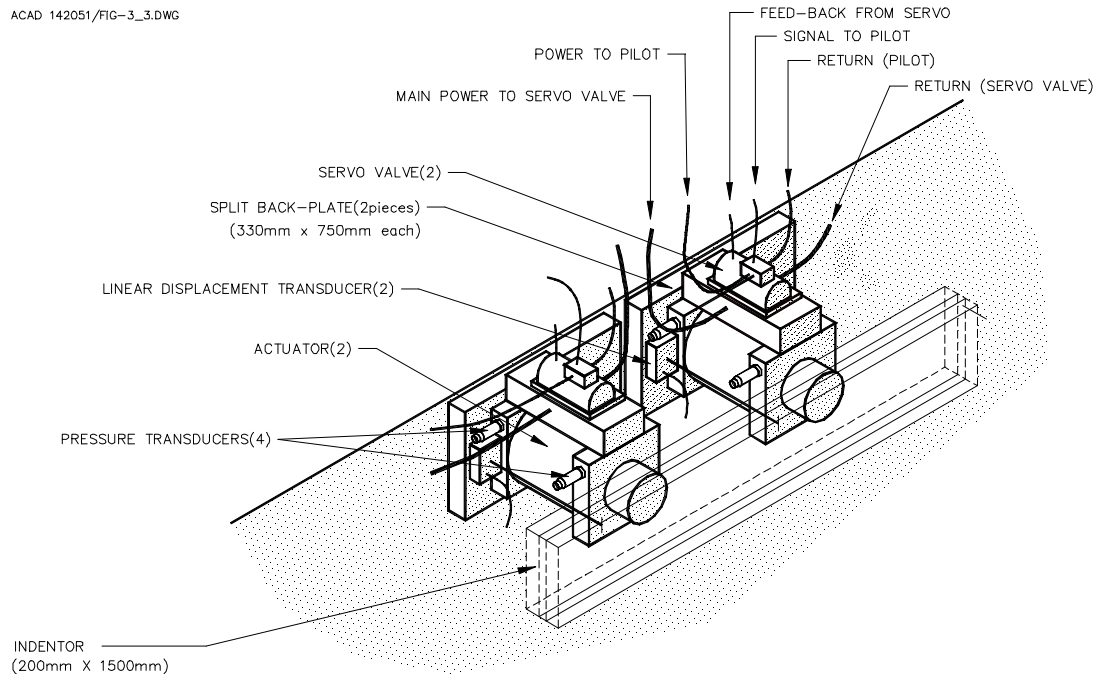

FIGURE 8.7: Schematic of Indentor Equipment

8.3.3 Data Attributes

TABLE 16: Data Acquisition System Characteristics for Fast Tests

Parameter	Value
Number of Channels	16.
A/D Resolution	12 bit.
Sampling Speed Per Channel	1000 Hz (nominal).
Capture Window	10 sec (nominal).
Data Storage	Direct to hard drive in Binary format.
Data Display	Pre-test signal levels in volts. Graph of loads in engineering units. Graph of displacements in engineering units. Graphs of local pressures in engineering units. Maximum value of signals in engineering units.

8.3.4 Data Quality and Number of Events

In this section the results of *Table 17* will be examined from a number of different perspectives. The tests can be divided into two groups:

- Tests 1 to 6 at high speed under deformation rate control (50 mm/s).
- Tests 7 to 11, which were at low speed (0.1 mm/s), without deformation control.

This change in test procedure was necessitated because of the failure of a seal during the test program, precluding the servo-control system from being used. This occurred during the damage loading phase of Test 7. Subsequent tests were conducted by using a small pump to pressurize the actuators, with the result that the tests were run at a low speed and with no displacement control.

TABLE 17: Results of Tuktoyaktuk Damaged ice Tests, 1997

Test No.	Type	Damage Pressure MPa	Failure Stress MPa	Displacement (mm)	Time to Peak Load (sec)	Stiffness MN/mm
1	F	--	1.58	5.24	0.113	0.09
02D	D-Fj	0.55	--	--	577	--
2	D-Fj	0.87	--	--	411	--
02F	F	--	0.65	2.99	0.128	0.065
3	D-Gr	3.78	--	30.71	1.811	0.037
03F	F	--	2.12	12.03	0.244	0.053
04D	D-Gr	1.59	--	8.34	1.187	0.057
04F	F	--	5.08	9.46	0.172	0.161
05D	D-Gr	0.85	--	12.54	1.366	0.02
5	D-Gr	1.82	--	13.2	0.626	0.041
05F	F	--	4.4	26.51	0.237	0.05
06D	D-Gr	1.71	--	18.82	0.881	0.027
06F	F	--	2.18	11.52	0.163	0.057
07D	D-Gr	2.2	--	25.36	1.196	0.026
07G	F	--	2.89	24.52	151	0.035
08D	D-Gr	1.82	--	21.96	216.2	0.025
08F	F	--	4.96	7.43	77.94	0.2
09D	D-Gr	3.98	--	19.54	92.9	0.061
09F	F	--	7.86	14.94	180	0.158
10D	D-Gr	5.35	--	23.5	153.5	0.068
10F	D	7.78	--	12.37	317.9	0.189
10G	D	7.99	--	36.41	482.1	0.066
11D	D-Gr	8.24	--	34.65	473.6	0.071

Explanation for the symbols in the column headed "Type" are as follows:

- F: Monotonic loading to failure.
- D-Fj: Damage loading with a flatjack.
- D-Gr: Damage loading with an expanded metal grid.

In addition to the directly measured values of stress, deformation and time, stiffness has been calculated. The stiffness for each loading has been defined as the maximum load divided by the maximum deformation at the instant of maximum load. The maximum load used for the stiffness calculation is the maximum pressure or stress of *Table 2* times the indentor area of 0.3 m^2.

8.3.5 Examples of Time Series Data

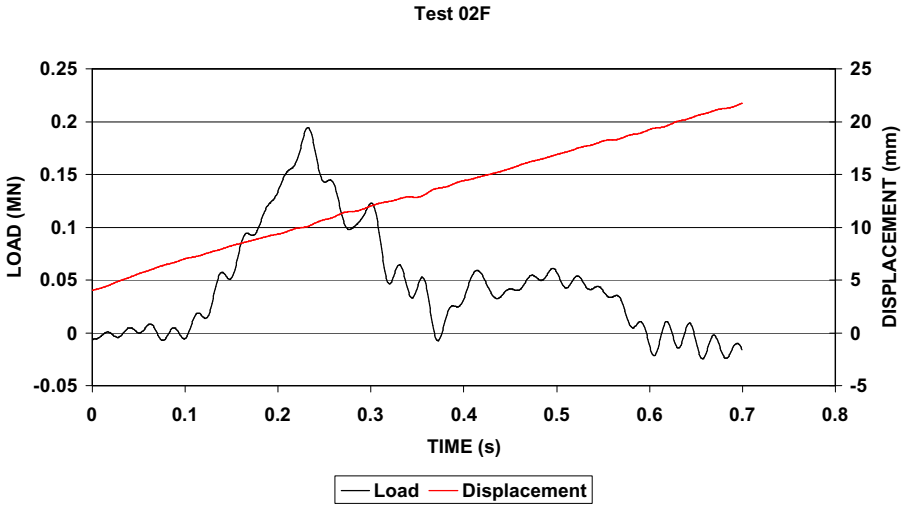

FIGURE 8.8: Load and Displacement Time Series, Test 02F

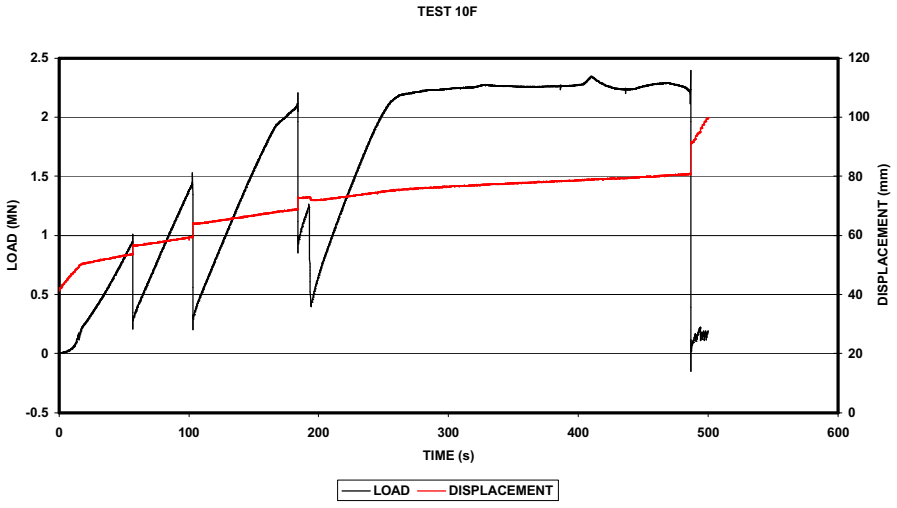

FIGURE 8.9: Load and Displacement Time Series, Test 04F

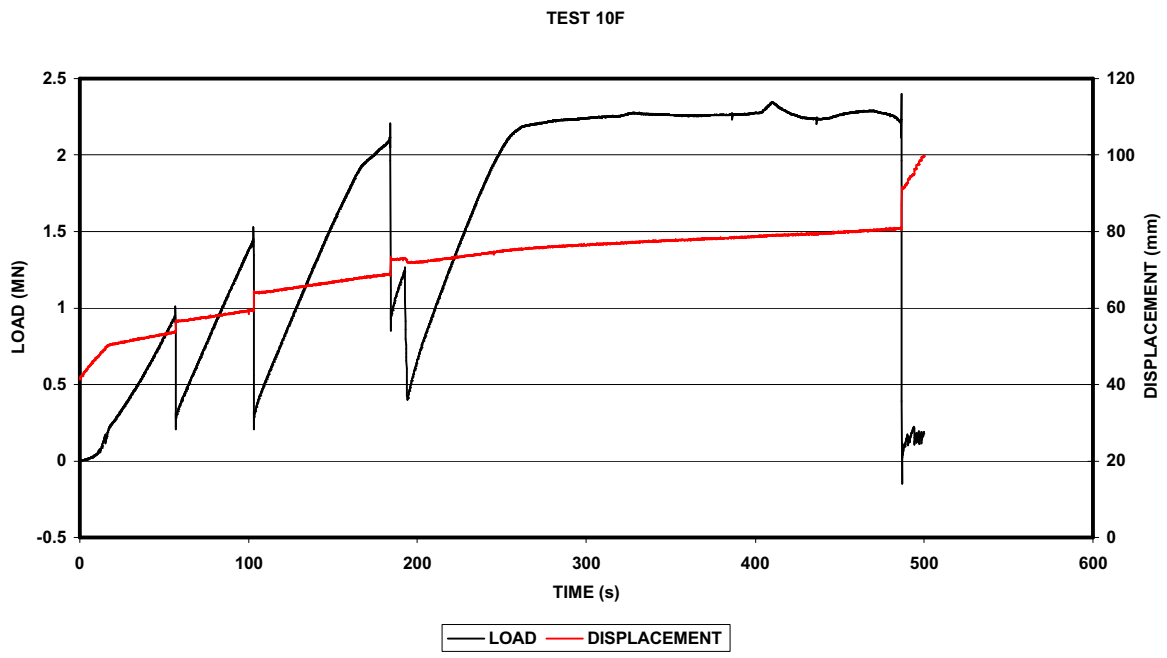

FIGURE 8.10: Load and Displacement Time Series, Test 10F

8.3.6 Comments on Relevance to Local Ice Loads Due to Icebergs

Tests were conducted on 1.8 m thick fresh water ice and are applicable to local loads due to iceberg. Ice temperatures during the tests were -20 deg. C or colder and thus data values may have to be adjusted for temperature effects.

9 Iceberg Impact Experiments

9.1 Summary

Data Source:	C-CORE Iceberg Impact Experiment
Geographic Location:	Grappling Island, Labrador
Time Period:	Summer 1995
Ice Types:	Icebergs, Bergy Bits, Growlers
Range of Contact Areas:	0.02 to 2.17 m^2
Relevance to Icebergs:	High

9.2 Background

The C-CORE Iceberg Impact Experiment was conducted at Grappling Island, near Packs Harbour, Labrador, in July, 1995. A 6 m x 6 m panel containing 36 instrumented triangular sub-panels was mounted to a rock face and icebergs were towed into the panel as illustrated in *Figure 9.1*. The iceberg loads measured in this experiment have yielded the most comprehensive data set documenting the iceberg impact process.

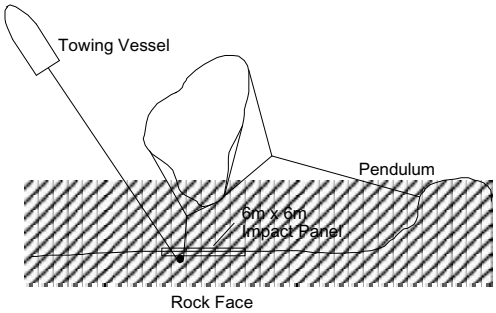

FIGURE 9.1: Illustration of the 1995 Iceberg Impact Experiment Set-Up

The overall purpose of the field program was to identify the relationship between iceberg crushing pressure, contact area, and shape, and to advance the understanding of the kinematics involved in iceberg collisions with structures. This was achieved through direct measurement and interpretation of contact loads and pressures resulting from full-scale iceberg impacts on an offshore structure. By deploying a large instrumented load measurement panel on a cliff, and towing ice pieces into the panel, realistic impact dynamics were achieved.

The load panel consists of a sub-frame of "I" beams with feet contacting the cliff at 16 points (on a 2 m grid) as illustrated in *Figure 9.2*. Each sub-panel, made of triangular steel plate, has a surface area of 1 m^2 and was connected to the frame via a 75-ton capacity load cell under each corner of the triangle. In total, there were 108 load cells in the panel. In addition to the force data from each load cell, each impact was recorded with both the overhead video camera (mounted on a jib boom 11 m above the water, looking down on the panel) and a hand-held video camera. The video record provides quantities such as iceberg size, impact speed, and impact angle, in addition to qualitative information on each impact.

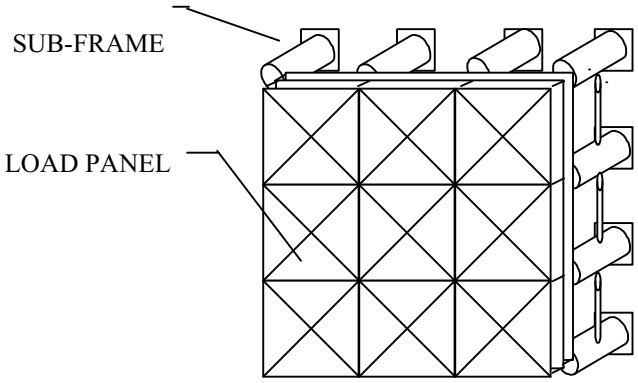

FIGURE 9.2: Triangular Load Panel and Sub-Frame

Twenty-nine iceberg impact events were recorded over a 10-day period, of which 21 were used in subsequent analyses. Impact speeds ranged from 0.3 m/s to 1.9 m/s, and ice masses ranged from 180 tons to approximately 1,000 tons.

The results indicated significantly lower ice loads than would have been deduced using existing techniques and knowledge base. The best fit pressure/area relationship for the 1995 iceberg impact data is:

$$P = 0.73A^{-0.65}$$

where A is the actual contact area and P is the corresponding average pressure. The constant *0.73* is considerably lower than values derived from previous studies, and is believed to be a product of the warm air and water temperatures.

Data release is subject to approval from all project participants.

9.3 Data Attributes

Twenty-nine iceberg impact events were recorded. One of these impacts could not be used because of a malfunction in the DA system. Another event had to be dropped as the registered load was too low. Additional five impacts have been dropped because the ice struck the side of the panel. Twenty-two events were considered good impacts. These data are summarized in *Table 18*. *Table 19* describes the columns in *Table 18*.

For each impact, the forces on the 108 load cells were sampled at a rate of 100 Hz and filtered at 50 Hz over a 20-second duration. The duration of impact ranges from 0.23 to 2.29 seconds, and the contact area range from 0.02 to 2.17 m^2. The Grappling Island ice was actively melting, relatively warm, and had a steep temperature gradient with cold ice in the interior.

The raw data are stored in an ASCII format containing matrices with 2,000 row (20 seconds of data collection at 100 Hz) and 110 columns (1 time channel, 108 load cells, and a voltage monitor).

Time series for global force, contact area, and local pressure for each impact were reduced from the force data from each load cell. The local pressure is highly dependent upon the estimates of contact area. Several collisions only impacted a single panel indicating the contact area was 1 m^2 throughout the crushing process. A triangle method, using the distribution of load on the three load cells of the individual panel, was used to identify the loaded sub-region on each triangular panel for each instant sampled in time. The method gave a better representation of the contact area. The local pressure was evaluated based on global force and the actual contact area.

Figure 9.3 shows processed data from a typical impact. The graphical display includes:

- A view of the collision from an overhead camera.
- A load versus time varying forces measured on the load cells.
- Changes in the distribution of impact loads over the area of panel as impacts progressed.
- Additional information including mass of the berg, initial contact velocity, force, pressure and calculated contact area.

9.4 Data Quality

The evaluation of critical information such as iceberg mass, contact surface shape, crushed area and eccentricity could only be approximated because accurate measurements on above-water profiles and underwater profiles including contact surface, were not taken during the experiment. This limited any conclusions that could be drawn from this effort.

The spatial resolution of the instrumented panel made it difficult to assess the contact areas during a collision. In some cases, impacts only registered on a single panel, suggesting that the contact area was uniform at 1 m^2. Therefore, contact areas were calculated using estimation techniques such as the triangle method. Subsequent Monte Carlo simulations indicated that the triangle method of contact area estimation gave reasonable results and provided a quantitative measure of the uncertainty in the area estimate.

There were two impacts in which panels with non-functioning load cells were contacted by the ice (Impact Nos. 23 and 28). In these instances, the forces in the non-functioning cells were assumed to be the average of the forces recorded in the two adjacent load cells.

9.5 Examples of Time Series Data

Examples of the changes in pressure, force, and contact area during three selected impacts are given in *Figures 9.4, 9.5 and 9.6*. For clarity, only selected portions of the impact are shown in these figures, but they all include the portion of the impact where the peak force occurred. In some of the impacts (e.g., Impact No. 28 in *Figure 9.6*) the variations in contact area and pressure are quite smooth. In others (e.g., Impact No. 31 in *Figure 9.5*), there are abrupt fluctuations in area. Although the "nominal" contact area might be expected to

increase rather steadily during an impact, our estimate of contact area is derived from the applied load, and spalling events will result in rapid reductions in actual, as opposed to nominal, contact area. The contact area based in applied force is therefore an underestimate of nominal contact area, and results in an overestimate of pressure, as defined in previous pressure/area analyses.

Although pressure/area relationships are normally defined at peak force only, the impact tests contain forces measured at 100 Hz over the entire duration of the impacts. This makes it possible to calculate pressure/area data points for several thousand instants in time. The 22 impacts have yielded 23,952 pressure/area pairs, which is well suited to probabilistic treatment.

9.6 Comments on Relevance to Local Ice Loads Due to Icebergs

The iceberg loads measured in this experiment have yielded the most comprehensive data set documenting the iceberg impact process. The mechanical behaviour of the Grappling Island ice is representative of conditions during real iceberg/structure interactions. However, the penetration depths in the Grappling Island tests (the distance into the ice to which ice was crushed) were not large, and most of the crushing occurred in the warm ice near the surface. If much larger penetration depths had been obtained, the crushing of cold, isothermal ice may have led to increased pressures. This is an important consideration if the pressure/area relationship from the Grappling Island data is extrapolated to larger contact areas corresponding to greater penetration depths.

Actual contact areas were estimated for the 1995 iceberg impact experiments. In practice, nominal contact areas are used for design and nominal areas have been estimated based on correlation with the above-mentioned sources. The triangle method of contact area estimation gives reasonable results. However, it is well known that the pressure distribution within the contact area is far from constant. Numerous indentor and ship ramming tests have shown that much of the force is applied through relatively small "critical zones" within the nominal contact area. The accuracy of the derived pressure/area relationship is a function of the accuracy of the technique used to estimate contact area. Analysis of these techniques indicate that both the constant and exponent in the pressure/area relationship are fairly insensitive to the estimation technique used, although there is considerable uncertainty for small contact areas, particularly those less than 0.5 m^2.

TABLE 18: Summary Table for the 22 Impacts Analyzed
(see *Table 19* for a Description of the Column Headings)

Impact No.	Angel of Impact (deg.)	Speed of Impact (m/s)	Mass (t)	Impact Duration (sec)	Time to Peak (sec)	Peak Force (MN)	Peak Contract Area (m^2)	Average Pressure (MPa)	Total Impact Energy (kJ)
11	16.8	0.57	50	1.14	0.65	0.43	0.96	0.44	81
21	19.3	1.59	200	0.7	0.22	0.69	0.86	0.81	253
22	32.4	1.54	200	0.3	0.2	0.67	0.35	1.79	237
23	3.2	1.86	190	0.51	0.26	0.88	2.17	0.37	329
24	2.7	1.64	180	1.08	0.08	0.16	0.32	0.49	242
25	37.8	0.77	1000	2.29	0.1	0.26	0.34	0.59	296
26	9.8	0.47	900	0.38	0.21	0.57	0.11	4.17	99
27	0.5	1.06	700	0.89	0.5	1.54	0.84	1.82	393
28	21.7	1.05	600	0.35	0.25	2.94	2.14	1.57	331
29	31.1	0.99	500	0.41	0.14	2.03	1.48	1.42	245
30	21.4	0.85	500	1.16	0.5	2.09	0.02	11.42	181
31	14.8	1.89	450	0.76	0.57	0.66	0.85	0.77	804
32	4.3	0.76	430	0.23	0.07	0.14	0.22	0.67	124
33	14.5	0.99	250	0.38	0.2	1.88	1.03	1.69	123
35	17.4	0.85	250	0.51	0.38	1.05	0.86	1.23	90
36	30.7	0.36	600	1	0.64	0.75	0.17	4.02	39
37	3.7	0.38	500	0.89	0.45	0.47	0.08	4.97	36
38	36.9	0.66	500	0.63	0.33	0.66	0.09	5.94	109
39	57.5	0.79	500	0.51	0.4	0.71	0.1	6.7	156
45	20.5	0.56	300	1.2	0.66	0.21	0.71	0.25	47
46	49.3	0.85	300	1.43	1.1	0.09	0.39	0.14	108
47	30.3	0.9	300	1.11	0.55	0.18	1.33	0.13	121

TABLE 19: Description of Columns in Summary Table

Column Title	Description
Impact No.	Impact data file number.
Angle of Impact	Angle of ice motion at impact from normal to the panel (i.e., 0 deg. = normal impact).
Speed of Impact	Impact speed in direction of motion.
Mass	Ice mass estimated from overhead and hand-held video record.
Impact Duration	Duration of main global load peak containing peak force value.
Time to Peak Force	Time from beginning of load to peak global force.
Peak Force	Peak global force (all panels).
Peak Contact Area	Contact area at peak force (triangle method).
Average Pressure	Peak force from all panels loaded above 0.06 MN/contact area at peak force using triangular method.
Total Energy	0.5 x mass (estimated from video) x speed^2.

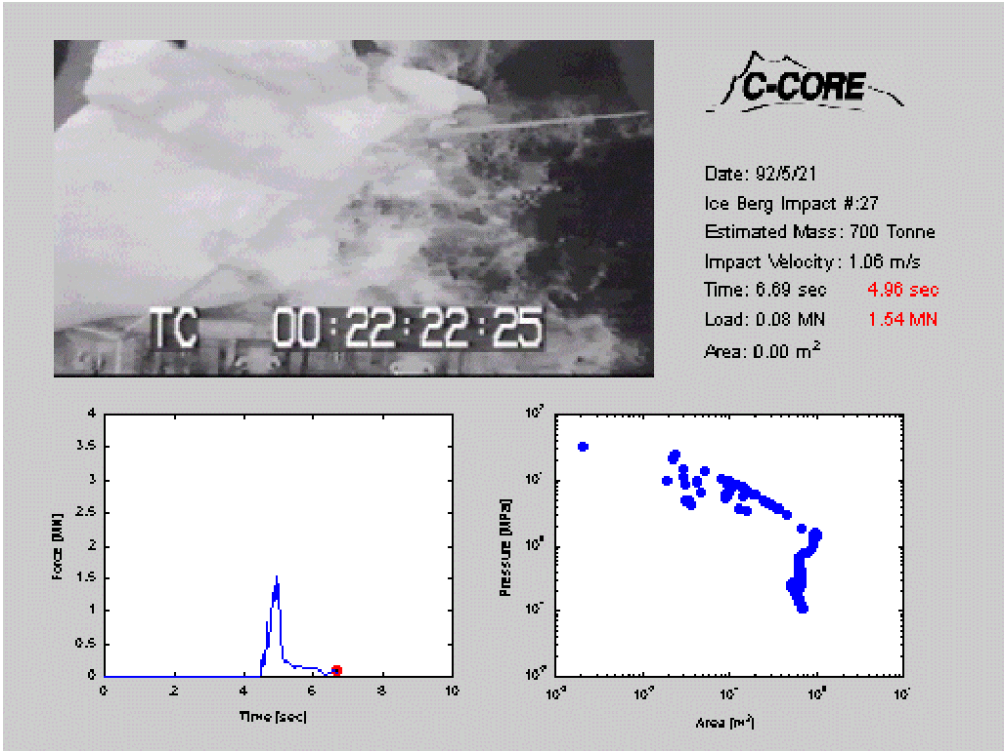

FIGURE 9.3: Graphical Display of Digital Image Sequence for Iceberg Impact No. 27

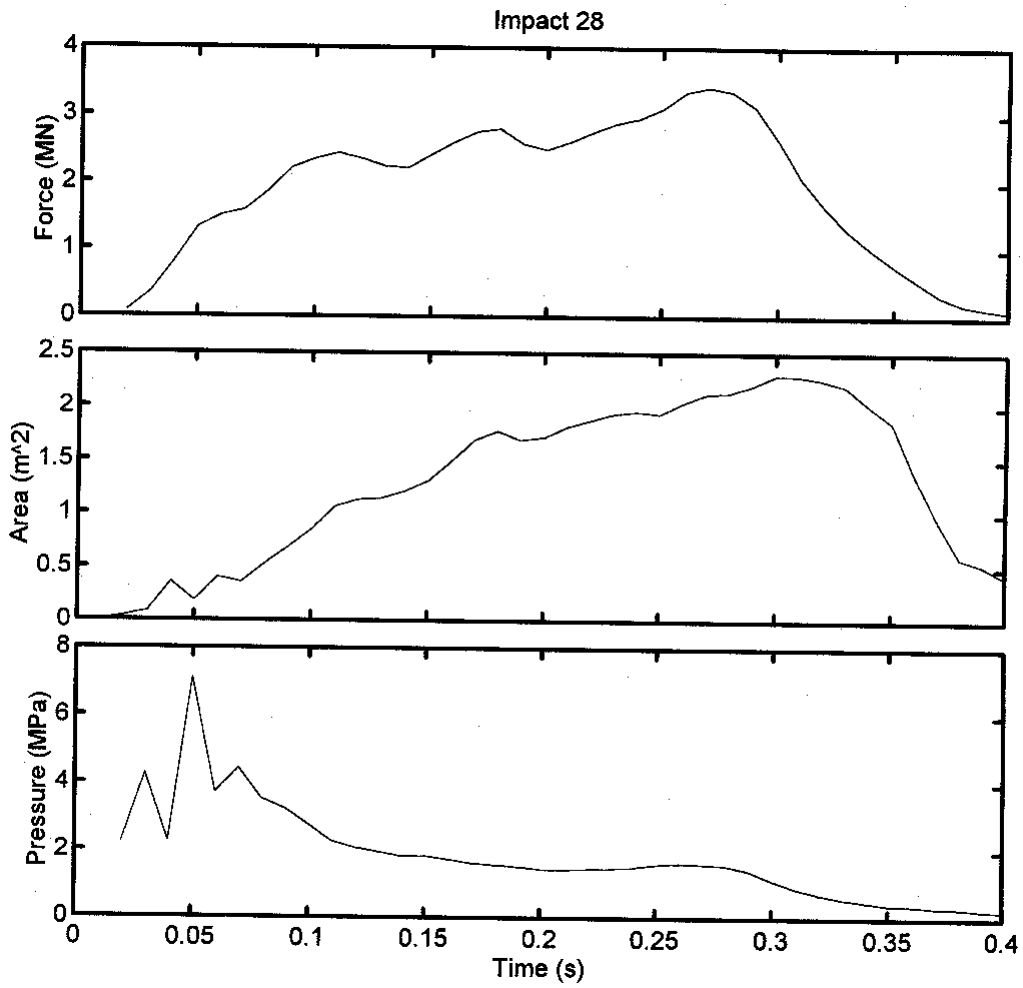

FIGURE 9.4: Example of Time Series Data for Iceberg Impact No. 28 Showing Global Load, Local Pressure, and the Associated Contact Area

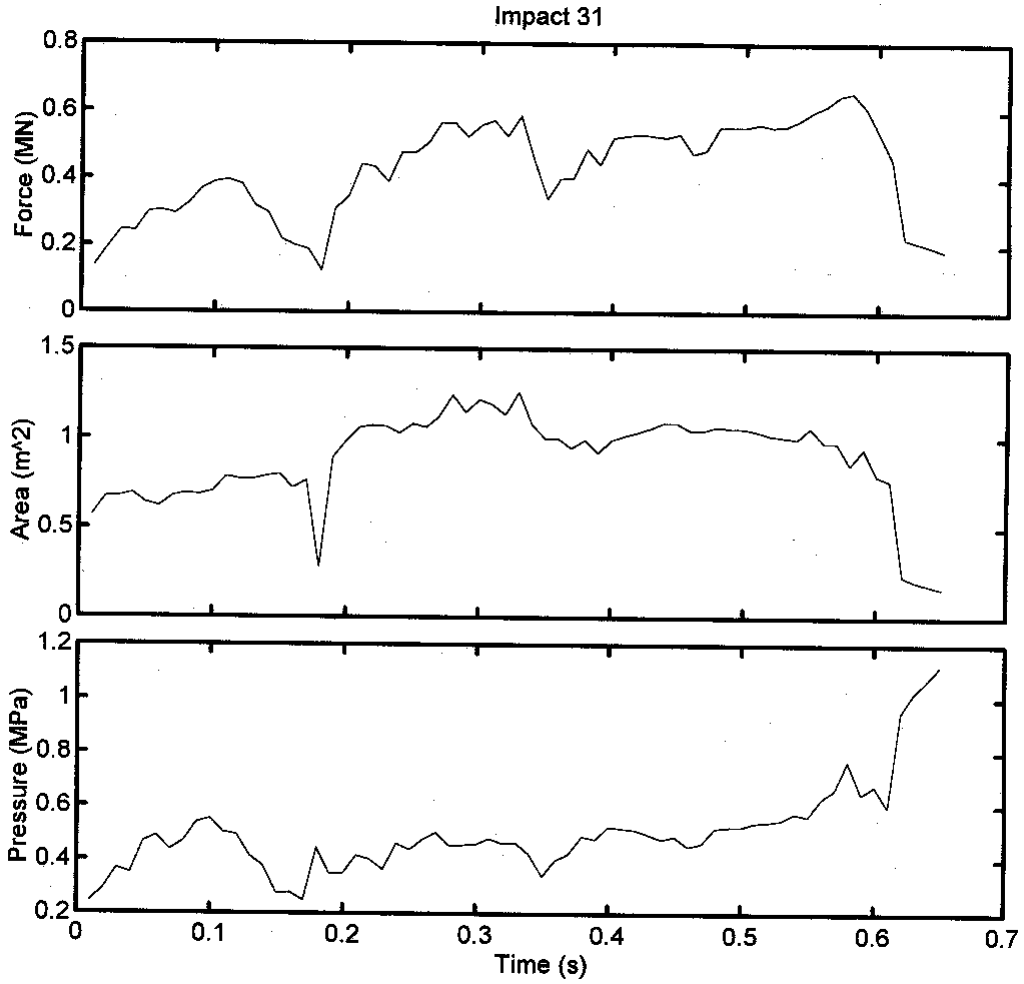

FIGURE 9.5: Example of Time Series Data for Iceberg Impact No. 31 Showing Global Load, Local Pressure, and the Associated Contact Area

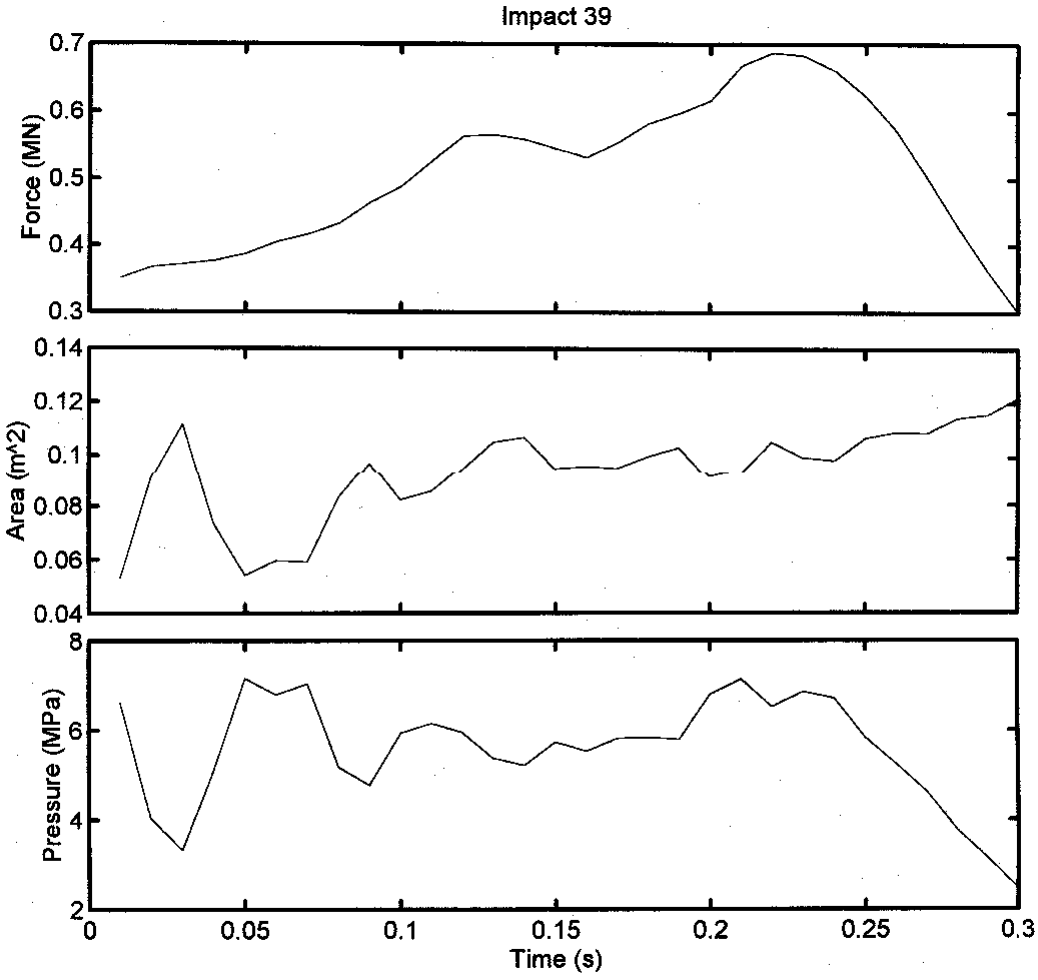

FIGURE 9.6: Example of Time Series Data for Iceberg Impact No. 39 Showing Global Load, Local Pressure, and the Associated Contact Area

10 Molikpaq Data

10.1 Summary

Data Source:	Molikpaq
Geographic Location:	Canadian Beaufort Sea
Time Period:	November 1985 - June 1986 (primary data set) November 1984 - June 1985 (secondary data set)
Ice Regime and Types:	Moving Pack Ice - ice types within the pack ice included first year Arctic sea ice and old ice
Range of Contact Areas:	From ~ 1 m^2 to ~ 15 m^2
Relevance to Icebergs:	High to Moderate - old ice Moderate to Low - first year ice

10.2 Background

General

The Molikpaq is a wide caisson structure that was used for offshore drilling operations in the Canadian Beaufort Sea from the mid to late 1980's. As deployed, it was a hybrid steel/sand structure, consisting of an octagonal steel annulus with dredged sand placed in its central core, see *Figure 10.1*). The Molikpaq was originally designed to have a set down draft of 21 m. In deeper water areas, the caisson was placed on a dredged subsea berm, with the berm height matched to the water depth at the deployment location, plus the depth of any foundation subcut that was required because of weak seabed conditions. The subsea berms built for the Molikpaq's deployments ranged from 8 m to 15 m in total thickness, and were designed with relatively narrow benchtops which extended about 15 m out from its toe, and side slopes of roughly 1 in 7.

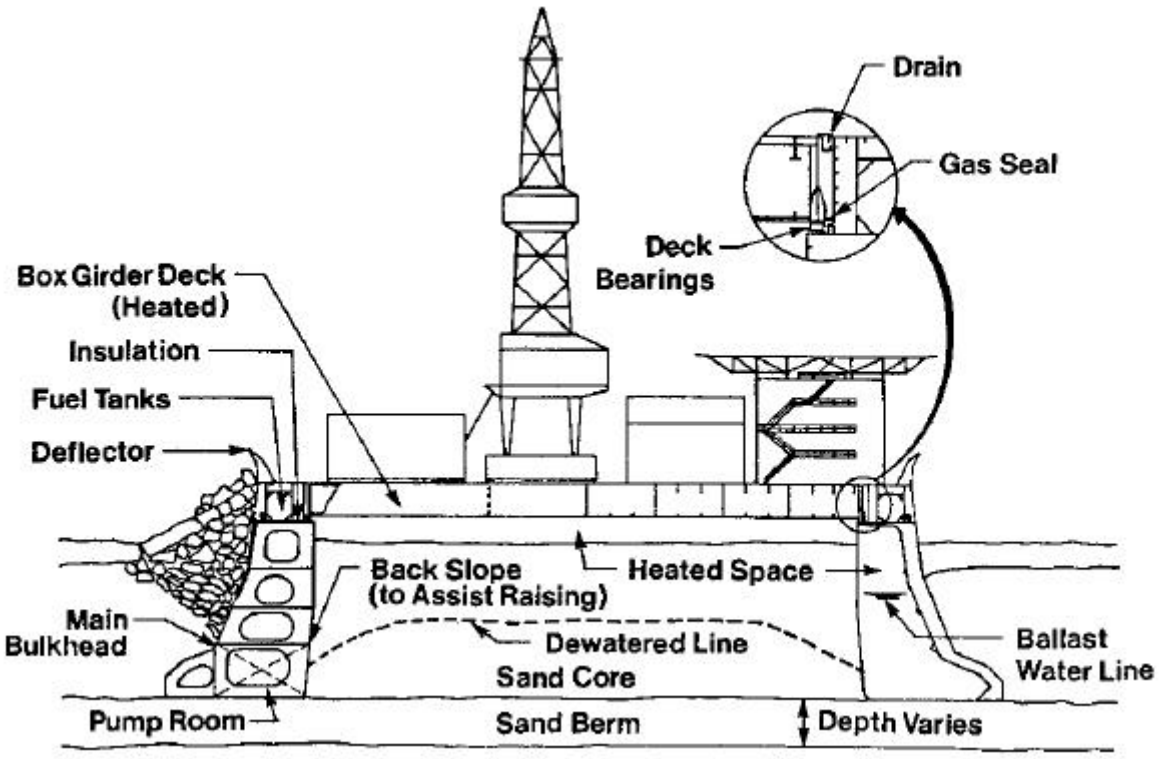

FIGURE 10.1: The Molikpaq at Amauligak

From its base, the height of the Molikpaq caisson was 33.6 m, including a 4.6 m ice deflector that extended above its deck. The caisson had outside dimensions of 111 m and 86 m at its base and deck respectively, and a typical as deployed waterline width of about 90 m. Data from the Molikpaq's 1985/86 and 1984/85 deployments, which involved set down drafts of 19.5 m, is of most interest for the purposes of this work. For these deployments, the caisson's geometry resulted in near vertical walls (8 degrees) being exposed to the oncoming ice cover at the waterline. At depths from ˜3 m to 13 m below the waterline, the caisson walls had a 23 degree slope, flaring out to about 40 degrees near its base.

In global terms, the Molikpaq's sliding resistance was provided by the weight of the ballasted steel caisson and its core fill, which had sufficient mass to resist the high horizontal ice loads expected during multi-year ice floe interactions in the Beaufort Sea. An unfactored global ice load of 620 MN was used in the structure's original design, while site specific deployments in the Beaufort's moving pack ice used design loads ranging from 500 MN to 800 MN. From a more local structural perspective, a system of closely spaced ribs supported the skin plate of the caisson, with loads sequentially passed through an arrangement of frames and

bulkheads to main vertical bulkheads spaced on 2.4 m centres. The caisson had a high strength ice wall located between +3 m and -9 m with respect to the waterline, which was capable of sustaining very high local ice pressures. In this zone, the skin plate was designed for point loads of 6.9 MPa, and local loads approaching 3.5 MPa and 2.5 MPa over areas of 6 and 12 m^2, respectively. The ice wall was also covered with a low friction coating to reduce the frictional component of ice loads, and to mitigate the potential for ice adfreeze.

Instrumentation

During all of its Beaufort Sea deployments, the Molikpaq was well instrumented. Together with systematic documentation of the interacting ice cover, the structure's instrumentation provided a substantial full scale data base on ice/structure interaction processes and loads. Typically, more than 500 sensors were installed on the steel caisson and in its sand core, berm and foundation, to measure ice loads and various platform responses. Direct observations of the ambient ice conditions and ice/structure interaction behaviours were also acquired by onboard monitoring personnel, supplemented by time lapse video coverage.

For the purposes of this work, the key components of the Molikpaq's instrumentation and monitoring system are the ones that provided information about local ice loads, the ice conditions causing these loads, and the associated ice failure behaviour. Medof panels, which were mounted on three of the caisson outer faces to directly measure local ice loads, are of particular importance. A brief description of these panels and the data acquisition system used to obtain various measurement records is given as follows:

Medof Panels

Local ice loads were measured on the face of the Molikpaq with Medof panels. These panels were 1.135 m wide and 2.715 m high, had a 13 mm thick front plate, a capacity of 20 MN, and were configured to measure the total ice load acting on the plate, regardless of how it was distributed or where it acted. The front and rear plates of the Medof panels were separated by an array of urethane disks about 2 mm in thickness. The remaining space between the disks was filled with a calcium chloride solution. When a load was applied to the front plate, the disks deformed, allowing the plates to come closer together, displacing the fluid up a stand pipe. A sensitive pressure transducer was used to measure the pressure head at the base of the stand pipe and thus, give a measure of the loads acting on the panel. Data from the Medof panels is properly interpreted as an average pressure on the area of the panel.

Figure 10.2 shows the location of the Medof panels. They were installed on the north, northeast and east faces of the Molikpaq. Based on predominant pack ice drift directions in the Beaufort Sea, significant ice load events were expected to occur most frequently from these directions. A total of 31 panels in arrays of 4 or 5 panels were distributed on these three faces. Each array was two panels across and two panels vertically, with the waterline passing 0.2 m above the lower edge of the upper row of panels. Three of the arrays had a fifth panel placed directly beneath the other four. Each panel had an area of 3 m^2, with the 4and 5 panel arrays having total areas of 12 m^2 and 15 m^2 respectively. Temperature sensors were embedded into the caisson's outer plate directly behind the panel arrays, which allowed thermal corrections to be made.

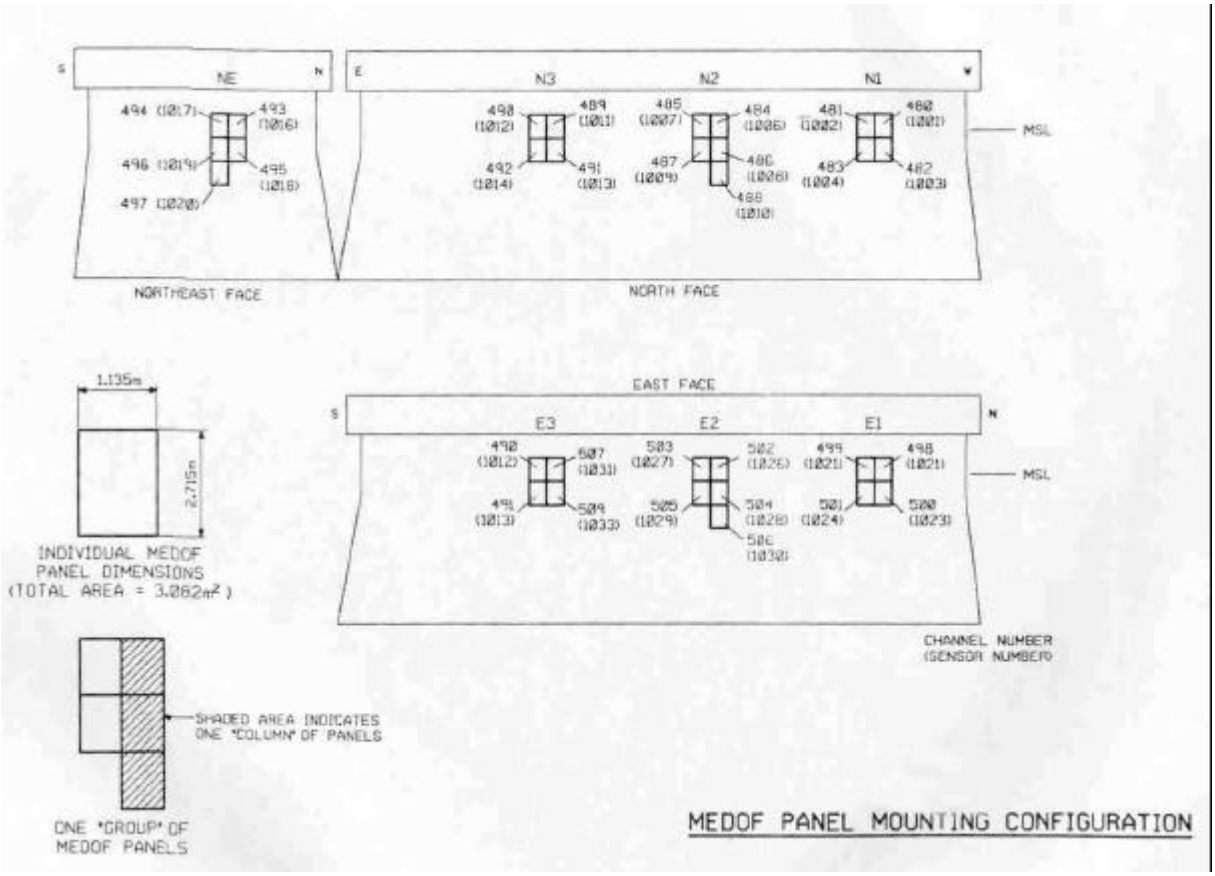

FIGURE 10.2: Medof Panel Mounting Configuration

Although the Molikpaq's Medof panels provided a direct measure of ice loads, they did have limitations. For example, the panels were susceptible to creep during slow loading events (in the order of hours), which can lead to an overestimation of loads. At the other end of the spectrum, the response time of the panels to load changes was in the order of several seconds. Therefore, they are inaccurate for the measurement of cyclic ice loads with frequencies in the range 0.5 or higher. However, the Medof panels did sense the average load during cyclic load events with good accuracy (in the order of 10%).

Data Acquisition System

A sophisticated data acquisition system was installed on the Molikpaq to monitor the outputs of the Medof panels and all of the other sensors. Normally, the DA system monitored outputs and recorded the mean, minimum and maximum of all channels every three minutes on day files. When certain trigger levels were exceeded, fast files were recorded at a frequency of 1 Hz for all channels. Finally, for even more extreme trigger levels, burst files were recorded at 50 Hz for a limited number of channels. Day files were continuously obtained while the fast files were about one hour long, and the burst files 1 to 1.5 minutes long. It should be noted that fast files are the key source of the Medof panel data outlined here. In this regard, the burst files did not contain Medof panel recordings while the day files only provided maximum values for each panel every three minutes.

Equally important to the measurement of ice loads on the Molikpaq were two video cameras that monitored ice conditions and ice action along the east and north faces of the Molikpaq. These cameras were connected to time lapse video recorders, and provided a near continuous record of how the ice was failing against the Molikpaq at any instant in time. Supplementary visual observations were also obtained onboard on a routine basis, to document specific ice/structure interaction events and to provide estimates of ice thickness, ice types, ice drift speeds and so forth.

Type of Ice Conditions and Ice/Structure Interactions Encountered

The local ice load data collected during the Molikpaq's first two deployment, at Tarsiut P-45 and Amauligak I-65, drilled in 1984/85 and 1985/86, is of primary interest here. These two well sites were located in the Beaufort Sea's moving pack ice zone, in 25.5 m and 31 m of water, respectively. At these locations, there was no permanent accumulation of grounded ice rubble around the caisson, due to its deep set down draft (19.5 m from the waterline to the top of the berm). As a result, the structure was directly exposed to pack ice action throughout both winter periods (*Figures 10.3 and 10.4*). Since the pack ice was in near continuous motion, the Molikpaq experienced a wide range of ice conditions, including level first year ice of various thicknesses, pressure ridges, rubble fields and on occasion, second and multi-year ice floes. Over these two winters, hundreds of kilometres of pack ice moved past the caisson.

FIGURE 10.3: The Molikpaq Exposed to Pack Ice

A wide variety of ice/structure interaction behaviours and failure modes were observed at the Molikpaq. Limit stress ice interactions tended to predominate, although limit momentum and limit driving force interactions were also observed. Mixed modal ice failures that involved bending, rubbling, splitting and some localized ice crushing were most common. Large width continuous ice crushing was much more rare, only occurring about 1% of the time. Ice load levels were strongly dependent upon the manner in which the ice failed against the caisson's outer walls. The highest ice load levels were associated with continuous crushing against the Molikpaq, with some of these crushing events including periods of pulsating (or cyclical) ice loads that resulted in ice induced vibrations of the structure.

FIGURE 10.4: Ice Failure Against Molikpaq Caisson's Outer Walls

The local ice loads that were measured during ice crushing failures against the Molikpaq are of most relevance to the question of iceberg impact loads, the issue which underlies this study. In this regard, the following points are noted:

- First year ice interactions with the Molikpaq are less relevant to the issue of iceberg interaction pressures than those involving crushing in thick old ice floes.

- The boundary conditions that are associated with first year ice (< 2 m) interactions at large aspect ratios (10 to 20) are such that there is little confinement in the failing ice, due to the proximity of free boundaries, even when it is crushing.

- Crushing failures in old ice with thicknesses in excess of 5 m have "better" boundary conditions, since there is considerably more confinement over the Medof panel areas.

Period of Data Collection

As noted above, the local ice load data that is most relevant to this work was acquired on the Molikpaq over the winters of 1984/85 and 1985/86. The intermittent fast file records and "continuous" day file statistics from the winter of 1985/86 are of primary interest here, since the data quality is high and readily available in PC compatible form. There is some relevant information from the 1984/85 winter period, but its quality is not as good as the 1985/86 data and it is in a less accessible format (i.e., it only resides on paper records and old tapes, rather than in PC compatible form).

Level of Analysis to Date

The Molikpaq data has been subjected to extensive analyses since the late 1980's. However, most of this work has focussed on questions surrounding ice/structure interaction dynamics and global ice load levels. Some assessments have been carried out to look at the data from a local ice loading perspective, but this work has not been extensive nor comprehensive.

Confidentiality

The Molikpaq ice load data that was acquired in the Beaufort Sea is no longer confidential. In the mid 1990's, NRC-CHC became the custodians of the data, and continue with this role.

10.3 Data Attributes

The key attributes of the local ice load information that is readily accessible from the 1985/86 Molikpaq data set are summarized as follows:

- Thirty-four fast file records that contain local ice load time series for all of the Medof panels (29 of the 31 panels were working in 1985/86) are available, and easily accessible in PC compatible form.

- Each fast file record is approximately one hour in length and contains local ice load data recorded at a frequency of 1 Hz.

- This represents an enormous amount of local ice load data in a wide range of different pack ice situations (i.e., different ice types, thicknesses, speeds, temperatures, failure modes, etc.). For example, in these 34 fast file records, there are more than 350,000 measurements at one second intervals over the 3 m^2 Medof panel areas (29 panels x 34 fast files x ˜ 1 hour/fast file x 3,600 seconds/hour).

- Depending upon the ice thickness that was interacting with the Molikpaq at any point in time during these fast file records, the range of contact areas on the Medof panels varied between ˜ 1 m^2 to ˜ 15 m^2. Contact areas cannot be directly determined from the instrument data, but in many cases, can be reasonably inferred from the observed ice thicknesses.

- As noted earlier, the degree of confinement and boundary conditions varied depending upon the particulars of each specific interaction, with the thicker old ice interactions favouring more confinement. In cases where old ice thicknesses were in the order of 5 m or more and continuous crushing was seen, full contact over the 3 m^2 Medof panel areas is quite certain, at least for the second row of panels.

- Ice types, concentrations, thicknesses, drift speeds and directions, degree of ridging, ice failure modes, and so forth are quite well known from the visual observations and video records obtained onboard. Although no on-ice measurements of ice temperature and salinity were made, reasonable estimates can be obtained from air temperatures (for ice temperatures) and from experience (for ice salinities).

Day file data containing maximum Medof panel values at three minute intervals across most of the 1985/86 winter season is also available. This data has recently been transferred from the original Molikpaq records into PC compatible format by NRC-CHC. The day file data is more limited than the 1 Hz fast file information, as it does not reflect true time series measurements However, it can be used to generate statistics about peak local load levels over 3 m^2 areas and also as a check, to ensure that no significant loading events were "missed" by the fast files and their triggers. This data set contains almost 200 days of maximum ice load values on the individual Medof panels at three minute intervals but, for this work, is considered to be of secondary importance.

Similarly, the Medof panel information from the 1984/85 winter period is also viewed as a secondary data source. In this regard, the Medof panels were not fully operational until mid-way through the winter of 1985, and data acquisition was not fully automated until the winter of 1985/86. Without undue effort, the best that can be done with the 1984/85 Molikpaq data is to compare some of the peak local load values (about 25 events in total) from the late winter period with the 1985/86 data. This information is readily available in existing reports but in digital form, only resides on old tapes at NRC-CHC. The data on these tapes is difficult and problematic to transfer into a PC compatible format.

10.4 Data Quality and Number of Events

By way of summary, the Molikpaq data that is considered to be of most use for future local ice load evaluations is the 1985/86 Medof panel information, as recorded on fast files at 1 Hz. For work directed towards iceberg impact loads and pressures, the fast files acquired during crushing interactions in old ice are of higher importance than those obtained in first year ice, since ice contact areas are typically higher, as is the degree of confinement in the failing ice.

Ten fast files involving Molikpaq interactions with thick old ice areas are readily available in PC compatible form, as time series. Another 24 fast files are available for first year ice interactions. With regard to the fast file data in old ice, each record spans a time period of about an hour, and each contains a differing number of specific crushing events. Without reviewing all of this data in detail, it is not possible to specify the number of significant local ice loading events the records contain. However, a minimum of several hundred load peaks over different areas are probable for crushing failures, and many more if other failure modes are considered.

The strength of the Medof panels is that they provide a direct measure of the local ice loads applied over their 3 m^2 surface area, albeit a spatially averaged value. They are not sensitive to how the ice loads are distributed on them, and there is no need to infer ice load levels and distributions from strain measurements, as is often done on ship hulls. In terms of weaknesses, the Medof panels do not provide any information about local ice loads applied over areas of less than 3 m^2, unless the ice contact area is well known. If it is, the Medof panel data can be used to calculate (or infer) smaller area loads and pressures. The frequency response of the Medof panels is also limited to a threshold of about 0.5 Hz or slightly less. As a result, higher frequency variations in applied ice load levels (should they occur and if they are significant) are not sensed by the panels.

The development of local ice load time series from the Medof panel data is straightforward. In this regard, the individual panel measurements recorded at 1 Hz provide a time series of the loads on their 3 m^2 surface areas directly. Ice loads over larger areas that are formed by horizontally and vertically contiguous Medof panels are simply obtained by adding individual panel load measurements together, since they are concurrently recorded values.

The Medof panel groups on the north, northeast and east faces of the Molikpaq include areas ranging from 3 m^2 to 15 m^2 (in steps of 3 m^2), with the largest area coverage provided by the 5 panel arrays located at N2 and E2 (two of the Medof panels on the NE face failed in December 1985). The large area load measurement coverage of the Medof panel groups is another strength of the data and in fact, makes it unique when compared to most other data sources.

10.5 Examples of Time Series Data

Three examples of local ice loads and pressures from the 1985/86 Molikpaq data set are given as follows. These examples all involve old ice interactions with the Molikpaq, and peak ice thicknesses well in excess of 5 m. Since these thicknesses would completely load the lower two rows of Medof panels, complete contact has been assumed over the lower two Medof panel rows, for local ice pressure determinations. In contrast, the upper row of panels, which is largely above the waterline (see *Figure 10.2*), did not show any significant ice loading activity. Because of this, the ice loads measured on these upper panels have not been included when calculating larger area pressure values.

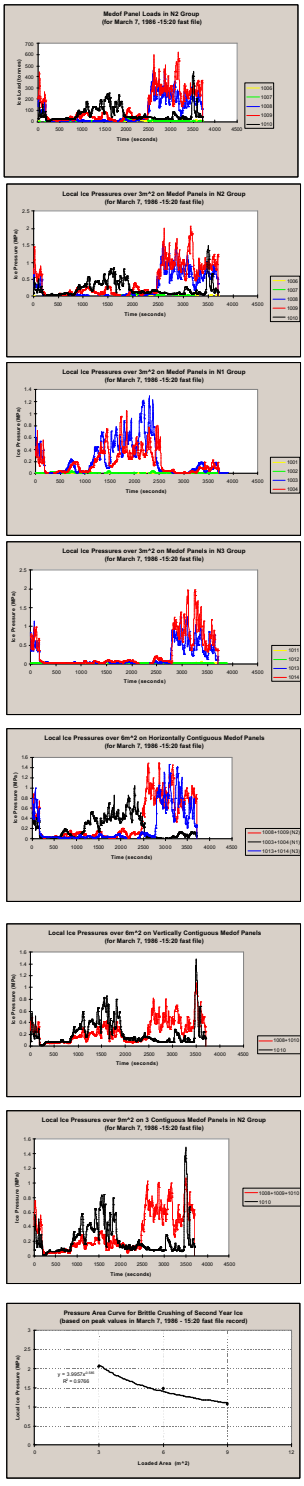

FIGURE 10.5: Molikpaq Time Series Data, March 7, 1986

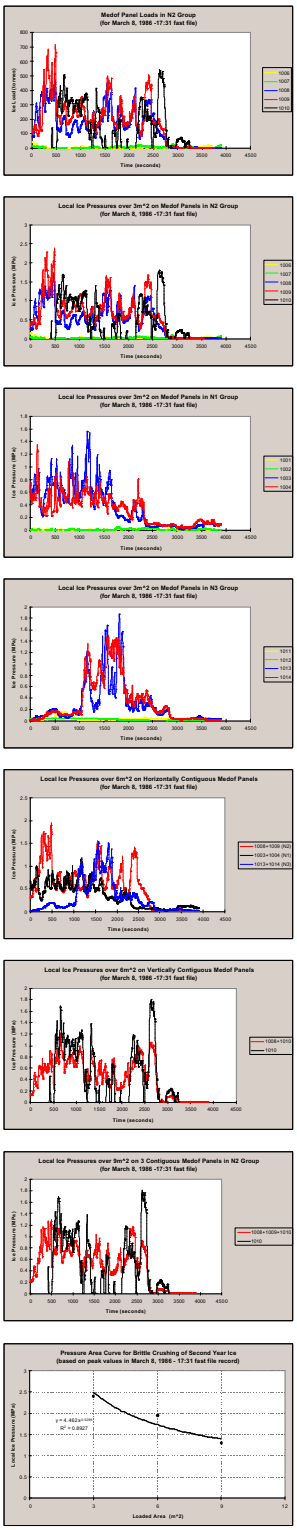

FIGURE 10.6: Molikpaq Time Series Data, March 8, 1986

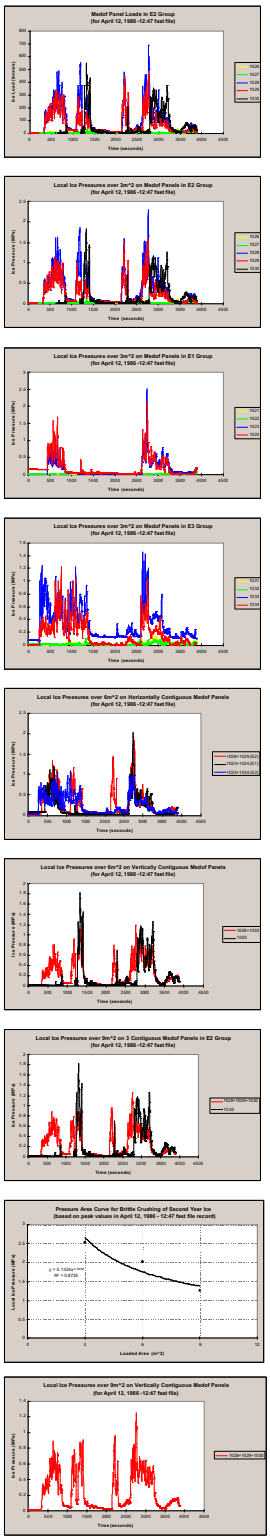

FIGURE 10.7: Molikpaq Time Series Data, April 12, 1986

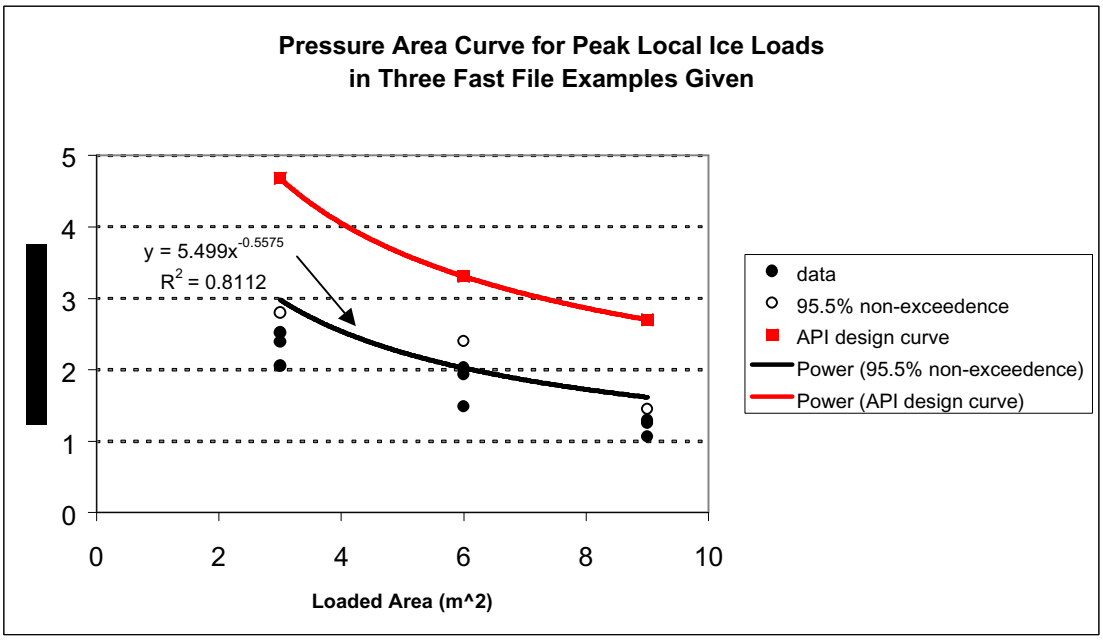

FIGURE 10.8: Pressure Area Curve for Peak Local Ice Loads in Three Fast File Examples Given

10.6 Comments on Relevance to Local Ice Loads Due to Icebergs

The Molikpaq old ice interaction data is very relevant to local loads from iceberg impacts.

11 Louis S. St-Laurent Data

11.1 Summary

Data Source:	1994 Louis S. St-Laurent North Pole Voyage
Geographic Location:	Arctic Ocean Transit from Bering Strait to North Pole exiting the ice North of Svalbard
Time Period:	July and August 1994
Ice Types:	Pack Ice: high concentrations of First, Second, and Multi-year ice
Range of Contact Areas:	Bow Panel 0.75 m^2 to 22.5 m^2 Side Panel 0.25 m^2 to 2.1 m^2 Shear Gauges Side Panel 1.2 m^2 to 17 m^2 Bottom Panel 0.8 m^2 to 5.6 m^2
Relevance to Icebergs:	High

FIGURE 11.1: CCGS Louis S. St-Laurent

11.2 Background

The Canadian Coast Guard Ship (CCGS) Louis S. St-Laurent shown in *Figure 11.1*, in conjunction with the United States Coast Guard Cutter (USCGC) Polar Sea, was deployed for an Arctic voyage during the summer of 1994. The primary mission was to conduct scientific research on the Arctic Ocean. (Ritch et al, 1997and Ritch et al, 1999).

The primary objectives of the ship technology program were to:

- Collect hull/ice interaction data on three areas of the Louis S. St-Laurent hull structure, the bow, the shoulders and the bottom, as shown in *Figure 11.2*.

- Collect vessel manoeuvring and powering data to fully characterize the vessel operations during the recorded hull/ice impact events.

- Collect environmental and ice data to fully characterize ice conditions during the recorded hull/ice impact events.

- Determine load patterns and load intensities on the three areas under consideration on the basis of the collected hull/ice interaction data. From this information it is possible to determine data trends and correlate impacts with ship motion and ice conditions; develop extreme load profiles and establish relationships for the frequency, magnitude, and pattern of loads on the three instrumented hull areas; compare the developed relationships with those specified in the Revised Canadian Arctic Shipping Pollution Prevention Regulations (CASPPR) Hull Construction Standards; and make recommendations as appropriate.

The Louis S. St-Laurent is the largest icebreaker in the Canadian Coast Guard fleet and in Canada. The vessel is a patrol and escort icebreaker that principally works the Gulf of St. Lawrence in the winter and the Arctic in the summer. The ship has a triple-screw, diesel-electric propulsion system and a conventional wedge-shaped icebreaking bow. The principal characteristics of the Louis S. St-Laurent are summarized in *Figure 11.2*.

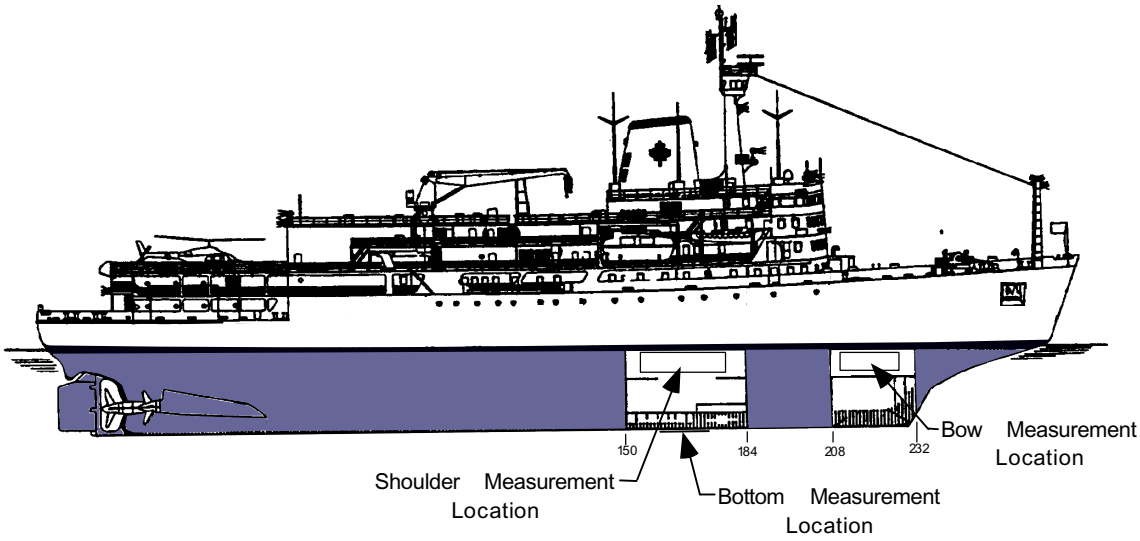

Principal Characteristics

Length Overall		392.4 ft.	119.6 m
Waterline Length		354.0 ft.	107.9 m
Maximum Beam		80.0 ft.	24.4 m
Waterline Beam		79.7 ft.	24.3 m
Full Load Draft		32.0 ft.	9.8 m
Full Load Displacement		14,800 LT	15,000 MT
Shaft Power	(Continuous)	24,000 HP	17.9 MW
	(Maximum)	27,000 HP	20.1 MW
Accommodations	100 persons		
Helicopters	2, Messerschmidt BO 105		

FIGURE 11.2: Outboard Profile and Principal Characteristics of the CCGS Louis S. St-Laurent

Voyage Description

The data were collected during the "Arctic Ocean Section '94" which took the vessel across the Arctic Ocean from the Pacific Ocean to the Atlantic Ocean. The trackline is shown in *Figure 11.3* (St. John et al, 1994). The ships operated together for the most part, alternating the lead and following a north-north-easterly course to the gap in the Lomonosov Ridge. From there the two ships proceeded to the North Pole. At about 45 nm from the Pole, the Polar Sea suffered a propeller casualty when a blade sheared from the starboard wing propeller.

The North Pole was reached on August 22nd after 27 days and 1,419 miles transiting in the ice. The average speed underway was 3.68 kt. The Russian nuclear icebreaker Yamal happened to be at the North Pole at the same time and the three ships were able to rendezvous. The decision was made to exit the ice in the most expedient manner because of the propeller casualty to the Polar Sea, and to conduct scientific research when easier ice conditions or open water was achieved. The shortest route to the ice edge was toward the Fram Strait. The Yamal offered to assist in breaking track for the Polar Sea and the Louis S. St-Laurent because she was heading in that direction to get to Murmansk. The three ships followed a course along longitude 35 degrees E to about 84 degrees N, where the Yamal parted company heading for Murmansk. The Louis S. St-Laurent and the Polar Sea proceeded into open water across the top of Svalbard and into the Fram Strait and then onto to Halifax, Nova Scotia, arriving on September 9th.

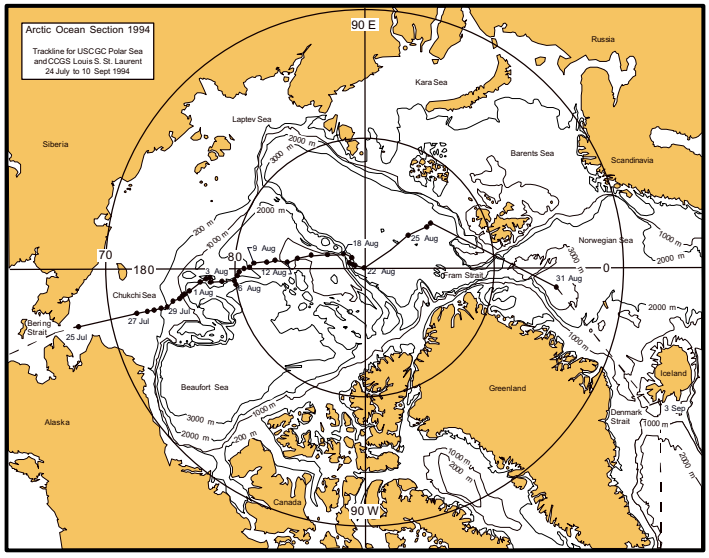

FIGURE 11.3: Trackline for the Louis S. St-Laurent and the Polar Sea for AOS '94

Overview of the Instrumentation and Measurement Program

Several different automated data acquisition systems were installed aboard the Louis S. St-Laurent for the program. The hull loads data acquisition system acquired strain gauge data from three locations on the hull of the ship: the bow, the shoulder, and the bottom. The location of the three instrumented areas are shown in *Figure 11.2*. A ship navigation data acquisition system and a video monitoring system were also installed to provide speed, position, power, and ice condition documentation to support the load measurements. In addition, two observers aboard the Polar Sea provided hourly average ice conditions, weather conditions, and operation details of both ships.

Bow Measurement Area

The bow measurement area was in the starboard wing tank outboard of the bubbler machinery compartment, in the portion of the bow structure that was recently replaced. The layout of the strain gauges in the bow area is shown in *Figure 11.4*. A total of 24 gauges were installed in this area. These gauges were placed on the web approximately 50 mm from the shell plate at the location of maximum strain as indicated by the finite element models. Each gauge consisted of a two-element gauge placed to measure shear strain in the frame.

Six main frames (214, 217, 220, 220, 223, 226 and 229) were instrumented near top and bottom between Stringer Nos. 9 and 10. On Frame Nos. 220, 223 and 226, an additional 12 gauges were placed midpoint between each stringer interval. These "small panels" measured the load over an area approximately 0.75 m^2. The upper most and lowest gauges on each frame measured the load over an area of approximately 3.7 m^2.

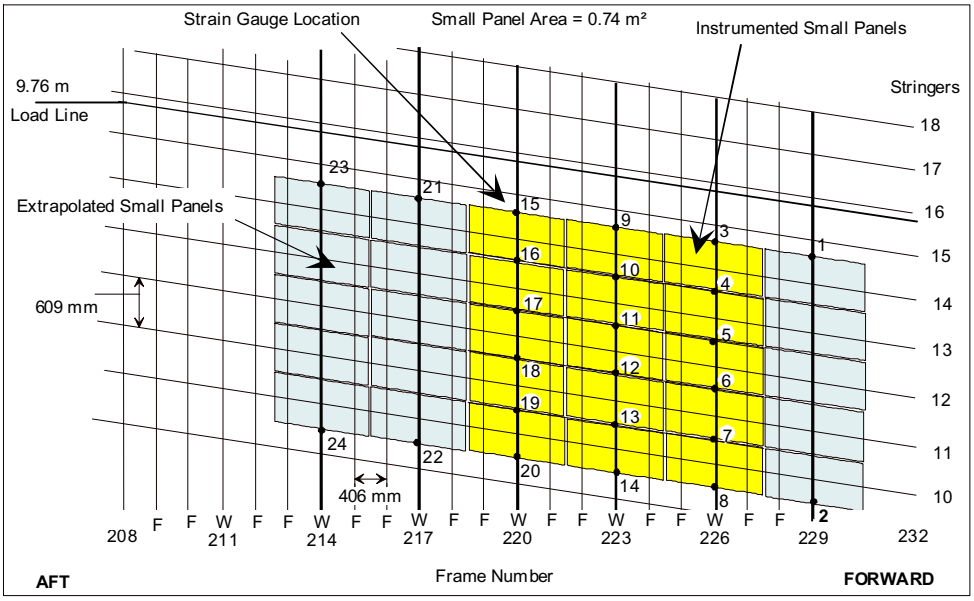

FIGURE 11.4: Layout of Strain Gauges in the Bow Area

Shoulder Measurement Area

The shoulder measurement area was located in the starboard heeling tank just aft of the new bow. The structure in this area is very complicated and difficult to instrument. The structure in this area is a grillage of heavy web frames, stringers, and ice frames. Recently the structure had been strengthened from the original design by the placement of two heavy braces athwartship in the opening of each full floor that formed the web frames of the tank. This addition makes the web frames act essentially as a bulkhead. Cross braces were added to the webs of each web frame to prevent web buckling and new stringers were added in between each original stringer for additional stiffening.

The installed strain gauge layout is shown in *Figure 11.5*. In order to cover a large enough hull area to capture the expected ice load footprint it was decided to instrument a number of the stringers for bending and to provide information about the loads over small areas to instrument the frame in shear. Twelve half-bridge strain gauges were placed midspan on the stringer flange as shown in *Figure 11.5*. An additional 16 half bridge strain gauge elements were placed on Frame Nos. 165 to 168 just above and below Stringer Nos. 3, B and 5, as shown in *Figure 11.5*. Each instrumented stringer measures the load over an area of 1.20 m^2 to 1.44 m^2 (12.9 ft^2 to 15.5 ft^2), and the shear gauges on the frames provides the measurement of small area pressures over 0.24 m^2 (2.6 ft^2).

Due to the nature of the measurement technique used the data based on the bending gauges is of lower quality and valid only at the point in time for which detailed re-analysis was performed. It is recommended that only the data obtained directly from the shear gauges be used.

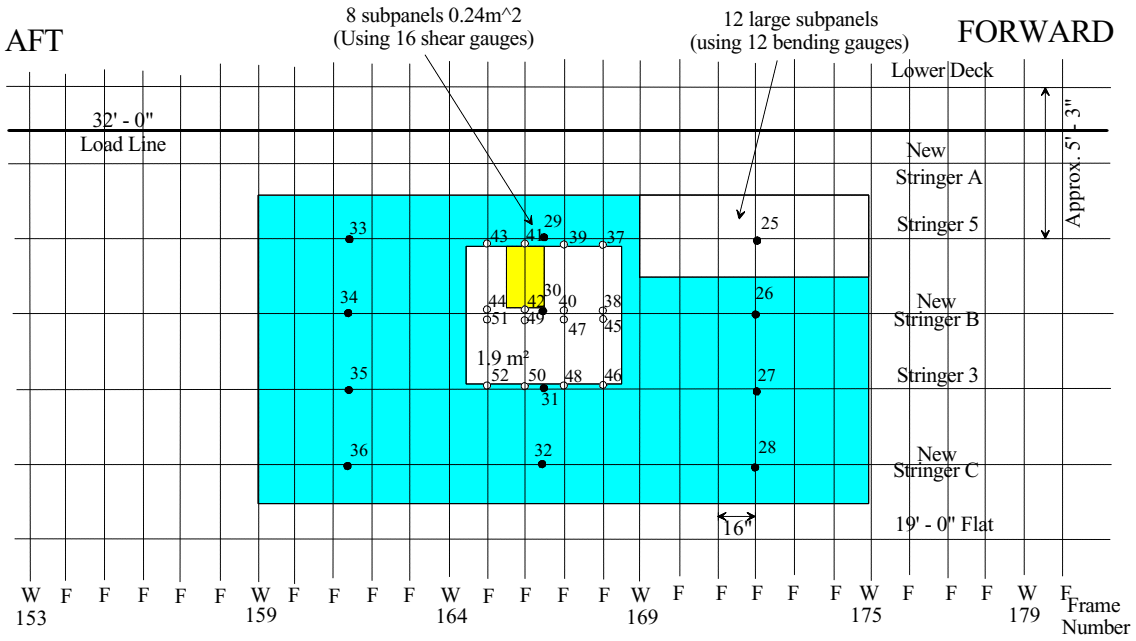

Figure 2 - Layout of Strain Gauges in STBD Heeling Tank

(Note: number next to gauge location indicates channel number)

FIGURE 11.5: Schematic of Side Panel (Ritch et al, 1997)

Bottom Area

A portion of the bottom was instrumented but is not applicable to local ice loads on icebergs.

11.3 Data Attributes

Data Availability

The data was originally collected as a joint project between the Canadian Coast Guard, and the US Coast Guard.

The original data was collected on HP computers and stored in HP format on floppy disks and 20 MB tapes. The original data was in AD counts only.

In 1999, under a project sponsored by Canadian Coast Guard the original HP format data was reprocessed into individual small panel pressures based on the techniques described in the "Measured methods... " section. The processed data was stored as ACSII data files on CD-ROM's. The data is stored in ISO 9660 format and can be read on any platform. Full details on the data storage formats are provided on the CD set. Marine Prairie & Northern Region, Canadian Coast Guard own these CD-ROM's.

There are 1730 time series events measured on the bow and 1290 applicable side panel events. The pressure on each instrumented cell (and frame) is output for each time step. Based on this data the user would need to develop an algorithm/software for calculating the loaded areas and total load.

The CD contains an EXCEL spreadsheet, summarizing the peak value loads and pressures, and loaded area for each event, along with the associated ship speed and ice conditions.

During the re-analysis of the data for use in other projects Ritch processed 93 events using the algorithms developed for this project. For the 93 specific bow loading events, the time history of total load, loaded area, along with the individual cell pressures are output in ASCII format.

Included on a second CD are all the raw or measured strain time history data files in ASCII format.

In addition to the digital data a video camera was placed to record the general view looking forward and a second camera was located at the shoulder, pointed downwards to record ice thickness. Video was recorded throughout the voyage from this camera.

Duration of Records

Each recorded event is six to ten seconds long.

Frequency of Data Recording

The data acquisition system was set-up as a transient recorder. The data acquisition system scanned continuously. When an impact greater than a set threshold on any of the three measurement areas would trigger an event. In some cases, simultaneous impacts were recorded on two or all three of the measurement areas. If the multiple impact cases are counted separately, 3,200 individual impacts were recorded of which 1,800 were on the bow area. This number represents the largest set of hull-ice impact events recorded on a single deployment.

Range of Contact Areas

- Bow Panel: 0.75 m^2 to 22.5 m^2
- Side Panel: 0.25 m^2 to 2.1 m^2 Shear Gauges
- Side Panel: 1.2 m^2 to 17 m^2
- Bottom Panel: 0.8 m^2 to 5.6 m^2

Ice Conditions and Ice Types (Salinity and Temperature)

A full range of ice types and conditions were encountered. Ice conditions as well as weather and ship operating conditions were observed continuously from the bridge of the Polar Sea while the ships were underway. The ice conditions were quite heavy, and high concentrations resulted in considerable operation in a continuous icebreaking or ramming mode. The average ice concentration for the trip to the North Pole was 94 percent. *Figure 11.6* presents the observed average hourly ice concentration and *Figure 11.7* the average ice thickness. The average ice thickness increased linearly from 1.0 m at the ice edge to 2.0 m at the North Pole. The highest concentrations occurred in the latitudes 73 degrees to 82 degrees N. The corresponding maximum observed hourly average ice thickness for this route was 3.54 m. Ice properties were also collected by the National Research Council of Canada's Institute for Marine Dynamics (NRC-IMD) and are reported separately (Williams, 1994).

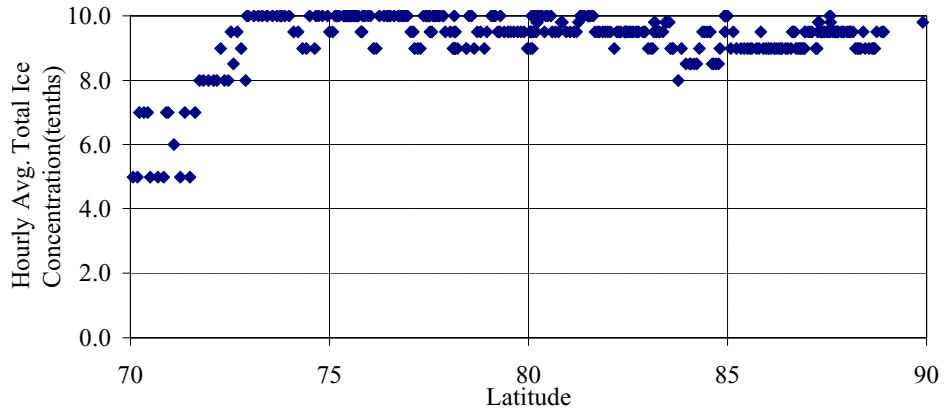

FIGURE 11.6: Ice Concentration – Ice Edge to the North Pole (Ritch et al, 1997)

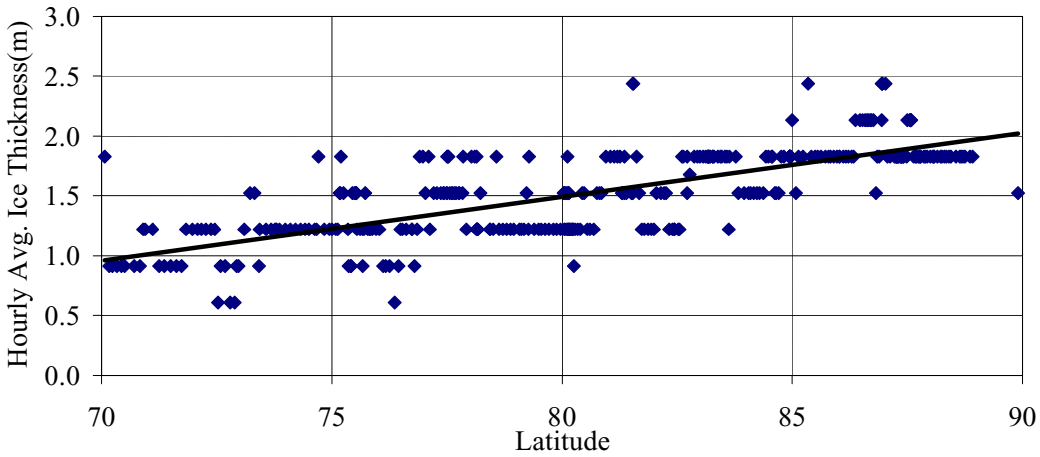

FIGURE 11.7: Average Hourly Ice Thickness –
Ice Edge to the North Pole (Ritch et al, 1997)

Ice Thickness, Ice Mass, Etc.

Hourly average level Ice thickness from 0.6 m to 3.1 m with maximum thickness of level ice 7.6 m. No specific ice features have been associated with each event. In some cases using video analysis events have been defined as ramming or glancing blow.

Ice Speed (Or Indentation, Ship Speed) Ice Direction

The vessel speed was measured using a GPS system. In the summary spread sheets a vessel speed is associated with each event. This speed us based on a running average of one second measurements. The actual time history of the ship's location throughout the voyage are available. The range of event vessel speeds are from near zero to 16 knots.

Measurement Methods, Resolution, Response Frequency, Etc. Method of Determining Contact Areas

The method of measuring individual strains on frames provides individual strain data with high resolution and high response rates. As part of the analysis process a finite element model of the structure was developed. Based on the model an influence matrix was developed and is used to convert the measured strain into pressures on each measurement area. This method attempts to take into account the load carrying behaviour of the structure. There are some uncertainties associated with this method.

As described in the introduction only three frames were instrumented in detail. In order to extend the detailed area during the analysis phase pseudo strains were predicted on Frame Nos. 214, 217 and 229 based on the measured strains at the top and bottom of these frames and the distribution of strain on the adjacent full instrumented frame. Based on these pseudo strains the loads on the "small panels" on 214, 217 and Frame No. 229 were extrapolated as described in the analysis report.

The side area was instrumented using both shear and bending gauges. The shear gauge provide good information on loads and pressures over a small area. There was some difficulty in determining loads from the bending gauges.

The original contractor developed software to calculate contact areas and loads. The contact areas are calculated by finding the highest loaded cell at each time step, then determining which of the adjacent cells are loaded. This algorithm requires the loaded area to be a single contiguous region. The results of this analysis at the time of peak pressure and loads have been summarized in EXCEL spreadsheets on the CD. These summary sheets include for each event the peak load, pressure, vessel speed, ice conditions, aspect area, and the pressures on the individual cells at the peak.

The resulting pressure/area envelope curves have been widely reported. A sample is shown in *Figure 11.8*.

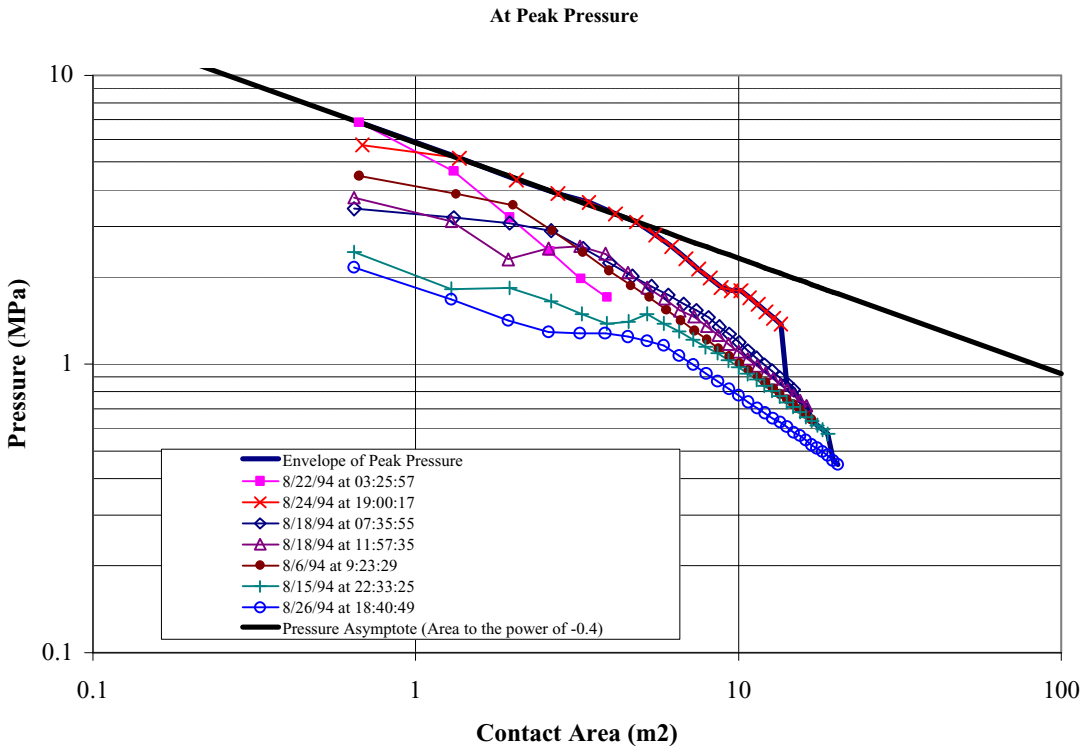

FIGURE 11.8: Derived Pressure/Area Envelope (Ritch et al, 1997)

Data Availability (Who Owns It, Where From) and Format (Tapes, Paper, Disks, Etc.)

The data was originally collected as a joint project between the Canadian Coast Guard, and the US Coast Guard.

As described in the data attributes section above, the original HP format was reprocessed into ASCII data format on CD-ROM's written is ISO 9660 (can be read on any platform) and are held by Marine Prairie & Northern Region, Canadian Coast Guard.

11.4 Data Quality and Number of Events

The time series data is of high quality with a large number of recorded events.

11.5 Examples of Time Series Data

As noted above the bulk of the time history data are stored as time histories of pressure on individual cells. In the in the OMAE paper (Ritch et al, 1994) two time histories for load, pressure, area and aspect ratio are reported. There are 93 similar analyzed event included on the CD-ROM (Ritch, 1999). Similar analysis is possible with all other data files. Two example time histories provided.

Based on the data reduction method described above, force and pressure time histories for each data event were produced. The form of each of these events varied significantly, but many events could be classed as either "sharp impact" or "blow" and "slide loads". A "sharp impact" is an event in which the loading occurs very quickly and moves little across the panel (*Figure 11.9*). A "sliding load" is an event in which the load moves onto the instrumented area from the forward end and slides across the panel. This is characterized as a long event in which the peak load moves progressively aft (*Figure 11.10*).

The duration of the loading for the "sharp impact" event (*Figure 11.9*) is about 0.4 seconds and then drops suddenly. This sudden drop could be due to either a large ice cusp failure or the vessel bouncing off the ice. The load is centred on Frame No. 217. It is interesting to note that the loaded area is reasonably constant throughout the event (10 m^2 to 15 m^2) and the maximum pressure on a single cell occurs at the same instant as the maximum load. This event was the maximum total load recorded during the voyage, and it occurred while following the Yamal and Polar Sea when the vessel contacted the edge of the broken channel.

The "sliding" event (*Figure 11.10*) lasts about 5 seconds during which the centre of loading moves progressively aft. The total load and the loaded area do not change rapidly through the course of the event.

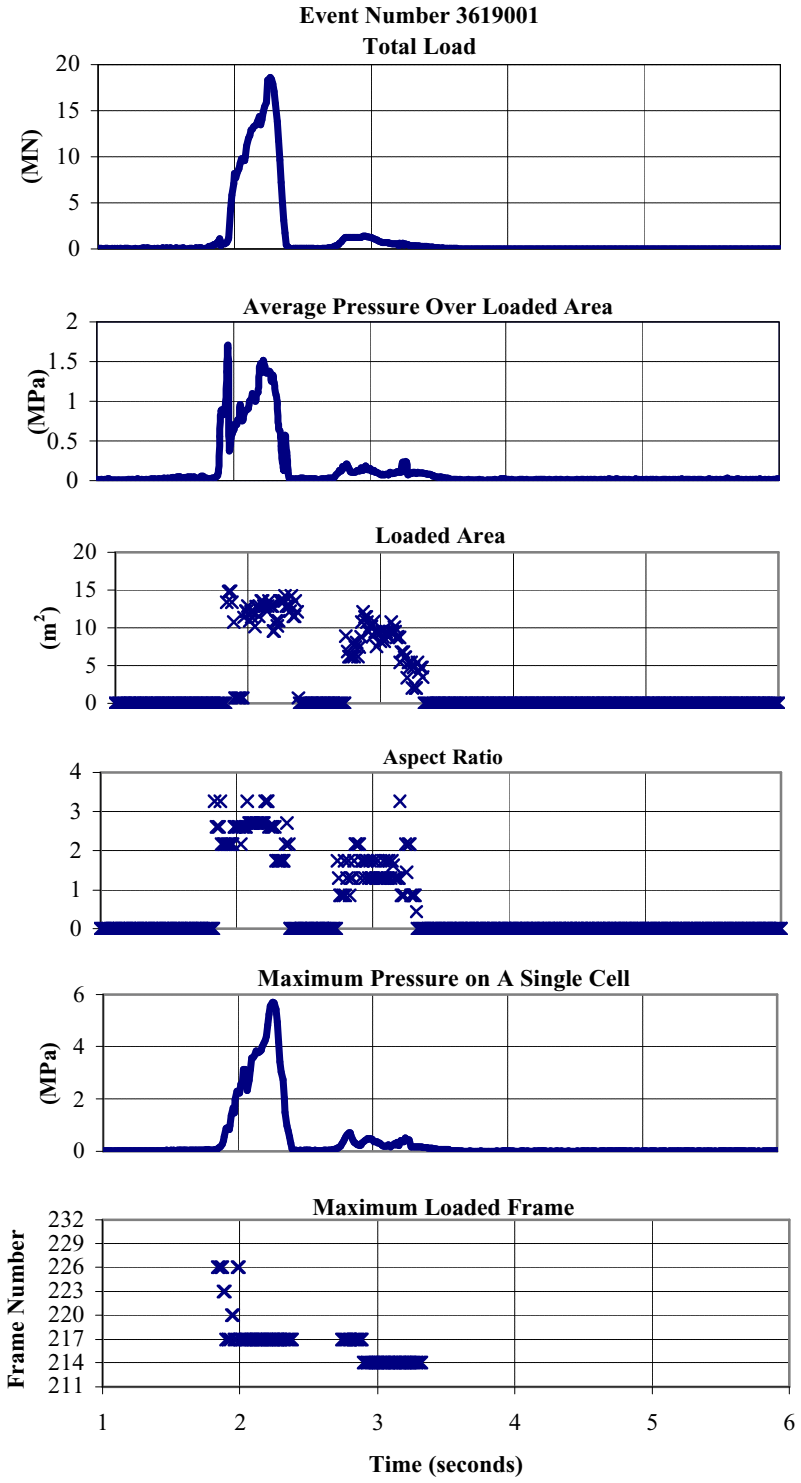

FIGURE 11.9: Sample Time History for "Sharp Impact" Event (Ritch et al, 1999)

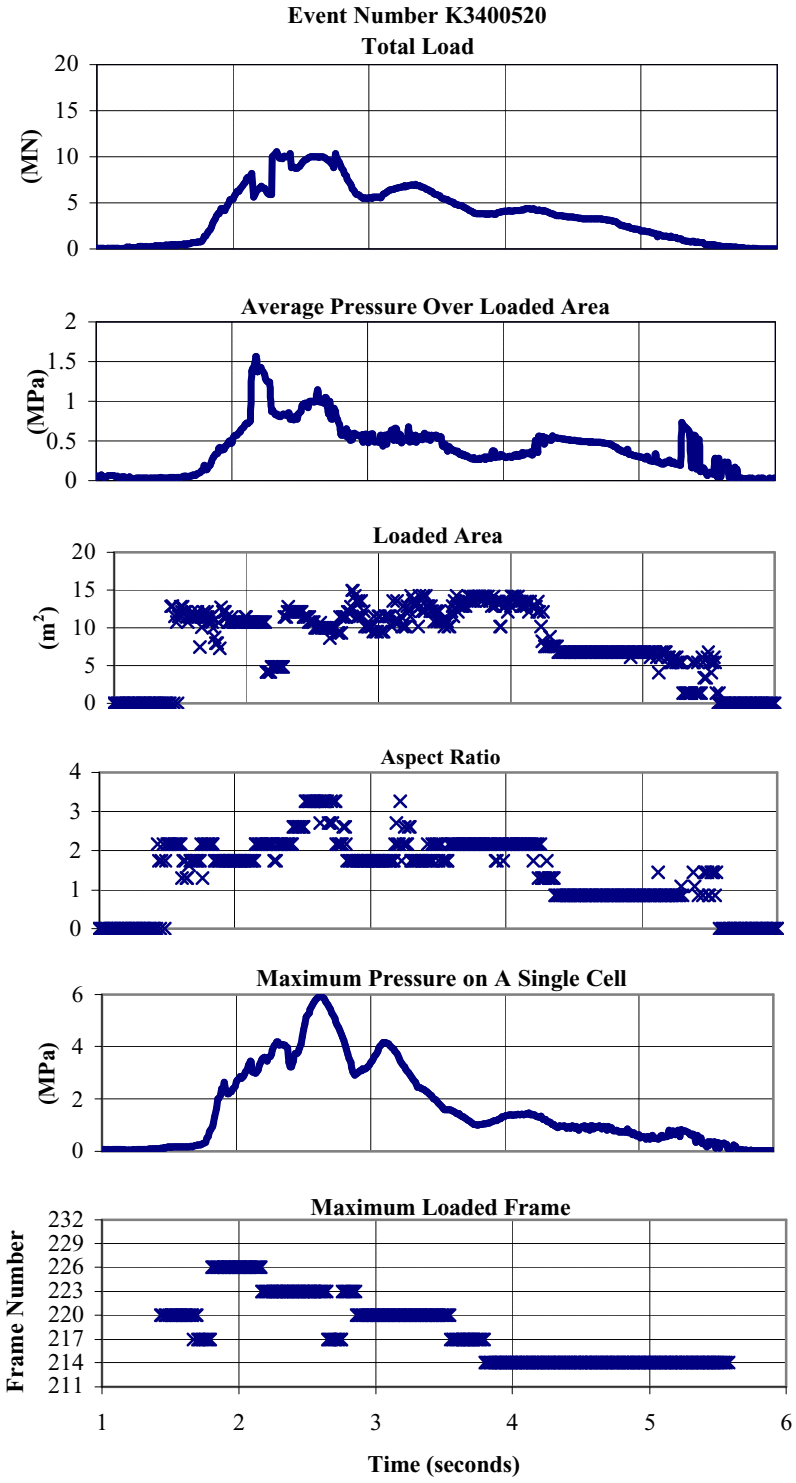

FIGURE 11.10: Sample Time History of a "Sliding" Event (Ritch et al, 1999)

Suitability of Data to Probabilistic Treatment

The data collection systems were run continuously as transient recorders while the vessel was underway, making the data ideally suited for long-term load estimation. Because of the large number of events over a relatively long period of time, this data provides excellent statistical data on ice loads/pressures. Based on this the data has been analyzed to predict the extreme loading events in the original report (Ritch et al, 1997) and subsequent reports (Browne et al, 2000). *Figure 11.11* shows an example of the data being used to predict the extreme value pressure for various ice regimes based on CAC classification.

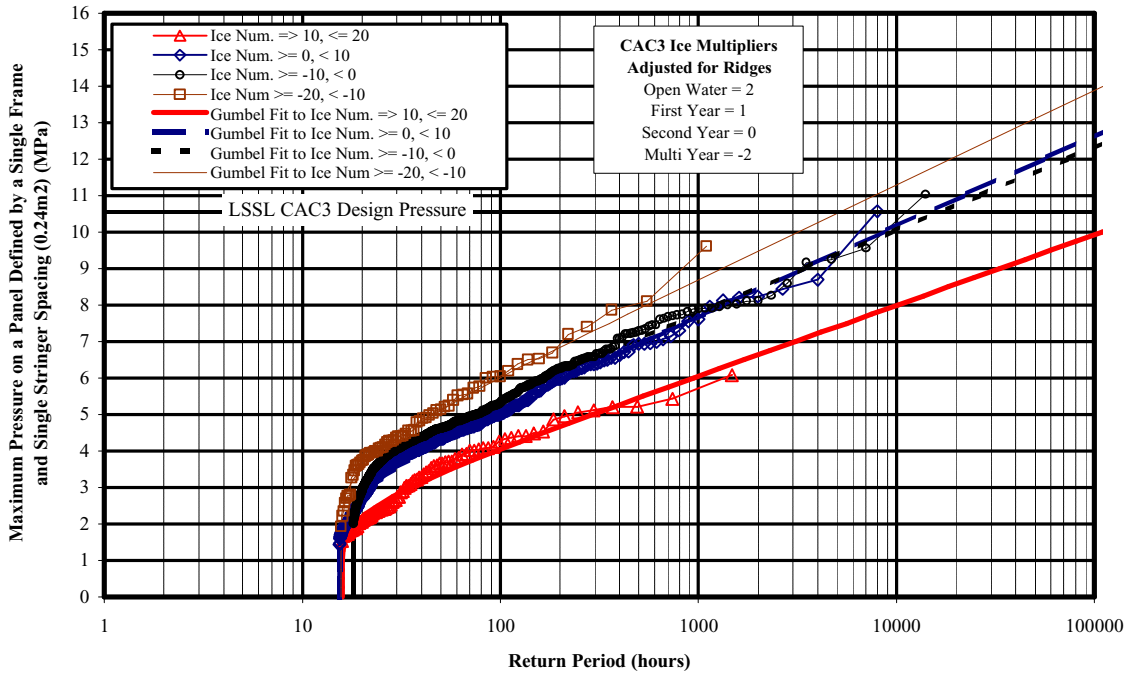

FIGURE 11.11: LSSL 1991 – Extreme Value Prediction for Local Pressure (Browne et al, 2000)

11.6 Comments on Relevance to Local Ice Loads Due to Icebergs

Ship ice interaction data especially with multi-year ice provides the largest source of interaction data and is directly relevant to ice loads due to icebergs especially growlers and bergy bits. The main issue in using these data are:

- Potential differences in properties between glacial ice and multi-year ice.
- The amount of confinement since the sea ice is of limited thickness.

- Sea ice is likely to fail initially in crushing but as the loads increase other modes of failure will likely limit the magnitude of the total force.

- The general ice conditions have been recorded but the specific ice type and size for each event are difficult to specify. In some cases detailed analysis of the video can provide more information on the nature of the impact.

12 Oden 1991 Data

12.1 Summary

Data Source:	Oden 1991 North Pole Voyage
Geographic Location:	Arctic Ocean
Time Period:	August to September 1991
Ice Types:	Pack Ice: First Year Arctic Sea Ice: Multi-year ice
Range of Contact Areas:	0.65 m^2 to 21 m^2 (26 m^2 with interpolation)
Relevance to Icebergs:	High

FIGURE 12.1: Oden

12.2 Background

The Swedish icebreaker Oden, as shown in *Figure 12.1*, was involved in a three ship deployment to the central Arctic Basin, the International Arctic Ocean Expedition 1991, to conduct a broad range of scientific measurements in the Arctic Ocean. The expedition left Tromsø, Norway, and followed a track to the west of Spitzbergen, Franz Josef Land, the Lomonosov Ridge, and Makarov Basin, ultimately reaching the geographic North Pole. The return trip was via the north coast of Greenland to Spitzbergen and back to Tromso. As part of the scientific effort, a ship technology program was sponsored by the US and Canadian Coast Guards, the National Maritime Administration of Sweden and the Swedish Polar Secretariat. The program included measurement of ice impact loads on the hull, rudder loads, propulsion plant dynamics, and ship performance as well as observing the ice conditions along the route (St. John et al, 1994).

Two different load measurement systems were employed; one that measured the total vertical load on the bow and one that measured the distribution of impact pressure across a large portion of the bow shell plating. The total vertical force was determined by measuring the shear force in the hull girder just forward of the ice knife and the bow acceleration. The local pressures on the hull were measured by strain gauging the webs of the ice frames in shear at regular intervals through the waterline. Eight ice frames were measured at five locations resulting in 32 areas of 0.65 m^2 over which the average pressures were computed.

The ice loads and ship performance data collection took place during operational transiting between successive scientific stations, although a number of dedicated ramming tests were carried out on September 27th near the edge of the polar pack.

Description of Oden

Two and *Figure 12.2* present the profile and plan views of the Icebreaker Oden. The vessel was designed and built by Goteverken Arendal (GVA Technology) in their yard at Gothenburg, Sweden. The design was done in association with Canadian Marine Drilling Limited (Canmar) of Calgary, Canada. The ship was delivered in December 1988. It is operated by the National Maritime Administration of Sweden (Sjöfartsverket).

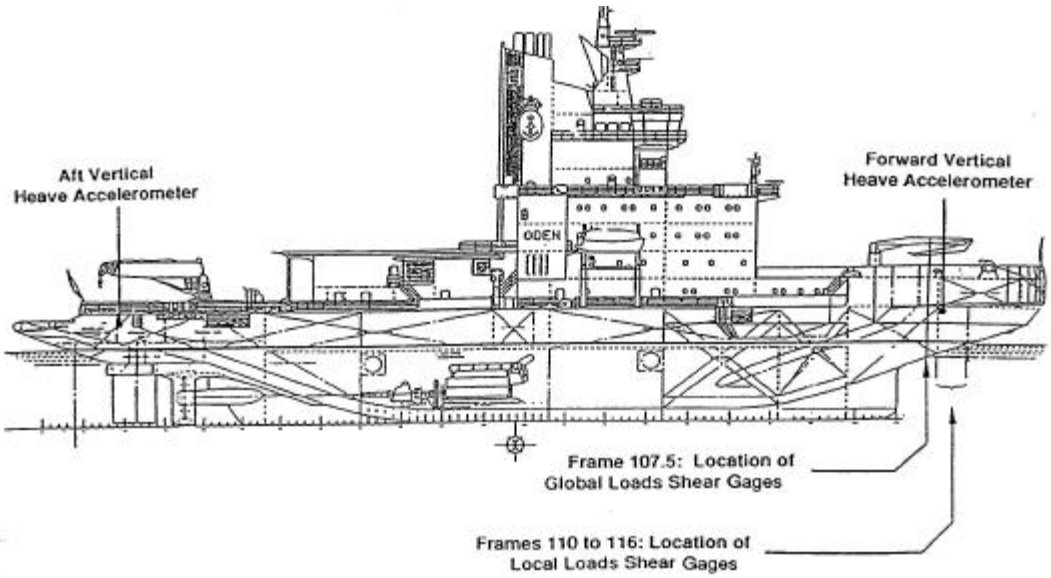

FIGURE 12.2: Side Profile of Oden Showing Location of the Instrumented Area (St. John et al, 1993)

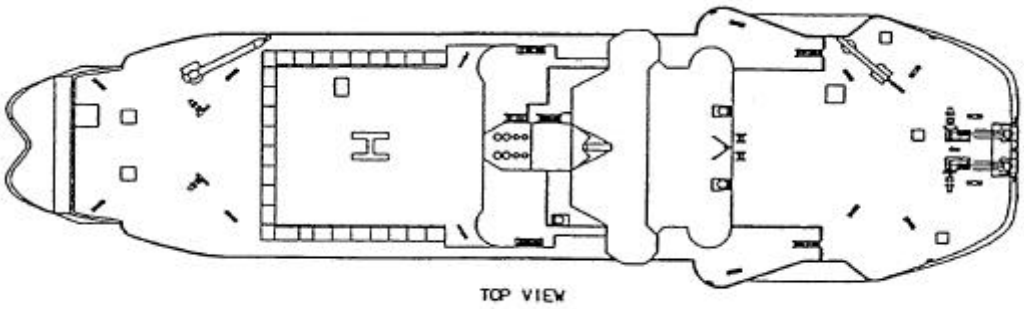

FIGURE 12.3: Top View of Oden (St. John et al, 1993)

Description of the Instrumentation

The hull loads measurement program covered two different aspects of global loads on the bow and local ice loads over a large area in the flat portion of the bow. Only the local loads instrumentation is described, which are directly applicable to local pressures.

The local ice impact loads measurement system aboard Oden consisted of a series of 40 strain gages located on eight frames in the bow of the ship. The strain was measured at five locations on each frame. The local loads measured area was divided into two sections because of the presence of a longitudinal bulkhead which could not be instrumented.

Each strain gage measured the shear strain in the frame from which the shear force can be computed. The difference between the shear force at two different locations on a frame determined the ice load between those locations. This results in there being four small panels on each frame. It is assumed all the shear force difference is due to ice acting on the shell area bounded by adjacent gages and the midpoint between adjacent frames. Thus with the installed gages the system measured the impact pressure over 32 areas of a size 770 by 850 mm. The location of the instrumented area and the layout of the small panels are shown in *Figure 12.4*.

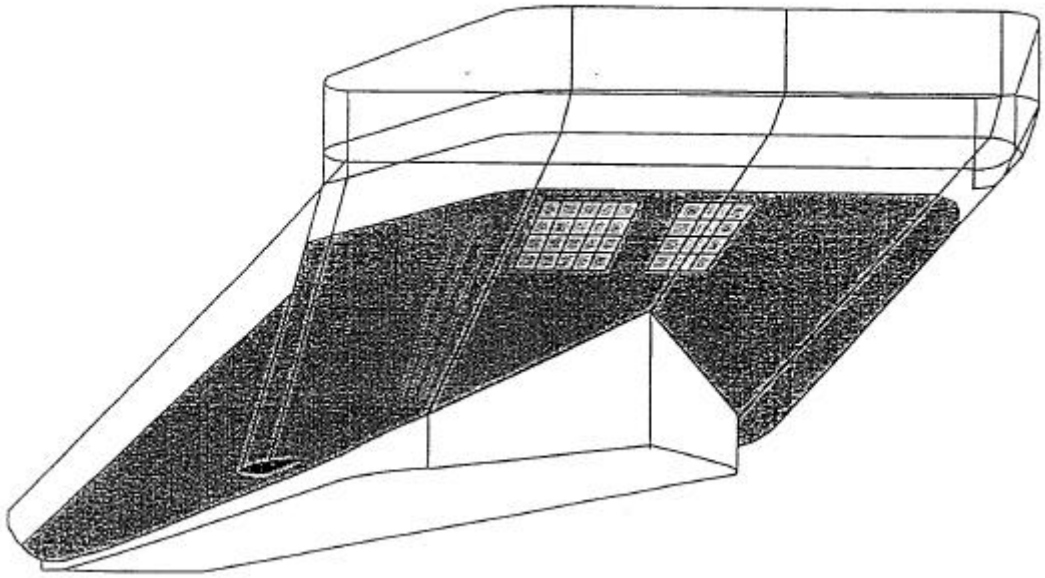

FIGURE 12.4: Location of Instrumentation on the Bow of the Oden 1991 (St. John et al, 1994)

12.3 Data Attributes

Availability of Time Series and Approximate Numbers of Time Series
Data Availability (Who Owns It, Where From) and Format (Tapes, Paper, Disks, Etc.)

The data was originally collected under a joint Canadian Coast Guard, US Coast Guard and the National Maritime Administration of Sweden (Sjöfartsverket).

The original data was collected on HP computers and stored in HP format. This original data was supplied to CCG in HP format on 20 MB data tapes.

In 1999, under a project sponsored by CCG the original HP format data was reprocessed into individual load cell pressures based on the techniques described in the "Measured methods... " section. There are 785 time series events measured on the bow. For each event, time history of the pressure on each small panel (and frame) was recorded. The strain time-history data series for each event are also included on the CD-ROM.

The data is stored in ASCII format, using the ISO 9660 format and can be read on any platform. Full details on the data storage formats are provided on the CD set. The CD-ROM also contains the original analysis report and digital copies of several reports detailing ice property measurements and log of the hourly ice observations made from the bridge. Marine Prairie & Northern Region, Canadian Coast Guard own these CD-ROM's.

Included in the analysis report is a table summarizing the peak loads, ship speed, and ice conditions for each recorded event.

In addition to the digital data a video camera was placed to record the general view looking forward (time lapse video). Video was recorded throughout the voyage from this camera.

Duration of Records

The data records were typically six seconds, but some longer files were recorded.

Frequency of Data Recording

Data was recorded at a sample rate of 50 Hz/channel. The data acquisition system acted as a transient recorder. The data acquisition system was configured such that high shear strain in either of several local strain gauges or global load gauges would cause a data file to be stored.

Range of Contact Areas

0.65 m^2 to 21 m^2 (26 m^2 with interpolation).

Ice Conditions and Ice Types (Salinity and Temperature)

Ice conditions as well as weather and ship operating conditions were observed continuously from the bridge of the Oden while the ships were underway. Hourly averages and maximums along with ice concentrations, weather etc. were recorded.

The ice conditions inside the permanent polar pack in which the Oden operated during the International Arctic Ocean Expedition 1991 were mostly 90 percent and often 95 percent total ice concentration. Nonetheless, extensive networks of leads and cracks, varying in width from hundreds of metres to less than the beam of the ship were found at all latitudes up to and including the pole. The data are divided into northbound and southbound legs. The heaviest ice conditions on the northbound leg were between 84 degrees N and 86 degrees N latitude and several locations north of latitude 88 degrees N as the pole was approached. The southbound trip had easier conditions leaving the pole but became difficult again at about 85 degrees N latitude.

The average thickness of the floes transited by the vessel was in the range of 1.8 to 2.5 m (6 to 8 ft.) for most of the trip.

During the voyage a total of 58 oceanographic station stops were made for the purpose of carrying out general science. At 22 of these station stops extensive measurement and sampling of sea ice properties were carried out by a combined effort of the various scientific teams onboard. Ice cores were taken at these 22 locations. A total of 26 multi-year ice cores were taken of varying lengths to 3.55 m (11.6 ft.). The temperature, salinity and density were recorded. These reports are available on the CD-ROM.

Ice Speed (Or Indentation, Ship Speed) Ice Direction

The vessel speed was measured using a GPS system. In the summary spread sheets a vessel speed is associated with each event. This speed is based on a running average of one second measurements. The actual time history of the ship's location throughout the voyage is available.

Measurement Methods, Resolution, Response Frequency, Etc. Method of Determining Contact Areas

The method of measuring individual strains on frames provides individual strain data with high resolution and high response rates. The Oden's structure is a very simple combination of shell plate and frames with no stringers interconnecting stringers and is therefore simple to analyze.

Initially the measured strains were converted to local panel pressures based on simple beam and shell plate theory. The load on an individual panel is calculated as the shear strain difference between adjacent strain gauges and the frame shear area. This assumes each frame only carries the load applied to the shell plate that extends half way between itself and the adjacent frames.

In order to check this a finite element model of several frames was developed to check the load distribution between adjacent frames for a given load on the shell plate. The FE model also was used to adjust the shear area and take into account the brackets on the upper end of each frame. The FE analysis use of the simple beam theory was adequate and this simple method was used to analyze the measured data.

During the initial analysis of the data analysis St. John, the region area between the two instrumented area was ignored. In subsequent analysis, (St. John et al, 1994) the pressure on this non-instrumented area was interpolated based on the pressures measured on either side.

During the analysis process the data was processed to obtain a pressure/area relationship envelope *Figure 12.5* (St. John et al, 1994).

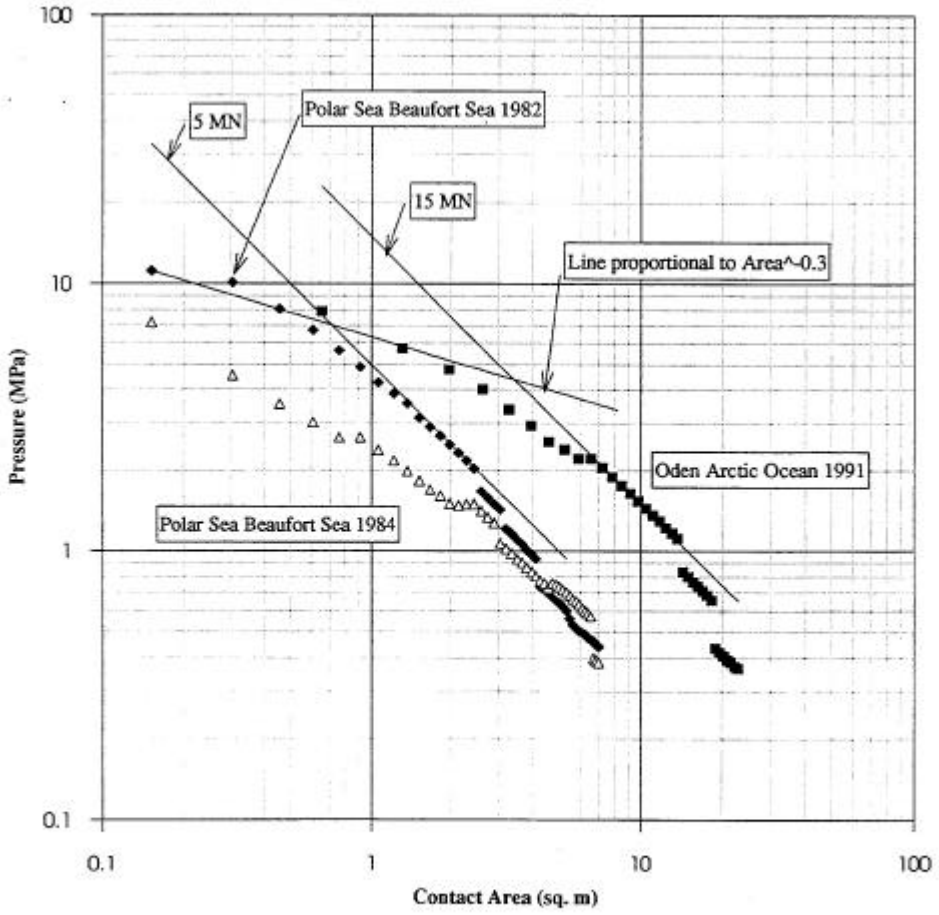

Figure 29. Comparison of the extreme envelope curves of pressure for the *Oden* and *Polar Sea* data sets in similar ice conditions. (1 MPa = 145 psi, 1 m^2 = 10.8 ft^2)

B21

FIGURE 12.5: Oden 1991 Pressure/Area Envelope Relationship (St. John et al, 1994)

12.4 Examples of Time Series Data

The original hull analysis report showed only limited number of time series. Based on the process data from the CD-ROM's a method was developed for this project to plot the full recorded time histories of total load, maximum single panel load, aspect ratio, loaded area, and maximum load frame. The loaded area is based on finding the maximum loaded small panel and then looking for all bordering adjacent panels that at the same time step are loaded. This forms a contiguous area of loading. If within this area a panel has zero load but is bordered by other loaded cells it is included as part of the loaded area.

Figure 12.6 shows the time history for the highest small panel pressure measured. The peak value is 7.9 MPa. At this point in time the total force is 6.1 MN and the loaded area is 10 m^2.

The original report and the subsequent papers do show load histories as bar graphs as shown in *Figure 12.7*. The event shown shows an example of highly localized the load can be. The peak pressure is 7.1 MPa and the peak force is 10.6 MN. The loaded area at this point in time is 14.3 m^2.

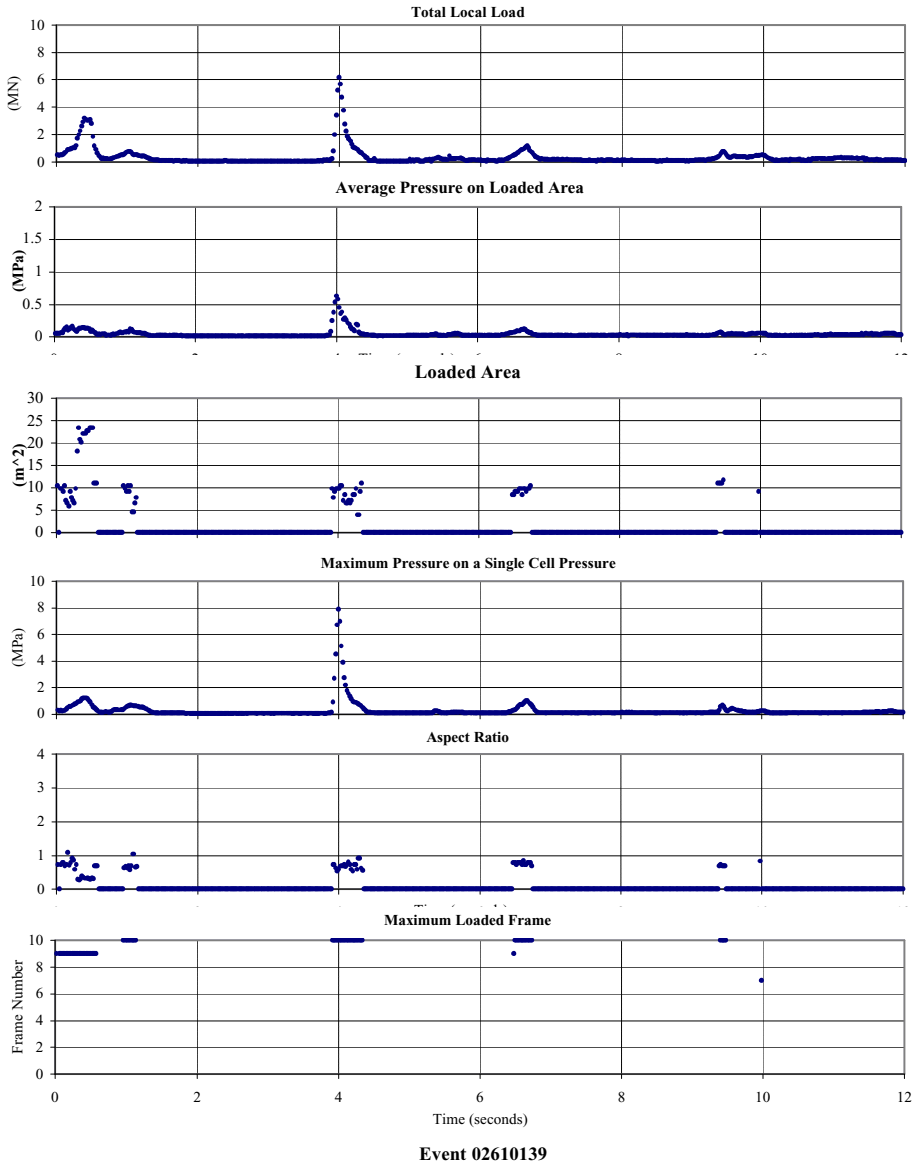

FIGURE 12.6: Oden 1991 Event 02610139 – Time History

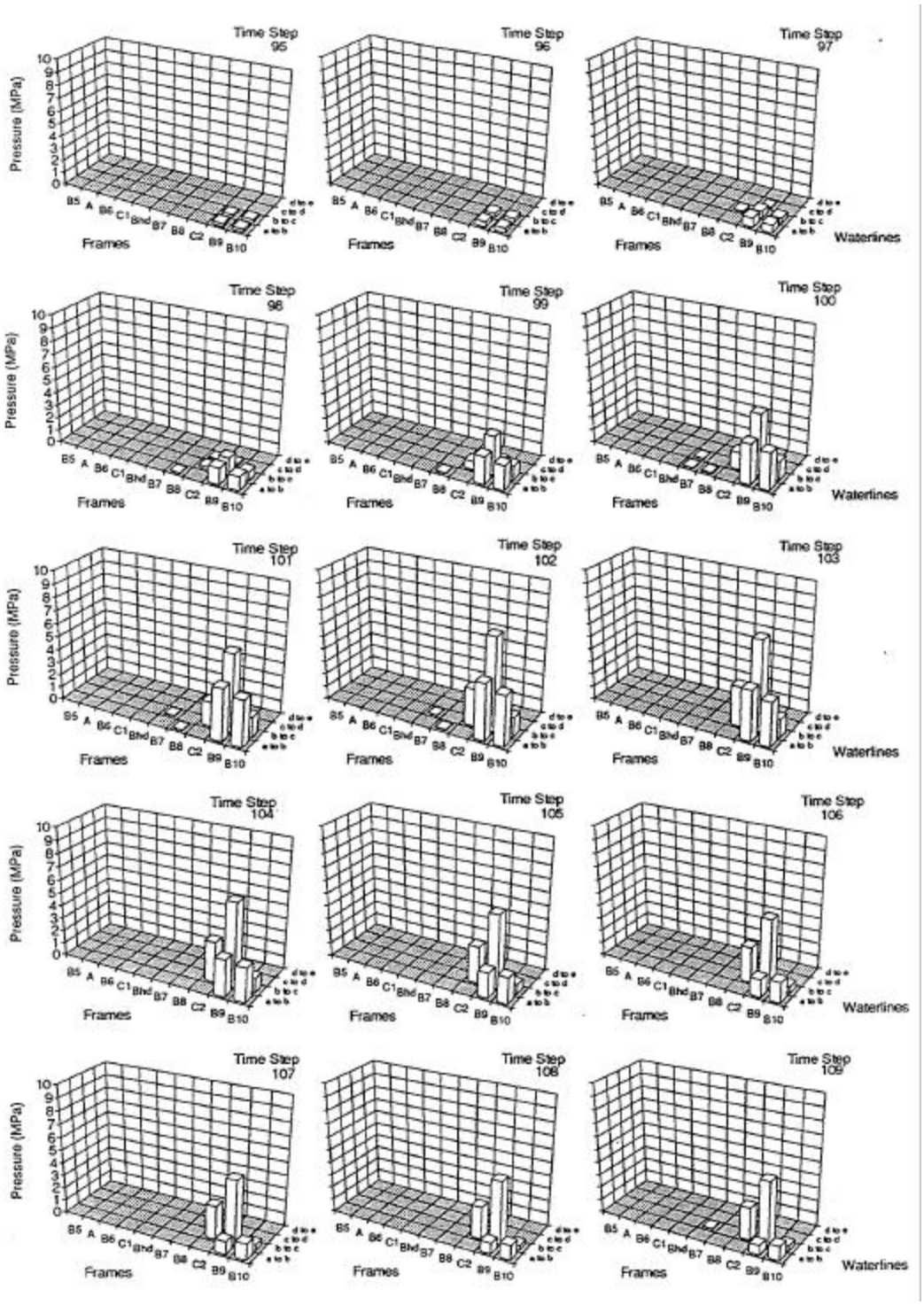

FIGURE 12.7: Oden 1991 – Pressure Distribution at Several Time Steps for Event 0500515 (St. John et al, 1994)

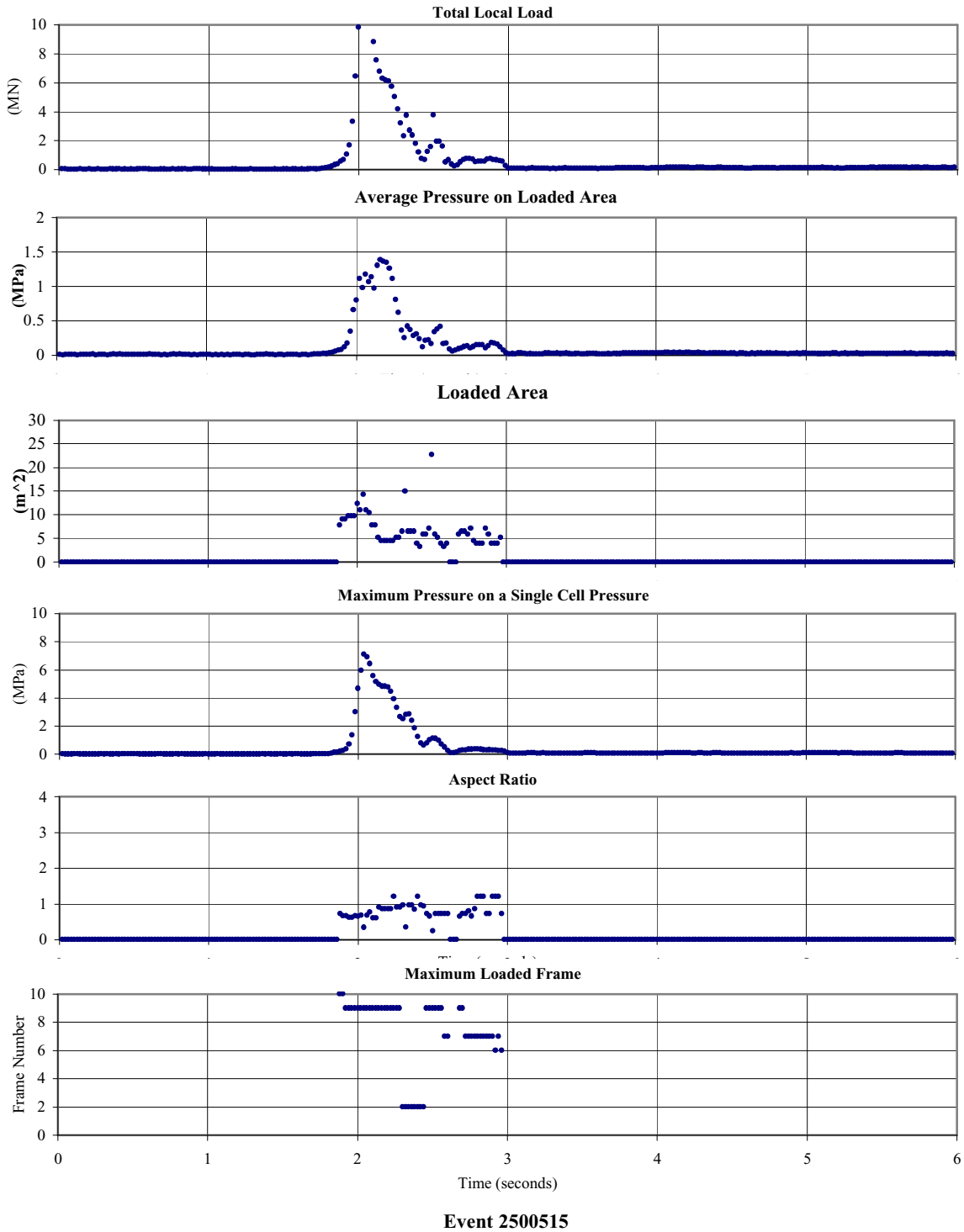

FIGURE 12.8: Oden 1991 – Time History for Event 0500515

Suitability of Data to Probabilistic Treatment

The data collection systems were run continuously as transient recorders while the vessel was underway, making the data ideally suited for long-term load estimation.

Because of the large number events over a relatively long period of time this data provides excellent statistical data on ice loads/pressures. Based on this the data had been analyzed to predict the extreme loading events.

Figure 12.9 shows a example of the data being used to predict the extreme value pressure for various ice regimes based on CAC classification.

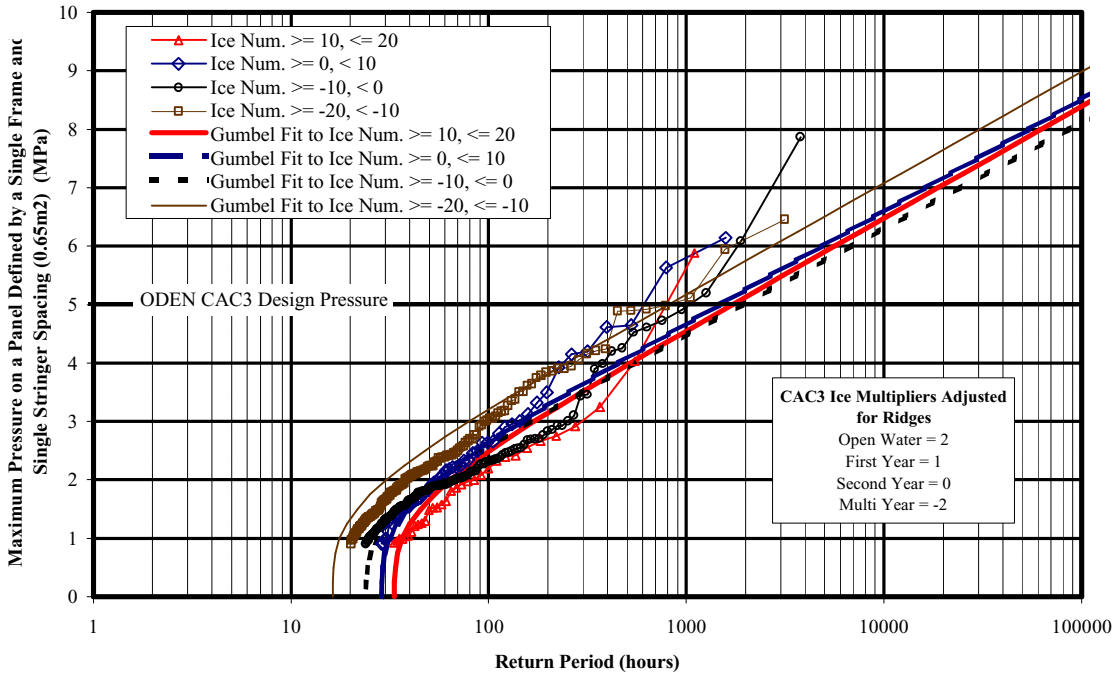

FIGURE 12.9: Oden 1991 Prediction of Extreme Ice Pressure (Browne et al, 2000)

12.5 Comments on Relevance to Local Ice Loads Due to Icebergs

Ship ice interaction data especially with multi-year ice provides the largest source of interaction data and is directly relevant to ice loads due to icebergs, especially growlers and bergy bits. The main issue in using these data are:

- Potential differences in properties between glacial ice and multi-year ice.

- The amount of confinement since the sea ice is of limited thickness.

- Sea ice is likely to fail initially in crushing but as the loads increase other modes of failure will likely limit the magnitude of the total force.

- The general ice conditions have been recorded but the specific ice type and size for each event are difficult to specify. In some case detailed analysis of the video can provide more information on the nature of the impact.

13 Oden 1996 Data

13.1 Summary

Data Source:	Oden 1996	
Geographic Location:	Arctic Ocean	
Time Period:	August and September 1996	
Ice Types:	Pack Ice: First year Arctic Sea Ice: Multi-year ice	
Range of Contact Areas:	Side Shell:	Minimum 0.88 m^2 (1.m high by 0.88) Maximum 21 m^2 (3.0 m high by 7.04)
	Bow Panel Minimum:	Minimum 0.65 m^2 Maximum 9.8 m^2
Relevance to Icebergs:	High	

13.2 Background

A Ship Technology Program was carried out onboard the Swedish Icebreaker Oden during leg two of her 1996 Arctic Ocean Expedition (Ritch et al, 2002). Oden's mission during this expedition was to serve as a platform for the collection of geological, geophysical, meteorological and biological data on the Arctic Ocean environment, as well as providing an opportunity to obtain data relevant to the ice strength design of ice-going shipping operating in Polar Pack Ice.

The objective of the Ship Technology Programme was to obtain full scale measurements of the ice loads acting on the hull side shell just aft of the midships area, together with comparative measurements in the bow waterline area so that the magnitude distributions of the ice impact loads in these two areas could be compared. While extensive full scale measurements of bow ice loads have been made on many different ice going vessels there is very little full scale data available to support the specification of ice strengthening requirements in other parts of the hull. Continuing incidence of damage to side shell structures in ice-going shipping throughout the world has suggested that current design practice underestimates the ice loads that can act in this area.

The 1996 voyage consisted of two legs with a crew change between each leg. The Ship Technology field crew consisted of two persons, one of whom was on the vessel for the full trip while the second joined the vessel for the second leg only. The contracted period for data collection was during the second leg only, but a number of data events of interest were collected during the first leg as well.

The expedition departed Gothenburg Sweden on July 12, 1996. Oden's route took her north, across the top of Norway and into the Barents Sea between Novaya Zemlya and Franz Josef Land, then northeast to approximately N87^{o}, E140^{o} where two weeks of ocean floor geological drilling was attempted. On August 25th the crew change was carried out with the vessel at N86^{o}, E130^{o}, using Russian planes and helicopters to carry leg two personnel to the ship via St. Petersburg and the Siberian port of Dixon. Following the crew change Oden proceeded east between N85^{o} and N87^{o} to E180^{o} and from there, north., arriving at the Geographic North Pole on September 10th. The vessel then returned south between E5^{o} and E20^{o} reaching the edge of the Polar pack at about N82^{o} on September 19th.

For this programme two locations on Oden's hull were instrumented. The main instrumented area was on the vessel's starboard side just aft of midships. This is the area that sustained the heaviest damage during this icebreaker's 1991 Arctic Expedition. The second area included three of the longitudinal frames in way of the bow waterline area that had been previously instrumented for measurement of bow local loads during the ship's 1991 Arctic Ocean Expedition. Three video systems were also installed to collect the views looking forward over the bow to the horizon, looking aft over the instrumented side shell area, and vertically downward over the starboard side to be used for determining ice thickness. A log of ship operations and hourly ice observations was kept by project personnel whenever the vessel was under way throughout leg two. Ice cores were taken when the vessel was stopped using the Transport Canada developed RAPID-CORE system to determine ice properties.

Side Shell Loads Measurement System

A total of 32 strain gauge shear rosettes were installed in Number Four Void Tank starboard, four gauges per frame on Frame Nos. 48 to 55 inclusive, providing an instrumented panel 3.45 m high by 7.04 m wide extending from near the waterline to just above the turn of the bilge.

The location of this panel is shown in the starboard side elevation of *Figure 13.1*. The locations of the gauges on each frame are shown in *Figure 13.2*.

All strain gauge installations consisted of half bridge rosettes oriented to measure shear in the webs of the frames normal to the side shell.

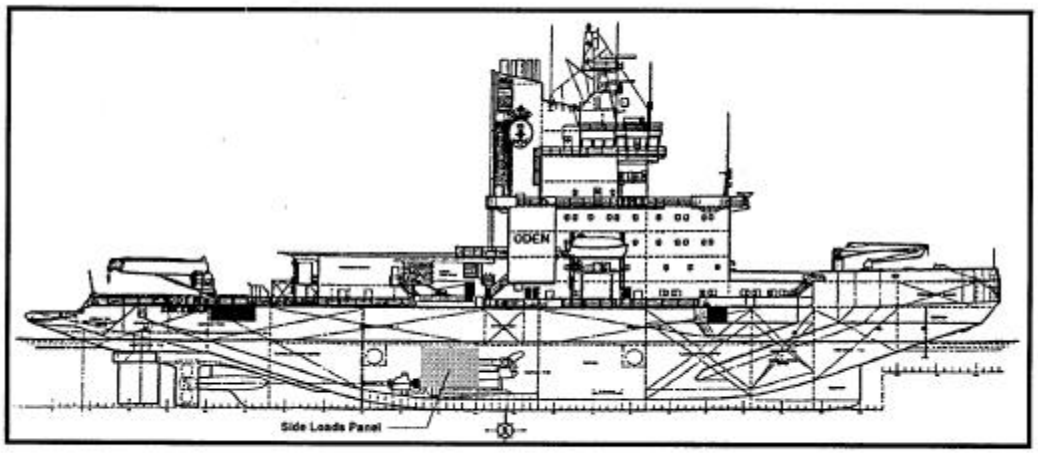

FIGURE 13.1: Location of Instrumented Side Shell Panel

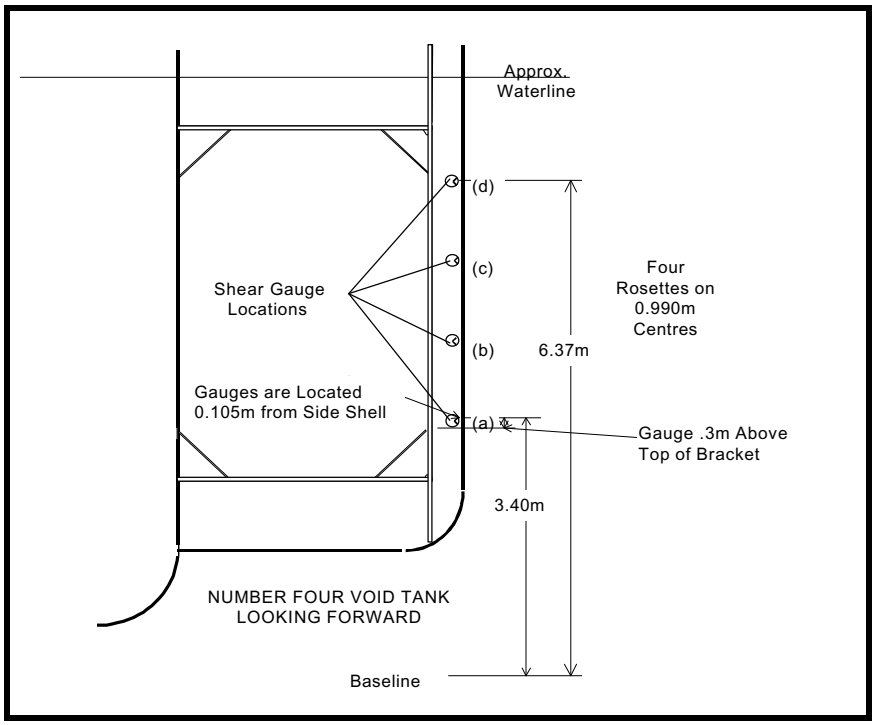

FIGURE 13.2: Locations of Shear Rosettes on Side Frames

Bow Area Loads Measurement System

In addition to the side shell instrumentation the strain gauges which were used in the 1991 trials were re-connected. The three frames selected were B7, B8 and C2 as shown. The extent of both the 1991 and the 1996 instrumented areas can be seen.

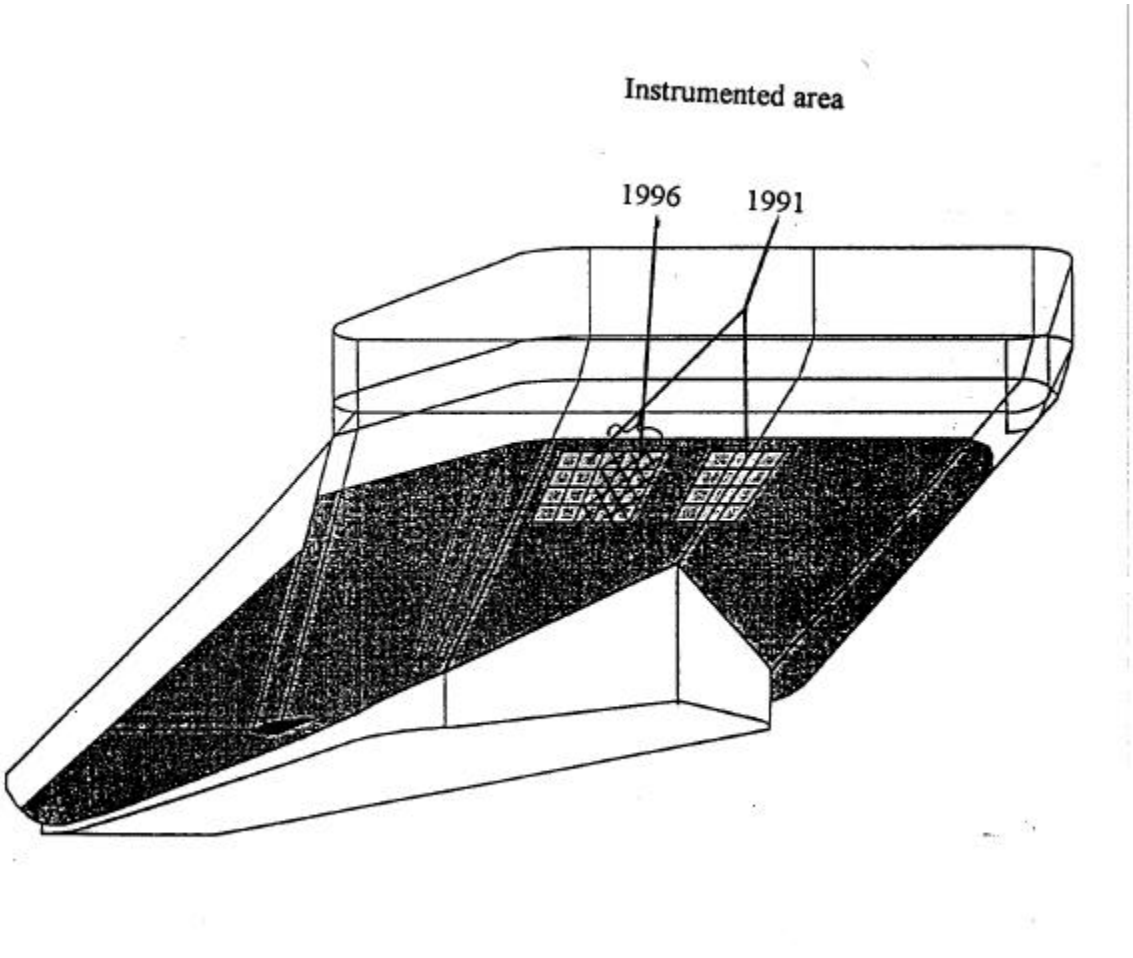

FIGURE 13.3: Locations of Instrumented Bow Frames
(Section at Frame No. 110 Looking Forward)

13.3 Data Attributes

The project was funded by Transport Canada, Marine, Prairie and Northern Region, Canadian Coast Guard, Fleet Technical Services, Panel on Energy Research and Development and supported by Polar Research Secretariat of the Royal Swedish Academy of Sciences.

A total of 1,179 and 1,133 data files were collected on the bow and side shell data acquisition systems, respectively. The data collection systems were run continuously as transient recorders while the vessel was underway, making the data ideally suited for long-term load estimation.

The time history data files have been stored in the form of ASCII files formatted for a PC. Each file contains information about calibration factors, dates, times scan rate, etc. The measured data has been converted into face shear micro strain.

Detailed analysis to determine pressures, pressure/area relationships and comparisons to other data sets has not been done under the original project. Estimates were of loads were performed using simple beam theory. As part of the information delivered under the original project an estimate of the maximum load on a single cell and a frame were made and summarized in tables. Included in these tables as ship speed and ice conditions for each event.

Under a subsequent project the bow loads were converted into pressures and compared to other data sets (Browne et al, 2000).

In addition to the digital data collected video images were recorded throughout the voyage looking forward and looking vertically downwards over the side to gather ice thickness information. Ice properties were collected using the RAPIDCORE sampling device.

Throughout the voyage a constant bridge watch was kept recording hourly average and maximum ice conditions, ship operations, weather etc. The vessel speed was measured continuously throughout the voyage using a GPS system.

Although the side data has not been analyzed in detail it does provide a unique set of data. The side is a vertical surface. Because the Oden has a very high degree of manoeuvrability as is moves through the pack ice it often rotates very quickly. This often results in the instrumented side area slamming against the ice edge. This result can thus bee seen as a vertical wall (shipside) slamming against an ice edge. This could be analogous to ice hitting a vertical structure.

Transport Canada owns this data.

Duration of Records

Record lengths varied from six to ten seconds long.

Frequency of Data Recording

Data was recorded at a rate of 100 Hz/channel.

Range of Contact Areas

- Side Shell: Minimum 0.88 m^2 (1 m high by 0.88)
  Maximum 21 m^2 (3.0 m high by 7.04)

- Bow Panel Minimum: Minimum 0.65 m^2
  Maximum 9.8 m^2

Ice Conditions and Ice Types (Salinity and Temperature)

The ice conditions consisted of heavy pack ice consisting of all ice types.

Figure 13.4 shows a graph of the ice concentration versus North Latitude and *Figure 13.5* shows the maximum thickness versus North Latitude.

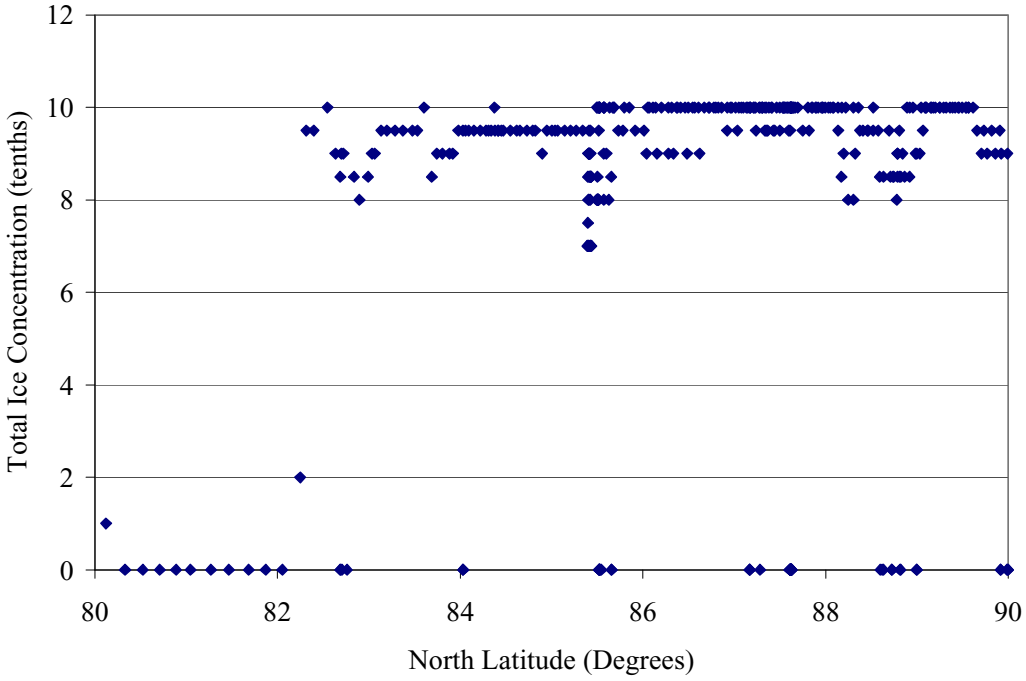

FIGURE 13.4: Oden 1996 – Ice Concentration

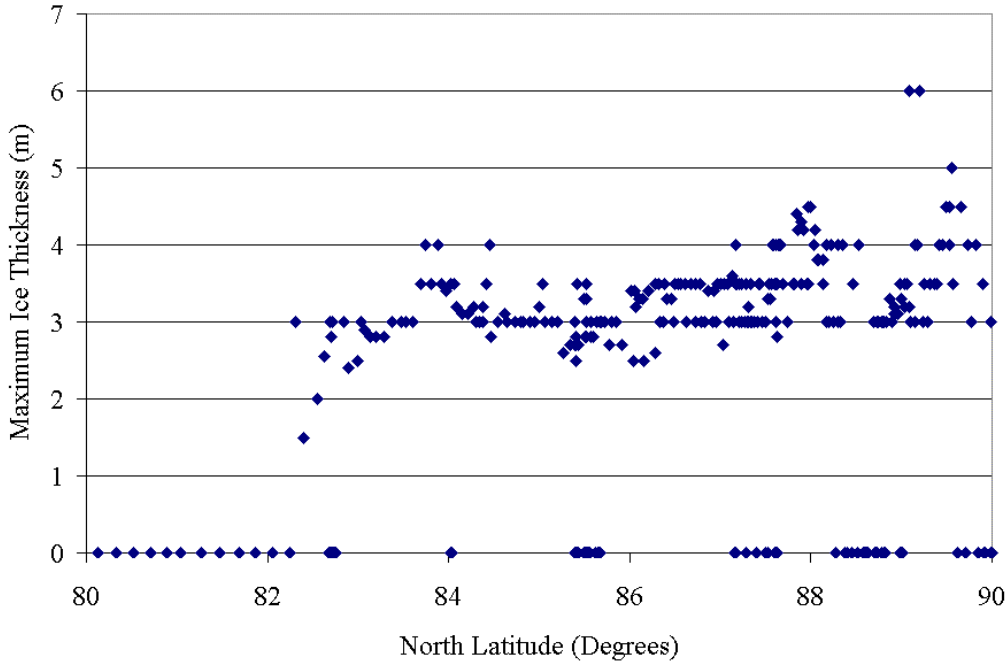

FIGURE 13.5: Oden 1996 – Maximum Ice Thickness

Ice Speed (Or Indentation, Ship Speed) Ice Direction

The ship speed was continuously measured using a GPS system. Each data event has been associated with a vessel speed. For the side loads the rotation of the vessel should be considered in estimating the ice-ship contact speed.

Measurement Methods, Resolution, Response Frequency, Etc. Method of Determining Contact Areas

The bow measurement and analysis technique is the same as used in the Oden 1991 data set. Browne (2000) analyzed the peak loads.

The side data has not been analyzed in detail. Under the original project estimates were made using simple beam theory and shear areas. Because the ship structure is quite simple in this area not a major effort would required to full analyze this data. All shear strain time history data was supplied to Transport Canada in ASCII PC format.

13.4 Examples of Time Series Data

As described above the time history data has not been fully reduced into pressures and loaded areas. A preliminary effort was made under the original project to calculate peak loads on frames and single cells.

To reduce the measured data from the hull load panels to engineering units, frame load calculations were performed based upon simple beam theory. The peak frame load on the bow was 8.2 MN while the peak frame load on the side shell was 5.4 MN. The peak bow sub panel pressure was 6.7 MPa on 0.65 m^2 area and 7 MPa on a 0.88 m^2.

Suitability of Data to Probabilistic Treatment

The data collection systems were run continuously as transient recorders while the vessel was underway, making the data ideally suited for long-term load estimation. There are a large number events over a relatively long period of time and therefore this data provides excellent statistical data on ice loads/pressures.

Figure 13.6 shows a one such prediction made by Browne (2000).

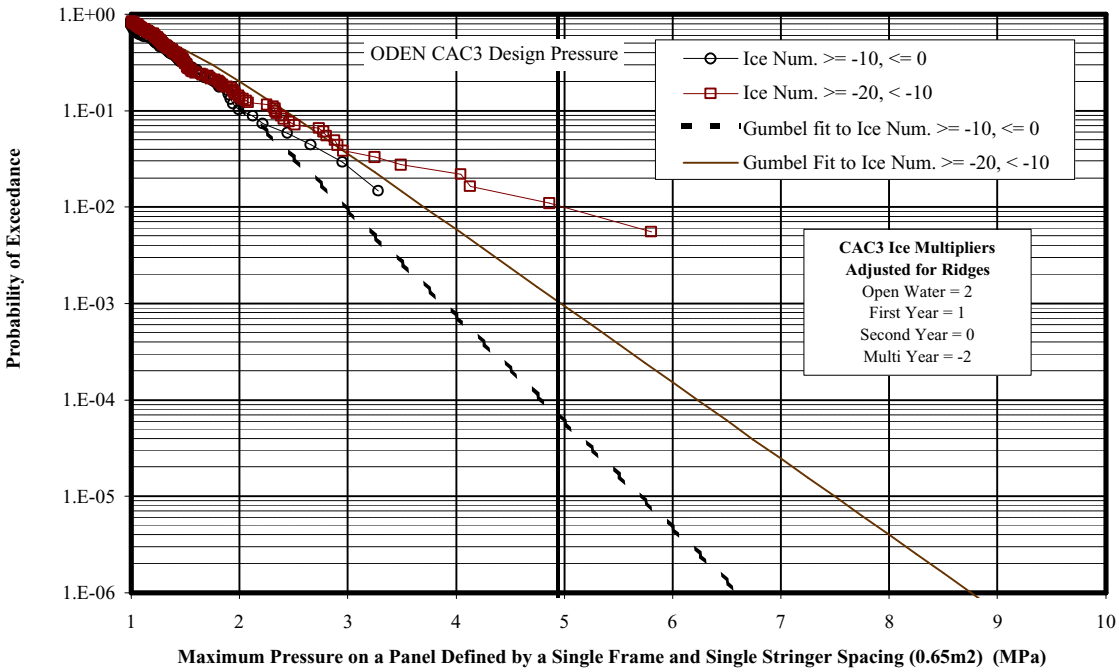

FIGURE 13.6: Oden 1996 Prediction of Long-Term Pressures

13.5 Comments on Relevance to Local Ice Loads Due to Icebergs

Same as other ship measured data.

14 Kigoriak 1981 Data

14.1 Summary

Source:	Kigoriak Rams
Location:	Beaufort Sea
Time Period:	August and October 1981
Ice Types:	Thick first and second year ice (August); multi-year ice (October)
Speeds:	Up to 7.2 ms^{-1} (August), up to 4.2 ms^{-1} (October)
Contact Areas:	Of the order of 50 - 80 m^2 (August), and 20 m^2 (October)
Relevance to Icebergs:	High

14.2 Background

In August and October 1981, two ramming trials into thick ice were conducted by Dome Petroleum using the Canmar Kigoriak. The tests were intended to be a scaled down version of a collision between a tanker and an iceberg. The ice was required not to break in bending and “massive" floes are mentioned in the "Design of Test Program". In the actual program, in the August series 157 rams were conducted on extremely heavy (up to 30 m thick and 1.2 km wide) first and second year ice floes. The borehole jack strength of the ice was on average 7.4 MPa. In the second series (October), 240 rams were made into thick (up to 12 m) multi-year ice. The borehole jack strength was on average 18.2 MPa. Salinities were 1.75 and 2.1 for the two test series respectively. The uniaxial strength showed a mean of 2.9 MPa (range 1.8 to 3.7) for the August series and a mean of 4.3 MPa (range 3.0 to 7.4) in the October series. These values compare well with the values for iceberg and glacial ice (*Figure 14.1*). It is interesting also to note that the local pressures measured were higher for the August test series than the October series. This might result partly from the fact that the impact velocities were higher in August than October. On the other hand, very little velocity-dependence was found in the results. The crushing failures would doubtless have a crushed "layer" associated with the process, which is highly softened as compared to the parent material. The uniaxial strength might not have as dramatic an effect as might be expected.

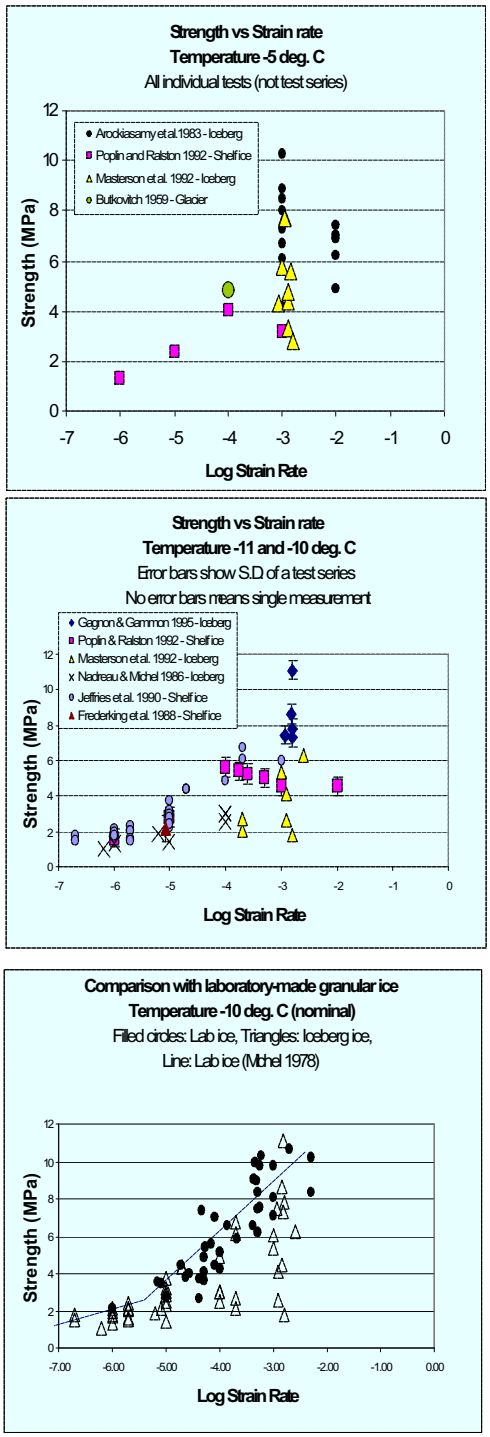

FIGURE 14.1: Uniaxial Strength of Glacial (Iceberg, Glacier and Shelf) Ice

Many measurements were taken; of importance to the present are the forces on the panels A_1 and A_2 (*Figure 14.2*).

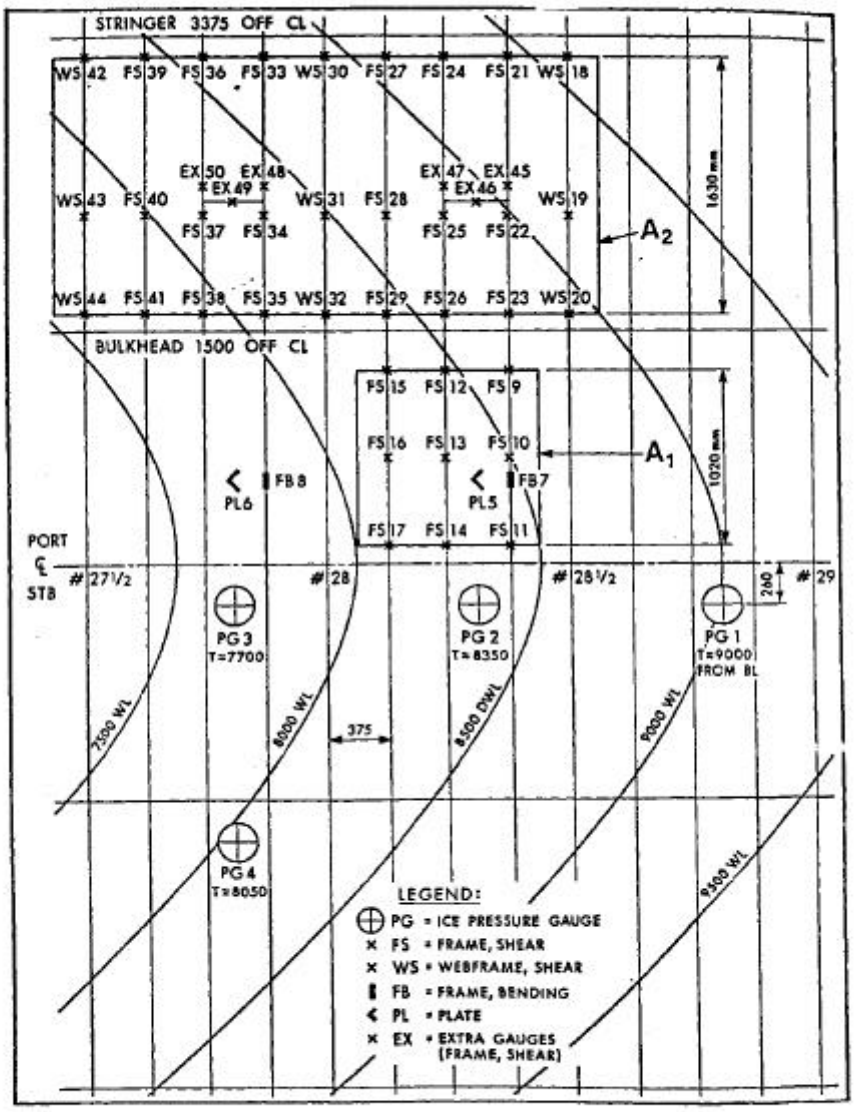

FIGURE 14.2: Panels A_1 and A_2

Using shear strain gauges, the forces on the panel could be determined, and also the distribution within the panels (*Figure 14.3*).

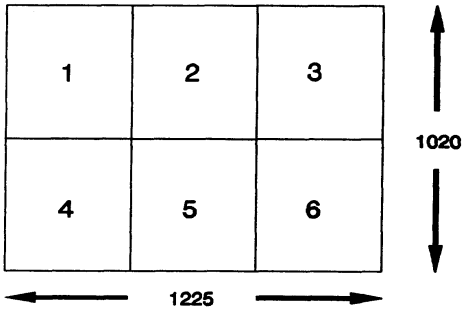

Schematic Diagram of the 1.25 m^2 Instrumented Panel (A1).

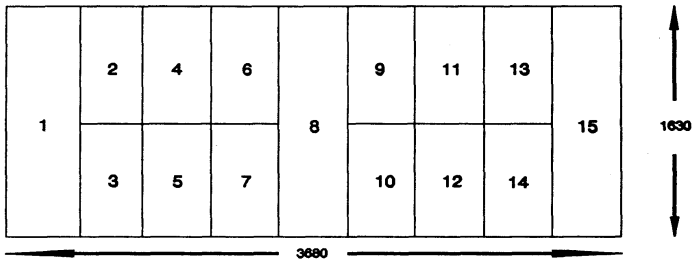

Schematic Diagram of the 6.0 m^2 Instrumented Panel (A2).

FIGURE 14.3: Schematic Diagrams of Instrumented Panels

The results of the force measurements are designated F_1 and F_2 in *Tables 20 and 21*.

TABLE 20: Test Results of the August Rams (Series A)

Run	F_1 (kN)	P_1 (MPa)	A_1 (m^2)	F_2 (kN)	P_2 (MPa)	A_2 (m^2)	FTOT (MN)
1	440	1	0.44	1540	1.1	1.4	4.92
2	0	0	0	0	0	0	6.97
3	0	1	0	1820	1.4	1.3	7.58
4	430	0.4	1.08	1060	1.5	0.71	6.92
5	410	1	0.41	1540	1.1	1.4	7.72
6	2010	4.4	0.46	2600	1	2.6	11.45

Run	F_1 (kN)	P_1 (MPa)	A_1 (m^2)	F_2 (kN)	P_2 (MPa)	A_2 (m^2)	FTOT (MN)
7	3620	3.4	1.06	3260	1.3	2.51	13.8
8	3150	2.9	1.09	4610	1.6	2.88	17.5
9	3270	3.7	0.88	4610	1.3	3.55	11.15
10	2520	2.9	0.87	8640	2.9	2.98	7.88
11	0	1	0	3260	2.9	1.12	16.2
12	0	1	0	2500	1	2.5	15.2
13	0	0	0	0	0	0	13.5
14	0	0	0	0	0	0	17
15	0	0	0	0	0	0	0
16	1700	2	0.85	4990	3.2	1.56	17.3
17	0	0	0	0	0	0	16
18	0	0	0	0	0	0	13.6
19	0	0	0	0	0	0	11.71
20	0	0	0	0	0	0	13.65
21	0	0	0	0	0	0	0
22	160	0.7	0.23	0	1	0	0
23	0	0	0	0	0	0	0
24	0	1	0	2690	1.1	2.45	0
25	0	1	0	960	0.9	1.07	0
26	0	1	0	2690	1.1	2.45	0
27	0	0	0	0	0	0	0
28	0	0	0	0	0	0	0
29	380	0.9	0.42	0	1	0	0
30	750	1.1	0.68	2300	0.9	2.56	0
31	0	0	0	0	0	0	0
32	0	0	0	0	0	0	0
33	1450	3.4	0.43	580	0.7	0.83	0
34	0	0	0	0	0	0	0
35	1130	1.7	0.66	1060	0.6	1.77	0
36	630	2.9	0.22	0	1	0	0
37	3480	3.2	1.09	0	1	0	0

Run	F_1 (kN)	P_1 (MPa)	A_1 (m^2)	F_2 (kN)	P_2 (MPa)	A_2 (m^2)	FTOT (MN)
38	0	0	0	0	0	0	0
39	1700	2.6	0.65	0	1	0	0
40	2640	2.5	1.06	4800	3	1.6	0
41	5910	5.5	1.07	0	1	0	0
42	1200	2.7	0.44	2500	1.8	1.39	0
43	4030	3.7	1.09	0	1	0	0
44	1130	1.1	1.03	1150	1	1.15	0
45	0	0	0	0	0	0	0
46	440	2	0.22	0	1	0	0
47	690	1.1	0.63	0	1	0	0
48	3150	2.9	1.09	9410	2.8	3.36	0
49	750	1.2	0.63	0	1	0	0
50	2080	1.9	1.09	2690	1.1	2.45	0
51	0	0	0	0	0	0	0
52	1380	1.3	1.06	1730	1	1.73	0
53	1450	1.7	0.85	4220	1.2	3.52	0
54	820	1.8	0.46	0	1	0	0
55	1070	1	1.07	8060	2.7	2.99	0
56	0	0	0	0	0	0	0
57	0	0	0	0	0	0	0
58	5660	5.3	1.07	1340	1.2	1.12	0
59	630	1	0.63	1340	1.5	0.89	0
60	0	0	0	0	0	0	0
61	0	0	0	0	0	0	1.47
62	1070	1.6	0.67	1920	1.4	1.37	4.9
63	0	0	0	0	0	0	16.95
64	0	1	0	3070	1.1	2.79	14
65	0	0	0	0	0	0	15.9
66	0	1	0	770	1.2	0.64	17.25
67	0	0	0	0	0	0	16.95
68	0	0	0	0	0	0	0.64

Run	F_1 (kN)	P_1 (MPa)	A_1 (m^2)	F_2 (kN)	P_2 (MPa)	A_2 (m^2)	FTOT (MN)
69	1950	2.3	0.85	580	0.9	0.64	3.48
70	1010	1.2	0.84	3170	1.3	2.44	10.85
71	3920	4.7	0.83	770	0.4	1.93	0
72	0	0	0	0	0	0	0
73	90	0.4	0.23	0	1	0	0
74	1070	1.2	0.89	0	1	0	0
75	570	0.5	1.14	1340	0.7	1.91	0
76	1010	2.3	0.44	3560	1.4	2.54	0
77	690	0.8	0.86	960	1.1	0.87	0
78	380	0.9	0.42	0	1	0	0
79	380	0.9	0.42	12100	3.1	0.68	0
80	940	0.9	1.04	1150	2.5	0.46	0
81	3900	6.2	0.63	1540	0.6	2.57	0
82	0	0	0	0	0	0	0
83	1130	0.9	1.26	5380	1.6	3.36	0
84	0	1	0	6140	1.5	4.09	0
85	1380	1.6	0.86	2880	1.6	1.8	0
86	0	1	0	580	0.4	1.45	0
87	2390	2.7	0.89	3460	0.9	3.84	0
88	0	0	0	0	0	0	0
89	820	0.9	0.91	4220	1	4.22	0
90	1510	2.3	0.66	0	1	0	0
91	0	0	0	0	0	0	0
92	0	0	0	0	0	0	0
93	690	2.9	0.24	0	1	0	0
94	1950	3	0.65	4030	1.5	2.69	0
95	1380	3.2	0.43	3070	1.4	2.19	0
96	1510	1.7	0.89	2020	0.9	2.24	0
97	880	2.1	0.42	0	1	0	0
98	1200	1.9	0.63	2880	0.9	3.2	0
99	1010	1.2	0.84	0	1	0	0

Run	F_1 (kN)	P_1 (MPa)	A_1 (m^2)	F_2 (kN)	P_2 (MPa)	A_2 (m^2)	FTOT (MN)
100	0	0	0	0	0	0	0
101	0	1	0	1730	3.8	0.46	0
102	1130	1.7	0.66	1730	1.5	1.15	0
103	0	1	0	580	0.6	0.97	0
104	0	1	0	1150	0.6	1.92	0
105	0	0	0	0	0	0	0
106	0	1	0	770	3.3	0.23	0
107	3210	3	1.07	2690	1.3	2.07	0
108	2140	2.4	0.89	7490	1.9	3.94	0
109	2330	2.6	0.9	1540	0.9	1.71	0
110	190	0.9	0.21	4800	1.3	3.69	0
111	1130	1.7	0.66	4800	1.9	2.53	0
112	0	0	0	0	0	0	0
113	1640	2.5	0.66	2690	1.2	2.24	0
114	380	1.7	0.22	2820	2.1	1.34	0
115	1130	1.3	0.87	2880	0.9	3.2	0
116	1130	1.3	0.87	1920	0.5	3.84	0
117	1320	2.1	0.63	2110	1.9	1.11	0
118	0	0	0	0	0	0	0
119	750	0.6	1.25	3260	2.4	1.36	0
120	0	0	0	0	0	0	0
121	440	1	0.44	0	1	0	0
122	3150	3.6	0.88	1730	1.5	1.15	0
123	440	0.7	0.63	2110	1.6	1.32	8.72
124	5160	6	0.86	960	0.4	2.4	11.56
125	690	1.5	0.46	2300	0.8	2.88	10.72
126	4280	4.9	0.87	1340	1.2	1.12	12.2
127	0	0	0	0	0	0	10.95
128	0	0	0	0	0	0	16.5
129	0	0	0	0	0	0	13.1
130	0	1	0	960	0.9	1.07	17.6

Run	F_1 (kN)	P_1 (MPa)	A_1 (m^2)	F_2 (kN)	P_2 (MPa)	A_2 (m^2)	FTOT (MN)
131	0	1	0	3260	1.8	1.81	17.25
132	0	0	0	0	0	0	15.35
133	0	0	0	0	0	0	12.35
134	0	0	0	0	0	0	16.15
135	0	1	0	1320	1	1.32	0
136	5850	5.4	0	1920	0.7	2.74	0
137	0	1	0	2880	1.1	2.62	0
138	0	1	0	5180	1.8	2.88	0
139	0	1	0	1150	0.6	1.92	0
140	0	1	0	560	0.4	1.4	0
141	750	3.5	0.21	0	1	0	0
142	2520	2	1.26	2500	2.2	1.14	0
143	0	1	0	3070	2.7	1.14	0
144	0	0	0	0	0	0	0
145	2580	2	1.29	3460	0.6	5.77	0
146	3710	2.9	1.28	0	1	0	0
147	0	1	0	7300	1.2	6.08	0
148	6040	4.7	1.29	580	0.1	5.8	0
149	570	0.4	1.43	960	0.2	4.8	0
150	0	0	0	0	0	0	0
151	1450	1.1	1.32	1150	0.2	5.75	0
152	2580	2	1.29	3460	0.6	5.77	0
153	0	0	0	0	0	0	0
154	570	0.4	1.43	1920	0.3	6.4	0
155	4590	3.6	1.28	2300	0.4	5.75	0
156	1320	1	1.32	5180	0.9	5.76	0
157	0	0	0	0	0	0	0

TABLE 21: Test Results of the October Rams (Series B)

Run (B)	F_1 (kN)	P_1 (MPa)	A_1 (m^2)	F_2 (kN)	P_2 (MPa)	A_2 (m^2)	FTOT (MN)
1	0.00	0.00	0.00	0.00	0.00	0.00	0
2	630.00	2.90	0.22	0.00	0.00	0.00	0
3	1380.00	1.30	1.06	2110.00	0.70	3.01	0
4	0.00	0.00	0.00	0.00	0.00	0.00	0
5	1010.00	0.80	1.26	0.00	0.00	0.00	0
6	630.00	0.70	0.90	1340.00	0.50	2.68	0
7	750.00	1.90	0.39	0.00	0.00	0.00	0
8	0.00	0.00	0.00	3650.00	1.20	3.04	0
9	3710.00	3.50	1.06	0.00	0.00	0.00	0
10	0.00	0.00	0.00	0.00	0.00	0.00	0
11	0.00	0.00	0.00	0.00	0.00	0.00	0
12	0.00	0.00	0.00	0.00	0.00	0.00	0
13	2010.00	2.30	0.87	0.00	0.00	0.00	0
14	0.00	0.00	0.00	0.00	0.00	0.00	0
15	0.00	0.00	0.00	0.00	0.00	0.00	0
16	0.00	0.00	0.00	0.00	0.00	0.00	0
17	0.00	0.00	0.00	0.00	0.00	0.00	0
18	0.00	0.00	0.00	0.00	0.00	0.00	0
19	0.00	0.00	0.00	0.00	0.00	0.00	0
20	0.00	0.00	0.00	0.00	0.00	0.00	0
21	0.00	0.00	0.00	0.00	0.00	0.00	0
22	0.00	0.00	0.00	0.00	0.00	0.00	0
23	0.00	0.00	0.00	0.00	0.00	0.00	0
24	0.00	0.00	0.00	0.00	0.00	0.00	0
25	0.00	0.00	0.00	0.00	0.00	0.00	0
26	1510.00	2.40	0.63	0.00	0.00	0.00	0
27	1570.00	3.80	0.41	0.00	0.00	0.00	0
28	2960.00	4.60	0.64	0.00	0.00	0.00	0
29	0.00	0.00	0.00	0.00	0.00	0.00	0
30	1380.00	2.20	0.63	0.00	0.00	0.00	0

Run (B)	F_1 (kN)	P_1 (MPa)	A_1 (m^2)	F_2 (kN)	P_2 (MPa)	A_2 (m^2)	FTOT (MN)
31	4470.00	5.10	0.88	0.00	0.00	0.00	0
32	0.00	0.00	0.00	0.00	0.00	0.00	0
33	1380.00	2.10	0.66	2500.00	0.90	2.78	0
34	2260.00	1.80	1.26	1730.00	1.50	1.15	0
35	630.00	2.90	0.22	0.00	0.00	0.00	0
36	1450.00	2.20	0.66	0.00	0.00	0.00	0
37	1640.00	2.60	0.63	0.00	0.00	0.00	0
38	0.00	0.00	0.00	0.00	0.00	0.00	0
39	1010.00	2.40	0.42	0.00	0.00	0.00	0
40	0.00	0.00	0.00	0.00	0.00	0.00	0
41	0.00	0.00	0.00	0.00	0.00	0.00	0
42	0.00	0.00	0.00	0.00	0.00	0.00	0
43	0.00	0.00	0.00	0.00	0.00	0.00	0
44	0.00	0.00	0.00	0.00	0.00	0.00	0
45	0.00	0.00	0.00	0.00	0.00	0.00	0
46	0.00	0.00	0.00	0.00	0.00	0.00	0
47	0.00	0.00	0.00	0.00	0.00	0.00	0
48	1070.00	4.90	0.22	0.00	0.00	0.00	0
49	0.00	0.00	0.00	0.00	0.00	0.00	0
50	0.00	0.00	0.00	0.00	0.00	0.00	0
51	0.00	0.00	0.00	0.00	0.00	0.00	0
52	1320.00	2.10	0.63	0.00	0.00	0.00	0
53	440.00	2.00	0.22	0.00	0.00	0.00	0
54	690.00	0.80	0.86	0.00	0.00	0.00	0
55	1320.00	2.10	0.63	0.00	0.00	0.00	0
56	1640.00	1.50	1.09	0.00	0.00	0.00	0
57	1130.00	5.20	0.20	0.00	0.00	0.00	0
58	2140.00	5.20	0.41	1730.00	1.30	1.33	0
59	2260.00	5.20	0.41	0.00	0.00	0.00	0
60	1570.00	1.90	0.83	2690.00	1.20	2.24	0
61	3270.00	3.00	1.09	1340.00	1.20	1.12	0

Run (B)	F_1 (kN)	P_1 (MPa)	A_1 (m^2)	F_2 (kN)	P_2 (MPa)	A_2 (m^2)	FTOT (MN)
62	2200.00	2.10	1.05	0.00	0.00	0.00	0
63	690.00	0.80	0.86	1730.00	0.70	2.47	0
64	0.00	0.00	0.00	2300.00	0.90	2.56	0
65	750.00	3.20	0.23	0.00	0.00	0.00	0
66	0.00	0.00	0.00	0.00	0.00	0.00	0
67	3270.00	4.90	0.67	0.00	0.00	0.00	0
68	0.00	0.00	0.00	0.00	0.00	0.00	0
69	0.00	0.00	0.00	0.00	0.00	0.00	0
70	0.00	0.00	0.00	0.00	0.00	0.00	0
71	0.00	0.00	0.00	960.00	1.10	0.87	0
72	3400.00	3.20	1.06	1730.00	1.50	1.15	0
73	0.00	0.00	0.00	0.00	0.00	0.00	0
74	0.00	0.00	0.00	0.00	0.00	0.00	0
75	630.00	0.70	0.90	0.00	0.00	0.00	0
76	0.00	0.00	0.00	0.00	0.00	0.00	0
77	1070.00	2.50	0.43	1540.00	1.40	1.10	0
78	0.00	0.00	0.00	0.00	0.00	0.00	1.2
79	0.00	0.00	0.00	0.00	0.00	0.00	5
80	0.00	0.00	0.00	0.00	0.00	0.00	4.75
81	0.00	0.00	0.00	1540.00	1.00	1.54	2.13
82	0.00	0.00	0.00	2500.00	2.20	1.14	2.84
83	0.00	0.00	0.00	0.00	0.00	0.00	0
84	0.00	0.00	0.00	0.00	0.00	0.00	3.76
85	0.00	0.00	0.00	1340.00	1.50	0.89	1.35
86	0.00	0.00	0.00	0.00	0.00	0.00	4.72
87	0.00	0.00	0.00	0.00	0.00	0.00	6
88	0.00	0.00	0.00	0.00	0.00	0.00	0
89	0.00	0.00	0.00	0.00	0.00	0.00	5
90	0.00	0.00	0.00	0.00	0.00	0.00	0.51
91	0.00	0.00	0.00	0.00	0.00	0.00	0.4
92	0.00	0.00	0.00	0.00	0.00	0.00	8.2

Run (B)	F_1 (kN)	P_1 (MPa)	A_1 (m^2)	F_2 (kN)	P_2 (MPa)	A_2 (m^2)	FTOT (MN)
93	0.00	0.00	0.00	0.00	0.00	0.00	4.52
94	0.00	0.00	0.00	0.00	0.00	0.00	0
95	440.00	1.00	0.44	0.00	0.00	0.00	0
96	0.00	0.00	0.00	0.00	0.00	0.00	0
97	0.00	0.00	0.00	0.00	0.00	0.00	0
98	0.00	0.00	0.00	0.00	0.00	0.00	0
99	0.00	0.00	0.00	0.00	0.00	0.00	0
100	0.00	0.00	0.00	0.00	0.00	0.00	0
101	0.00	0.00	0.00	0.00	0.00	0.00	0
102	0.00	0.00	0.00	0.00	0.00	0.00	0
103	380.00	0.90	0.42	0.00	0.00	0.00	0
104	0.00	0.00	0.00	0.00	0.00	0.00	0
105	940.00	4.40	0.21	1920.00	1.70	1.13	0
106	0.00	0.00	0.00	0.00	0.00	0.00	0
107	0.00	0.00	0.00	0.00	0.00	0.00	0
108	0.00	0.00	0.00	1340.00	1.20	1.12	0
109	0.00	0.00	0.00	0.00	0.00	0.00	0
110	0.00	0.00	0.00	0.00	0.00	0.00	0
111	940.00	1.10	0.85	0.00	0.00	0.00	0
112	0.00	0.00	0.00	0.00	0.00	0.00	0
113	3590.00	3.30	1.09	0.00	0.00	0.00	0
114	1890.00	2.20	0.86	1730.00	0.80	2.16	0
115	250.00	0.60	0.42	0.00	0.00	0.00	0
116	0.00	0.00	0.00	0.00	0.00	0.00	0
117	0.00	0.00	0.00	0.00	0.00	0.00	0
118	1640.00	2.40	0.68	1730.00	1.90	0.91	0
119	0.00	0.00	0.00	0.00	0.00	0.00	0
120	0.00	0.00	0.00	0.00	0.00	0.00	0
121	3270.00	3.10	1.05	2110.00	1.90	1.11	0
122	1570.00	1.50	1.05	0.00	0.00	0.00	0
123	0.00	0.00	0.00	4220.00	1.70	2.48	0

Run (B)	F_1 (kN)	P_1 (MPa)	A_1 (m^2)	F_2 (kN)	P_2 (MPa)	A_2 (m^2)	FTOT (MN)
124	0.00	0.00	0.00	0.00	0.00	0.00	0
125	2010.00	1.60	1.26	0.00	0.00	0.00	0
126	0.00	0.00	0.00	0.00	0.00	0.00	0
127	940.00	1.40	0.67	0.00	0.00	0.00	0
128	0.00	0.00	0.00	0.00	0.00	0.00	0
129	570.00	2.40	0.24	0.00	0.00	0.00	0
130	0.00	0.00	0.00	0.00	0.00	0.00	0
131	1260.00	1.50	0.84	0.00	0.00	0.00	0
132	0.00	0.00	0.00	0.00	0.00	0.00	0
133	0.00	0.00	0.00	0.00	0.00	0.00	0
134	880.00	2.10	0.42	0.00	0.00	0.00	0
135	1760.00	2.70	0.65	0.00	0.00	0.00	0
136	630.00	0.70	0.90	0.00	0.00	0.00	0
137	5720.00	9.10	0.63	1540.00	0.80	1.93	0
138	0.00	0.00	0.00	0.00	0.00	0.00	0
139	0.00	0.00	0.00	0.00	0.00	0.00	0
140	0.00	0.00	0.00	0.00	0.00	0.00	0
141	0.00	0.00	0.00	0.00	0.00	0.00	1.7
142	0.00	0.00	0.00	0.00	0.00	0.00	1.2
143	0.00	0.00	0.00	0.00	0.00	0.00	0.7
144	0.00	0.00	0.00	0.00	0.00	0.00	1.04
145	0.00	0.00	0.00	0.00	0.00	0.00	2.5
146	0.00	0.00	0.00	0.00	0.00	0.00	0
147	0.00	0.00	0.00	0.00	0.00	0.00	4.37
148	0.00	0.00	0.00	0.00	0.00	0.00	2.74
149	0.00	0.00	0.00	2500.00	2.20	1.14	0
150	0.00	0.00	0.00	0.00	0.00	0.00	0
151	380.00	0.80	0.48	0.00	0.00	0.00	0
152	380.00	1.80	0.21	0.00	0.00	0.00	0
153	0.00	0.00	0.00	0.00	0.00	0.00	0
154	0.00	0.00	0.00	0.00	0.00	0.00	0

Run (B)	F_1 (kN)	P_1 (MPa)	A_1 (m^2)	F_2 (kN)	P_2 (MPa)	A_2 (m^2)	FTOT (MN)
155	0.00	0.00	0.00	0.00	0.00	0.00	0
156	0.00	0.00	0.00	0.00	0.00	0.00	0
157	630.00	1.50	0.42	0.00	0.00	0.00	0
158	0.00	0.00	0.00	0.00	0.00	0.00	0
159	0.00	0.00	0.00	0.00	0.00	0.00	0
160	4150.00	6.60	0.63	0.00	0.00	0.00	0
161	3330.00	5.30	0.63	0.00	0.00	0.00	0
162	1510.00	2.40	0.63	0.00	0.00	0.00	0
163	0.00	0.00	0.00	0.00	0.00	0.00	0
164	0.00	0.00	0.00	0.00	0.00	0.00	0
165	0.00	0.00	0.00	0.00	0.00	0.00	0
166	0.00	0.00	0.00	0.00	0.00	0.00	0
167	0.00	0.00	0.00	0.00	0.00	0.00	0
168	3400.00	3.10	1.10	0.00	0.00	0.00	0
169	2830.00	4.50	0.63	0.00	0.00	0.00	0
170	0.00	0.00	0.00	0.00	0.00	0.00	0
171	0.00	0.00	0.00	0.00	0.00	0.00	0
172	0.00	0.00	0.00	0.00	0.00	0.00	0
173	0.00	0.00	0.00	0.00	0.00	0.00	0
174	750.00	1.20	0.63	0.00	0.00	0.00	0
175	0.00	0.00	0.00	0.00	0.00	0.00	0
176	2900.00	2.50	1.16	0.00	0.00	0.00	0
177	0.00	0.00	0.00	0.00	0.00	0.00	0
178	5410.00	4.20	1.29	0.00	0.00	0.00	0
179	0.00	0.00	0.00	0.00	0.00	0.00	0
180	0.00	0.00	0.00	0.00	0.00	0.00	0
181	0.00	0.00	0.00	0.00	0.00	0.00	0
182	630.00	0.90	0.70	0.00	0.00	0.00	0
183	0.00	0.00	0.00	0.00	0.00	0.00	0
184	2330.00	5.70	0.41	0.00	0.00	0.00	0
185	0.00	0.00	0.00	0.00	0.00	0.00	0

Run (B)	F_1 (kN)	P_1 (MPa)	A_1 (m^2)	F_2 (kN)	P_2 (MPa)	A_2 (m^2)	FTOT (MN)
186	6100.00	5.70	1.07	0.00	0.00	0.00	0
187	0.00	0.00	0.00	0.00	0.00	0.00	0
188	4280.00	6.50	0.66	0.00	0.00	0.00	0
189	4970.00	7.50	0.66	0.00	0.00	0.00	0
190	2890.00	4.40	0.66	0.00	0.00	0.00	0
191	440.00	2.10	0.21	0.00	0.00	0.00	0
192	2580.00	3.90	0.66	0.00	0.00	0.00	0
193	1260.00	1.50	0.84	0.00	0.00	0.00	0
194	3400.00	3.20	1.06	0.00	0.00	0.00	0
195	1380.00	2.10	0.66	0.00	0.00	0.00	0
196	0.00	0.00	0.00	0.00	0.00	0.00	0
197	3710.00	5.90	0.63	0.00	0.00	0.00	0
198	1700.00	2.70	0.63	0.00	0.00	0.00	0
199	2830.00	4.50	0.63	0.00	0.00	0.00	0
200	0.00	0.00	0.00	0.00	0.00	0.00	0
201	1010.00	2.20	0.46	0.00	0.00	0.00	0
202	0.00	0.00	0.00	0.00	0.00	0.00	0
203	0.00	0.00	0.00	0.00	0.00	0.00	0
204	0.00	0.00	0.00	0.00	0.00	0.00	0
205	0.00	0.00	0.00	0.00	0.00	0.00	0
206	0.00	0.00	0.00	0.00	0.00	0.00	0
207	1640.00	2.50	0.66	0.00	0.00	0.00	0
208	0.00	0.00	0.00	0.00	0.00	0.00	0
209	0.00	0.00	0.00	0.00	0.00	0.00	0
210	1130.00	1.80	0.63	0.00	0.00	0.00	0
211	2200.00	3.40	0.65	0.00	0.00	0.00	0
212	750.00	1.70	0.44	0.00	0.00	0.00	0
213	630.00	0.70	0.90	960.00	0.90	1.07	0
214	0.00	0.00	0.00	1540.00	0.80	1.93	0
215	0.00	0.00	0.00	2690.00	1.00	2.69	0
216	1510.00	1.40	1.08	2500.00	1.60	1.56	0

Run (B)	F_1 (kN)	P_1 (MPa)	A_1 (m^2)	F_2 (kN)	P_2 (MPa)	A_2 (m^2)	FTOT (MN)
217	1070.00	1.20	0.89	0.00	0.00	0.00	0
218	2330.00	2.10	1.11	0.00	0.00	0.00	0
219	0.00	0.00	0.00	0.00	0.00	0.00	0
220	0.00	0.00	0.00	0.00	0.00	0.00	0
221	1380.00	3.40	0.41	0.00	0.00	0.00	0
222	1700.00	1.60	1.06	1730.00	1.60	1.08	0
223	1450.00	3.40	0.43	0.00	0.00	0.00	0
224	630.00	2.90	0.22	3070.00	1.30	2.36	0
225	0.00	0.00	0.00	0.00	0.00	0.00	0
226	0.00	0.00	0.00	0.00	0.00	0.00	0
227	630.00	1.00	0.63	0.00	0.00	0.00	0
228	0.00	0.00	0.00	0.00	0.00	0.00	0.1
229	0.00	0.00	0.00	0.00	0.00	0.00	0.7
230	0.00	0.00	0.00	0.00	0.00	0.00	0.45
231	0.00	0.00	0.00	0.00	0.00	0.00	2.75
232	0.00	0.00	0.00	0.00	0.00	0.00	3.8
233	0.00	0.00	0.00	0.00	0.00	0.00	2.7
234	0.00	0.00	0.00	0.00	0.00	0.00	3.5
235	0.00	0.00	0.00	0.00	0.00	0.00	4.59
236	0.00	0.00	0.00	0.00	0.00	0.00	9.2
237	0.00	0.00	0.00	0.00	0.00	0.00	5.95
238	0.00	0.00	0.00	0.00	0.00	0.00	4.63
239	0.00	0.00	0.00	0.00	0.00	0.00	0
240	0.00	0.00	0.00	0.00	0.00	0.00	0

14.3 Data Attributes

The data is not available in electronic form, but excellent summaries exist (Dome Petroleum, 1982, Riska et al, 1982). The local pressures reached a peak during the impact phase of the rams, and the peak values of F_1 and F_2 during this phase were deduced by the VTT team. The data were obtained for each ram; a few were discarded where the data was not recorded. The VTT report contains several examples of the time series plots of data.

Because of the large size of the ice masses, the ice would be highly confined. The total nominal contact areas were limited by the size of the vessel. But is should be noted that the results are consistent with a probabilistic analysis in which no limit is placed on the number or size of high-pressure zones. See the analysis in *Section 16*.

15 Data Suitability

15.1 Iceberg Interaction Scenarios

In order to consider the suitability of the ice pressure data which has been catalogued, it will be useful to discuss the possible types of interactions between icebergs and oil and gas facilities on the Grand Banks. There are four types of facilities that have to be designed for the consequences of iceberg interaction; these are:

1) Fixed Platforms
2) Floating Platforms
3) Tankers and Supply Vessels
4) Seafloor Facilities

Local loads generated during the interaction process can be relevant to all these. However, we will assume that sea floor facilities such as pipelines and wellhead templates will be buried to avoid direct iceberg contact, and we will therefore consider only the first three scenarios in this discussion.

15.1.1 Fixed Platforms

By definition, fixed platforms are not able to be moved in order to avoid an iceberg collision. Ice management can be applied to tow icebergs away, but for the largest icebergs, towing is not feasible. Therefore, fixed platforms (such as Hibernia) are designed to withstand the impacts from all iceberg sizes and the global ice load is controlled by collisions with bergs having the highest kinetic energies.

In fact, the inputs to an impact load calculation are various, and include the iceberg mass, speed, crushing strength, eccentricity, shape of the interacting surfaces and structure stiffness. It is beyond the scope of this study to review this topic in detail. However it is important to understand the magnitudes of the global contact zones and their shapes in order to consider the boundary conditions for the generation of local loads within the interaction process (recognizing that average global ice pressures are used in the calculations).

Contact areas controlling maximum global loads during large iceberg impacts are in the range of several 100 square metres. For example, using a simple energy dissipation model, it can be shown that if an iceberg of 3.6 million tonnes impacts an 80 m diameter structure at 1 m/s with an eccentricity of 50 m, the contact area builds up to about 700 m^2 before the iceberg is stopped. This is beyond the experience and data for iceberg crushing processes. As well, most data on local loads comes from either experiments or measurements where the local area is much closer to a free boundary than would be the case for most similar areas within the 700 m^2 contact zone.

We do have some experience from the Molikpaq of global contact areas in the hundreds of square metres for sea ice. However, the shape of the contact areas expected during iceberg impacts will have nominal aspect ratios (width/thickness) of less than say 3, this compares to the range of 50 to 100 for the larger areas of contact for sea ice. In other words, all large area data for sea ice (and accompanying local loads) is for failures with free edges within 1 to 2 m of the crushing area. This implies that data for sea ice at large areas is for failures which are less confined than the corresponding areas for iceberg impacts.

Based on the above, the validity of the pressure/area relationships derived for sea ice applied to large scale iceberg impacts is not obvious. Clearly, the confidence level in using such data will need to be linked to plausible and (hopefully) proven physics models. Questions such as the following need to be answered:

a) Is the conceptual model for ice crushing shown earlier and repeated as *Figure 15.1*, generally valid?

b) If so, what controls the width of the zone around the edges where spalling (flaking) can occur?

c) Once in the interior where spalling is unlikely, are the sizes of the high pressure zones constant, or do they vary in size with contact area?

d) How likely is a large scale facture within the interior zone, how can this effect be linked to a size effect of this zone.

It is beyond the scope of this study to address these questions in detail. However, it can be appreciated that these questions are actually being implicitly addressed when we extrapolate data on local (and global) loads obtained from the data sets referenced in this report, to the scenario of large iceberg impacts with a fixed platform.

Pragmatically, given that no other data will likely be available on large scale iceberg impacts, we have to decide how to combine and qualify the data derived from ship impacts and from indentation tests. In ship impacts, the contact areas are relatively small and unconfined, whereas in indentation tests the areas are also small, but the confinement may be more comparable to small areas within large contact areas.

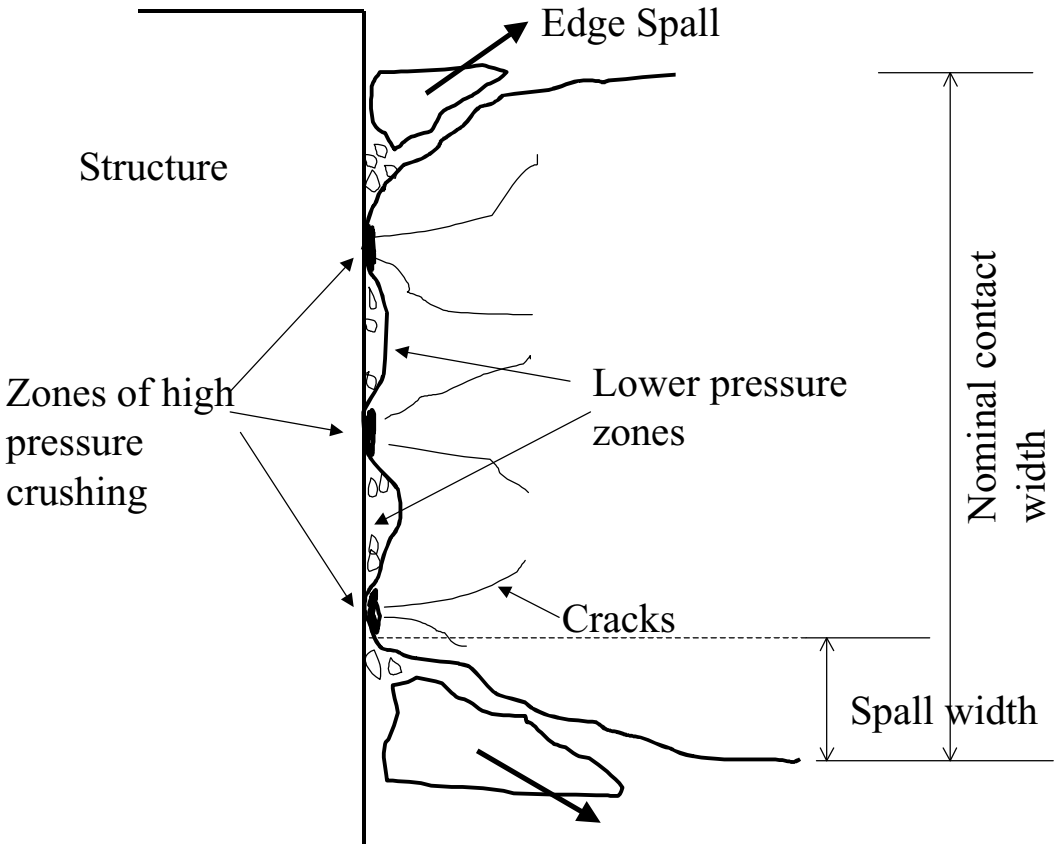

FIGURE 15.1: Conceptual Model for Ice Crushing

15.1.2 Floating Platforms

The rationale for using a floating platform is that it can be designed for lower iceberg impact loads because it can be moved to avoid large icebergs. Furthermore, smaller icebergs can be towed. Even so, it is usual to consider a "design iceberg" as one, which in a probabilistic sense, slips through the ice management defence system. A typical design iceberg for an FPSO is in the 50,000 to 100,000 tonne range. Impact calculations allow for the momentum exchange between iceberg and vessel as well as energy absorbed by ice crushing against the hull.

Typical calculations for an FPSO with a mass of 200,000 t subject to an impact with a 100,000 t iceberg travelling at about 0.9 m/s, give nominal contact areas in the 25 - 60 m^2 range. These are also beyond experience, but are much closer to some of the data sets referenced in this study.

Some of the questions raised in the previous discussion for fixed platforms are also relevant to floating platforms. However, instinctively we can be more comfortable in use of the existing data because the contact areas and boundary conditions in the data sets are closer to the application. However, the issue of contact shape and aspect ratio, hence degree of confinement needs to be kept in mind.

15.1.3 Tankers and Vessels

These will use their detection and manoeuvring capabilities to avoid collisions with icebergs. Even so, they need capability to withstand collisions with undetectable ice masses. However, the contact areas and boundary conditions will be very close to some of the ship impact data sets referenced in this study and their use should be valid.

15.2 Pressure/Area Curves

Pressure/area relationship for ice crushing became a popular approach to ice loads especially after Sanderson (1988) assembled as much data as he could onto the well known single graph. The choice of log scales gave this plot a convincing appearance even though much of the data was from dissimilar tests and measurements.

The form of relationship below was shown to fit the data:

$$p = cA^{-d}$$

Where p is the pressure over the area A, c is a value of pressure (nominally over unit area) and d is a power.

An upper bound to the Sanderson curve was shown to be about:

$$p = 10A^{-0.5}$$

Masterson and Frederking (1993) plotted ice pressures from a variety of indentation tests, ship impact measurements and full scale measurements on Beaufort Sea structures. This plot was included in both the CSA and API codes. It should be noted that this data set did include some iceberg indentation tests from Pond Inlet, these were for contact areas up to about 3 square metres. This plot gives a mean of about:

$$p = 4A^{-0.5}$$

and a mean plus two standard deviations of about:

$$p = 8A^{-0.5}$$

More recently, Jordaan et al (1996) used a probabilistic approach to the problem and from ship data derived a mean of:

$$p = 3A^{-0.4}$$

Despite the obvious validity of these relationships for the data from which they are derived, care is needed in their use. As discussed earlier, their use for the global loads caused by large iceberg impacts may be questioned because we are extrapolating their application to very large contact areas with shapes quite different from the larger areas in the data base. It is also questionable as to whether they should be used during the build up of contact area during iceberg impact calculations because of the different boundary conditions (this will be discussed further later).

15.3 An Alternative Scheme for Iceberg Impact Crushing Pressures

In the absence of any real data at large areas for iceberg crushing, the following scheme is proposed. It is similar to the concept originally proposed by Jordaan discussed earlier and shown in *Figure 15.1*. In this case however, the intent will be to only use actual data from iceberg tests. These are; the Pond Inlet tests, representing confined iceberg crushing; The Grappling Island tests representing unconfined iceberg crushing under real conditions:

- Assume the contact zone is made up of two regions (see *Figure 15.2*).

- The outer region is an unconfined region where failures can propagate to the free edges. This region is assumed to fail at similar pressures to those derived from the Grappling Island cliff impact tests. A further reduction over these pressures might be invoked due to a pseudo aspect-ratio effect due to non-simultaneous failures around the periphery.

- The inner region is a confined zone. Crushing is manifested by the rapid growth and decay of high pressure zones. Average maximum crushing pressures across this zone can be based on the Pond Inlet tests. Later in the development of the model, the inclusion of a scheme based on a formalization of the theory of the physics of high pressure zones might be substituted.

- The model will be sensitive to shape of the contact zones. This is illustrated in *Figure 15.3* - with typical results.

- Whether an additional size effect can be applied to the confined zone is open to debate. Intuitively one would expect this, but we have no experience or data for large iceberg failures on structures. On the other hand we do see that when icebergs calve, massive cracking and global failures can occur at relatively low stresses due to change of buoyancy and gravity forces. In the calculation scheme we have allowed the use of a size effect on the central area in order to assess its effects.

15.3.1 Some Initial Results (Large Icebergs)

We have applied the two region model on a trial basis to assess results for a variety of ranges of inputs. *Figure 15.3* is a plot of pressure versus area for the square contact zone. Due to the dominance of the unconfined edges on the small areas, there is actually a "reverse" size effect. The average pressure eventually slowly trending upwards from about 2.5 MPa at 100 m^2 to about 3.25 MPa at 900 m^2. This is the most conservative interpretation and can be fully justified from existing measurements on icebergs.

Figure 15.4 shows the application of a modest size effect ($A^{-0.1}$). This is beyond any experience for icebergs, except anecdotal. In this case, global pressures for typical areas relevant to global loads is about 1.8 to 1.9 MPa.

This model is also considered important in the context of the problem of impact between an iceberg with a ship or platform, when some or all of the energy of the impact is absorbed in ice crushing. The ultimate force during such an impact is very sensitive to how the force builds up. A rapid build up of force with penetration leads to a lower absorption of energy for a given force and hence to a larger ultimate force in order to absorb a given amount of collision energy. It is for this reason that early designs such as the Hibernia platform used the "teeth" around the perimeter.

It is suggested that using a pressure/area curve of the form, $p = cA^{-d}$, for the build up of load during a collision is incorrect, and is likely to yield conservative results. This is because in the initial stages of an impact, the ice is not as confined as it is in the data sets which govern the pressure/area equation. It is recommended that an ice pressure build-up based on the concept discussed here be used. Such an ice pressure relationship is shown in *Figure 15.4*. This is based on using a constant ice crushing pressure in the core region of 3.5 to 4 MPa (justified as a confined value from the Pond Inlet tests). In the outer spalling region a pressure of between 1.5 MPa and 1.0 MPa is used depending on the perimeter length of the zone (this range is justified by the Grappling Island data). It should be noted that the results are also dependent on the assumed width (thickness) of the spalling zone. In this case we assumed it was 1 m. It should also be pointed out that at large areas, there may be additional size effects which prevail and effectively reduce the 4 MPa central zone pressure.

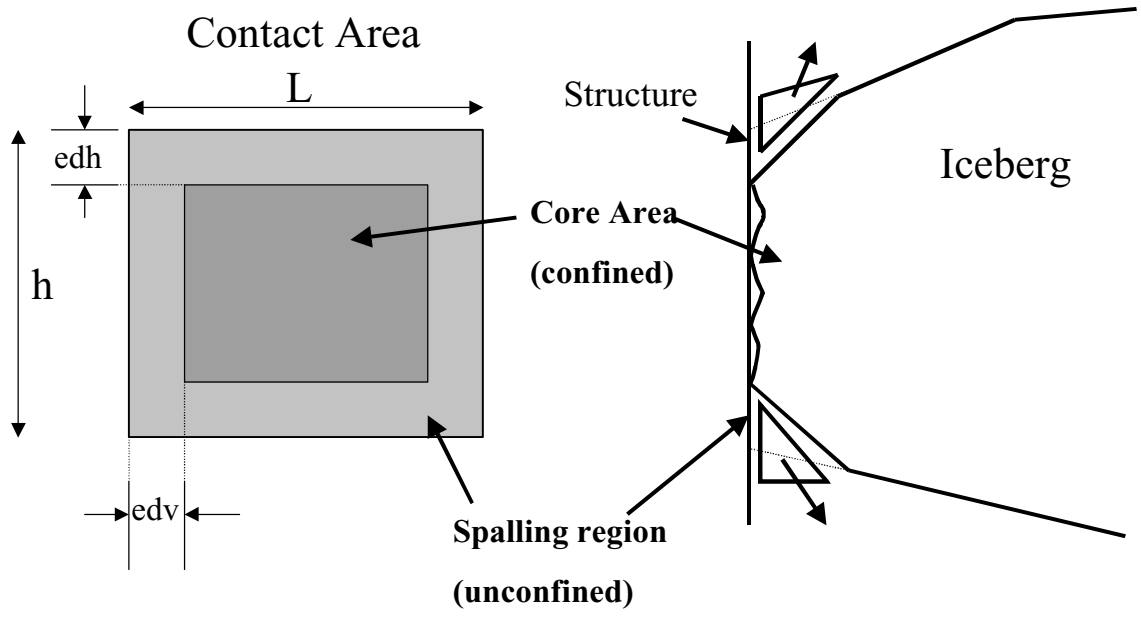

FIGURE 15.2: Crushing Model Concept

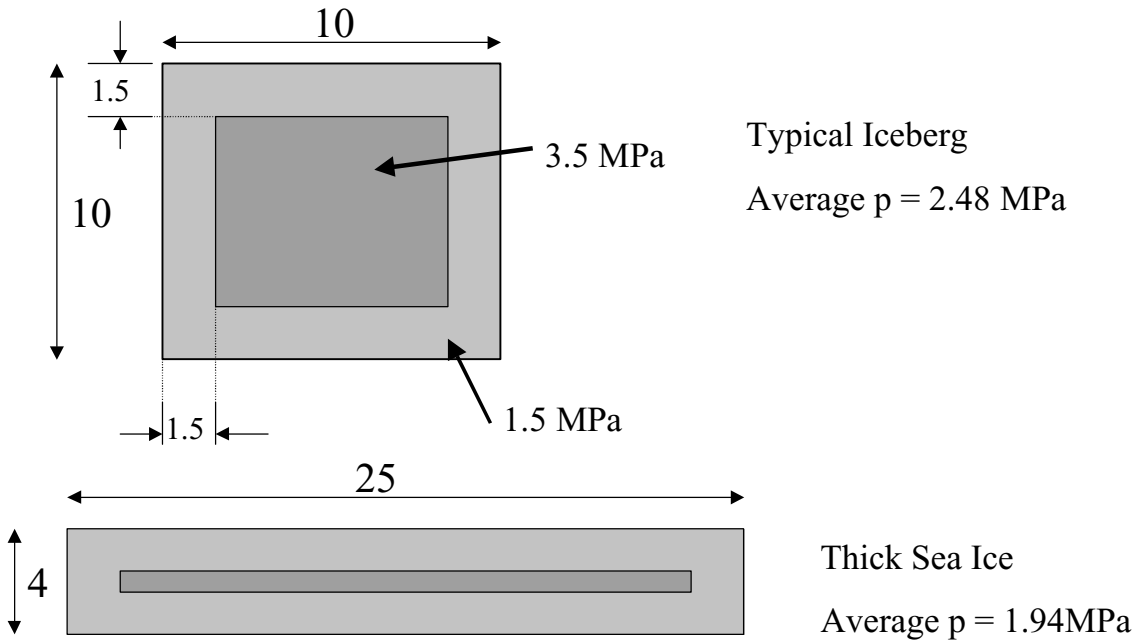

FIGURE 15.3: Effect of Shape for Typical Ice Pressure Inputs to the Core and Spalling Regions

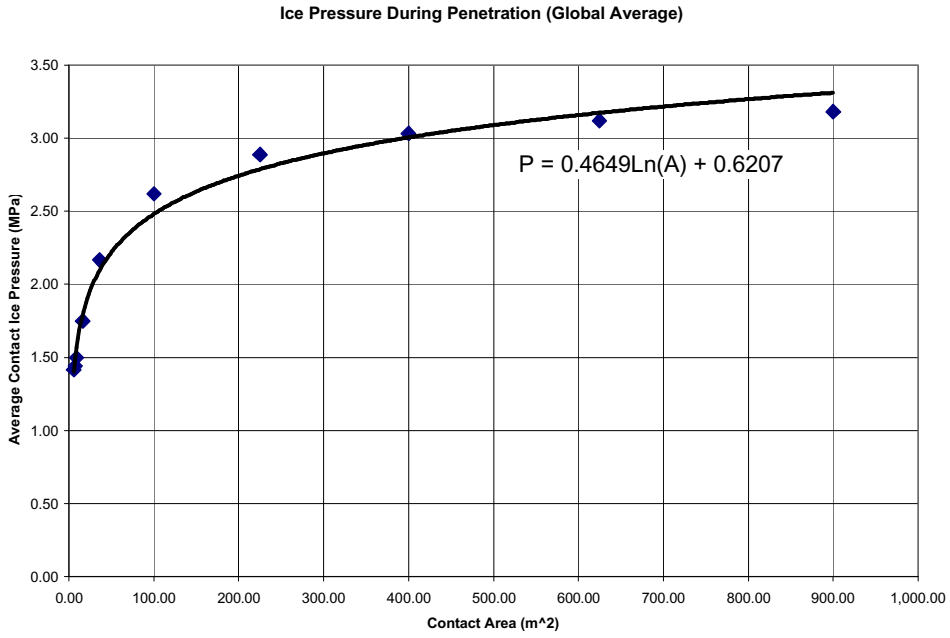

FIGURE 15.4: Global Pressure Versus Area Curve Based on Iceberg Test Data With No Size Effect on Confined Region

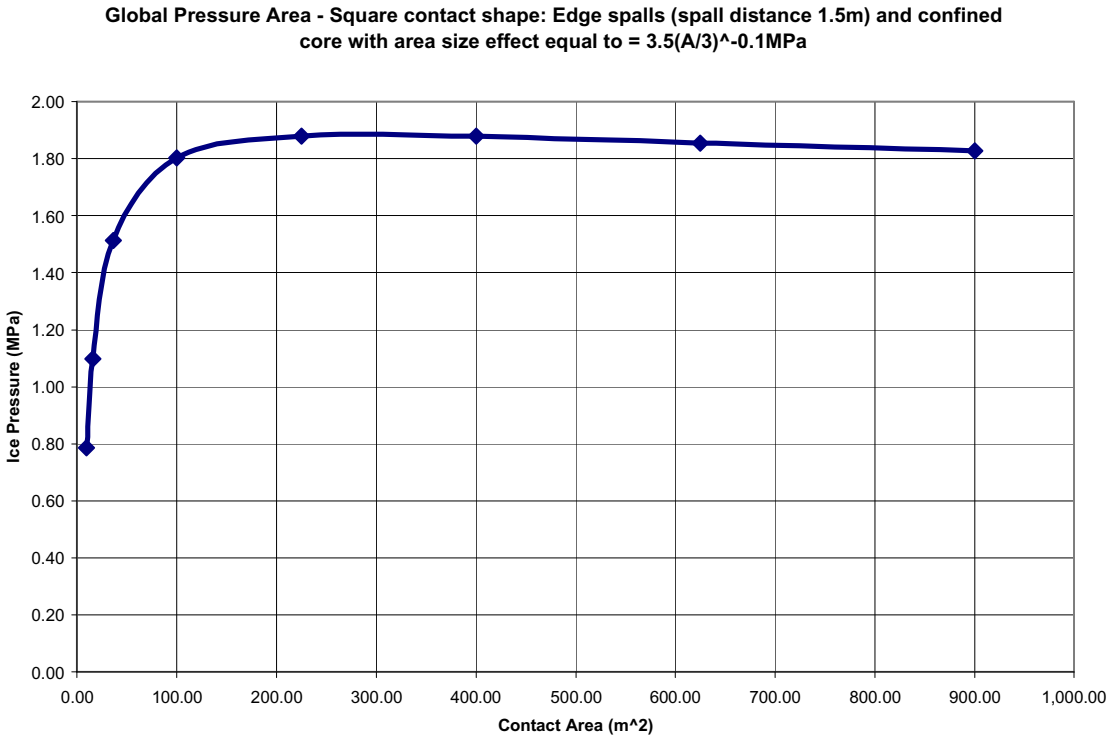

FIGURE 15.5: Effect on Global Pressures Applying a Modest Size Effect to the Confined Core Region

16 Discussion of Probabilistic Approaches

16.1 General Safety Issues

One overall objective in design is to achieve consistent safety in time. Exposure to hazards is an important part of this approach. Very rare hazards are not treated as having the same consequences as frequent ones. Damage is usually accepted in such cases, but it is important to contain this damage to an agreed acceptable level. Design for earthquakes is a case in point; aspects such as ductility of the structure become more important in an effort to maintain integrity while accepting some level of damage. The same philosophy has been used in arctic ship design: some denting of plates is accepted as a part of the operation. Similar approaches could be used in dealing with problems of the Grand Banks.

With regard to exposure, one can contrast the situation for CAC1 vessels which can conduct say 10,000 rams in multi-year ice per year, as compared to CAC4, in which several (e.g., 10 to 20) are expected. The difference in design requirements in the ASPPR Equivalent Standards reflects the different exposure in the two cases. It is not appropriate to use a single design curve for local pressure if different exposures are anticipated. In the following, a methodology is outlined for analyzing this factor in a rational manner.

In obtaining safety levels, both load and resistance of the structure are involved. The specification of load varies a lot from one area of application to another. The CSA standard specifies loads at the 10^{-2} and 10^{-4} levels of annual exceedance probability levels, the latter being applicable for rare loads. Certainly this will be the case for Grand Banks ice loads. The CSA was composed on the basis that the usual resistance formulation would be used, for instance the ultimate load calculated on the basis of structural layout and geometry, section properties and material strength. The effect of the load and the resistance are compared after load and resistance factors are applied. This strategy can lead to excessive damage if not supplemented by criteria for damage states (this is noted also in the CSA code). A case in point is the analysis by Carter et al. (1992) of the local load provisions in the ASPPR revisions (now the Equivalent Standards). The design method consisted of the use of a load corresponding approximately to the mode of the annual maximum, not the usual practice of an extreme (e.g., 1% exceedance) value. The resistance was calculated on the basis of the first two plastic hinges forming-thus neglecting the reserve capacity associated with membrane action. This amounted to a check that denting would not occur frequently; ultimate safety was provided by the reserve capacity noted, which could be 10 times the load associate with three-hinge bending failure (although no explicit check was included). No calculations of ultimate capacity was proposed. Design load specifications are related to consequences of failure. Depending on the latter, and the strategy, the specified value could be at the 10^{-2}, 10^{-4} or some other level.

16.2 Modelling of Local Ice Pressures

Global pressures in ice-structure interaction are defined as the total interaction force divided by the nominal contact area. This area is defined by the projection of the structure onto the original ice feature (without fractures) at the required amount of penetration. This can be determined accurately if the shape of the ice feature is known. Analysis of global failure pressures in ice, both from ship rams and from interactions with indentors and structures, show that the global pressures decrease, on average, with the nominal contact area, on average $\propto (\text{area})^{-0.5}$. During the interaction, pieces of ice spall off, so that the actual contact area is less. Fractures result in parts of the nominal area carrying little or no pressure, as illustrated in *Figure 16.1*. Most of the force is transmitted through "high-pressure zones". There are also areas of lower pressure where soft granular ice is extruded from these zones. The crushing process in ice includes all of these phenomena. High-pressure zones tend to move and fluctuate in intensity continually.

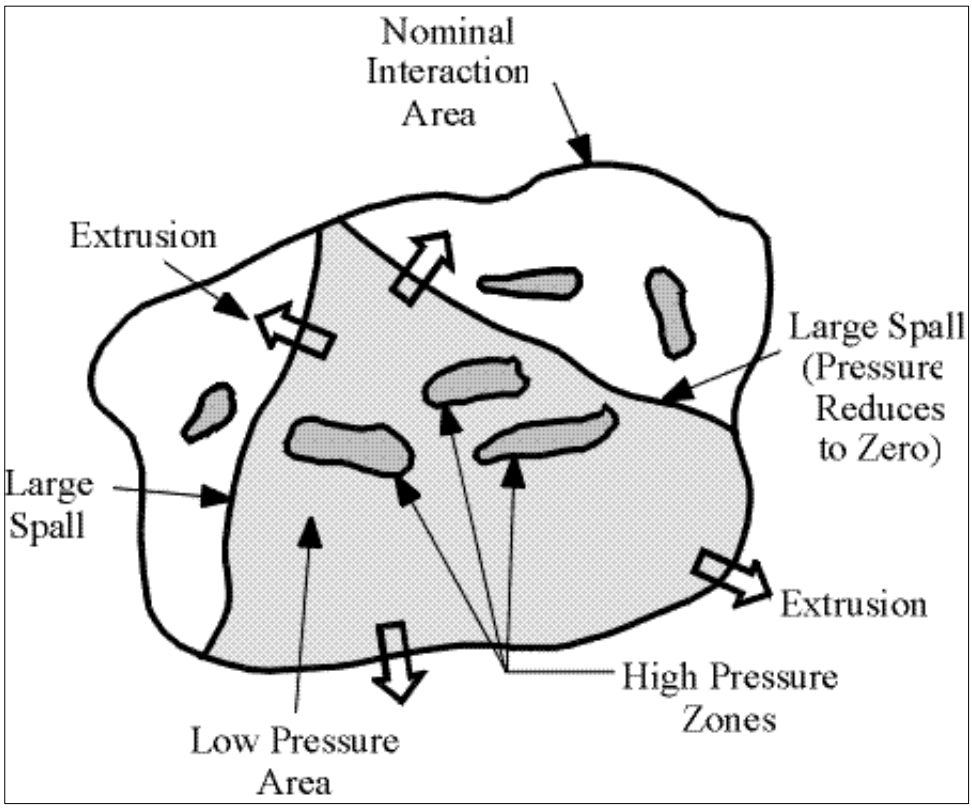

FIGURE 16.1: Local Ice Model

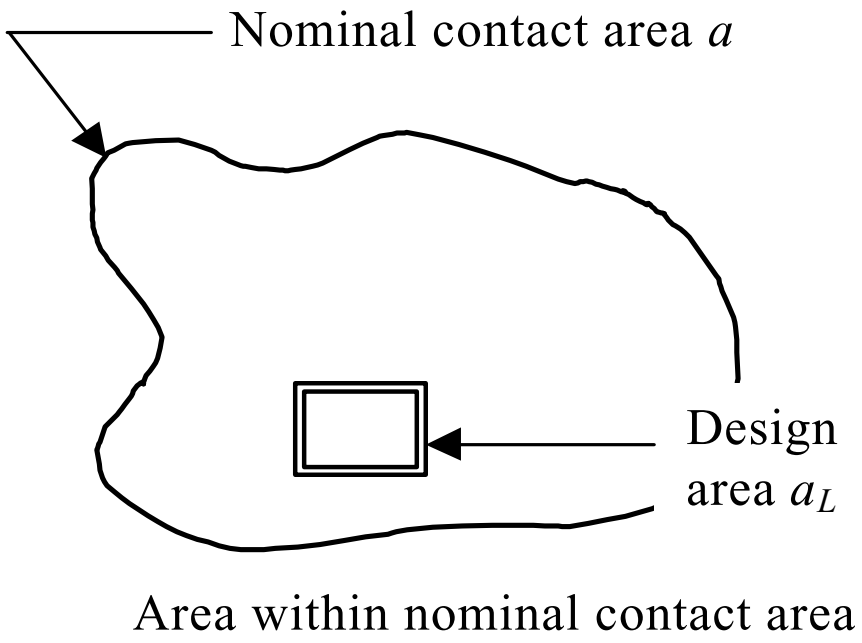

FIGURE 16.2: Design Local Area

Since global average pressures decrease with nominal contact area, one can deduce that fractures are more in evidence at higher contact areas. This counteracts the effect of confinement, insofar as the fractures reduce considerably the contact area. This will certainly be a random process, with some "internal" fractures. It should be noted that the methodology presented below does not place any limit on the size of high-pressure zones.

For design of local areas, a particular panel could be somewhere within the total interaction area, as shown in *Figure 16.2*. An interaction might last, say, 50 seconds, and the nominal area might increase to more than 100 m^2. The design area would receive pressures that depend on the location and movement of high-pressure zones. This is a dynamic situation and is quite different from the pressure received by a nominal area that is equal to the design area. It is therefore important to develop two different pressure/area relationships, for:

- global pressures; and,
- local pressures.

The present report addresses the second of these.

16.3 Principles for Probabilistic Analysis

Ideally, the data must reflect the random situation to be obtained in a real interaction. These are distinguished by continual fluctuations of load, including times of zero pressure when fractures occur. One can contrast the Pond Inlet and other medium scale results, in which the contact area is limited with, ship or the Grappling Island results. The medium scale results do not simulate the process to be expected in a design area within a large interaction, and the situation is highly confined, with a small contact area some distance away from a free surface. *Figure 16.3* illustrates the concept of non-simultaneous failure. This is intimately linked to the scale effect for global loads. The medium scale tests may not capture this effect. The exposure time is also most important; different situations must be related by means of a comparison of how long the panel is exposed to the loading.

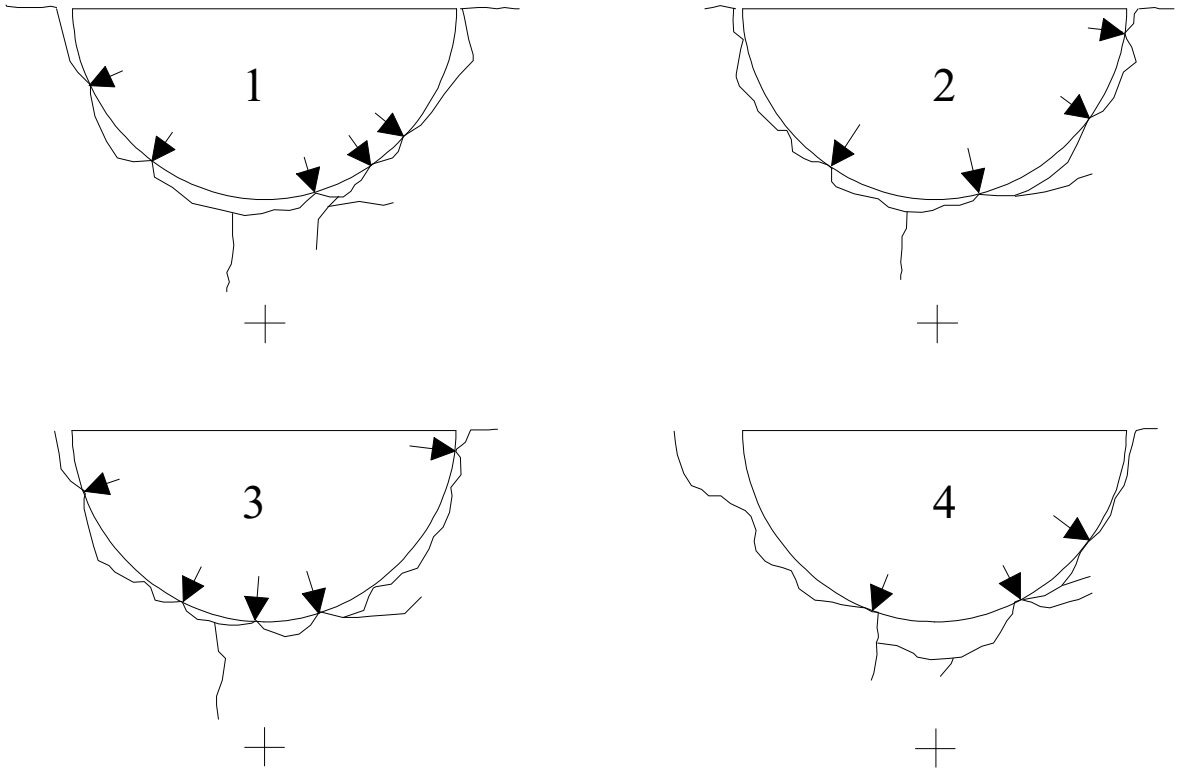

FIGURE 16.3: Non-Simultaneous Failure

Let *X* be a random quantity denoting the maximum pressure on area a for a given exposure. This will be termed an "event". The probability density function pdf is denoted $f_X(x)$, and cumulative distribution function cdf is denoted $F_X(x)$. These are as shown in *Figure 16.4*, together with the probability of exceedance, p_e. These curves would represent our uncertainty regarding the pressure in a single event. An example is given in *Figure 16.5* where a histogram of measured values has been plotted. If one fits a curve of probability density, then this would be one way of obtaining the pdf. There is no fixed maximum value, so that in design one chooses a value at an annual probability of exceedance p_e that ensures a reasonable safety level. The procedure is acceptable if one event in a year occurs. (We use a time basis of one year; this could be any other periods, such as structure lifetime, if desired).

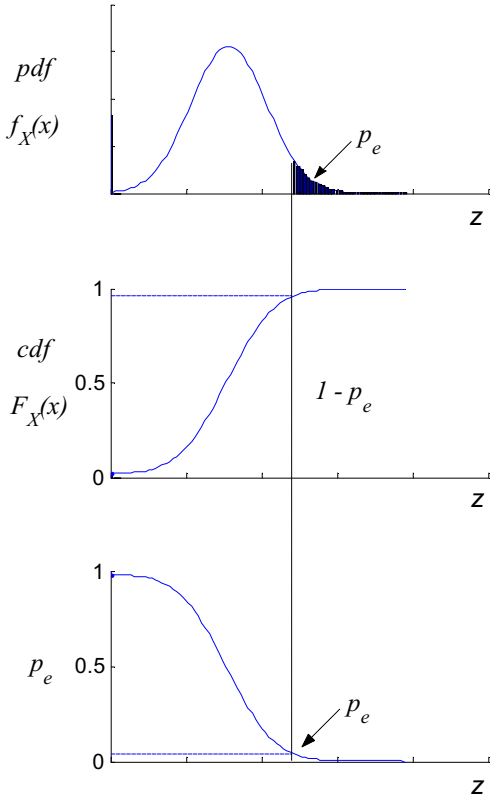

FIGURE 72: Probability Density Function (pdf), Cumulative Distribution Function (cdf) and Probability of Exceedance (p_e) Curves

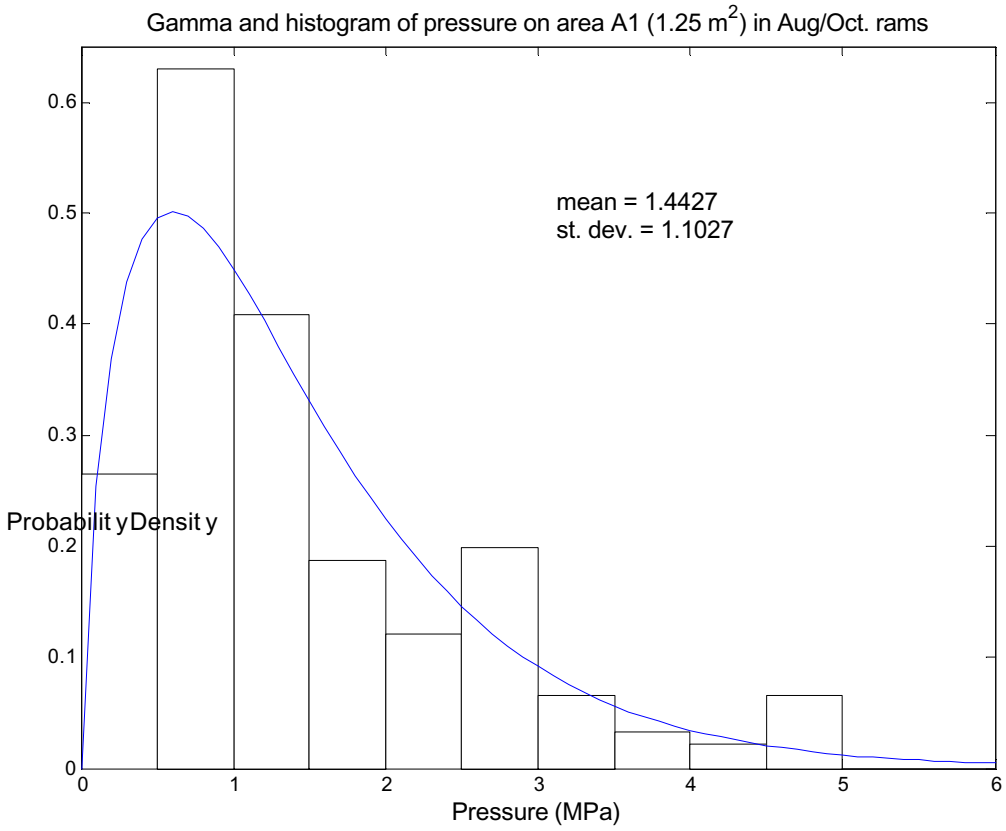

FIGURE 16.5: Histogram of Measured Values

The situation is complicated if one now considers two rams in a year. What we need is the maximum pressure in two rams, called *Z*, also random:

$$Z = max\ (X_1, X_2)$$

If we take the distributions of each ram as being independent and identically distributed (iid), say following a distribution such as *Figure 16.5* then:

$$F_z(z) = Pr\ (both\ X_1\ and\ X_2\ \#\ z) = F_X^2(z)$$

For example, if $f_X(x) = exp(-x)$, $F_X(x) = 1 - exp\ (-x)$, and:

$$F_Z(z) = \{1 - exp(-x)]^2$$

This will yield different results from taking more extreme values of p_e on the parent distribution $f_X(x)$ to compensate for the fact that there are now more than one ram.

The same method applies if there are *n* rams in the period:

$$Z = max\ (X_1, X_2, X_3, ..., X_i, ..., X_n)$$

If we judge again that each X_i has the same cdf $F_X(x)$ and that the random quantities are stochastically independent (*iid*):

$$F_Z(Z) = Pr\ (all\ X_i \# z) = FX^n\ (z)$$

The local pressure model is based on ship impacts (Jordaan et al., 1993). The distribution of pressure in individual rams such as those in *Figure 16.5* have exponential tails of the form:

$$p_e = exp[-(x - x_0) / a] \qquad \text{Equation 1}$$

where p_e = probability of exceedance = $1\text{-}F_X(x)$, and x_0 and a are constants. See the next section for an example of fitting of this relationship.

It is reasonable to assume a Poisson arrival process of loading events, not necessarily with a constant arrival rate. This results in the following expression for the distribution of extreme load *Z* which can be derived by writing the expression for zero arrivals in the process, with rate $?[1\text{-}F_X(z)]$, where *Z* = max $(X_1, X_2, X_3,\ldots,X_i,\ldots,X_n)$ extreme value, and *?* = number of arrivals in a year.

$$F_z(z) = exp\ \{-u \quad [1 - F_x(z)]\} \qquad \text{Equation 2}$$

The choice of period of time could be a year, as this facilitates comparison with other risk indices, or the lifetime of the structure, or any other time period that is useful for the question being studied. Using Equation 1, Equation 2 takes the form of the double exponential or Gumbel distribution:

$$F_z(z) = exp\{-exp[-(z - x_0 - x_1) / a]\} \qquad \text{Equation 3}$$

where x_1 = ln *?*. It should be noted that if $? < 1$, a "spike" of probability at zero load will be found (see *Figure 16.6*). This is usual in Grand Banks applications.

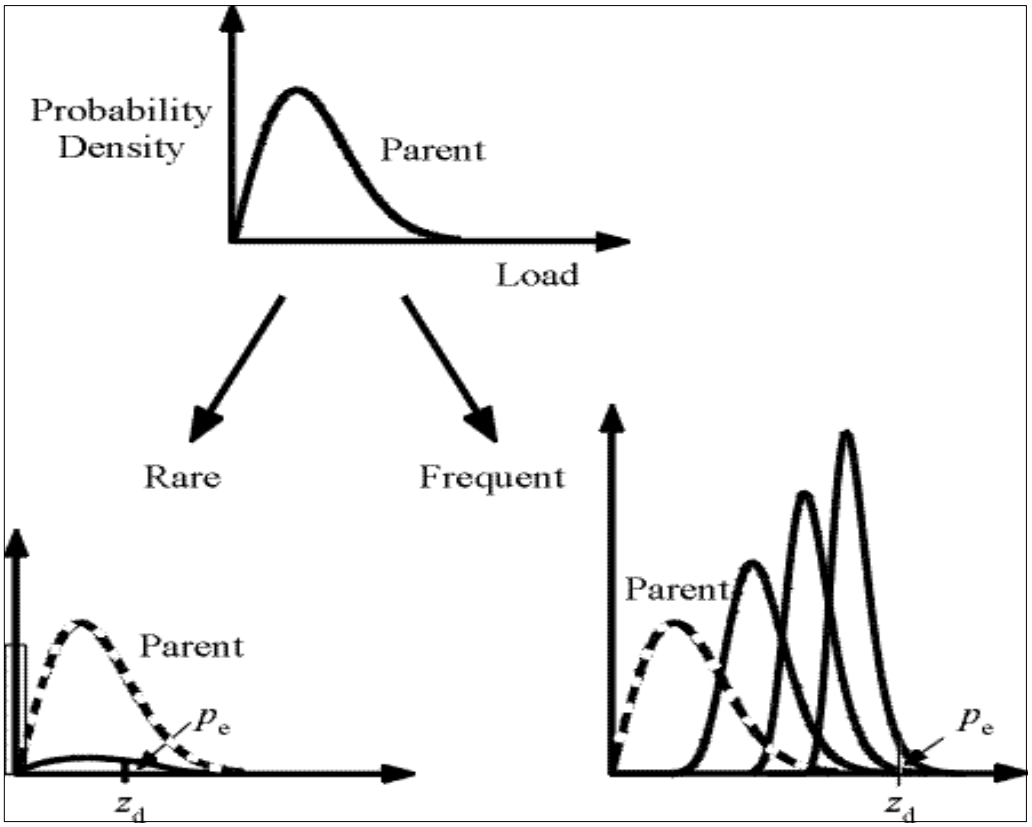

FIGURE 16.6: pdf for Rare and Frequent Events

The calibration using the Kigoriak ramming tests (see *Section 14*) is described below. This has been supplemented with data from the Louis S. St-Laurent, and compared with reasonable agreement to the updated ASPPR regulations (see Jordaan and Xiao, 1999).

16.4 Analysis

The Kigoriak data has been entered into an Excel spreadsheet. Only events where pressures recorded were used (in many rams, no pressures were recorded, probably in many cases because of fractures in the ice). Rather than a full histogram such as that in *Figure 16.5*, it was decided to concentrate on the tail of the distribution, see *Figures 16.7 and 16.8*. These plots were done on the basis that the 1.25 m^2 and 6.0 m^2 panels were the "design areas" under consideration, so that the pressures were simply the force (F_1 or F_2) divided by the panel area (1.25 m^2 or 6.0 m^2). There is information in the data set on the distribution of the force; the areas on which the force is applied within the 1.25 m^2 and 6.0 m^2 areas are also given (subareas a_1 and a_2, leading to p_1 and p_2). These were analyzed

in various ways, of interest here is the analysis of Maes and Hermans (1991), and also of Brown (1996). They performed a statistical analysis of the various patterns that can occur to constitute the recorded subareas and produced the results show on *Figure 16.9*. Maes and Hermans (1991) conducted a substantial and independent check on the results. The slight "kink" in the plot for the 1.25 m^2 results was found to result from an anomalous result for one subarea.

As a result, the following relationship was developed:

$$a = 1.25a^{-0.7}$$

with a = design area in m^2, in the range 0.6 to 6 m^2. This is also shown in *Figure 16.9*.

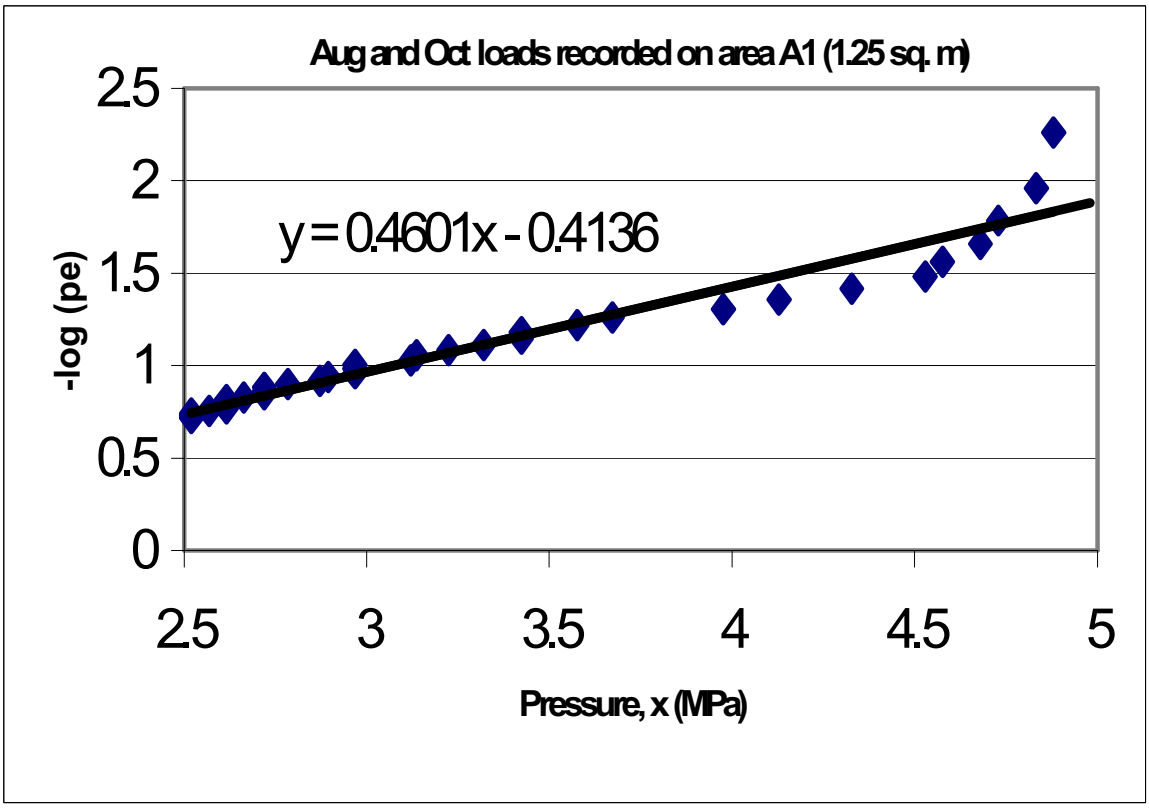

FIGURE 16.7: Pressure Versus Probability (To Log Scale) for an Area at 1.25 m^2

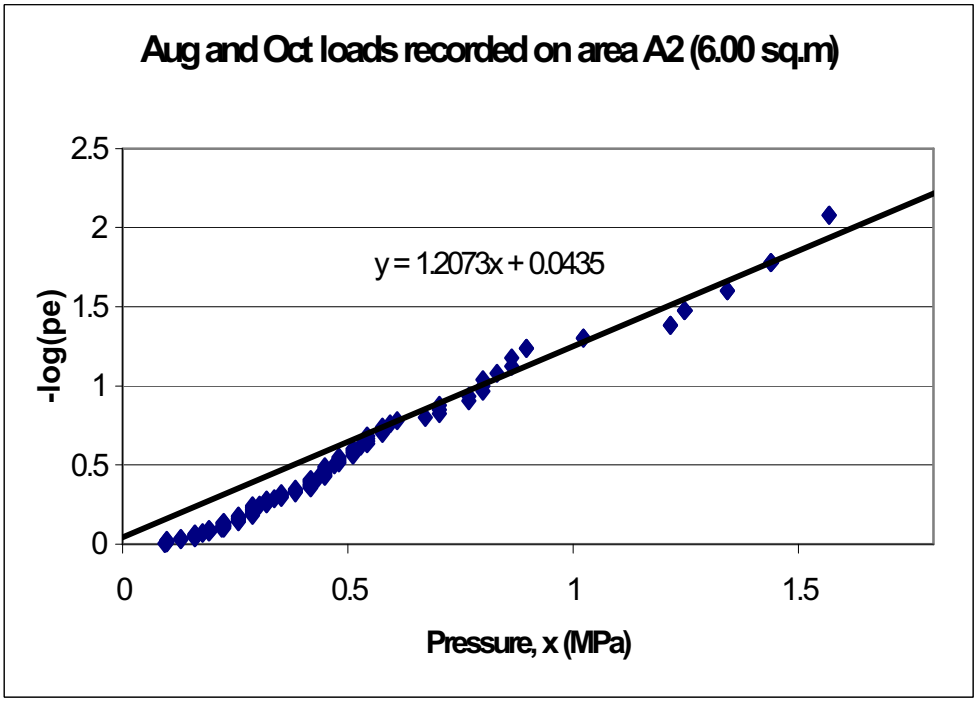

FIGURE 16.8: Pressure Versus Probability (To Log Scale) for an Area at 6.0 m^2

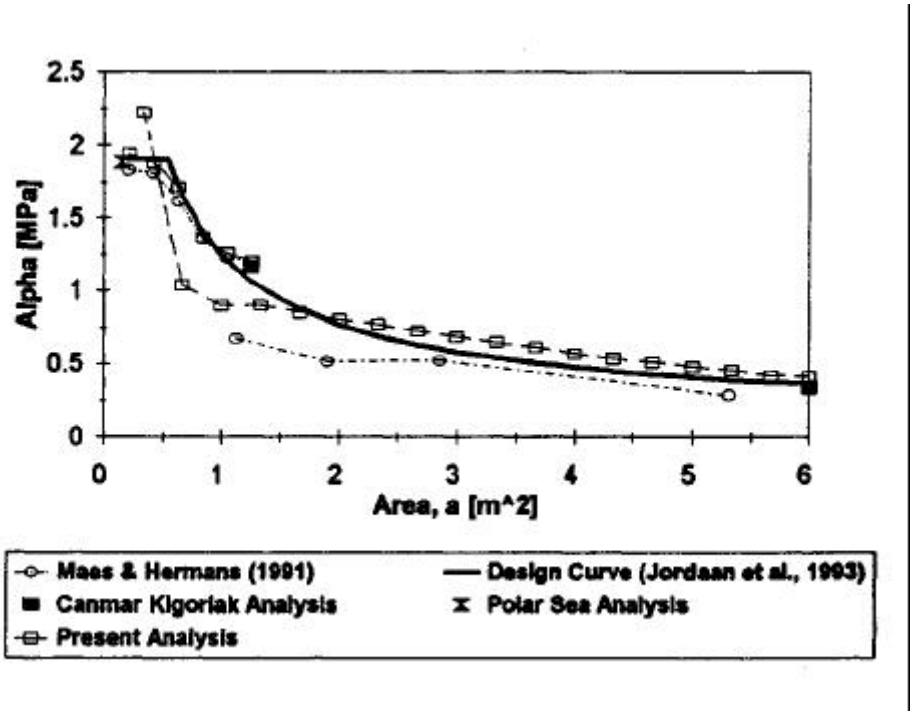

FIGURE 16.9: Lot of ∀ (from Equation 4) Versus Design Area a

16.5 Other Supporting Evidence

A probabilistic model of high-pressure zones has been developed based on the idealization of the high-pressure zones as point loads, as illustrated in *Figure 16.10* (Jordaan et al, 1993, Johnston et al, 1998, and Zou, 1996). For the analysis, a spatial Poisson process was used to model the random number of point loads on a design area, with the size of each load being random as well. This has been compared to the Equation 4 above, based on the Kigoriak data on ship rams. Good agreement was found. This is shown in *Figure 16.11*. It should be noted that there is no limit on size or number of the high-pressure zones.

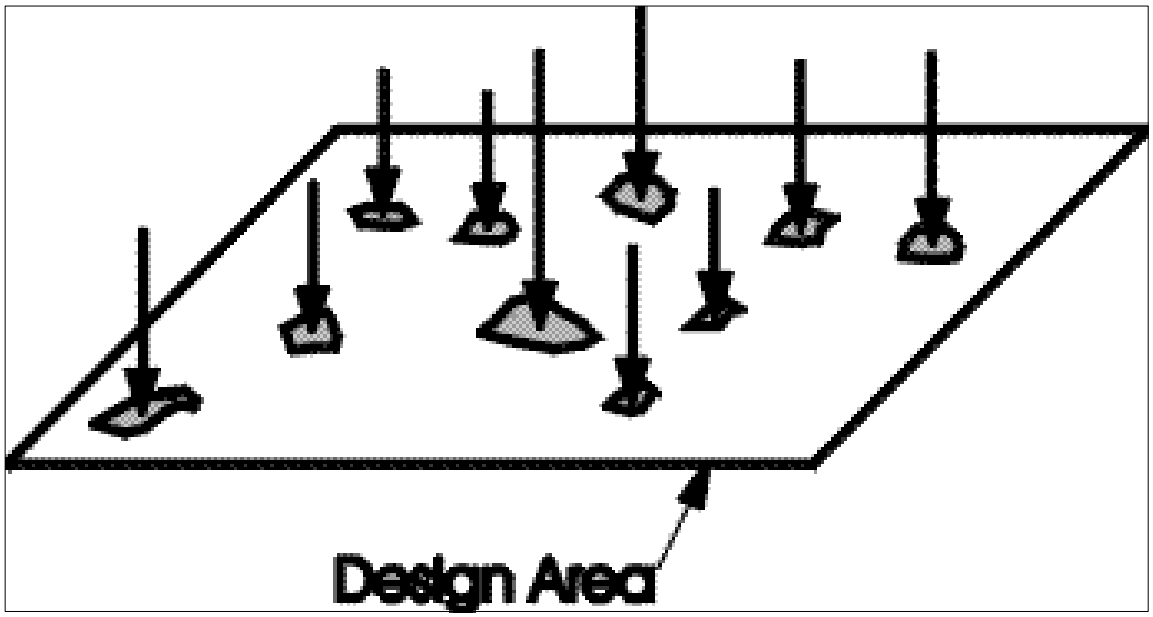

FIGURE 16.10: High-Pressure Zones as Point Loads

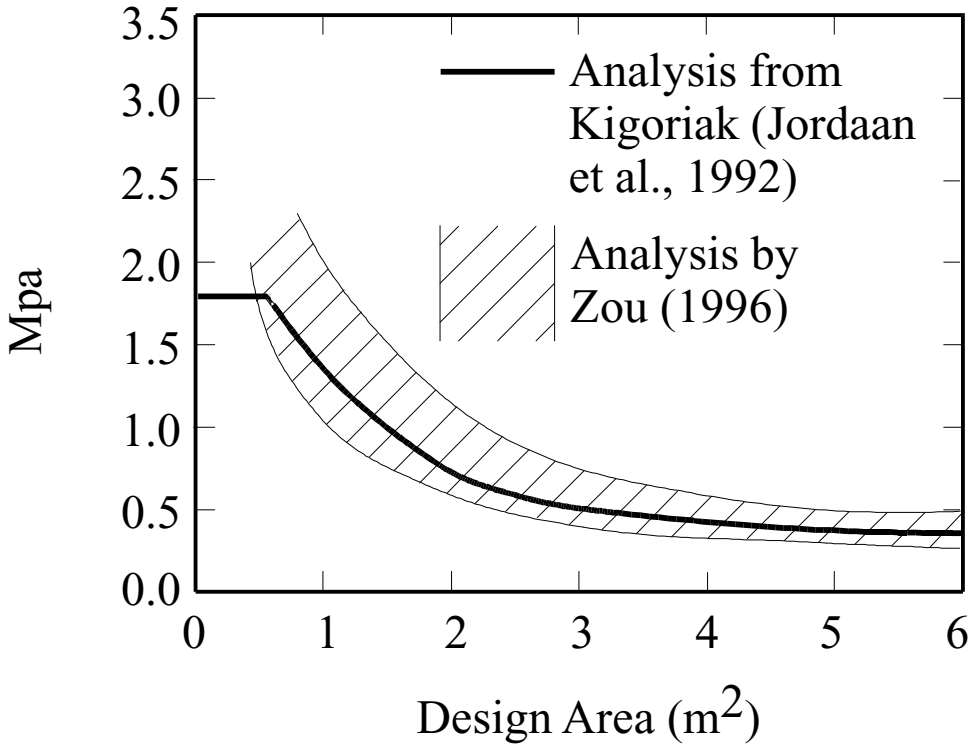

FIGURE 16.11: Kigoriak Results

Further support for the relationship comes from the ASPPR revisions (now the Equivalent Standards); see Carter et al. (1992). The relationship above is in good agreement with the design curves in the ASPPR approach, which is based on considerable experience with local pressures in the Arctic.

16.6 Design Application

The parameter *n* includes a factor that relates to the exposure of the structure as compared to ship rams, and also includes a factor related to the frequency of impacts of the structure with icebergs. The average duration of the ship rams is estimated as 0.7 secs. From Equation 3 we can obtain an expression for z_e:

$$Z_e = a \{ -1n[-1nF_Z(Z_e)] + 1nm\}$$

We can solve for z_e using this equation:

$$z_e \cong \alpha \left(\ln n + \ln \mu \right).$$

This is a good approximation for large *?μ*; *?* is the return period.

Some results are plotted in *Figure 16.12* for a fixed platform: annual arrival rate = 0.11, duration = 8 secs., and for a floater: arrival rate = 0.05, duration = 4 secs.

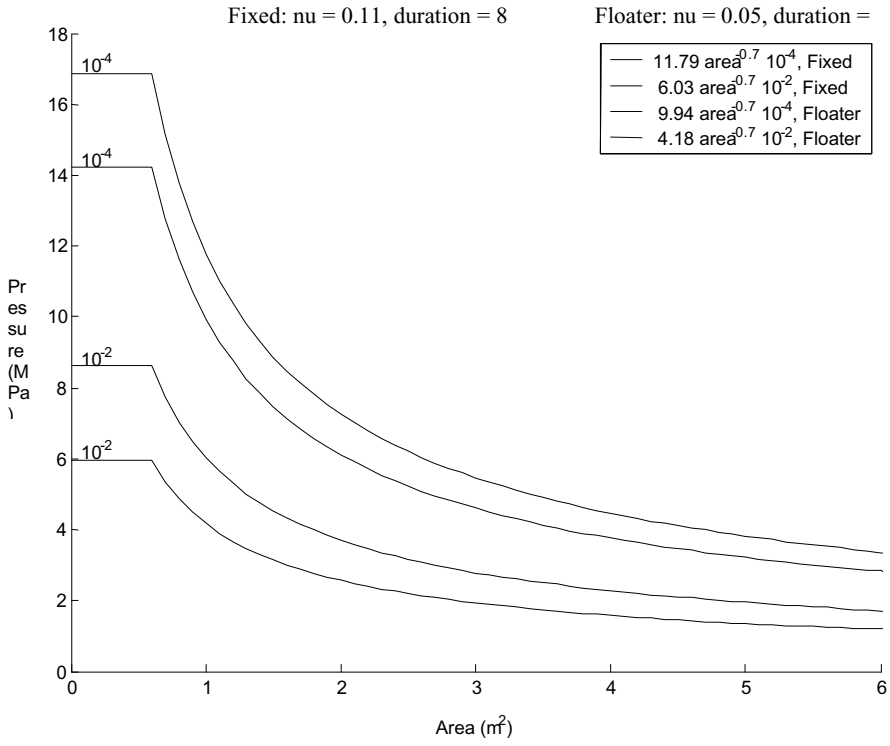

FIGURE 16.12: Pressure Versus Area Design Curves

It can be seen that there is a sharp drop-off in pressure with area, as compared to the values used in previous work. There is still a high demand for resistance at small area, of the order of 1 square metre. At the same time, the comments in the section "General Safety Issues" above should be taken into account.

17 Conclusions and Recommendations

All the data sets catalogued in this study are useful in providing insights into the nature and magnitudes of local ice loads. However, only a limited amount of data is available on iceberg crushing strengths that might be used directly for local load criteria. These are the Pond Inlet indentation tests and the Grappling Island impact tests. These data sets have their limitations. For example, it might be argued that the Pond Inlet tests represent conditions which are too confined for many situations. The Grappling Island tests are not as confined, but the impacts are of limited magnitude and the full crushing pressures that might occur in relatively modest real-world interactions (even with floaters), were unlikely to be simulated.

As well, the data from these tests are not very amenable to statistical treatment and therefore cannot directly provide the basis for a probabilistic methodology.

A probabilistic approach based on the analysis of ship data (mainly from the Kigoriak) is described in this study. The ship data contains numerous events and therefore provides a good basis for probabilistic analysis. However, views on the use of data from interactions of ships with sea ice for iceberg criteria are mixed. There are strong proponents arguing that the strength and confinement conditions are similar. There are others who are concerned that in many impacts, this is not the case, especially if the data is used for local loads within a large crushing area as can occur with a large iceberg and a fixed platform.

The recent experiments with the Terry Fox impacting small icebergs, which are not yet available, will be very relevant to the problem. The results need to integrated into the catalogue of available data as soon as possible.

However, even these data are unlikely to involve large contact areas and therefore the issue of local ice loads on small areas within larger areas of iceberg crushing may remain.

As discussed in this report, even though large contact areas have been experienced on Arctic platforms such as the Molikpaq, the shape of the contact areas is different. Large contact areas for sea ice will usually be at high aspect ratios, with the centre of the crushing zone still within a metre or two of a free edge. However, most iceberg impacts will involve aspect ratios close to one. Local areas at the centre of the crushing zone will likely be more confined. Whether this leads to higher local ice pressures is open to discussion and depends on the physics of the process, which is poorly understood. Nevertheless, it is recommended that pressure/area curves be qualified by aspect ratio effects. Pressure/area data which is for aspect ratios not suitable for iceberg interactions should be separated, the remaining pressure/area data should then be examined to see if it can be reliably processed for iceberg design criteria.

One data set that, if re-examined, may give new insights on the effects of aspect ratio is the Molikpaq data. In particular, the records of the Medof panels should be examined in detail. There is a considerable amount of data never examined. For example, in 34 fast file records, there are more than 350,000 measurements at 1 second intervals over the 3 m^2 Medof panel areas.

Depending upon the ice thickness that was interacting with the Molikpaq at any point in time during these fast file records, the range of contact areas on the Medof panels varied between ~ 1 m^2 to ~ 15 m^2. Furthermore, the degree of confinement and boundary conditions varied depending upon the particulars of each specific interaction, with the thicker old ice interactions favouring more confinement. In cases where old ice thicknesses were in the order of 5 m or more and continuous crushing was seen, full contact over the 3 m^2 Medof panel areas is quite certain, at least for the second row of panels.

Thus the Molikpaq data can be sorted by contact area and aspect ratio. It will be worth conducting such an exercise, first to provide new reliable local load data and second to examine the effects of aspect ratio or ice thickness on local loads.

Another issue relating to ice pressures on small areas relates to the use of the pressure/area curve during impact calculations (in which the nominal contact area builds up from small values to larger values as the interaction proceeds). It is common practice to use a pressure/area relationship which can lead to high values at the beginning of the interaction when areas are small. Such high pressures are unlikely because these initial small areas are unconfined. An alternative to the conventional approach is described in this report. It results in a pressure/area relationship where the pressure increases with area up to a peak value, after which size effects may cause it to decrease according to the conventional pressure/area relationship.

Despite the uncertainties discussed above, there is little doubt that local ice pressures should be treated within a probabilistic framework and that the design values need to take account of the exposure of a structure to ice action as discussed in this report. This is especially important for the Grand Banks where iceberg interactions with fixed platforms is a rare event.

18 References and Bibliography

Akagawa, S., Nakazawa, N., Sakai, M., Matsushita, H., Terashima, T., Takeuchi, T. and Saeki, H., 2000. Ice failure mode predominantly producing peak-ice-load observed in continuous ice load records, Proceedings of the Tenth International Offshore and Polar Engineering Conference, The International Society of Offshore and Polar Engineers, Vol. I, pp 613-620.

Arockiasamy M., El-Tahan H., Swamidas A.S.J., Russell W. and Reddy D.V., 1983. Semi-submersible response to bergy-bit impact. Int. Symp. RINA Offshore Eng. Group, Royal Institute Naval Architects, paper 14.

Blanchet, D., 1990. Ice design criteria for wide Arctic structures. Canadian Geotechnical Journal, Vol. 27, No. 6, pp. 701-725.

Blanchet, D., Churcher, A.C., Fitzpatrick, J.P. and Badra-Blanchet, P., 1989. An analysis of observed ice failure mechanisms for laboratory, first-year and multi-year ice. In Working Group of Ice Forces, 49th State-of-the-Art Report. Edited by G.W. Timco, US Army Cold Regions Research and Engineering Laboratory, Hanover, NH, Special Report 89-5, pp. 77-124.

Blenkarn, K.A., 1970. Measurements and analysis of ice forces on Cook Inlet structures. Proceedings OTC 1970, Houston. Paper 1261.

Blount, H., Glen, I.F., Comfort, G. and Tam, G., 1981. Results of Full Scale Measurements Aboard CCGS Louis S. St-Laurent During a 1980 Fall Arctic Probe, Report for Canadian Coast Guard by Arctic Canada Ltd., Vols. I and II.

Brown, P.W., Jordaan, I.J., Nessim, M.A. and Haddara, M.M.R., 1996. Optimization of bow plating for icebreakers. Journal of Ship Research 40 (1) 70-78.

Browne, R. and Ritch, R., 2000. North Pole Voyages Analysis for AIRSS Identification and Measurement of Factors Influencing Hull Damage Risk, Canadian Hydraulics Centre TP13573E.

Browne, R. and Ritch R., 2000. North Pole Voyages Analysis for AIRSS; Identification and Measurement of Factors Influencing Hull Damage Risk Through analysis of :Louis S. St-Laurent and Oden North Pole Voyage Data, Canadian Hydraulics Centre.

Brown, T.G., 2001. Four years of ice force observations on the Confederation Bridge. Proc. of 16th Intl. POAC Conf. Ottawa, Canada Aug 2001.

Carter, J.E., Frederking, R.M.W., Jordaan, I.J., Milne, W.J., Nessim, M.A. and Brown, P.W., 1992. Review and Verification of Proposals for the Arctic Shipping Pollution Prevention Regulations. Memorial University of Newfoundland, Ocean Engineering Research Centre, Report submitted to Canadian Coast Guard, Arctic Ship Safety.

Croasdale, K.R., 1970, “The Nutcracker Ice Strength Tests” Imperial Oil Ltd. APOA Project No. 1.

Croasdale, K.R., 1971. The nutcracker ice strength tests. Arctic Petroleum Operators' Association, Calgary, Alta., APOA Project 9.

Croasdale, K.R., 1985. Ice Investigations at a Beaufort Sea Caisson, 1985. A report prepared for the National Research Council, Ottawa and the US Dept of the interior.

Croasdale, K.R. and Frederking, R., 1987. Field Techniques for Ice Force Measurements. Working Group on Ice Forces, 3rd IAHR State of the Art Report. CRREL Special Report 87-17.

Crocker, G., Croasdale, K.R., Mckenna, R., Guzzwell, J. and Bruneau, S., 1996. C-CORE Iceberg Impact Experiment Phase 2 Final Report. C-CORE Publication 96-C16, St John's, Nfld.

Danys, J.V. and Bercha, F.G., 1975. Determination of ice forces on a conical offshore structure. Proc. 3rd Intl. POAC Conf. Univ. of Alaska. Aug 1975.

Dome Petroleum Limited, 1982. Full Scale Measurement of the Ice Impact Loads and Response of the Kigoriak August and October, 1981. Dome Petroleum Limited, Calgary, Alberta, Canada.

Edgecombe, M., St. John, J., Liljestrom, G., Ritch, R., 1992. Full-Scale Measurements of the Hull-Ice Impact Loads Onboard the Oden During the 1991 International Arctic Ocean Expedition Canadian Publication Number TP 11252E, Canadian Coast Guard Northern, Arctic Ship Safety, Ottawa.

Engelbrektson, A., 1977. Dynamic ice loads on lighthouse structure. Proceedings, 4th International Conference on Port and Ocean Engineering under Arctic Conditions, St. John's, Nfld., Vol 2, pp. 654-663.

Engelbrektson, A., 1983. Observations of a resonance vibrating lighthouse structure in moving ice. Proceedings, 7th International Conference on Port and Ocean Engineering under Arctic Conditions, Helsinki, Finland, Vol. 2, pp. 855-864.

Frederking, R.W. et al, 1985. Ice force results from the modified Yamachiche Bend Lightpier, winter 1983 -84. Proc. of Can. Coastal Conf. 1985, St. John's Nfld.

Frederking, R.W. et al, 1989 “Field Tests of Ice Indentation at Medium Scale: Ice Island” Report for Can. C.G. and NRC.

Frederking, R., Timco, G.W., Jeffries, M.O. and Sackinger, W.M., 1988. Initial measurements of physical and mechanical properties of ice from Hobson's Choice Island. Proc. IAHR Symposium on Ice, vol. 1, 23-27, Aug. 1988, Sapporo, Japan 188-198.

Gagnon, R.E. and Gammon, P.H., 1995. Triaxial experiments on iceberg and glacier ice. Journal of Glaciology 41, 528-540.

Gagnon, R.E., Jones, S.J., Frederking, R., Spencer, P.A. and Masterson, D.M., 1998. “Large Scale Hull Loading of First-Year Sea Ice, International Northern Sea Route Programme (INSROP) Working Paper No. 114 – 1998, I.1.7, September 18, 1998.

Gagnon, R.E., Jones, S.J., Frederking, R., Spencer, P.A. and Masterson, D.M., 1999. "Large Scale Hull Loading of Ice in Tuktoyaktuk Harbour, 18th International Conference on Offshore Mechanics and Arctic Engineering (OMAE 99), St. John's, NF, July 11-16, 1999, Paper No. 99-1129.

Hawkins, J.R., James, D.A. and Der, C.Y., 1983. Design, construction and installation of a system to measure environmental forces on a caisson retained island. Proceedings, 7th International Conference on Port and Ocean Engineering under Arctic Conditions, Helsinki, Finland, Vol. 4, pp. 770-779.

Iyer, S.H. and Masterson, D.M., 1991. "Field and Laboratory Strength Values of Multi-Year Ice Off Herschel Basin", Proceedings, 1991 Offshore Mechanics and Arctic Engineering Conference, Stavanger, Norway.

Jeffries, M.O., Sinha, N.K. and Sackinger, W.M., 1990. Deformation of natural ice island ice under constant strain rate uniaxial compression. Proc. 10th Int. Symp on Ice (IAHR), Helsinki, University of Technology, Espoo, Finland 1, 238-251.

Johnson, J.B., Cox, G.F.N. and Tucker, W.B., 1985. Kadluk ice stress measurement program. Proceedings, 8th International Conference on Port and Ocean Engineering under Arctic Conditions, Narssarssuaq, Greenland, Vol. 1, pp. 88-100.

Johnston, M.E., Croasdale, K.R. and Jordaan, I.J., 1998. Localized pressures during ice-structure interaction: relevance to design criteria. Cold Regions Science and Technology; 27:105-117.

Jordaan, I.J., Fuglem, M. and Matskevitch, D.G., 1996. Pressure-area Relationships and the Calculation of Global Ice Forces, Proceedings, IAHR Symposium on Ice, Beijing, China, Vol. 1, pp. 166-175.

Jordaan, I.J., Maes, M.A., Brown, P.W. and Hermans, I.P., 1993. Probabilistic analysis of local ice pressures. Journal of Offshore Mechanics and Arctic Engineering. 115:83-89.

Jordaan, I.J., Xiao, J. and Zou, B., 1993. Fracture and damage of ice: towards practical implementation. Proceedings,1st Joint Mechanics Meeting of ASME, ASCE, SES, Charlottesville Virginia, AMD 163 (Ice Mechanics): 251-260.

Jordaan, I.J. and Xiao, J., 1999. Compressive ice failure. Ice in Surface Waters, Proceedings, IAHR Symposium on Ice, 1998 HT Shen (ed) Potsdam, New York, p. 1025-1031.

Jones, S.J., Spencer, P.A., Masterson, D.M. and Gagnon, R.E., 1995. "Flaking Tests to Measure Large Scale Strength of Ice", IST'95, INSROP Symposium Tokyo '95, October 1-6, Tokyo, Japan.

Kamio, Z., Takawaki, T., Matsushita, H., Takeuchi, T, Sakai, M., Terashima, T., Akagawa, S., Nakazawa, N. and Saeki, H., 2000. Medium scale field indentation tests: physical characteristics of first-year sea ice at Notoro Lagoon, Hokkaido, Proceedings of the Tenth International Offshore and Polar Engineering Conference, The International Society of Offshore and Polar Engineers, Seattle, USA, pp 562-568.

Kry, P.R., 1981. Scale effects in continuous crushing of ice, Proc. 5th IARH Ice Symp., Universite Laval, Quebec, 1981.

Kry, P.R., 1980. Ice forces on wide structures. Canadian Geotechnical Journal, Vol. 17, No. 1, pp. 97-113.

Kry, P.R., Lucente, R.F. and Hedley, R.E., 1978.”Continuous Crushing of Ice. Esso Resources Canada Ltd. Report IPRT-28ME-78, APOA Project 106.

Liljestrom, G. (Editor) Icebreaker ODEN Trafficability Data, Swedish Polar Research Secretariat.

Lipsett, A.W. and Gerard, R., 1980. Field Measurements of Ice Forces on Bridge Piers, 1973 - 1979. Alberta Research Council Report, SWE 80-3. Edmonton, Alberta.

Maattanen, M., 1977. Ice-force measurements at the Gulf of Bothnia by the instrumented Kemi I Lighthouse, Proceedings, 4th International Conference on Port and Ocean Engineering under Arctic Conditions, Sept. 26-30, 1977. St. John's, Newfoundland. Vol. 2, pp. 730-740.

Maattanen, M., Hoikkanen, A.N. and Avis, J., 1996. Ice Failure and Ice Loads on a Conical Structure – Kemi-1 Cone Full Scale Ice Force Measurement Data Analysis. Proceedings IAHR Ice Symposium, pp 8-16, Beijing, China.

Maes, M.A. and Hermans, I.P., 1991. Review of Methods of Analysis of Data and Extreme Value Techniques for Ice Loads. Queen's University. Report submitted to Memorial University of Newfoundland.

Masterson et al, 1993, Iceberg Impact Simulations at Medium Scale IAHR 1993, pp 930-966.

Masterson, D.M., Frederking, R.M.W., Jordaan, I.J. and Spencer, P.A., 1993. "Description of Mult-Year Ice Indentation Tests at Hobson's Choice Ice Island - 1990", 1993 OMAE Conference, Glasgow, Scotland, June, 1993 (Paper 93-127) (pg. 145-155).

Masterson, D.M. and Frederking, R.M.W., 1992. Local contact pressures in ships and structure/ice interactions. Cold Regions Science and Technology. Elsevier Science Publishers B.V.

Masterson, D.M. and Frederking, R.M.W., 1993. Local contact pressures in ship/ice and structure/ice interactions, Cold Regions Science and Technology.

Masterson, D.M. and Iyer, S.H., 1988, "Failure Criteria for Multi-Year Ice Based on Medium Scale Field and Small Scale Laboratory Tests", Proceedings, IAHR Symposium, Sapporo, Japan.

Masterson, D.M., Graham, W.P., Jones, S.J. and Childs, G.R., 1997. “A comparison of uniaxial and borehole jack tests at Fort Providence ice crossing, 1995” Canadian Geotechnical Journal 34: 471-475.

Masterson, D.M., Nevel, D.E., Johnson, R.C., Kenny, J.J. and Spencer, P.A., 1992. The medium scale iceberg impact test program. In : Proc. IAHR Ice symposium, Banff, Alberta.

Masterson, D.M., Spencer, P.A., Nevel, D.E. and Nordgren, R.P., 1999. “Velocity Effects from Multi-Year Ice Tests”, 18th International Conference on Offshore Mechanics and Arctic Engineering (OMAE 99), St. John’s, NF, July 11-16, 1999, Paper 99-1127.

Masterson, D.M., Spencer, P.A. and Frederking, R.M.W., 1994 "Medium-Scale Uniform Pressure Tests on First-Year Sea Ice, 1993, Presented at OTC Houston, Texas May 1994, Paper No. 7614.

Masterson, D.M. and Spencer, P.A., 2000. Ice Forces vs. Aspect Ratio, Proceedings IUTAM Symposium on Scaling Laws in Ice Mechanics and Ice Dynamics, Fairbanks AK, USA.

Michel, B., 1978. The strength of polycrystalline ice. Can. J. Civ. Eng. 5, 285-300.

Matsushita, H., Kamio, Z., Sakai, M., Takeuchi, T., Terashima, T., Akagawa, S., Nakazawa, N. and Saeki, H., 2000. Consideration of failure mode of a sea ice sheet, Proceedings of the Tenth International Offshore and Polar Engineering Conference, The International Society of Offshore and Polar Engineers, Vol. I, pp 577-582.

McFadden, T., Haynes, D., Burdick, J. and Zarling, J., 1981. Ice force measurements on the Yukon River bridge. Proceedings, ASCE Specialty Conference. The Northern Community, Seattle, WA, pp. 749-777.

Metge, M., 1976. Ice conditions and ice defense at Netserk B-44 and Adgo P-25 during the winter of 1974-75. Arctic Petroleum Operators' Association, Calgary, Alta., APOA Project 104-1.

Montgomery, C.J., Gerard, R. and Lipsett, A.W., 1980. Dynamic response of bridge piers to ice forces. Canadian Journal of Civil Engineering, 7: 345-356.

Nadreau, J.P and Michel, B., 1986. Secondary creep in confined ice samples. Proc. 8th IAHR Ice Symp., Iowa City, Iowa, Vol. 1, 307-318.

Nakazawa, N., Akagawa, S., Kawamura, M., Sakai, M., Matsushita, H., Terashima, T., Takeuchi, T., Saeki, H. and Hirayama, K., 1999. Medium scale field indentation test (MSFIT) - Results of 1998 winter tests, Proceedings of the Ninth International Offshore and Polar Engineering Conference, The International Society of Offshore and Polar Engineers, Vol. 2, pp 498-504.

Neill, C.R., 1970. Ice pressure on bridge piers in Alberta, Canada. IAHR Ice Symposium, Reykjavik, Iceland, 1970.

Neill, C.R., 1974, “Selected Aspects of Ice Forces on Piers & Piles”. Canadian Society of Civil Engineers. Atlantic Regional Conference, Fredericton, N.B. Nov. 1974.

Nelson, R.D. and Sackinger, W.M., 1975. Ice stress measurements at Adgo and Netserk Islands, 1974 - 75. APOA project No. 104 -3 (Available through Arctic Inst. of North America, Univ of Calgary).

Nevel, D., 1986. Iceberg impact forces, Proc. 8th IAHR Ice Symp., Iowa City, IA.

Oshima, M., Narita, H., Yashima, N. and Tabuchi, H., 1980. Model and field experiments for development of ice resistant offshore structures. Proceedings, 12th Offshore Technology Conference, Houston, TX, Vol. 4, Paper 3885, pp. 307-314.

Pilkington, G.R., Blanchet, D. and Metge, M., 1983. Full-scale measurements of ice forces on an artificial island. Proc. 7th Intl. POAC Conf. Helsinki, 1983.

Poplin, J.P. and Ralston, T.D., 1992. Physical and mechanical properties of Hobson's Choice Ice Island cores. Cold Regions Science and Technology 20, 207-223.

Riska, K. et al, 1982. Measurement of Ice Pressures and Forces on Canmar Kigoriak during Repeated Trials in 1981. VTT Report LAI-332/82.

Riska, K., Rantala, H. and Joensun, A., 1990. “Full Scale Observations of Ship Ice Contact.” Helsinki University of Technology Research Report M97.

Ritch, R., Edgecombe, M. and Liljestrom, G., 2002. Measurement of hull side shell ice loads at full scale: Oden 1996 Arctic Ocean Expedition. Technical Report TP12919E, submitted to Transport Canada, Marine, Prairie and Northern Regions.

Ritch, R. and St. John, J., 1997. Ice Load Measurements on the CCGS Louis S. St-Laurent during the 1994 Arctic Ocean Crossing, Analysis and Conclusions, Fleet Systems, Canadian Coast Guard, June 1997.

Ritch, R., St. John, J., Browne, R.P. and Sheinberg, R., 1999. Ice load impact measurements on the CCG Louis S. St-Laurent during the 1994 arctic ocean crossing, OMAE99-1141.

Saeki, H., Hirayama, K., Honda, H., Akagawa, S., Takeuchi, T., Nakazawa, N., Terashima, T., Matsushita, H. and Saeki, H., 1998. Medium scale field indentation tests (MSFIT) - Results of 1997 winter, Proceedings of the Eighth International Offshore and Polar Engineering Conference, The International Society of Offshore and Polar Engineers, Vol. 2, pp. 364-369.

Sanden, E.J. and Neill, C.R., 1968. Determination of actual forces on bridge piers due to moving ice. Proceedings, Toronto Convention, Canadian Good Roads Association, Toronto, Ont., pp. 405-420.

Sanderson, T.J.O., 1988. Ice Mechanics: Risks to Offshore Structures; Graham & Trotman.

Sayed, M., Frederking, R.M. and Croasdale, K.R., 1986. Ice stress measurements in a rubble field surrounding a caisson-retained island. In Ice technology. Edited by T.K.S. Murphy, J.J. Cannon and C.A. Brebbia. Springer-Verlag, pp. 255-262.

Schwarz, J., 1970. The pressure of floating ice-fields on piles. IAHR Ice Symposium, Reykjavik, Iceland, 1970.

Schwarz, J., 2001. Ice Force Measurements within the Loleif Project. POAC, 2001. Ottawa.

Semeniuk, A., 1977. Ice pressure measurements at Arnak L-30 and Kannerk G-42. Arctic Petroleum Operators' Association, Calgary, Alta., APOA Project 122-1.

Sodhi, D.S., Kato, K. and Haynes, F.D., 1983. Ice force measurements on a bridge pier in the Otauquechee River, Vermont. US Army Cold Regions Research and Engineering Laboratory, Hanover, NH, Report 83-20.

Sodhi, D., Takeuchi, T., Akagawa, S., Nakazawa, N. and Saeki, H., 1998. Medium scale indentation tests on sea ice at various speeds, Journal of Cold Regions Science and Technology, 28, pp 161-182.

Spencer, P.A. and Masterson, D.M., 1993. "A Geometrical Model for Pressure Aspect-Ratio Effects in Ice-Structure Interaction", OMAE '93 Conference, Glasgow, Scotland, June 1993 (93-215).

St. John, J. and Minnick, P., 1993 Swedish Icebreaker Oden Ice Impact Load Measurements During International Arctic Ocean Expedition 1991 Instrumentation and Measurement Summary, Science an Technology Corp. USCG Contract DTCG23-91-D-ENM026.

St. John, J., Sheinberg, R., Ritch, R. and Minnick, P., 1994. Ice Impact Load Measurement Aboard the ODEN During the International Arctic Expedition 1991, ICETECH 1994 Conference.

Strilchuk, A.R., 1977. “Ice Pressure Measurements Netserk F-40, 1975-76. Imperial Oil Ltd., Report No. IPRT-14ME –77. APOA Project 105.

Takeuchi, T., Masaki, T., Akagawa, S., Kawamura, M., Nakazawa, N., Terashima, T., Honda, H., Saeki, H. and Hirayama, K., 1997. Medium scale field indentation tests (MSFIT) - Ice failure characteristics in ice/structure interactions, Proceedings of the Seventh International Offshore and Polar Engineering Conference, The International Society of Offshore and Polar Engineers, Vol. 2, pp 376-382.

Takeuchi, T., Akagawa, S., Kawamura, M., Sakai, M., Terashima, T., Kamio, Z., Matsushita, H., Nishimaki, H., Kurokawa, A. and Saeki, H., 2000. Examination of factors affecting total ice load using medium scale field indentation test data, Proceedings of the Tenth International Offshore and Polar Engineering Conference, The International Society of Offshore and Polar Engineers, Vol. I, pp 607-612.

Taylor, T.P., 1973, “Ice Crushing Tests, 1973”. Imperial Oil Report. APOA 52.

Taylor et al, 1981. An Experimental Investigation of the Crushing Strength of Ice. Proc of POAC, Quebec City, 1981.

Weaver, J.S. and Berzins, W., 1983. The Tarsiut Island monitoring program. Proceedings, 15th Offshore Technology Conference, Houston, TX, Vol. 2, Paper 4519, pp. 67-74.

Weiss, R.T., Wright, B. and Rogers, B., 2001. In-ice performance of the Molikpaq off Sakhalin Island. Proc. of 16th Intl. POAC Conf. Ottawa, Canada Aug 2001.

Wetmore, S.B., 1984. Concrete island drilling system. Super Series (Super CIDS). Proceedings, 16th Annual Offshore Technology Conference, Houston, TX, Vol. 3, pp. 215-226.

Williams, F.M., 1994. The Canada/US 1994 Arctic Ocean Section-Ice Mechanical Properties Measurements, Report TR-1994-29, Institute of Marine Dynamics, National Research Council Canada, St. John's, Newfoundland, Canada.

Wright, B, Croasdale, K.R. and Metge, M., 1998. “Molikpaq Ice Load Data”. Report to EPR, 1998.

Wright, B.D., Pilington, G.R., Woolner, K.S. and Wright, W.H., 1986. Winter ice interactions with an arctic offshore structure. Proceedings, 8th International Association of hydraulic Research Ice Symposium, Iowa City, IA.

Zou, B., 1996 Ships in Ice: the Interaction Process and Principles of Design. Ph.D. Thesis. Memorial University of Newfoundland.

APPENDIX A

Data Format Template

LOCAL ICE LOAD DATA RELEVANT TO GRAND BANKS STRUCTURES

OUTLINE FOR DATA SOURCE FORMAT

1 Summary

Data Source: e.g. Molikpaq

Geographic Location: e.g. Beaufort Sea

Time Period: e.g. Winters of 1984/85: 85/86

Ice Types: e.g. Pack Ice: First year Arctic Sea Ice: Multi-year ice

Range of Contact Areas:

Relevance to Icebergs: High, medium or low

2 Background

Brief description of the data source (instrumented structure or indentation tests or ship). Overview of type of instrumentation and/or measurement methods. Location, type of ice encountered or tested. Period of testing or data collection.

Level of data analysis to date. Comments on boundary conditions. Confidentiality of data (if any). (About one to two pages)

3 Data Attributes

1. Availability of time series and approximate numbers of time series.

2. Duration of records.

3. Frequency of data recording.

4. Range of contact areas.

5. Comments on degree of confinement and boundary conditions.

6. Ice conditions and ice types (salinity and temperature).

7. Ice thickness, ice mass, etc.

8. Structural stiffness and response (if any).

9. Ice speed (or indentation, ship speed) ice direction.

10. Measurement methods, resolution, response frequency etc. Method of determining contact areas.

4 Data Availability (Who Owns It, Where from)And Format (Tapes, Paper, Disks, Etc.)

5 Data Quality and Number of Events

Example of how local ice loads are determined with strengths and weaknesses of data. (e.g., low frequency response of Medof panels).

Number of events and time series available.

Development of local loads with time.

6 Examples of Time Series Data

Present three examples of times series data for local loads and associated contact areas.

Describe how contact area is determined for each data point and how it changes with time (if relevant). Plot contact areas and aspect ratio with the local loads and ice pressure on same time axis. Indicate if area over which pressure is determined is part of a larger contact area. If so, also plot gross contact area, aspect ratio and or some other measure of confinement (e.g. distance to free edges. Provide a commentary on this issue for each time series.

Suitability of data to probabilistic treatment.

COMMENTS ON RELEVANCE TO LOCAL ICE LOADS DUE TO ICEBERGS

Consider both large icebergs and bergy bits, and the issues of confinement, ice speeds, ice temperature, ice salinity etc.